An investigation of inter-seasonal near-surface ground heat transfer and storage

José Javier Muñoz Criollo

School of Engineering

Cardiff University

This thesis is submitted to Cardiff University in fulfilment of the requirements for the Degree of Doctor of Philosophy

December 2014

DECLARATION

This work has not been submitted in substance for any other degree or award at this or any other university or place of learning, nor is being submitted concurrently in candidature for any degree or other award.

Signed …… (candidate)

Date ……

STATEMENT 1

This thesis is being submitted in partial fulfillment of the requirements for the degree of PhD

Signed …… (candidate)

Date ……

STATEMENT 2

This thesis is the result of my own independent work/investigation, except where otherwise stated. Other sources are acknowledged by explicit references. The views expressed are my own.

Signed …… (candidate)

Date ……

STATEMENT 3

I hereby give consent for my thesis, if accepted, to be available online in the University's Open Access repository and for inter-library loan, and for the title and summary to be made available to outside organisations.

Signed …… (candidate)

Date ……

Acknowledgements

I would like to express my gratitude to my supervisors Dr. Peter J. Cleall and Dr. Stephen W. Rees. Their continuous help, encouragement and endless patience have made possible the completion of this thesis. Their sincere support and trust have inspired me to give my very best during the last years.

I would like to thank also to the Mexican government through their National Council for Science and Technology (CONACyT) and the Secretariat of Public Education (SEP) for the funding awarded to me for the pursuing of this degree at Cardiff University and to the Transport Research Laboratory (TRL) for supplying and allowing the use of the data published in (Carder et al, 2007) for the purposes of this thesis.

During the course of my PhD studies several people have helped me one way or another for the achievement of my objectives. In particular I would like to thank the staff at the Research Office at the School of Engineering of Cardiff University for their continuous guidance and efforts to unravel the messed thoughts of a PhD student.

I also would like to acknowledge the help provided by Dr. Snehasis Tripathy, the technicians Len Czekaj and Paul Malpas from the School of Engineering of Cardiff University, Dr. Peter Brabham from the Earth and Ocean Sciences of Cardiff University and Dr. Maria Victoria Villar Galicia from the CIEMAT for their kind help in the experimental aspects of this investigation. An area in which I wasn't particularly skilled nor knowledgeable and that could have made my stay in Cardiff University less enjoyable if it not were for their thoughtful assistance.

To the staff in charge of ARCCA in Cardiff University for technical assistance in the numerical aspects of this research. Their always accessible attitude have facilitated the journey through the learning curve that represents the use of advanced computing equipment.

Finally, to my friends, just for being there and having a beer (or a cider) and a slice of pizza with me. For the endless hours of random (really random and lateral) talks that in some way have kept me sane. A very special thank you is deserved to Iris

Acejo for her saintlike patience and endless cheering without which I would have cracked a long time ago.

To all of you. Thank you..... Javier Muñoz

Carder, D. R., Barker, K. J., Hewitt, M. G., Ritter, D., and Kiff, A. [2007]. Performance of an Interseasonal Heat Transfer Facility for Collection, Storage and Re-Use of Solar Heat from the Road Surface. PPR302. Transport Research Laboratory.

Abstract

This thesis presents a numerical, analytical and experimental investigation of inter-seasonal heat transfer processes in soils. Particular attention is given to the energy balance at the soil surface and its impact on the performance of thermal energy storage devices in shallow regions of the ground. For this purpose, a transient three-dimensional theoretical framework representing the relevant processes has been developed. A numerical solution has also been developed using the finite element method for spatial discretization and the finite difference method for time-stepping. The resulting model takes into account conductive and convective heat transfer between the fluid inside pipe heat exchangers and the surrounding soil. An alternative simplified 2D approach has also been developed and compared to the full 3D model. The determination of representative initial conditions and far-field (bottom) boundary conditions for the simulation of shallow ground heat storage facilities has also been investigated. To this end, a novel (1D) analytical approach has been developed to estimate realistic soil temperature profiles and seasonal thermal energy storage variations that can be used as input for more comprehensive analysis. Comparisons have been made to 1D numerical analysis.

The proposed numerical model has been used to study a full-scale experiment undertaken by others involving the use of an inter-seasonal heat storage facility. As part of this study, key material properties have been measured using soil samples recovered from the experimental site. The results have revealed the importance of correctly representing the energy balance at the soil surface. Inclusion of soil/atmosphere interaction has been shown to be of critical importance for the correct assessment of buried heat transfer devices. The region of thermal influence and its seasonal variation have been established and the main limitations of the proposed model identified. General guidance for the design and installation of inter-seasonal heat transfer facilities has been provided based on the obtained results.

List of Figures

List of tables

List of Symbols

A_i	Pipe internal area	m^2
$\boldsymbol{A_U}$	Laplace matrix for moisture flow	
$\boldsymbol{A_V}$	Laplace matrix for heat flow	
$\boldsymbol{A_W}$	Laplace matrix for heat advection	
C_e	Coefficient of evaporation for fully dense canopies	dimensionless
c_f	Transfer coefficient for aerodynamic resistance	dimensionless
C_f	Volumetric moisture capacity	J/m^3K
C_{fc}	Coefficient for forced convection	dimensionless
C_{nc}	Coefficient for natural convection	dimensionless
$c_{p,a}$	Specific heat capacity at constant pressure of soil air particles	J/kgK
$c_{p,b}$	Soil bulk specific heat capacity at constant pressure	J/kgK
$C_{p,b}$	Soil bulk volumetric heat capacity at constant pressure	J/m^3K
$c_{p,f}$	Specific heat capacity at constant pressure of fluid inside pipe	J/kgK
$c_{p,s}$	Specific heat capacity at constant pressure of soil solid particles	J/kgK
$c_{p,w}$	Specific heat capacity at constant pressure of soil water particles	J/kgK
C_{sh}	Coefficient of sheltering	dimensionless
C_w	Specific moisture capacity function	1/m
C_θ	Specific moisture capacity	1/m
D_{sh}	Shading factor	dimensionless
D_w	Unsaturated diffusivity	m^2/s
e_a	Atmospheric vapour pressure	kPa
$e_{a,sat}$	Atmospheric saturation vapour pressure	kPa
$e_{ss,sat}$	Soil surface saturation vapour pressure	kPa
E_i	Total bulk volumetric energy	J/m^3
$e_{c,sat}$	Saturated vapour pressure of canopy cover	kPa
E_p	Precipitation mass rate per unit area	kg/m^2s
e_{ss}	Soil surface vapour pressure	kPa
E_s	Thermal energy stored in column of soil	J/m^2
E_v	Evaporative mass rate per unit area	kg/m^2s
f	Friction factor	dimensionless
f_i	Boundary condition i	
F_{12}	View factor between surface 1 and 2	dimensionless
F_i	Initial condition	
$\boldsymbol{F_U}$	Load vector for moisture flow	
$\boldsymbol{F_V}$	Load vector for heat flow	
$\boldsymbol{F_W}$	Load vector for heat advection	
h	Pressure head	m
h_i	Heat transfer coefficient at boundary i	W/m^2K
H_a	Relative humidity	%
h_C	Convective heat transfer coefficient	W/m^2K
$h_{C,c}$	Convective heat transfer coefficient of canopy cover	W/m^2K

h_E	Evaporative heat transfer coefficient	W/m^{2}kPa
$h_{E,c}$	Evaporative heat transfer coefficient of canopy cover	W/m^{2}K
h_h	Discrete approximation of pressure head	m
h_f	Convective heat transfer coefficient of pipe wall	W/m^{2}K
h_{sat}	Pressure head under saturated conditions	m
h_{ss}	Pressure head at the soil surface	m
K	finite element	
K_w	Unsaturated hydraulic conductivity	m/s
$K_{w,sat}$	Saturated hydraulic conductivity	m/s
L_c	Characteristic length of pipe	m
L_{MO}	Monin-Obukhov length	m
L_s	Depth of column of soil	m
L_p	Length of pipe	m
L_v	Latent heat of evaporation for water	J/kg
$\dot{m}_f$	Mass flow rate of the fluid flowing through the pipe	kg/s
$\boldsymbol{M_U}$	Mass matrix for moisture flow	
$\boldsymbol{M_V}$	Mass matrix for heat flow	
$\boldsymbol{M_W}$	Mass matrix for heat advection	
N	Cloud cover factor	dimensionless
Nu	Nusselt number	dimensionless
Pr	Prandtl number	dimensionless
q_C	Convective heat flux per unit area	W/m^2
q_E	Evaporative heat flux per unit area	W/m^2
q_{ep}	Volume flow rate per unit area due to evaporation and precipitation	kg/m^{2}s
Q_f	Pipe internal heat generation	W/m^3
q_G	Conductive heat flux per unit area	W/m^2
q_T	Thermal energy flux per unit area	W/m^2
q_I	Infrared radiation per unit area	W/m^2
$Q_{I,1}$	Infrared heat flux rate from surface 1	W
$q_{I,1}$	Infrared heat flux rate per unit area from surface 1	W/m^2
$Q_{I,2}$	Infrared heat flux rate from surface 2	W
$q_{I,2}$	Infrared heat flux rate per unit area from surface 2	W/m^2
$q_{I,in}$	Incoming infrared radiation per unit area	W/m^2
Q_{max}	Maximum possible heat transfer rate on pipe	W
Q_p	Heat flux rate through pipe wall	W
q_p	Pipe heat transfer per unit area	W/m^2
Q_{real}	Actual heat transfer rate on pipe	W
q_S	Solar radiation per unit area	W/m^2
q_{sh}	Solar radiation reaching the surface after taking into account a shade factor	W/m^2
$q_{ss,in}$	Total amount of energy reaching the soil surface per unit of area	W/m^2
$q_{ss,out}$	Total amount of energy leaving the soil surface per unit of area	W/m^2
q_w	Total moisture flow	kg/m^{2}s
r	radius	m

R	Global solar radiation per unit area	W/m^2
r_a	Aerodynamic resistance	s/m
r_e	External pipe radius	m
Re	Reynolds number	dimensionless
r_i	Internal pipe radius	m
R_{max}	Max noon solar radiation per unit area	W/m^2
r_s	Stomata resistance	s/m
T	Temperature	˚C
t	Time	s
T_*	Average absolute temperature	K
$T_{1,\mathrm{K}}$	Absolute temperature of surface 1	K
$T_{2,\mathrm{K}}$	Absolute temperature of surface 2	K
T_∞	Temperature of surrounding environment	K
T_a	Air temperature	˚C
$T_{a,amp}$	Amplitude of air temperature	˚C
$T_{a,ave}$	Average air temperature	˚C
$T_{a,\mathrm{K}}$	Absolute air temperature	K
T_c	Temperature of canopy cover	˚C
$T_{c,\mathrm{K}}$	Absolute temperature of canopy cover	K
T_f	Temperature of fluid inside pipe	˚C
$T_{f,i}$	Pipe inlet temperature	˚C
$T_{f,o}$	Pipe outlet temperature	˚C
T_{pw}	Temperature of pipe wall	˚C
t_{ref}	Reference time	s
T_s	Temperature of soil	˚C
$T_{s,\mathrm{K}}$	Absolute temperature of soil	K
$T_{sky,\mathrm{K}}$	Absolute sky temperature	K
T_{ss}	Soil surface temperature	˚C
$T_{ss,\mathrm{K}}$	Absolute soil surface temperature	K
$\boldsymbol{U}$	Vector of unknown coefficients for moisture flow	
U_b	Base line value	
U_Δ	Value after change in one variable	
u_f	Velocity of fluid inside pipe	m/s
U_p	Pipe overall heat transfer coefficient	W/m^{2}K
u_s	Wind speed	m/s
V	Volume	m^3
$\boldsymbol{V}$	Vector of unknown coefficients for heat flow	
V_i	Volume of constituent i	m^3
$\boldsymbol{W}$	Vector of unknown coefficients for heat advection	
x,y,z	Cartesian coordinates	m
z_0	Soil surface roughness length	m
z_{0T}	Soil surface roughness for sensible heat transfer	m
z_{0m}	Soil surface roughness for momentum	m
z_{0v}	Soil surface roughness for vapour transfer	m
z_T	reference high at which temperature is measured	m
z_u	reference high at which wind speed is measured	m

Greek symbols

α	Coefficient for the estimation of vapour pressure at the soil surface	dimensionless
α_b	Soil bulk thermal diffusivity	m^2/s
α_c	Solar albedo for canopy cover	dimensionless
α_S	Solar albedo	dimensionless
β	Coefficient for the estimation of vapour pressure at the soil surface	dimensionless
β_m	Eigenvalues	
γ	Psychrometric constant	kPa/°C
Γ	Finite element spatial boundary	
Γ_1	Finite element spatial boundary 1	
Γ_2	Finite element spatial boundary 2	
γ_f	Specific gravity of fluid inside pipe	$kg/m^3/kg/m^3$
ε_1	Infrared emissivity of surface 1	dimensionless
ε_2	Infrared emissivity of surface 2	dimensionless
ε_c	Canopy cover infrared emissivity	dimensionless
ε_p	Pipe heat transfer effectiveness	dimensionless
ε_{sky}	Sky infrared emissivity	dimensionless
ε_{ss}	Soil surface infrared emissivity	dimensionless
η	Parameter for time discretization	dimensionless
θ_a	Air content	dimensionless
ϑ_K	Error indicator for element K	
θ_s	Zenith angle of the sun	
θ_v	Virtual temperature	K
θ_w	Moisture content	dimensionless
$\theta_{w,sat}$	Moisture content under saturated conditions	dimensionless
θ_{wp}	Wilting point moisture content	dimensionless
κ_s	Intrinsic permeability of the soil	m^2
λ	Thermal conductivity	W/mK
λ_b	Soil bulk thermal conductivity	W/mK
λ_f	Thermal conductivity of fluid inside pipe	W/mK
λ_i	Thermal conductivity of constituent i	W/mK
λ_{pw}	Thermal conductivity of pipe wall	W/mK
μ_f	Dynamic viscosity of fluid inside pipe	kg/ms
μ_w	Dynamic viscosity of water	kg/ms
ν	Density of canopy cover	dimensionless
ξ	Generalized heat transfer coefficient	W/m^2K
ρ_a	Density of air	kg/m^3
ρ_b	Soil bulk density	kg/m^3
ρ_f	Density of fluid inside pipe	kg/m^3
ρ_s	Density of soil solid particles	kg/m^3
ρ_w	Density of water	kg/m^3
ς	Size of mesh element	
υ_m	Mean velocity of fluid inside pipe	m/s

ϕ	Finite element test function	
χ_a	Fraction of air	dimensionless
χ_i	Fraction of constituents i	dimensionless
χ_s	Fraction of solid particles	dimensionless
χ_w	Fraction of water	dimensionless
Ψ_h	Empirical stability parameter for temperature	dimensionless
Ψ_m	Empirical stability parameter for momentum	dimensionless
Ω	Finite element domain	
ω_1	Annual period	s
ω_2	Daily period	s

Constants

g	Acceleration due to gravity	9.81 m/s^2
R_c	Solar constant	1.362 W/m^2
R_w	Gas constant for water vapour	461.5 J/kgK
κ	Von karman constant	0.41
σ	Steffan-Boltzmann constant	5.6704×10^{-8} W/m^2K^4
P_a	Atmospheric pressure	101.325 kPa

Mathematical operators

Δ	Difference operator
∇	Vector differential operator
∂	Partial derivative
$\hat{n}$	Normal unitary vector

Superscripts

n	At previous time step
$n+1$	At current time step
$n+1/2$	Between previous and current time steps

Subscripts

i,j	Counters
h	Numerical approximation of given variable

Chapter 1 Introduction

1.1 Motivation.

Commercial and residential buildings consume almost 40% of the primary energy (fossil fuels) in the United States and Europe, and nearly 30% in China. This has motivated the development of new technologies and standards to increment the energy efficiency of buildings to bring them to an ideal of zero energy usage (Deng et al. 2014). Furthermore, as personal income arises in populous and hot developing countries, their use of air conditioning is likely to increase as well (Sivak 2013). In China, in 1990, less than one percent of urban households owned an air conditioner; by 2003 this number rose to 62 % (McNeil and Letschert 2007). Moreover, if global warming continues its current trend, more energy will be required in buildings both for heating and cooling to mitigate changes in weather. For this reason, several countries have undergone ambitious efforts to reduce their carbon production and energy consumption (Raupach et al. 2014).

From a different perspective, oil prices have traditionally driven research on renewable energies and energy efficiency technologies, increasing during oil crises and declining when the prices drop. However, these same fluctuations in energy prices and the related political pressures attached to them converts the topic of renewable energies and energy efficiency into a national security issue (Hope 2014; U.S. Department of Defense 2013).

The aforementioned reasons show the necessity to devote efforts towards the reduction of current and future energy demands through research in new technologies for the improvement of energy efficiency and sustainability that contribute towards cutting down CO2 emissions, fighting global warming and making countries more energy independent.

One of these fields is energy storage. The technologies developed in this area allow to store and transport several kinds of energy obtained from surpluses due to either efficiency improvements or to gradients (spatial or temporal) in energy availability. An example of this is the seasonal thermal energy supply in summer and the thermal energy demand (e.g. building heating) in winter. Energy storage techniques help to

reduce the discrepancy between supply and demand contributing in this way to increase global energy efficiency.

1.1.1 Energy storage in soils

This thesis investigates the storage of thermal energy in regions of the soil close to its surface by means of engineering thermal devices. Particular attention is given to inter-seasonal thermal storage that utilizes the heat capacity of the ground (or other suitable medium) to store the surplus thermal energy from one season so that it can be used at a subsequent time. The relatively high specific heat capacity and low thermal conductivity of many soils allows the usage of the stored energy to be delayed in time with only relatively small energy losses. In general the storage process is carried out in the summer months when there is high solar energy availability (and in some cases waste heat availability from various heating and ventilation systems) while the utilization occurs in the winter months when energy demands increase.

Typical applications for inter-seasonal heat storage systems may include; heating for buildings, ice-prevention in highway pavements, and winter thermal maintenance of aircraft stands (Morita and Tago 2000). Sources of solar thermal energy for these systems are, for example, road surfaces (Bobes-Jesus et al. 2013) and roof solar collectors (Kroll and Ziegler 2011). When the former is used, the operation of the system is highly dependent on the interactions between the ground surface and the atmosphere since this determines the amount of energy available for the system. In this context, a correct understanding of the energy fluxes at the surface of the ground and a capability to represent them in a reliable manner is of clear importance. In turn, this will provide aid in performance assessment, decision making, design and implementation.

Research in ground thermal energy storage and the aspects that influence it contributes to improved energy efficiency in several different fields. The following section provides a summarized background regarding the classification and current use of ground thermal energy storage.

1.1.2 Research context

Inter-seasonal heat storage can be viewed as a sub-topic of the wider area of research, namely Thermal Energy Storage (TES) when classified according to the

storage period. TES can also be broadly subdivided into three categories according to the technology used:

- *Latent heat storage* involves a phase change from liquid to solid of a suitable material. The main advantages of this process are a high energy storage potential that translates into smaller volumes needed to store the same amount of energy and almost constant temperatures that reduce heat losses (Pomianowski et al. 2013). This technology is currently under active research due to its potential to increment the energy efficiency on buildings (Memon 2014; Entrop et al. 2011) with the majority of studies focusing on the integration of Phase Change Materials (PCM) into the construction elements of buildings such as walls, ceiling and floors (Pomianowski et al. 2013).
- *Thermo-chemical energy storage* uses reversible chemical reactions to store thermal energy in chemical bonds. Under the influence of a heat supply, a chemical compound is dissociated into its components which can be stored separately. When these components are put in contact the chemical compound is restored with a heat release. With this process, thermal energy can be stored with negligible losses since heat is not kept in sensible or latent form but as a chemical compound (N'Tsoukpoe et al. 2009). Applications based on this technology are currently not available due to high material costs, corrosive reactants and difficult temperature control. However, several efforts are being performed to overcome these obstacles, including the development of an Thermochemical accumulator demonstrated by the Solar Energy Research Centre (Sweden) and their industrial partner, ClimateWell AB (Kalaiselvam and Parameshwaran 2014).
- *Sensible heat storage* is based on the specific heat of a storage medium and has the lowest energy density requiring large volumes for its implementation. Despite these shortcomings, this technology is the most wide spread currently due to being relatively inexpensive, especially in applications with a low number of storage cycles as is the case of inter-seasonal heat storage (International Renewable Energy Agency and International Energy Agency 2013).

The concept of inter-seasonal heat storage is usually applied using sensible heat technology due to the limited amount of cycles (1 per year) that are achieved in the lifetime of the system and the relatively low construction costs. These systems, due to the large volume usually required, are typically placed in the ground and are commonly referred as Underground Thermal Energy Storage (UTES) systems. They are implemented in four main ways: aquifers, boreholes, caverns and water tanks/pits (Xu et al. 2014).

- *Aquifer thermal energy storage* (ATES) technology makes use of the permeable layer where the aquifer is present as storage medium and the water in it as the heat carrier. The process involves the extraction of water from the aquifer and its reinjection at a modified temperature (Seibt and Kabus 2006).
- *Borehole thermal energy storage* (BTES) typically consist of several vertical heat exchangers buried deep in the ground. Hot water is pumped in the summer through the heat exchangers elevating the temperature of the surrounding soil. A good example of the implementation of BTES is the Drake Landing Solar Community in Alberta, Canada (McClenahan et al. 2006) and the experimental study of a piled ground heat exchanger system for residential building applications performed at Sutton Bonington, UK (Wood 2009).
- *Cavern thermal energy storage* (CTES) makes use of either natural or manmade large caverns to store large amounts of hot water. An example of this technology is the recent relaunch of a solar energy test plant with seasonal storage in a cavern in Lyckebo Sweden (Hussein and Ivarsson 2013; Park et al. 2013).
- *Water tank/pit storage* makes use of artificial structures built in shallow regions of the ground. The construction costs in this last category are lower than the previous methods since the associated excavation expenses are considerably reduced, although expenses for insulation must be considered in order to minimize heat losses to the surface (Novo et al. 2010; Ochs et al. 2006; Xu et al. 2014).

1.1.2.1 International and national initiatives

Thermal storage development has received a boost from a number of international initiatives:

- The International Energy Agency (IEA) supports international energy technology research, development and knowledge transfer through technology initiatives. Some of these initiatives are directly related to the area of inter-seasonal thermal storage (International Energy Agency 2014a) for example: the Annex 7, Annex 17 and Annex 23 from the Energy Conservation through Energy Storage programme (IEA-ECES) (International Energy Agency 2014b); the Task 7, Task 32 and Task 45 from the Solar Heating and Cooling programme (IEA-SHC) (International Energy Agency 2014c); and the Annex IX from the District Heating and cooling programme (IEA-DHC) (International Energy Agency 2014d).
- The European Union through its Intelligent Energy Europe program have supported the widespread use of heat storage technologies by funding the projects such as PREHEAT (Policy reinforcement regarding heat storage technologies) (Ellehauge 2006).
- The International Renewable Energy Agency (IRENA) in collaboration with the International Energy Agency's Energy Technology Systems Analysis Programme (IEA-ETSAP) has published a set of 10 technology briefs that provide technical background information, analyses market potential and barriers and provides insights for policy makers on key types of renewable energy technology including thermal energy storage (International Renewable Energy Agency 2014).

Examples of national initiatives around the world in the area of UTES include the approval by the Canadian government of a national standard for the "Design and installation of earth energy systems" and the German Solarthermie2000 and Solarthermie2000plus programs in which pilot and demonstration projects of seasonal heat storage for district heating have been realized (Solarthermie2000plus 2014).

1.1.2.2 Private sector

In the private sector area, there are various companies that specialize in the UTES field. Some examples are:

- PlanEnergy is an independent advisory company based in Denmark. The firm advises in solar energy projects that include collective installations, seasonal storage and certification. It has planned, designed and consulted on the construction of a wide range of solar thermal and short-term seasonal heat storage plants in Denmark (PlanEnergi 2014).
- Ooms, a Dutch construction company, in collaboration with WTH and TipSpit, have developed Road Energy Systems that extract energy from asphalt concrete. The system exploits the heat absorbing capacity of asphalt concrete, which is enhanced by its black color. The thermal energy produced can be transported to an underground storage system and be used to cool buildings, houses and roads in summer and to heat them in winter (Ooms Civiel 2014).
- Icax is a company that specializes in the implementation of inter-seasonal heat storage with technologies such as ThermalBanks. This is a bank of earth used to store heat between seasons, similar to the pit stores mentioned earlier. Solar thermal energy is captured using a collection pipe network directly under the surface (e.g. black tarmac roads). The thermal energy is released in winter to heat buildings using methods such as under floor heating (ICAX 2014).

1.2 Research and knowledge opportunities

In Section 1.1.2 a review of literature related with the storage of thermal energy in general and of storage of thermal energy in soils in particular was presented, it was found that the main subject in the literature is related with the materials used to store the thermal energy (in order to minimize losses and facilitate transportation), with the capture and extraction of thermal energy from different process and sources (including solar) and with the delivery of thermal energy for specific applications. However, it was also found that the description of boundary interactions between soil and atmosphere tend to be simplified usually due to assumptions regarding the depth of storage of the thermal energy in the soil. For shallow applications these

interactions become more important and it does the specific conditions of the surface (or surfaces). Furthermore, when the source of thermal energy is related with the sun, the presence of objects that might impact the availability of solar energy (clouds, trees) become relevant in the study of the performance of buried geo-environmental thermal storage devices. It was also noted during the literature review in Section 1.1.2 that one of the areas of interest in recent research regarding the storage of thermal energy in soils is related with the use of shallow regions of the ground and the capture and recovery of sensible thermal energy through the year in order to minimize costs and broaden the applicability of a mature engineering field.

1.3 Aims & Objectives

The main aims of this study are:

i) identify the impact that relevant factors occurring on the soil surface have on the potential thermal energy available to be stored in the ground.

ii) develop a general transient three-dimensional theoretical framework represent the transient processes of storage and extraction of thermal energy from the ground that occur in heat exchange devices buried in the soil.

iii) develop a numerical solution of the above theoretical framework. This will be achieved via the finite element method for spatial discretization and a finite difference time-stepping method.

iv) measure key material properties where necessary.

v) offer insight on the effect that assumptions made regarding far-field (lower) boundaries have on the overall computational effort to simulate a such facilities.

vi) develop an analytical approach to estimate initial soil temperature profiles that can be used as input data for more comprehensive numerical models.

vii) compare and contrast 2D simplification of the field problem with a more comprehensive 3D model.

viii) provide general guidance on the design and efficiency of seasonal heat storage facilities.

1.4 Scope and limitations

In this thesis a numerical model is proposed to study the transient behaviour of buried engineering devices for storage and extraction of thermal energy in regions close to the soil surface. The model is constructed using the finite element method and is capable of solving the transient one-way coupled heat and moisture transfer equation in soil in 3D. The equations describing the movement of moisture are assumed to be independent of the temperature field, while the thermal properties of the domain are assumed to be a function of the moisture content field. The model takes into account the presence of heat exchange devices buried in the ground and the transport of heat within them and between them and the soil.

The main scope of the study is limited primarily to the interactions of thermal energy at the boundaries between the soil and the atmosphere and between the soil and buried heat exchangers and their impact on the amount of energy stored in the ground. The model is verified using experimental data reported by others (Carder et al. 2007).

Giving this scope, the main limitations of the model are summarized as follow:

- No mechanical deformations or chemical reactions are considered in the model.
- The model is applicable for unsaturated conditions. No saturated conditions or combination of saturated/unsaturated conditions are taken into account.
- No snow melting processes are considered, although coupled evaporative processes are taken into account.

1.5 Contents Summary

The division of the thesis and the summary of each Chapter is summarized as follows:

- Chapter 2 seeks to present targeted reviews of the main approaches used to estimate soil thermal properties, theoretical representation of solar collectors on highways and pavements, with special focus on the transfer of heat between horizontal pipes and soil, representation of heat transfer process at the soil surface, coupled heat and moisture transfer processes in the soil,

analytical and numerical methods used in the estimation of soil temperature profiles and the study of thermal devices buried in the ground.

- Chapter 3 presents the governing equations that describe the transfer of heat and mass in soil and the flow of heat within pipe systems. The key assumptions made in the development of these equations are also introduced. The main heat transfer approaches considered at the soil surface are described.
- Chapter 4 presents the numerical solution of the partial differential equations that describe the heat and moisture transfer within soils and the advection of heat by a fluid using the finite element method. The general numerical implementation of different kinds of boundary conditions is also presented. Since the particular method of discretization adopted allows changes in mesh refinement between time steps in transient simulations, an algorithm for the selection of elements based on the gradient of the independent variable (temperature, pressure head) is also presented.
- Chapter 5 presents experimental results reported by UK's Transport Research Laboratory (TRL) (Carder et al. 2007) who under the auspices of the British Highways Agency, performed an experimental study about the feasibility of implementing an inter-seasonal heat storage system aimed to provide maintenance to road surfaces by preventing the formation of frost that otherwise would be hazardous to road users. The results of the TRL work are used in this study to validate the numerical model proposed.
- Chapter 6 provides a summary of the information gathered in the literature about the experimental area discussed in Chapter 5. It presents the procedures followed for soil sampling (a site visit was undertaken by the author at the beginning of February 2012 in order to take samples of soil and observe the current state of the surface of the soil), the laboratory tests performed on the recovered samples and the results obtained.
- Chapter 7 presents the development of new 1d analytical solutions for the transient heat transfer equation. The equation is solved using ad-hoc developed equations for two main meteorological variables with relatively simple heat transfer coefficients. Results of a verification exercise to test the numerical model presented in Chapter 4 and the results of a validation test for

the analytical solution, using the experimental data from the test case presented in Chapter 5, are also shown.

- Chapter 8 shows 1D analyses of measured field data from soil columns to provide both partial validation of the model presented in Chapters 4 and to investigate methods of defining appropriate initial and boundary conditions. The following aspects are considered in detail: boundary conditions at the top of the domain, boundary conditions at the bottom of the domain, initial conditions, use of different sources of meteorological data, thermal energy stored in the domain, variation of thermal properties with moisture content.
- Chapter 9 shows the validation of the numerical model presented in Chapter 4 in 2D using the experimental measurements from the test case presented in Chapter 5. The main objectives of this chapter are to: assess the impact that shading cast by adjacent objects has on the thermal performance of an ground storage device; and propose and validate an algorithm in 2D to represent the operation of a ground inter seasonal heat storage device consisting of pipe heat exchangers.
- Chapter 10 shows the validation of the numerical model presented in Chapter 4 in 3D using the experimental measurements from the test case presented in Chapter 5. The main objectives of this chapter are: use results obtained in Chapter 8 and Chapter 9 regarding boundary conditions and shade levels on the road surface to build a numerical model in three dimensions, compare the results obtained from a three dimensional model with results obtained from a two dimensional model (Chapter 9) regarding thermal performance of the inter-seasonal heat storage device.
- Chapter 11 presents the overall conclusions of the study and makes suggestions for further work.
- Appendix A presents thermal properties of a fluid commonly used in thermal engineering applications: water-ethylene-glycol mixtures.
- Appendix B This explores the impact of varying fluid temperature and mean velocities on the convective heat transfer coefficient between the walls of a pipe and the fluid flowing in its interior.

1.6 References

Bobes-Jesus, V., Pascual-Muñoz, P., Castro-Fresno, D., and Rodriguez-Hernandez, J. [2013]. Asphalt Solar Collectors: A Literature Review. Applied Energy 102 (February): 962–970. doi:10.1016/j.apenergy.2012.08.050.

Carder, D. R., Barker, K. J., Hewitt, M. G., Ritter, D., and Kiff, A. [2007]. Performance of an Interseasonal Heat Transfer Facility for Collection, Storage and Re-Use of Solar Heat from the Road Surface. PPR302. Transport Research Laboratory.

Deng, S., Wang, R. Z., and Dai, Y. J. [2014]. How to Evaluate Performance of Net Zero Energy Building – A Literature Research. Energy 71 (July): 1–16. doi:10.1016/j.energy.2014.05.007.

Ellehauge, K. [2006]. Policy Reinforcement Regarding Heat Storage Technologies - Present State of the Support for Thermal Storage Technologies. WP2.

Entrop, A. G., Brouwers, H. J. H., and Reinders, A. H. M. E. [2011]. Experimental Research on the Use of Micro-Encapsulated Phase Change Materials to Store Solar Energy in Concrete Floors and to Save Energy in Dutch Houses. Solar Energy 85 (5): 1007–1020. doi:10.1016/j.solener.2011.02.017.

Hope, C. [2014]. Make Your Home More Energy Efficient to Help Fight Putin, Says Energy Secretary. [Online]. Available at: http://www.telegraph.co.uk/news/earth/energy/11162264/Make-your-home-more-energy-efficient-to-help-fight-Putin-says-Energy-secretary.html. [Accessed: 12-Jan-2015].

Hussein, W. and Ivarsson, E. [2013]. Solar Heating in Storvreta. Bachelors, Sweden: Uppsala University. http://uu.diva-portal.org/smash/record.jsf?searchId=1&pid=diva2:626749.

ICAX. [2014]. [Online]. Available at: http://www.icax.co.uk/thermal_energy_storage.html. [Accessed: 13-May-2014].

International Energy Agency. [2014a]. IEA - Energy Technology Initiatives. [Online]. Available at: http://www.iea.org/techinitiatives/. [Accessed: 12-May-2014].

International Energy Agency. [2014b]. IEA - Energy Conservation through Energy Storage. [Online]. Available at: http://www.iea-eces.org/. [Accessed: 12-May-2014].

International Energy Agency. [2014c]. IEA - Solar Heating and Cooling. [Online]. Available at: http://www.iea-shc.org/. [Accessed: 12-May-2014].

International Energy Agency. [2014d]. IEA - District Heating and Cooling. [Online]. Available at: http://www.iea-dhc.org/home.html. [Accessed: 12-May-2014].

International Renewable Energy Agency. [2014]. IRENA | Publications | Reports and Papers | IRENA-IEA-ETSAP Technology Briefs. [Online]. Available at: http://www.irena.org/menu/index.aspx?mnu=Subcat&PriMenuID=36&CatID=141&SubcatID=283. [Accessed: 12-May-2014].

International Renewable Energy Agency and International Energy Agency. [2013]. Thermal Energy Storage - Technology Brief E17. IRENA-IEA-ETSAP. http://www.irena.org/DocumentDownloads/Publications/IRENA-ETSAP%20Tech%20Brief%20E17%20Thermal%20Energy%20Storage.pdf.

Kalaiselvam, S. and Parameshwaran, R. [2014]. Thermochemical Energy Storage. In Thermal Energy Storage Technologies for Sustainability, edited by S. K. Parameshwaran, 57–64. Boston: Academic Press.

Kroll, J. A. and Ziegler, F. [2011]. The Use of Ground Heat Storages and Evacuated Tube Solar Collectors for Meeting the Annual Heating Demand of Family-Sized Houses. Solar Energy 85 (11): 2611–2621. doi:10.1016/j.solener.2011.08.001.

McClenahan, D., Gusdorf, J., Kokko, J., Thornton, J., and Wong, B. [2006]. Okotoks: Seasonal Storage of Sol Ar Energy for Space Heat in a New Community. In Proceedings of ACEEE 2006. Vol. 11. Pacific Grove: American Council for an Energy-Efficient Economy.

McNeil, M. A. and Letschert, V. E. [2007]. Future Air Conditioning Energy Consumption in Developing Countries and What Can Be Done about It: The Potential of Efficiency in the Residential Sector. In European Council for an Energy Efficient Economy Summer Study Proceedings. http://www.eceee.org/conference_proceedings/eceee/2007.

Memon, S. A. [2014]. Phase Change Materials Integrated in Building Walls: A State of the Art Review. Renewable and Sustainable Energy Reviews 31 (March): 870–906. doi:10.1016/j.rser.2013.12.042.

Morita, K. and Tago, M. [2000]. Operational Characteristics of the Gaia Snow-Melting System in Ninohe, Iwate, Japan. Geo-Heat Center 21 (4): 5–11.

Novo, A. V., Bayon, J. R., Castro-Fresno, D., and Rodriguez-Hernandez, J. [2010]. Review of Seasonal Heat Storage in Large Basins: Water Tanks and Gravel–water Pits. Applied Energy 87 (2): 390–397. doi:10.1016/j.apenergy.2009.06.033.

N'Tsoukpoe, K. E., Liu, H., Le Pierrès, N., and Luo, L. [2009]. A Review on Long-Term Sorption Solar Energy Storage. Renewable and Sustainable Energy Reviews 13 (9): 2385–2396. doi:10.1016/j.rser.2009.05.008.

Ochs, F., Heidemann, W., Müller-Steinhagen, H., and Koch, H. [2006]. Soil-Water Pit Heat Store with Direct Charging System. In . Pomona, NJ, USA, 31 May - 2 June 2006.

Ooms Civiel. [2014]. Road Energy System® | Ooms Civiel. [Online]. Available at: http://www.ooms.nl/en/7/301/road_energy_system.aspx. [Accessed: 12-May-2014].

Park, D., Kim, H.-M., Ryu, D.-W., Choi, B.-H., Sunwoo, C., and Han, K.-C. [2013]. The Effect of Aspect Ratio on the Thermal Stratification and Heat Loss in Rock Caverns for Underground Thermal Energy Storage. International Journal of Rock Mechanics and Mining Sciences 64 (December): 201–209. doi:10.1016/j.ijrmms.2013.09.004.

PlanEnergi. [2014]. Solar Heating and Seasonal Heat Storage - PlanEnergi. [Online]. Available at: http://www.planenergi.eu/solar-heating-and-seasonal-heat-storage.html. [Accessed: 12-May-2014].

Pomianowski, M., Heiselberg, P., and Zhang, Y. [2013]. Review of Thermal Energy Storage Technologies Based on PCM Application in Buildings. Energy and Buildings 67: 56–69. doi:10.1016/j.enbuild.2013.08.006.

Raupach, M. R., Davis, S. J., Peters, G. P., Andrew, R. M., Canadell, J. G., Ciais, P., Friedlingstein, P., Jotzo, F., van Vuuren, D. P., and Le Quéré, C. [2014]. Sharing a Quota on Cumulative Carbon Emissions. Nature Climate Change 4 (10): 873–879. doi:10.1038/nclimate2384.

Seibt, P. and Kabus, F. [2006]. Aquifer Thermal Energy Storage: Projects Implemented in Germany. In . Pomona, NJ, USA, 31 May - 2 June 2006.

Sivak, M. [2013]. Will AC Put a Chill on the Global Energy Supply? American Scientist 100 (5): 330. doi:10.1511/2013.104.330.

Solarthermie2000plus. [2014]. [Online]. Available at: http://www.solarthermie2000plus.de/. [Accessed: 13-May-2014].

U.S. Department of Defense. [2013]. Clean Energy Tied to National Security, Official Says. [Online]. Available at: http://www.defense.gov/news/newsarticle.aspx?id=119237. [Accessed: 12-Jan-2015].

Wood, C. [2009]. Investigations into Novel Ground Source Heat Pumps. PhD Thesis, Dept. for the Built Environment: University of Nottingham.

Xu, J., Wang, R. Z., and Li, Y. [2014]. A Review of Available Technologies for Seasonal Thermal Energy Storage. Solar Energy 103: 610–638. doi:10.1016/j.solener.2013.06.006.

Chapter 2 Literature review

2.1 Introduction

Many books and scientific publications have been presented elsewhere dealing with the topics of heat transfer, coupled heat and moisture transfer and thermal and hydraulic properties of soils. In particular, notable contributions have been provided by: Sauer and Horton (2005), Hillel (2003), Arya (1988) and Koorevar (1983) who discuss in detail the process of thermal energy transfer in soil and the estimation of temperature profiles assuming no moisture movement conditions. In addition, Deb et al. (2011), Vasco (2010), Grifoll et al. (2005) Fredlund and Rahardjo (1993), Winterkorn (1962), de Vries (1958) and Philip and de Vries (1957) provide useful contributions on the transport of moisture under non-isothermal conditions. Regarding the study of thermal and hydraulic properties of soils the following references are recommended: Reeves et al. (2006), Hillel (2005), Abu-Hamdeh (2003), Rees et al. (2000), Pielke (1984), Farouki (1981) and de Vries (1963). All provide thorough reviews on thermal properties of soils as a function of moisture content and/or degree of saturation. Whereas, Grant (2005), Maidment (1993), Haverkamp et al. (1998) and Fredlund and Rahardjo (1993) provide the fundamental theoretical framework for moisture movement in unsaturated soils. Subsequently, this Chapter seeks to present targeted reviews of the following: i) the main approaches used to estimate soil thermal properties, ii) theoretical representation of solar collectors on highways and pavements, with special focus on the transfer of heat between horizontal pipes and soil, iii) representation of heat transfer process at the soil surface; iv) coupled heat and moisture transfer processes in soils, and v) analytical and numerical methods used in the estimation of soil temperature profiles and the study of thermal devices buried in the ground for thermal energy storage and extraction.

2.2 Heat Transfer in Soils

Thermal energy in a porous medium may be transferred by four processes; heat conduction, latent heat transferred by vapour movement, heat of wetting transfer, and heat convection.

- Heat conduction is the process in which heat is transferred within a solid. It is defined as the amount of heat passing through a unit cross sectional area in a unit of time under a unit temperature gradient applied in the direction of the heat flow.
- Latent heat transport arises when part of the moisture available in the soil undergoes a phase change due to thermal gradients. Usually it is small in magnitude but may have certain relevance in some cases (e.g. for vapour-dominated flow mechanisms) like in arid and semi-arid regions with rapidly drying soils (Feddes et al. 1988).
- Heat of wetting: is heat generated when dry soil is mixed with water and is only applicable to clayey materials which have a large value for the integral heat of wetting (Kay and Groenevelt 1974).
- Heat convection is related to the movement of moisture within the soil, without phase change, induced either by thermal, pressure or mechanical gradients. It is usually very small and may be neglected safely in the majority of cases (De Vries 1958), except under very humid conditions.

In general, heat conduction tends to dominate the heat transfer process within soils while the relative importance of the other processes vary depending on the specific conditions of the problem and how relevant the transport of moisture is for its physical description. In some cases it can be reasonable to assume that the amount of moisture being transferred in the domain has a negligible impact on the thermal distribution and heat transfer in the soil (Grant 2005; Romero et al. 2001; Nobre and Thomson 1993). Further discussion on this topic is provided in Section 2.5.2.

Quantities critical in the description of heat transfer in soils are their density and specific heat capacity. These quantities and the thermal conductivity depend on the relative presence of constituents (i.e. solid, liquid and gaseous phases) within the soil. This defines the physical means by which the process of heat transfer in soils is coupled to moisture content (or saturation). The following sections present common relations to estimate the thermal conductivity and specific heat capacity of soils. Relationships for soil density can be found in basic literature sources (Fredlund and Rahardjo 1993).

2.2.1 Thermal conductivity

Reeves et al. (2006), Hilllel (2005), Abu-Hamdeh (2003), Rees et al. (2000), Pielke (1984) Farouki (1981) offer reviews and descriptions on the main approaches to estimate thermal conductivity in soils. These authors in general agree that heat conduction is the process that dominates the transport of thermal energy within soils and is commonly used in thermal energy balances at the soil surface to represent thermal energy transferred between the atmosphere and the ground. Thermal conductivity occurs in all the soil constituents including water and air although the physical process and relative importance may vary compared with the thermal conduction through soil solids. Each constituent in the soil (in basic approaches considered to be composed only of solid particles, water and air) have a thermal conductivity that may depend on the temperature of the constituent. The common practice is to define a bulk thermal conductivity by averaging the thermal conductivities of the mixed elements present in the soil. In this Section only the most common approaches to perform this average are summarized while for a concise review the reader is directed to Rees et al. (2000).

The most common methods to calculate the thermal conductivity are mathematically similar to calculating an electrical conductivity when more than one resistance are present. In this context the value of thermal conductivity depends on the arrangement of the constituents besides their relative presence. Three scenarios can be summarized following this idea:

When the constituents (i.e. the solid, liquid and gaseous phases of the soil) can be assumed to have a distribution parallel to the flow of heat, the soil bulk thermal conductivity can be expressed as a weighted arithmetic mean:

$$\lambda_b = \sum_i \chi_i \lambda_i \qquad (2\text{-}1)$$

where χ_i and λ_i (W/mK) are the volume fraction and thermal conductivity of constituent *i* and λ_b is the resulting average bulk thermal conductivity of soil. The volume fraction of constituent *i* is given by:

$$\chi_i = \frac{V_i}{V} \qquad (2\text{-}2)$$

where V_i (m^3) is the volume occupied by constituent *i* and V (m^3) is the total volume of soil.

When the constituents can be assumed to follow a series distribution respect to the direction of heat flow, the thermal conductivity of the soil is given as a harmonic mean:

$$\lambda_b = \frac{\prod_i \lambda_i}{\sum_i \chi_i \lambda_i} \tag{2-3}$$

where Π and Σ are symbols to represent product and sum of multiple terms.

Woodside and Messmer (1961) have found that equations (2-1) and (2-3) tend to over-estimate and under-estimate, respectively, the thermal conductivity of the soil. These deviations could be explained from the fact that the constituents in the soil are more likely to be random-like distributed rather than following a perfect parallel or series distribution, although they can offer a reasonable first approximation. Woodside and Messmer also provided an alternative approach that was found to offer intermediate results between the arithmetic and geometric approaches.

$$\lambda_b = \prod \lambda_i^{\chi_i} \tag{2-4}$$

2.2.2 Specific heat capacity

In general the specific heat capacity at constant pressure of a material, c_p (J/kgK), is defined as the amount of thermal energy required to change by 1 K one unit of mass of the material (Çengel 2003). This quantity is required when non-steady calculations need to be performed. A related quantity is the volumetric heat capacity at constant pressure, C_p (J/m^3K), defined as the amount of thermal energy required to change 1 K one unit of volume of material (Çengel 2003).

Hillel (2005), Garrat (1994) and Fredlund and Rahardjo (1993) offer an expression to estimate the soil volumetric heat capacity at constant pressure from the specific heat capacities of the soil constituents weighted by their corresponding densities, it can be expressed as (assuming only solid particles, water an air are present in the soil):

$$C_{p,b} = \chi_s \rho_s c_{p,s} + \chi_w \rho_w c_{p,w} + \chi_a \rho_a c_{p,a} \tag{2-5}$$

where χ, ρ and c_p represent volume fractions (equation (2-2)), density (kg/m^3) and specific heat capacity (J/kgK) respectively; and the sub indices *s*, *w* and *a* stand for solid, water and air respectively. It can be seen that the volumetric heat capacity as defined by (2-5) is dependent on the degree of saturation of the soil by the inclusion of the volume fraction of water χ_w.

Alternatively, if the bulk specific heat capacity can be obtained by experimental means using for example the method suggested by the American Society for Testing and Materials (2008) then the volumetric heat capacity can be calculated as:

$$C_{p,b} = \rho_b c_{p,b} \tag{2-6}$$

where ρ_b (kg/m^3) is the soil bulk density and $c_{p,b}$ (J/kgK) is the soil bulk specific heat capacity.

2.3 Solar collectors for Highways & Pavements

This Section presents the heat transfer process between heat pipes embedded in highways and pavements. A general overview of the field of thermal energy storage (TES) and in particular of inter-seasonal thermal energy storage is given in the introduction of this study. It was mentioned that when the soil is used as storage medium it is commonly referred as Underground Thermal Energy Storage (UTES) (Xu et al. 2014) a sub-category of which (in terms of implementation) is Borehole Thermal Energy Storage (BTES) with excavation depths in the order of ~100 m. Wood et al. (2009) and Nabi and Al-Khoury (2012) offer good examples of the implementation of this category.

An additional way of implementing UTES is by using horizontal heat exchangers at shallower depths. Kupiec et al. (2015) presents a 1D mathematical model to describe the operation of a horizontal heat exchanger at a depth of 1.14 m. Their results were validated using experimental measurements obtained by Wu et al. (2010) who performed experimental measurements and numerical simulations of a horizontal slinky ground-source heat exchanger under UK weather conditions.

Regarding the applications of horizontal heat exchangers Kroll and Ziegler (2011) have propose to use them surrounded by an insulation layer as a mean to satisfy the thermal energy needs of small residential homes. In the field of building research,

Cogedo et al. (2012) compared the impact of different pipe distributions in the performance of horizontal ground heat exchangers finding that slinky configurations offer advantages over traditional straight arrangements. Liu et al. (2011) pointed out through numerical and experimental investigations the impact that the heat island effect has on the average soil temperature and moisture content in shallow regions of the soil (<3m) covered mostly by concrete and pavements surfaces. Santamouris (2013) proposed passive and active measures to counterbalance this phenomenon including the use of horizontal heat exchanger located under paved surfaces to harvest thermal energy.

While the use of passive techniques (e.g. modification of albedo and emissivity) to cool down paved surfaces are effective, active techniques offer the possibility to harvest the thermal energy that can be used for other applications. Bobes-Jesus et al. (2013) have provided an extensive review on the main findings of the existing research on asphalt solar collectors identifying the main heat transfer mechanisms and parameters involved in the solar energy collection process and summarizing the main different methodologies employed by other authors to study asphalt.

Zhou et al. (2015) carried out a small-scale pilot project to study the effectiveness of a pavement solar energy system, using BTES. Their system operated 24 h a day in summer (69 days) and winter (104 days). Under these settings they conclude that although the amount of electrical energy required to circulate the water through the system was minimal compared the thermal energy harvested, the thermal energy stored in summer was smaller than the extracted in winter reducing the soil temperature in the long term. They suggested that the system, instead of a continuous 24h operation, should be activated in winter only when freezing conditions appear on the surface.

2.3.1 Energy transfer between a solid and an embedded pipe with fluid flow.

Liquid or gas flow through pipes or ducts is commonly used in heating and cooling applications. The fluid in such applications is forced to flow by a fan or pump through a tube that is sufficiently long to accomplish the desired heat transfer (Çengel 2003). The required pumping power is determined by the geometric characteristics of the pipe and by the physical properties of the fluid being pumped

(e.g. viscosity). General physical descriptions of internal flow can be found in engineering textbooks such as Çengel (2003) and Roberson and Crowe (1989).

A directly related variable with the process of heat transfer in pipes is the heat convection coefficient that defines the amount of thermal energy that is transferred between the fluid inside the pipes and the surrounding medium (Çengel 2003). For discussions regarding the application of the theory of fluid flow in pipes in real ground heat exchangers the reader is directed towards Svec (1990; 1983) for water based heat exchangers and towards Krarti (1996) for air based heat exchangers.

2.4 Energy Balance at the soil/atmosphere interface

A critical aspect of the process of inter-seasonal heat storage in soils is the analysis of the energy balance at the surface of the soil. This boundary condition determines to a great extent how much thermal energy is transferred into the soil and becomes available for any thermal engineering application. It also determines how much energy will be lost between seasons to the atmosphere until the stored thermal energy is required.

According to Sauer and Horton (2005) the thermal energy balance at the soil surface can be expressed as:

$$q_G = q_S + q_I + q_C + q_E \tag{2-7}$$

where q_G (W/m^2) is the energy transferred into the ground by thermal conduction. As mentioned in Section 2.2.1 thermal conduction is the main process by which thermal energy is transferred into the soil and its magnitude is defined by the balance of the other four heat transfer processes: solar radiation (q_S) (W/m^2), infrared radiation (q_I) (W/m^2), convection (q_C) (W/m^2) and evaporation (q_E) (W/m^2).

The solar radiation term is defined by Duffie and Beckman (2006) as:

$$q_S = R\left(1-\alpha_S\right) \tag{2-8}$$

where α_S is the solar albedo of the soil surface and R (W/m^2) is the global radiation (a measurement commonly reported by meteorological stations (National Meteorological Library and Archive 2014)) composed of direct and diffuse solar radiation. The albedo is a dimensionless number that defines the ratio of reflected

radiation to incident radiation and is a function of the optical properties of the surface (mainly the colour and roughness) (Çengel 2003).

Duffie and Beckman (2006) suggest that the soil can be considered as a relatively small surface enclosed by a larger surface, the sky, and offer an expression for the infrared radiation in this scenario:

$$q_I = \varepsilon_{ss}\sigma(T_{\mathrm{sky,K}}^4 - T_{ss,\mathrm{K}}^4) \tag{2-9}$$

where ε_{ss} is the infrared emissivity of the soil surface and σ is the Stefan-Boltzmann constant equal to $5.6704\text{x}10^{-8}\text{W/m}^2\text{K}^4$. $T_{ss,K}$ (K) is the absolute temperature of the soil surface. $T_{sky,K}$ (K) is the theoretical absolute temperature of the sky considered as a black surface.

Iziomon et al. (2003) propose the following relationship to relate the absolute sky temperature to the absolute air temperature:

$$T_{sky,\mathrm{K}}^4 = \varepsilon_{sky} T_{a,\mathrm{K}}^4 \tag{2-10}$$

where ε_{sky} is the infrared emissivity of the theoretical atmospheric surface and $T_{a,K}$ (K) is the absolute temperature of air. A summary of different expressions proposed for ε_{sky} are presented in Section 2.4.3.

Penman (1948) and Edinger (1968) have shown that thermal convection and evaporation share a similar formulation. Thermal convection is driven by the temperature difference between the air above ground and the temperature of the soil surface, while evaporation is driven by the gradient of vapour pressures between the atmospheric air and soil surface. They can be expressed as:

$$q_C = h_C\left(T_a - T_{ss}\right) \tag{2-11}$$

$$q_E = h_E\left(e_{a,sat} - e_{ss}\right) \tag{2-12}$$

where h_C ($\text{W/m}^2\text{K}$) and h_E ($\text{W/m}^2\text{kPa}$) are convective and evaporative heat transfer coefficients respectively, $e_{a,sat}$ (kPa) is the atmospheric saturation vapour pressure and e_{ss} (kPa) is the water vapour pressure at the saturated soil surface. The particular formulation of these coefficients depends on the assumptions made for the

atmospheric boundary layer. Two possible formulations are presented in Section 2.4.2.

2.4.1 Influence of surface cover

The characteristics of the soil surface impacts certain aspects of the heat transfer process between the soil and the atmosphere. The optical properties of the surface influence the solar and infrared heat transfers while its roughness and moisture content influence convective and evaporative heat transfers. In addition, all these processes are influenced when the presence of vegetation is important. Three different surface scenarios relevant for the problem studied in this work are provided in this Section. These are: bare soil, soil covered by asphalt and soil covered with vegetation.

2.4.1.1 Bare soil

Several authors including Bitteli (2008), Hillel (2003), Alvenas and Jansson (1997), Kondo et al. (1990) and Penman (1948) have studied the heat transfer process between bare soils and the atmosphere. When the soil is bare only the characteristics of the material that compose the soil play an important role in the surface heat balance formulation, particularly its optical properties, roughness and moisture content. The latter being of special interest when evaporative processes or coupled interactions of heat and moisture transfer are considered.

Garrat (1994) has provided values for the solar and infrared optical properties used in equations (2-8) and equation (2-9) for wet and dry surface conditions. The solar albedo for a soil composed of clay is given by:

$$\alpha_S = 0.20 - 0.35 \quad (\text{dry clay}) \tag{2-13}$$

$$\alpha_S = 0.10 - 0.20 \quad (\text{wet clay}) \tag{2-14}$$

Herb et al. (2008) has offered a similar value:

$$\alpha_S = 0.15 \tag{2-15}$$

For infrared optical properties Garrat (1994) and Herb et al. (2008) have proposed:

$$\varepsilon_{ss} = 0.95 \quad (\text{dry clay}) \tag{2-16}$$

$$\varepsilon_{ss} = 0.97 \quad \text{(wet clay)} \tag{2-17}$$

In the case of the evaporative heat transfer process a typical method is the one proposed by Penman (1948). Penman offered an analysis that treated the soil surface as an open water body (saturated conditions). This method was chosen since it has the advantage of providing a surface defined by readily determined properties. Philip and de Vries (1957) proposed a modification for this method that take into account the possibility of unsaturated soil surface conditions. They modified the term corresponding to the surface vapour pressure (assumed saturated by Penman) in the following way:

$$e_{ss} = \exp\left(-\frac{h_{ss} g}{R_w T_{ss,\mathrm{K}}}\right) e_{ss,sat}(T_{ss}) \tag{2-18}$$

where h_{ss} (m) is the pressure head at the soil surface, g (9.81 m/s^2) is the acceleration due to gravity, R_w (461.5 J/kgK) is the gas constant for water vapour, $e_{ss,sat}$ (kPa) is the saturation vapour pressure at the soil surface and T_{ss} (˚C) and $T_{ss,K}$ (K) are the temperature and absolute temperature of the soil surface. In relation to equation (2-18) Alvenäs and Jansson (1997) notice that when the surface is unsaturated it is necessary to estimate the amount of moisture available for evaporation. This is calculated under the assumption that when an earlier saturated soil dries, the free water in larger pores evaporates first and the remaining water is retained mainly in smaller pores by strong capillary forces and the vapour pressure of the air in equilibrium with the pore water will therefore be lower than in the air close to a free water surface. Boast and Simmons (2005) also point out the importance to estimate the availability of moisture at the soil surface in relation to the evaporative heat transfer process.

Mahfouf and Noilhan (1991) have offered a comprehensive review of alternative methods to estimate the surface moisture availability or vapour pressure at the soil surface known as the α-method and the β-method. The α-method is given by:

$$e_{ss} = \alpha e_{ss,sat}(T_{ss}) \tag{2-19}$$

where the coefficient α represents the relative humidity of air at the soil surface. In the β-method the whole process of evaporation is described from the water level to the atmosphere. In this method equation (2-12) can be expressed as:

$$q_E = h_E \beta \left(e_a - e_{ss} \right) \tag{2-20}$$

Both coefficients α and β are functions of soil water content that compensate for the changes in soil surface humidity during drying.

Besides the moisture availability at the soil surface, other parameters influencing the level of evaporation and convection are the convective and evaporative heat transfer coefficients h_C and h_E used in equations (2-11) and (2-12) (specific expressions for these are provided in this Section). Garrat (1994) provides a theoretical formulation that shows how these parameters are a function of the dynamic roughness of the soil z_0 (m), the momentum roughness, z_{0m} (m) and the roughness lengths for sensible heat and vapour transfer, z_{0T} (m) and z_{0v} (m). The dynamic roughness z_0 was explained as a measure of the irregularities of the surface while the momentum roughness, z_{0m}, represented the height at which the wind speed can be considered to be zero assuming that the wind follows a logarithmic profile with height. Similarly, the roughness lengths for sensible heat z_{0T} and vapour transfer z_{0v} are the heights where their concentrations assume their surface value. According to Brutsaert (1982) z_0 is theoretically independent of the air flow above the soil surface, and is only a function of its geometrical nature – i.e. the arrangement and size of the particles at the surface (roughness).

Garrat (1994) offers useful values of surface roughness lengths for a range of natural surfaces. For bare soils it is suggested that:

$$z_0 = 0.001 - 0.01 \tag{2-21}$$

Garrat (1994) mentions that while the value of z_{0m} depends on the conditions at the lower atmospheric boundary layer and its interaction with the surface roughness, for relatively rough surfaces (most of earth's surfaces been considered in this category including bare soil surfaces) the momentum roughness can be assumed equal to the surface roughness:

$$z_{0m} = z_0 \tag{2-22}$$

With regards to the roughness lengths for sensible heat and vapour transfer, z_{0T} and z_{0v} the ASCE Hydrology Handbook (1996) suggest that, for most agricultural surfaces, their values can be considered to be proportional to z_{0m}:

$$z_{0T} = z_{0v} = 0.1 z_{0m} \tag{2-23}$$

This is a value that is in between those corresponding to smooth surfaces and permeable-rough (vegetated) surfaces. This value agrees with measurements of Kubota and Sugita (1994) who performed a series of experiments over a pasture field during a growing season and show that the scalar roughness for sensible heat flux may vary over the range of 10^{-1} to 10^{-7} m both diurnally and seasonally.

2.4.1.2 Pavement/bituminous cover

Jansson et al. (2006) provide solar optical properties for a paved surface (wet and dry). The solar albedo used by them is given by:

$$\alpha_S = 0.1 \quad (\text{dry pavement}) \tag{2-24}$$

$$\alpha_S = 0.10 – 0.20 \quad (\text{wet pavement}) \tag{2-25}$$

Herb et al. (2008) offer similar values (although without specifying if the surface is wet or dry):

$$\alpha_S = 0.12 \tag{2-26}$$

In relation with infrared optical properties Jansson et al. (2006) treat the paved surface as perfect black body:

$$\varepsilon_{ss} = 1 \tag{2-27}$$

while Herb et al. (2008) offer a slightly lower value:

$$\varepsilon_{ss} = 0.94 \tag{2-28}$$

Regarding the vapour pressure at the paved surface Herb et al. (2008) suggests that it can be considered impervious implying that there is no infiltration and neglecting evaporation except during rainfall events during which the surface is assumed to be saturated. Jansson et al. (2006) in the other hand, consider the asphalt as porous with a moisture content of 5 %. Scholz and Grabowiecki (2007) state that the way in

which the evaporation from the pavement should be addressed depends on the type of pavement (impermeable, porous or permeable pavements) and even for porous pavements, the level of evaporation will depend on the state of the surface since the pores are known to clog with time.

Chen et al. (1999) provide values for the aerodynamic characteristics of pavements. According to them the momentum roughness (z_{0m}) and heat roughness (z_{0T}) are given by:

$$z_{0m} = 5\text{x}10^{-4} \tag{2-29}$$

$$z_{0T} = 1\text{x}10^{-4} \tag{2-30}$$

2.4.1.3 Soil with vegetation cover (grass, tall grass, crops)

This subsection deals with the scenario of a soil surface covered partially by vegetation and is based on the work of Herb et al. (2008). They developed a model to predict temperatures for vegetated and impervious surfaces based on the works of Deardorff (1978) and Best (1998). Deardorff (1978) assumes the presence of a single layer of vegetation with negligible heat capacity on top of the soil. The density of the cover is characterized by a single quantity ν ($0 \leq \nu \leq 1$) which is an area average shielding factor associated with the degree to which the foliage prevents solar radiation from reaching the soil surface. If ν=0 it implies that the soil is completely exposed with no vegetation cover while if ν=1 it means that the soil is completely covered by vegetation. It is obvious that ν is a function of the type of vegetation present on top of the soil.

Geiger (1950) offers estimates for ν for different plant types based on the measures of Angstrom (1925). The measurements performed by Geiger (1950) and Angstrom (1925) imply that the vegetation density (and the amount of solar radiation that reaches the ground) varies seasonally. This is expected from the natural process of seasonal grow and decay (or sow and harvest) of most types of vegetation.

Vogel et al. (1995) has compared the model proposed by Deardorff (1978) with other models that estimate the heat transfer processes between the soil and the atmosphere with the presence of a canopy layer. For example, the estimation of latent heat flux offered by Deardorff (1978) is comparable with the estimates obtained with other

relatively simpler models (e.g. Penman-Monteith's model (Thom et al. 1975)). However, the advantage of the model proposed by Deardorff (1978) relies on the fact that it takes into account the radiative transfers (solar and infrared) and turbulent transfers of heat and moisture between the vegetation canopy-soil-atmosphere system and the thermal energy transferred to the ground by conduction. Although it does it at the expense of requiring more details regarding the structure and properties of the vegetation including the temperature and humidity of the air between the soil surface and canopy cover.

Best (1998) proposes an alternative model based on Deardorff (1978) that neglects the turbulent heat transfer interactions between the soil surface and the canopy cover for a relatively dense vegetation. With this assumption Best (1998) simplifies the model proposed by Deardorff (1978) since the temperature and humidity of the air between the soil surface and the canopy cover are no longer required. Another difference is that while Deardorff (1978) neglects the heat capacity of the canopy layer, Best (1998) does not, although he assumes that it is small. Herb et al. (2008), using both models, retains the simplifications introduced by Best (1998) but neglects the heat capacity of the canopy layer as suggested by Deardorff (1978). The model proposed by Herb et al. (2008) is composed of two energy balance equations, one for the canopy cover and one for the soil surface. The equation for the canopy cover is given by:

$$\begin{aligned}&(1-\alpha_c)\nu R+\nu\sigma\left(\varepsilon_{ss}\varepsilon_{sky}T_{\mathrm{a,K}}^4-2\varepsilon_c T_{c,\mathrm{K}}^4+\varepsilon_{ss}T_{ss,\mathrm{K}}^4\right)\\&+h_{E,\mathrm{c}}\left(e_a-e_{\mathrm{c},sat}(\mathrm{T}_v)\right)+h_{C,c}\left(T_a-T_c\right)=0\end{aligned} \tag{2-31}$$

where α_c, ε_c, T_c (˚C) and $T_{c,K}$ (K) are the solar albedo, infrared emissivity, temperature and absolute temperature of the canopy cover respectively. h_{Cc} (W/m^{2}K) and h_{Ec} (W/m^{2}kPa) are the convective and evaporative heat transfer coefficients between the canopy cover and the atmosphere. The convective and evaporative interactions between the canopy layer and the atmosphere are assumed to be turbulent (the expression for these coefficients is presented in the next Section) and inversely proportional to an aerodynamic resistance r_a (s/m), similarly to the coefficients corresponding to bare soil and pavement formulations, and to a stomata resistance r_s (s/m). Herb et al. (2008) provided expressions for these resistances:

$$r_a = \frac{1}{c_f u_s} \tag{2-32}$$

$$r_s = 200\left(\frac{R_{max}}{R + 0.03R_{max}} + \left(\frac{\theta_{wp}}{\theta_w} \right)^2 \right) \tag{2-33}$$

where c_f is a transfer coefficient, u_s (m/s) is wind speed, R_{max} is the maximum noon solar radiation that can be achieved, θ_w is the soil moisture content and θ_{wp} is the wilting point moisture content. c_f is given by:

$$c_f = 0.01\left(1 + \frac{0.3}{u_s} \right) \tag{2-34}$$

According to Deardorff (1978), the stomata resistance given by (2-33) takes into account the fact that many types of leaves transpire only from the underside and that older leaves transpire less than newer ones.

The balance equation for the soil surface is given by:

$$\begin{aligned} -\lambda_b \frac{dT_{ss}}{dx} = {} & (1-\alpha_S)(1-\nu) R \\ & + \sigma \varepsilon_{ss} \left[(1-\nu) \varepsilon_{sky} T_{a,\mathrm{K}}^4 - T_{ss,\mathrm{K}}^4 \right] + \nu \varepsilon_c \sigma T_{c,\mathrm{K}}^4 \\ & + (1 - C_e \nu) \left[h_E (e_a - e_{ss}) + h_C (T_a - T_{ss}) \right] \end{aligned} \tag{2-35}$$

where C_e is a constant that establishes the level of soil evaporation for fully dense canopies, e.g. setting $C_e < 1$ gives non-zero soil evaporation for the full canopy case. Since equation (2-31) is not linear with T_c it can be solved using Newton's method as suggested by Deardorff (1978). The calculated canopy temperature can then be used to calculate the ground surface heat flux using equation (2-35).

2.4.2 Convective and evaporative coefficients under turbulent and non-turbulent conditions

This Section introduces the formulation of the convective and evaporative heat transfer coefficients used in equations (2-11) and equation (2-12).

The coefficients are developed for three of the main approaches commonly found in the literature: turbulent atmospheric conditions, non-turbulent conditions and evaporation and convection through a layer of vegetation. For other coefficients,

Sartori (2000) provides a review of typical equations used for the calculation of the evaporation rate from free water surfaces, as discussed before this is a common approach that can be modified to suit unsaturated soil conditions.

The turbulent approach is used by Jansson (2012) to describe evaporation and convection from bare soils in the development of the model *CoupModel*. A model that simulates soil water and heat processes in many types of soils including bare soils or soils covered by vegetation. This approach is based on the theory of atmospheric boundary layer and is applicable when the rates of transfer and mixing are several orders of magnitude greater than the rate of molecular diffusion (Garratt 1994). Under these conditions the convective and evaporative heat transfer coefficients are defined as:

$$h_C = \frac{\rho_a c_{p,a}}{r_a} \tag{2-36}$$

$$h_E = \frac{\rho_a c_{p,a}}{r_a \gamma} \tag{2-37}$$

where ρ_a (kg/m^3) and $c_{p,a}$ (J/kgK) are the density and specific heat capacity of air, γ (kPa/K) is the psychrometric constant and r_a (s/m) is the aerodynamic resistance of the soil surface and is inversely proportional to the wind speed. Beljaars and Holtslag (1991) offer the following expression for r_a:

$$r_a = \frac{1}{\kappa^2 u_s}\left[\ln\left(\frac{z_u}{z_{0m}}\right) - \Psi_m\left(\frac{z_u}{L_{MO}}\right) + \Psi_m\left(\frac{z_{0m}}{L_{MO}}\right)\right] \left[\ln\left(\frac{z_T}{z_{0T}}\right) - \Psi_T\left(\frac{z_T}{L_{MO}}\right) + \Psi_T\left(\frac{z_{0T}}{L_{MO}}\right)\right] \tag{2-38}$$

where κ is the Von Karman constant, a dimensionless number used in the description of the logarithmic velocity profile of a turbulent fluid flow near a boundary with no-slip condition. Its value is commonly accepted to be 0.41 (Garratt 1994), z_u (m) and z_T (m) are the reference height at which the measurements of wind speed and temperature are performed respectively. L_{MO} (m) is the Monin-Obukhov length and is used to describe the effects of buoyancy on turbulent flows, particularly in the lower tenth of the atmospheric boundary layer. According to Garrat (1994) it is

usually obtained by an iterative process from its relation with the bulk Richardson number, a dimensionless number in meteorology relating vertical stability and vertical shear. The empirical stability functions Ψ_m and Ψ_T are a measure of the deviation of the atmospheric wind and temperature profile from the standard logarithmic law. However, Garrat states that measurements over low-roughness surfaces (e.g. short grass, bare soil, water) are consistent with the logarithmic law and such deviations can be neglected. In this case, equation (2-38) can be expressed as:

$$r_a = \frac{1}{\kappa^2 u_s} \ln\left(\frac{z_u}{z_{0m}}\right) \ln\left(\frac{z_T}{z_{0T}}\right) \tag{2-39}$$

Herb et al. (2008), Adams et al. (1990) and Ryan et al. (1974) adopt a non-turbulent approach. The term "non-turbulent" is used in this study purposely to contrast with the previous presented model developed for turbulent atmospheric conditions. The non-turbulent approach is characterized by the inclusion of terms that take into account natural convective processes on the soil surface that are neglected in turbulent scenarios. Under these conditions Herb et al. (2008) citing the work of Ryan et al. (1974), propose the following expressions for the convective and evaporative heat transfer coefficients:

$$h_C = \rho_a c_{p,a} (C_{fc} C_{sh} u_s + C_{nc} \Delta\theta_v^{0.33}) \tag{2-40}$$

$$h_E = \rho_a L_V (C_{fc} C_{sh} u_s + C_{nc} \Delta\theta_v^{0.33}) \tag{2-41}$$

where L_v (J/kg) is the latent heat of evaporation, C_{fc}, C_{nc} (m/sK$^{1/3}$) and C_{sh} are coefficients that weight the contribution of forced convection, natural convection and sheltering respectively and take value between 0 and 1, $\Delta\theta_v$ (K) is the difference in virtual temperature between the air and the soil surface.

Adams et al. (1990) showed that equation (2-41) tends to over predict evaporation by about 15–25% and stated that "most researchers have found that pure addition of forced and free convection over predicts evaporation". According to Satori (2000), a comparison between the Reynolds and Grashoff numbers is commonly used to decide whether forced or free convection should be used.

Deardorff (1978) and Best (1998) propose heat transfer coefficients for convection and evaporation when the treatment of the soil surface requires the consideration of a canopy cover. These are defined as:

$$h_{E,c} = \frac{\rho_a L_v \nu}{r_a + r_s} \tag{2-42}$$

$$h_{C,c} = \frac{\rho_a c_p \nu}{r_a} \tag{2-43}$$

2.4.3 Infrared heat transfer coefficient

This Section presents common relations found in the literature for the sky emissivity used in equation (2-10). According to Duffy and Beckman (2006) and other authors (Iziomon et al. 2003; Berdahl and Martin 1984) the atmosphere can be treated as a surface (as it were a dome) surrounding the soil. The atmosphere is actually composed of several layers of gas, each one of them at different temperatures and chemical composition and in continuous movement. Tomasi (1978) shows how the presence of water vapour and its radiative properties in the infrared define an atmospheric window between 8 μm and 14 μm. In this window, the atmosphere is basically transparent to infrared radiation, while outside of this window the infrared radiation is mostly absorbed. In conjunction, these properties determine the net incoming long wave radiation from the sky.

Duffy and Beckman (2006) explain that for the purposes of modelling, the sky is usually treated as a black body at an equivalent sky temperature $T_{sky,\mathrm{K}}$. Several relations have been proposed to relate $T_{sky,\mathrm{K}}$ to measured meteorological variables such as vapour pressure and air temperature. These relations try to account for all the atmospheric complexities mentioned before and in general they adopt the form of equation (2-10). They are summarized in Table 2-1. In particular, the expressions given by Brunt (1932) and Monteith (1961) in Table 2-1 where obtained with data from two locations in the UK (Benson and Kew respectively). Additionally Table 2-2 shows two common relations based only on air temperature.

It is important to remark that relations shown in Table 2-1 and Table 2-2 are defined for long wave radiation under clear skies and that are unsuitable if the effect of clouds needs to be included. The presence of clouds tends to increase the amount of

infrared thermal energy that reaches the soil. This is because, as explained before, the water vapour absorbs energy in the atmospheric window and re-emits it to the ground. Despite the inherent difficulty to obtain expressions for cloudy skies based on the seemingly random nature of clouds presence Edinger et al. (1968) and Iziomon et al. (2003) have performed measurements that lead them to propose the equations summarized in Table 2-3.

Brunt (1932)	$q_{I,in} = \left(a_1 + b_1 e_a^{0.5}\right)\sigma T_{a,\mathrm{K}}^4$	$a_1 = 0.55$ $b_1 = 0.0065\mathrm{kPa}^{-1/2}$
Monteith (1961)	$q_{I,in} = \left(a_2 + b_2 e_a^{0.5}\right)\sigma T_{a,\mathrm{K}}^4$	$a_2 = 0.53$ $b_2 = 0.0065\mathrm{kPa}^{-1/2}$
Berdahl and Martin (1984)	$q_{I,in} = \left(a_3 + b_3 e_a^{0.5}\right)\sigma T_{a,\mathrm{K}}^4$	$a_3 = 0.56$ $b_3 = 0.0059\mathrm{kPa}^{-1/2}$
Iziomon et al. (2003) - 1	$q_{I,in} = \left(a_4 + b_4 e_a^{0.5}\right)\sigma T_{a,\mathrm{K}}^4$	$a_4 = 0.50$ $b_4 = 0.0066\mathrm{kPa}^{-1/2}$
Swinbank (1963) - 1	$q_{I,in} = \left(a_5 + b_5 e_a^{0.5}\right)\sigma T_{a,\mathrm{K}}^4$	$a_5 = 0.64$ $b_5 = 0.0037\mathrm{kPa}^{-1/2}$
Fund and Ångström (1915) - 1	$q_{I,in} = \left(a_6 - b_6 10^{-c_6 e_a}\right)\sigma T_{a,\mathrm{K}}^4$	$a_6 = 0.82$ $b_6 = 0.25$ $c_6 = 0.0094\mathrm{kPa}^{-1}$
Fund and Ångström (1915) - 2	$q_{I,in} = \left(a_7 - b_7 10^{-c_7 e_a}\right)\sigma T_{a,\mathrm{K}}^4$	$a_7 = 1.017$ $b_7 = 0.331$ $c_7 = 0.002\mathrm{kPa}^{-1}$
Iziomon et al. (2003) - 2	$q_{I,in} = \left[1 - a_8 \exp\left(\frac{-b_8 e_a}{T_{a,\mathrm{K}}}\right)\right]\sigma T_{a,\mathrm{K}}^4$	$a_8 = 0.35$ $b_8 = 1\mathrm{kPa}^{-1}\mathrm{K}$

Table 2-1: Expressions dependent on atmospheric vapour pressure, e_a (kPa), and absolute air temperature T_{aK} (K) for clear sky incoming infrared radiation.

Swinbank (1963) - 2	$q_{I,in} = \left(a_9 T_{a,\mathrm{K}}^2\right)\sigma T_{a,\mathrm{K}}^4$	$a_9 = 9.34\,\mathrm{x}\,10^{-6}\,\mathrm{K}^{-2}$
Idso and Jackson (1969)	$q_{I,in} = \left(1 - a_{10}\exp\left[-b_{10}\left(273 - T_{a,\mathrm{K}}\right)^2\right]\right)\sigma T_{a,\mathrm{K}}^4$	$a_{10} = 0.261$ $b_{10} = 7.77\,\mathrm{x}\,10^{-4}\,\mathrm{K}^{-2}$

Table 2-2: Expressions dependent on the absolute air temperature $T_{a,K}$ (K) only for clear sky incoming radiation.

Edinger et al. (1968)	$q_{I,in} = \left[N + a_{11}(1-N)e_a^{b_{11}} \right] \sigma T_{a,\mathrm{K}}^4$	$a_{11} = 0.067\mathrm{kPa}^{-1}$ $b_{11} = 0.08$
Iziomon et al. (2003)	$q_{I,in} = \left[1 - a_{12} \exp\left(\frac{-b_{12} e_a}{T_{a,\mathrm{K}}} \right) \right] \left(1 + 64 c_{12} N^2 \right) \sigma T_{a,\mathrm{K}}^4$	$a_{12} = 0.35$ $b_{12} = 1\mathrm{kPa}^{-1}\mathrm{K}$ $c_{12} = 0.0035$

Table 2-3: Expressions for cloud-covered sky incoming infrared radiation. *N* is the cover factor being 0 for clear sky and 1 for completely cloudy.

Sky emissivities equations shown in Table 2-1 are plotted in Figure 2-1 and Figure 2-2. In Figure 2-1 air vapour pressure is calculated keeping air temperature constant at $T_{a,K}$=282.67K and varying relative humidity from 50% to 100%, this corresponds to an air vapour pressure range from approximately 6 Pa to 12 Pa. In Figure 2-2 air vapour pressure is calculated keeping relative humidity constant at H_a=80% and varying air temperature from 273.15K to 323.15K, this in turn corresponds to an air vapour pressure range from approximately 5 Pa to 100 Pa. From this it can be seen that air temperature has the strongest impact in the value of air vapour pressure. It can also be appreciated that the different sky emissivity models behave linearly in the range of air vapour pressures obtained with variations in relative humidity while in contrast the models behave non-linearly in the wider range of air vapour pressures obtained with variations in air temperature. This is an indication of the high level of uncertainty in the calculation of this term. In all cases the sky emissivity increase with the increase of water pressure, this is due to the higher amount of water molecules present on the atmosphere at higher vapour pressure values. These molecules absorb and reemit the infrared radiation to the ground.

Figure 2-3 shows two of the equations presented in Table 2-2. These equations depend only on air temperature. Their main advantage is the fewer meteorological variables required for estimate the value of sky emissivity. However, this can also reduce their accuracy. As it can be seen in Figure 2-3, these relations tend to be linear. In comparison, Figure 2-2 shows that equations that use vapour pressure in addition to air temperature tend approach asymptotically to 1 at higher values of vapour pressure. This could mean that equations in Table 2-2 underestimate the sky emissivity at higher temperatures (and higher vapour pressure values) but as discussed before, the inherent uncertainty among different models makes this possibility less important when compared with the advantages of requiring fewer meteorological input data.

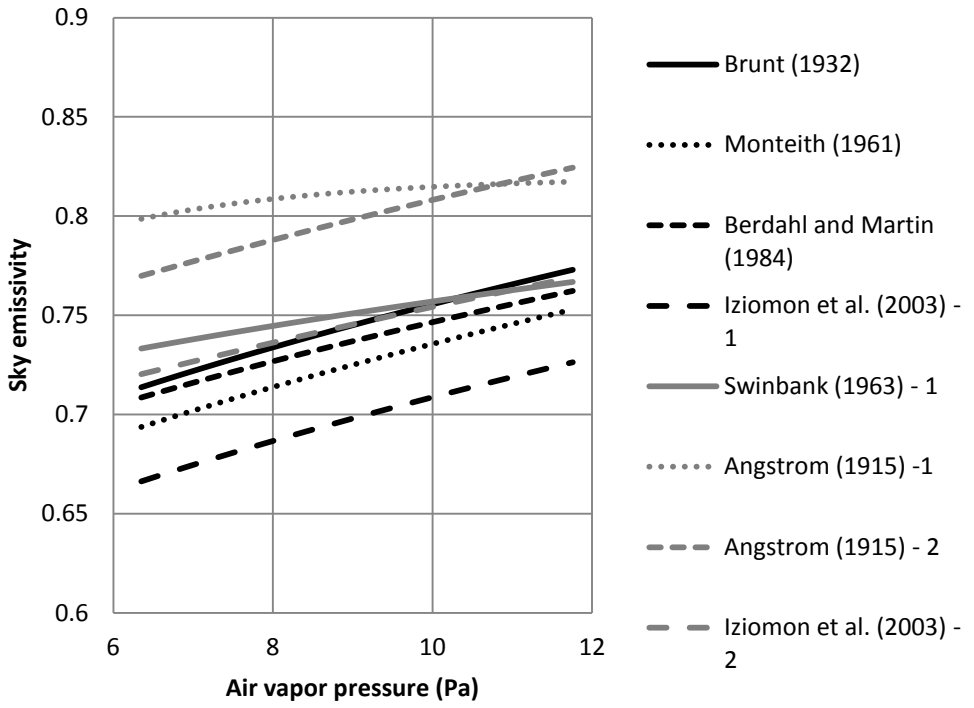

Figure 2-1: Sky emissivities for clear skies. From equations shown in Table 2-1. Air vapour pressure is calculated keeping air temperature constant at 282.67K and varying the relative humidity from 50% to 100%.

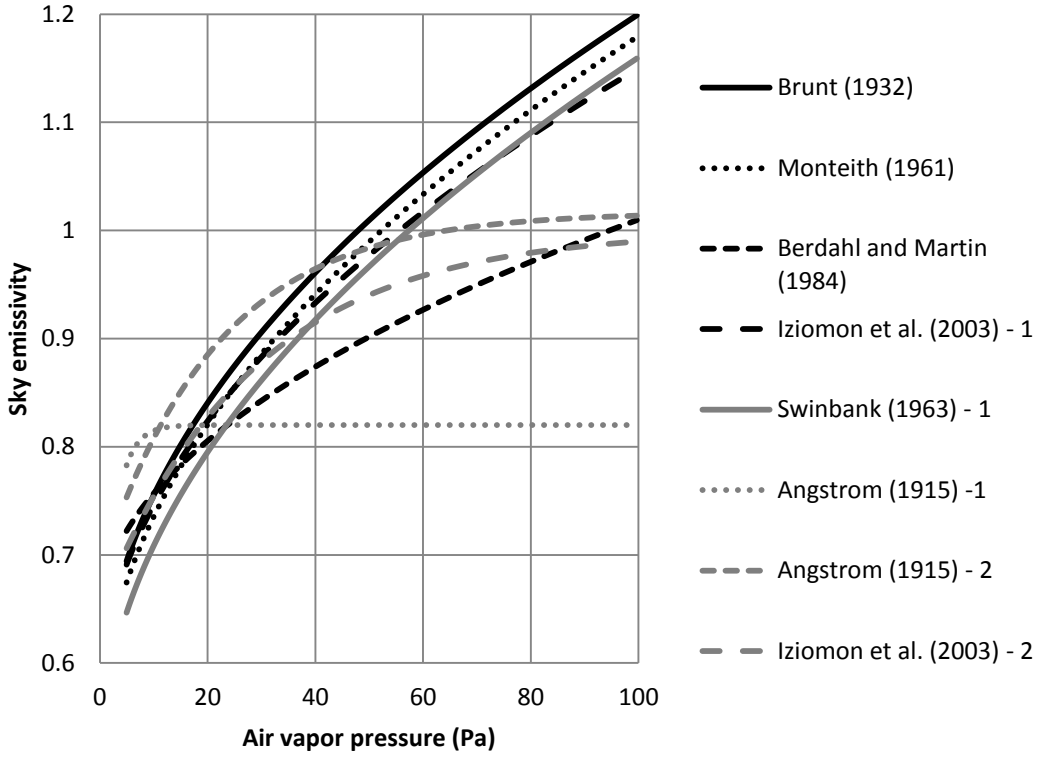

Figure 2-2: Sky emissivities for clear skies. From equations shown in Table 2-1. Air vapour pressure is calculated keeping relative humidity constant at 80% and varying the air temperature from 273.15K to 323.15K.

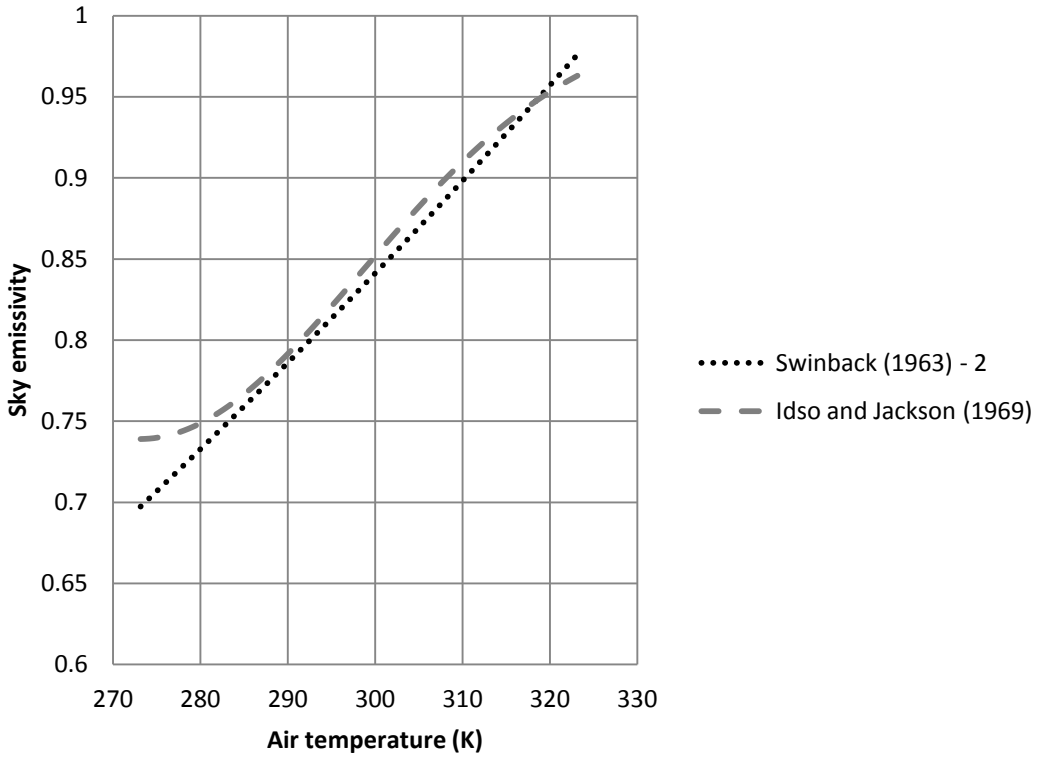

Figure 2-3: Sky emissivities for clear skies from two equations shown in Table 2-2. These relations are only dependent on air temperature.

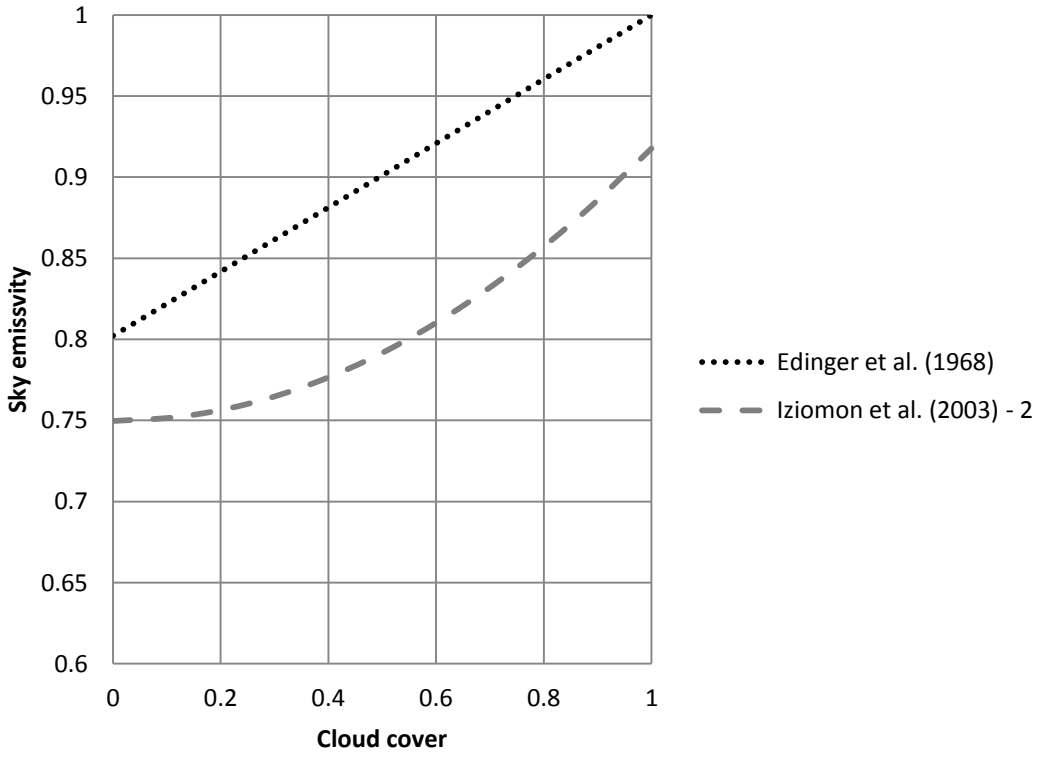

Figure 2-4: Sky emissivities for cloudy skies from equations shown in Table 2-3. Value of 0 for cloud cover corresponds to a clear sky while 1 corresponds to a completely cloud-covered sky.

Figure 2-4 shows equations presented in Table 2-3 using constant values of air temperature (282.67 K) and relative humidity (80 %). These equations correspond to cloudy skies. It can be seen that as the cloud cover factor increases, the value of sky emissivity increases as well. However, there could be difference of up to 0.1 between the two models. Again, as these models are based on experimental observations, these difference are probably due to meteorological difference from site to site. Nevertheless, as they take into account the presence of clouds it is expected to also offer more realistic values, especially on regions with a high level of cloudiness as is the UK.

2.5 Coupled heat and moisture transfer in soils

2.5.1 Moisture transfer in soils

The movement of moisture in unsaturated soils is a relevant physical process in many engineering applications. Under unsaturated conditions, the presence of air in the soil as an independent phase requires the consideration of multi-phase flow models. However, according to Rumynin (2012) a two phase problem is often suitable in the formulation and solution of many problems. In this approach only the motion of the liquid phase is considered with the assumption that ideal counter flow of pore air exists, implying that the air pressure at any point is always constant and equal to the atmospheric pressure. Fredlund and Rahardjo (1993) state that this assumption is applicable to soils with a degree of saturation less than approximately 80%. Under these assumptions the behaviour of the soil moisture can be describe by one partial differential equation (Fredlund and Rahardjo 1993).

Richards' equation is a non-linear partial differential equation derived using Darcy's law that describes the relationship between pressure head h (m), volumetric moisture content (θ_w, or saturation S) and hydraulic conductivity K_w (m/s). Celia et al. (1990) summarize the three common forms of Richards' equation:

The θ_w-based form expressed in terms of moisture content:

$$\frac{\partial \theta_w}{\partial t} = \nabla \cdot D_w(\theta_w) \nabla \theta_w + \frac{\partial K_w}{\partial z} \qquad (2\text{-}44)$$

$$D_w(\theta_w) \equiv \frac{K_w(\theta_w)}{C_w(\theta_w)} \tag{2-45}$$

The *h*-based form expressed in terms of pressure head

$$C_w(h)\frac{\partial h}{\partial t} = \nabla \cdot K_w(h)\nabla h + \frac{\partial K_w}{\partial z} \tag{2-46}$$

$$C_w(h) \equiv \frac{d\theta_w}{dh} \tag{2-47}$$

and the Mixed form expressed in terms of moisture content and pressure head

$$\frac{\partial \theta_w}{\partial t} = \nabla \cdot K_w(h)\nabla h + \frac{\partial K_w}{\partial z} \tag{2-48}$$

where $C_w(h)$ is the specific moisture capacity function and $D_w(\theta_w)$ is the unsaturated diffusivity. It is assumed that appropriate constitutive relationships between θ_w and h and between K_w and h (or K_w and θ_w) are available.

Celia et al. (1990) have recognized that numerical approximations based on either of the three formulations presented above can give significantly different results. In general, numerical schemes for solving the pressure head based Richards' equation are more commonly applied since such schemes are capable of dealing with both saturated and unsaturated conditions, applicable to heterogeneous soils. In this respect Marinoschi (2006) offers a comprehensive analysis of the solution of the Richards equation under saturated, unsaturated and saturated-unsaturated conditions. Marinoschi (2006) mentions that during the flow of a fluid in a porous medium its degree of saturation changes developing saturated and unsaturated zones and giving rise to free boundary problems inside the domain. Under this situation the solution to Richards's equation raises a difficult mathematical problem. Marinoschi (2006) shows how, for example, when the pressure head in the unsaturated soil comes close to the unsaturated value, the water capacity vanishes and forces Richards' equation to degenerate. Correspondingly, the diffusion coefficient expressed as a function of moisture exhibits a blow-up development around saturation.

2.5.2 Variation of soil thermal properties with moisture content

As discussed in Section 2.2, the thermal properties of soil are dependent on the soil moisture content, since the soil is a mixture of three main constituents, mainly solids,

water and air. Pielke (1984), Sellers (1965) and Marshall et al. (1996) have studied the variation of thermal diffusivity and thermal conductivity of soils with moisture content while Garrat (1994) have offered a summary of their studies and provides a list of representative values for bulk thermal conductivity (λ_b), bulk specific heat capacity $c_{p,b}$, bulk density (ρ_b) and bulk thermal diffusivity α_b for various types of soil at three water contents that cover the range from saturated to dry conditions. Table 2-4 shows data taken from Garrat (1994) for clay soils. It can be seen that the variations of density and specific heat capacity are mostly linear, while the variations in bulk thermal conductivity and bulk thermal diffusivity are non-linear but having the strongest changes close to the dry range of moisture content.

θ_w	λ_b (W/mK)	$c_{p,b}$ (J/kgK)	ρ_b (kg/m^3)	α_b (m^2/s)
0	0.25	890	1600	0.18
0.2	1.1	1170	1800	0.52
0.4	1.6	1550	2000	0.52

Table 2-4: Variation of thermal properties with water content for clay soils. Data taken from (Garratt 1994).

2.5.3 Variation of hydraulic properties with temperature

According to Grant (2005) the theoretical influence of temperature on hydraulic conductivity and gas-phase water concentration is well known and can yield precise estimates of these effects. Grant (1994) explained how the hydraulic conductivity has been found to be directly proportional to liquid density, the reciprocal of liquid viscosity, and the square of the mean grain diameter. The density of water changes little between its conventional melting and boiling temperatures and the approximate value of 1000 kg/m^3 can be used. The dynamic viscosity of water, μ_w (Pa s), at temperature T in the other hand can be fitted using the Vogel-Tamman-Fulcher equation:

$$\mu_w = \mu_0 \exp\left(\frac{B}{T + T_0}\right) \tag{2-49}$$

where μ_0=31.8903 Pa s, B=479.9 K and T_0=-154.05K. In addition, Grant (2005) also shows how the hydraulic conductivity is function of the degree of saturation. For higher degrees of saturation, the impact of temperature on the hydraulic conductivity is also higher. Conversely, for lower degrees of saturation the impact is reduced. Regarding the pressure head (equivalent to matric potential), Grant (2005) mentions that the relation between temperature and pressure head is not so well understood but

the effect of increasing temperature is in general to decrease the pressure head gradients within the soil due to differences in water content. The effect of temperature on pressure head appears to be well described by the relation:

$$h(T) = h(T_r)\frac{\beta_0 + T}{\beta_0 + T_r} \tag{2-50}$$

where T_r (K) is a reference temperature and β_0 (K) is a constant, which most soils has a value between -350 K and 450 K.

The above observations appear to agree with measurements from Romero (2001) who tested the hydraulic properties of natural kaolinitic-illitic clay in the range from 22 ˚C to 80 ˚C under isochoric conditions and found that at a given moisture content the total suction tends to decrease with increasing temperature, however the reduction at high moisture contents (>11%) is negligible. Nobre and Thomson (1993) studied the effects of transient temperature gradients on soil moisture dynamics using a two-dimensional coupled thermal energy transport and soil moisture flow numerical model in the context of remediation process via soil flushing and soil vapour extraction. They performed three hypothetical field-scale experiments, one of these focusing on the impact of an internal heat source on the coupled mechanisms of thermal energy transport and soil moisture dynamics. Their results from isothermal and non-isothermal simulations indicated that moisture velocities were smaller in the non-isothermal cases as compared with the isothermal cases. In addition, they also showed how the moisture flow through the domain had little impact on the spatial distribution of temperature indicating that the coupling of moisture flow and thermal energy transport may not be necessary for simulations of this nature.

2.6 Predicting temperature variations in the soil profile

This Section presents a summary of analytical and numerical methods used in the estimation of soil temperature profiles and the study of thermal devices buried in the ground.

2.6.1 Analytical methods

Analytical solutions have been applied to solve the diffusion equation and the diffusion-convection equation in soil in various different fields in order to estimate

the soil temperature profile. For example, Hagentoft (1996a; 1996b), Jacovides et al. (1996) and Hollmuller and Lachal (2014) have studied the heat diffusion problem in relation to the interaction between buildings and soil while Li and Cleall (2010) and Chen et al. (2009) have studied diffusion of contaminants in porous media composed of two or more layers. Convection and diffusion have been analysed together in relation with water infiltration by Gao et al. (2003) and by Wang et al. (2012) and general solute transport in porous media under various boundary conditions have been studied by Li and Cleall (2011). Huang and Wu (2012) have studied the infiltration of water in unsaturated soils using Richards' equation. Approximate analytical solutions have been used to study heat and moisture transfer including phase change (thawing) in soils by Kurylyk et al. (2014). In each of these approaches three main types of boundary conditions are considered. These are: first type (also known as Dirichlet type), which specify the value of the variable at the boundary; second type boundary conditions (also known as Neumann type) which specify the value of the derivative of a variable at the boundary; and third type boundary conditions (also known as Robin type), these specify both (as a linear combination) the value of the variable and its derivative at the boundary.

The limitations of analytical solutions typically result from the simplification of certain aspects of the problem. For example the approaches proposed by Michopoulos et al. (2010) and Mihalakakou et al. (1997) to estimate the temperature of the ground and the coupled heat diffusion and water infiltration analytical method proposed by Shao et al. (1998) relied on the assumption of fixed boundary conditions (constant or periodic). Chuangchid and Krarti (2001) use a similar assumption in order to include more complex geometries while Yumrutaş et al. (2005) modelled analytically the actual operation of a buried heat exchanger.

In recent years more attention has been given to describe in more detail the energy and mass transfer interactions at the soil surface. This has been accomplished for example by Wang (2012) and Wang and Bou-Zeid (2012) through the inclusion of time dependent boundary conditions of the second type, while others like Cleall and Li (2011) have taken into consideration even more descriptive boundary conditions of the third type. With regard to the boundary condition at the bottom of the domain, the common approaches found in the previous cited works is to either fix it at an estimated average temperature or assume an insulated (no heat flux) boundary

condition. The implication of this last assumption is to neglect any geothermal heat flux coming from the deepest layers of the ground. A map of geothermal heat fluxes at the soil surface published by Davies (2013) supports this assumption. However, where this assumption cannot be made, the inclusion of a constant heat flux at the bottom that takes into account this term is not difficult.

2.6.1.1 Analytical equations for meteorological variables

As mentioned in Section 2.6.1, the analytical approaches to estimate the temperature profiles near the soil surface rely on several assumptions including prescribing the transient behaviour of the soil at the surface. Carson (1963) and Mihalakakou (1997) used a first kind (Dirichlet) boundary condition to fix the variation with time of the soil temperature at the surface to follow same regular pattern found in both the annual and diurnal cycles of solar radiation and air temperature. They argued that if the fluctuations superimposed on these regular cycles (produced by clouds, warm or cold spells) are removed from available experimental data, the regular cycles can be studied and represented by analytical functions that can be used to fix the temperature at the surface of the soil.

Lumb (1964), Cinquemani et al. (1979), Frouin et al. (1989) and dos Santos and Mendes (2006) presented analytical relations to directly model the diurnal variations of solar radiation that can be applied to different fields including the estimation of soil temperatures. For example, for solar radiation, Lumb used the following equation:

$$R = R_c \cos\theta_s \left(a + b\cos\theta_s\right) \tag{2-51}$$

where θ_s is the sun's zenith angle defined as the angle measured from directly overhead to the geometric centre of the sun's disc, *Rc* (1.362 kW/m^2) is the solar constant defined as the amount of electromagnetic radiation per unit area that would be incident on a plane perpendicular to the rays at a distant of one astronomical unit from the sun, and *a* and *b* are coefficients that need to be adjusted depending on the location of interest.

The solar relation presented by dos Santos and Mendes (2006) adopted the following form:

$$R(t) = 300 + 100\sin\left(\pi + \frac{\pi t}{31536000}\right)\sin\left(\frac{3\pi}{2} + \frac{\pi t}{43200}\right) \qquad (2\text{-}52)$$

were t is the time in seconds. The value for total solar radiation given by (2-52) is valid between 6:00 am and 6:00 pm with peak values at noon, and, elsewhere it equal to zero.

Hillel (2003) presented an analytical model to represent the annual variations of air temperature that is given by:

$$T_a(t) = T_{a,ave} + T_{a,amp}\sin\left(\frac{2\pi t}{86400}\right) \qquad (2\text{-}53)$$

where $T_{a,ave}$ (˚C) is the average ambient temperature and $T_{a,amp}$ (˚C) is the diurnal amplitude.

dos Santos and Mendes (2006) suggested the use of the following equations for air temperature:

$$T_a(t) = 20 + 0.5\sin\left(\pi + \frac{\pi t}{31536000}\right) + 5\sin\left(\pi + \frac{\pi t}{43200}\right) \qquad (2\text{-}54)$$

A yearly average air temperature of 20 ˚C with daily variation of 5 ˚C and yearly variation of 5 ˚C for the peak values was considered for the authors.

Although other meteorological variables such as rain fall, wind speed or relative humidity are more challenging to describe analytically, dos Santos and Mendes (2006) has offered an expression for the latter:

$$H_a(t) = 0.60 - 0.1\sin\left(\pi + \frac{\pi t}{43200}\right) \qquad (2\text{-}55)$$

For ambient relative humidity, a daily variation between 50% and 70% was considered. No yearly peak variation was used in this case.

2.6.2 Numerical methods

Analytical methods are useful to estimate temperature profiles in the soil when the soil (or geometric) conditions can be simplified. Numerical methods, in the other

hand, can also be applied for these analyses not only in 1D, but in 2 and 3 dimensions, and can more readily accommodate complex geometries, non-linear material properties and transient processes.

Ma et al. (2008) and Qin et al. (2002) have used numerical methods to obtain a more detailed description of coupled problems involving the transfer of mass and thermal energy between the soil and the atmosphere in 2D and 3D conditions. Rajeev et al. (2012) and Liu et al. (2011) have used them to model the mechanical behaviour of soils, the performance of buried structures and climate prediction.

In the context of this thesis, the interest focuses in the numerical analysis of buried thermal energy storage devices. The methods and assumptions taken into account vary depending on the specific physical characteristics of the problem at hand. Yumrutaş et al. (2005), for example, offered a semi-analytic method to estimate the performance of a building's cooling system. They use an analytical solution to estimate the heat flux between the storage system and the surrounding soil, but solve numerically the behaviour of the cooling system itself. Since they assumed that the storage device is placed deep into the soil, constant soil temperature as initial condition and no (or reduced) heat flux interaction with the atmosphere was assumed. The same approach was used by Nabi and Al-Khoury (2012) to perform the numerical analysis of U-tube heat exchangers, ground heat storage devices buried at relatively high depths into the ground (~100 m); and by Shang et al. (2011) to analyse numerically the thermal energy recovery from the soil using ground-source heat pumps under intermittent operation. In these works the initial condition and bottom and distant (far-field) boundary conditions are considered constant and equal to the annual average soil temperature while the boundary condition at the surface, although not disregarded, is usually simplified. In comparison, the movement of the fluid inside the pipes is considered in great detail. In the numerical treatment of shallower heat storage devices, Kroll and Ziegler (2011), for example, suggested that the thermal energy interactions at the soil surface can also be simplified or assumed negligible provided that it is well insulated

Wu et al. (2010) performed 2-month experimental measurements and numerical simulations of a horizontal slinky ground-source heat exchanger. Their experimental system was placed near the surface of the soil (1-2 m depth) at a site near

Oxfordshire, UK. A commercial CFD package software (FLUENT) was used to build a numerical model to solve the 3 dimensional transient heat transfer equation without consideration of moisture movement in the domain. Experimental data measured at the beginning of the experiment and thermo physical properties measured from soil samples taken from the site were used as initial condition and as input data for the model. As heat carrier, a mixture of water and ethylene glycol at 30% was used. Similarly, Esen et al. (2007) and İnallı and Esen (2004) performed experimental measurements and numerical simulations in a year-long project that aimed to evaluate the thermal performance of shallow horizontal ground-source heat pump systems. In this case the experimental system was composed of two heat exchangers buried 1 m and 2 m in the ground. The fluid used as heat carrier was a mixture of water and ethylene glycol at 25%. A numerical model based on the finite difference method was build to solve the transient heat transfer equation, again, neglecting moisture movement in the domain. Congedo et al. (2012) performed a set of purely CFD numerical simulations in 3 dimensions in a cubic domain of 2 m per side. The authors compared the performance of horizontal ground heat exchangers with different pipe distributions using constant thermal properties and fixing the bottom boundary using experimentally measured data. The top boundary condition was defined using meteorological data recorded on site. Other authors have developed similar numerical models to study the behaviour of ground-source heat pump systems (Nam et al. 2008; Bittelli et al. 2010; Hollmuller and Lachal 2014).

In the area of building science, dos Santos and Mendes (2006) presented a purely numerical analysis in 3 dimensions using the finite volume method of the energy interactions of a building's envelope with the soil underneath. These authors took into account the simultaneous heat and moisture transfer within the soil. The size of the soil domain was 10 m in the x and y directions and 4 m in the z direction (depth). Two sets of boundary conditions were used at the top surface of the soil, one for the interaction soil-atmosphere and the other for the interaction soil-building. All other soil domain surfaces were considered adiabatic and impermeable. A pre-simulation period of several years was recommended for the correct estimation of temperature and moisture content profiles. Dos Santos and Mendes (2006) showed that very slight differences exist in terms of building's indoor air temperature between a purely conductive model for the ground and a model considering moisture movement,

however, the significant differences were found in terms of indoor air humidity. Rees et al. (2007) presented a 2-dimensional numerical simulation based on the finite element method of a year-long full-scale experiment that dealt with the energy interactions of a building's envelope and the ground. In this case, the moisture movement in the domain was neglected since the accuracy offered by standard uncoupled methods was considered enough for that application. The size of the domain was 12.95 m in the x direction and 14.626 m in the z direction (depth). The vertical boundary conditions were considered adiabatic while the bottom boundary was fixed to a suitable temperature. A 4 year-long pre-conditioning analysis was considered enough to obtain a suitable initial condition for the problem.

2.7 Concluding remarks

This Chapter has offered an overview of the scientific literature available related to the storage of thermal energy in soils using shallow heat exchangers.

The main physical properties governing the transfer of heat and moisture in the ground have been described, including the thermal conductivity and the specific heat capacity. The dependency of these properties with moisture content has been explained and simple relations for their estimation have been offered.

Special attention has been given the description of three main formulations describing the energy interactions at the soil surface for different soil covers (bare soil, pavement and vegetation covered). Heat transfer coefficients have been offered for the typical heat flux processes at the surface of the soil: solar radiation, infrared radiation, convection and evaporation.

The process of coupled heat and moisture transfer in a soil and the relative dependence of the hydraulic properties on the temperature field and conversely the dependence of thermal properties on soil moisture content have also been discussed. In general, both physical processes are related and need to be considered for a fully detailed description of moisture and heat flux within the soil. However, in practice, the relative dependence on temperature of the hydraulic properties appear to allow for some simplifications especially if the problem's specific characteristics (like the presence of an impermeable insulation layer near the surface of the soil) lead one to suppose that the soil moisture transfer can be considered as of second order of importance compared with the thermal transfer processes.

Analytical methods for the estimation of the soil temperature profile have also been discussed. The importance of these lie in the insight they offer about the physical processes happening in a problem. The main drawback is that they usually only allow for relatively simple scenarios to be solved. Very often, field scale problems require consideration of many different variables at the same time. In these conditions, numerical methods are more suitable. An overview of some numerical simulations regarding the treatment of buried thermal devices has been offered. Different numerical methods are used (finite differences, finite elements or finite volumes) and also different software packages are used (FLUENT, COMSOL, etc) or purpose-built in different languages (FORTRAN, C, C++, MATLAB), but it has been shown that in general they share very similar assumptions regarding the treatment of boundary conditions and the physical processes related with the transfer of heat in soils (usually neglecting moisture transfer).

2.8 References

Abu-Hamdeh, N. H. [2003]. Thermal Properties of Soils as Affected by Density and Water Content. *Biosyst. Eng.* **86** (1): 97–102. doi:10.1016/S1537-5110(03)00112-0.

Adams, E. E., Cosler, D. J., and Helfrich, K. R. [1990]. Evaporation from Heated Water Bodies: Predicting Combined Forced plus Free Convection. *Water Resour Res* **26** (3): 425–435. Scopus.

Alvenäs, G. and Jansson, P.-E. [1997]. Model for Evaporation, Moisture and Temperature of Bare Soil: Calibration and Sensitivity Analysis. *Agric. For. Meteorol.* **88** (1–4): 47–56. doi:10.1016/S0168-1923(97)00052-X.

American Society for Testing and Materials. [2008]. Test Method for Specific Heat of Rock and Soil. ASTM International. http://www.astm.org/Standards/D4611.htm.

Ångström, A. [1925]. The Albedo of Various Surfaces of Ground. *Geogr. Ann.* **7** (January): 323–342. doi:10.2307/519495.

ASCE, A. S. of C. E. [1996]. *Hydrology Handbook*. ASCE Publications.

Beljaars, A. and Holtslag, A. [1991]. Flux Parameterization Over Land Surfaces for Atmospheric Models. *J. Appl. Meteorol.* **30** (3): 327–341. doi:10.1175/1520-0450(1991)030<0327:FPOLSF>2.0.CO;2.

Berdahl, P. and Martin, M. [1984]. Emissivity of Clear Skies. *Sol. Energy* **32** (5): 663–664. doi:10.1016/0038-092X(84)90144-0.

Best, M. J. [1998]. A Model to Predict Surface Temperatures. *Bound.-Layer Meteorol.* **88** (2): 279–306. doi:10.1023/A:1001151927113.

Bittelli, M., Tomei, F., Pistocchi, A., Flury, M., Boll, J., Brooks, E. S., and Antolini, G. [2010]. Development and Testing of a Physically Based, Three-Dimensional Model of Surface and Subsurface Hydrology. *Adv. Water Resour.* **33** (1): 106–122. doi:10.1016/j.advwatres.2009.10.013.

Bittelli, M., Ventura, F., Campbell, G. S., Snyder, R. L., Gallegati, F., and Pisa, P. R. [2008]. Coupling of Heat, Water Vapor, and Liquid Water Fluxes to Compute Evaporation in Bare Soils. *J. Hydrol.* **362** (3-4): 191–205. doi:10.1016/j.jhydrol.2008.08.014.

Boast, C. and Simmons, F. [2005]. Evaporation of Water from Bare Soil. In , 494–502. Oxford: Elsevier. http://www.sciencedirect.com/science/article/B7GG2-4DGTX0B-2S/2/ae2a8ce8334b369ac1da74a3a00c2efd.

Bobes-Jesus, V., Pascual-Muñoz, P., Castro-Fresno, D., and Rodriguez-Hernandez, J. [2013]. Asphalt Solar Collectors: A Literature Review. *Appl. Energy* **102** (February): 962–970. doi:10.1016/j.apenergy.2012.08.050.

Brunt, D. [1932]. Notes on Radiation in the Atmosphere. I. *Q. J. R. Meteorol. Soc.* **58** (247): 389–420. doi:10.1002/qj.49705824704.

Brutsaert, W. [1982]. *Evaporation into the Atmosphere: Theory, History and Applications*. Springer Netherlands.

Carson, J. E. [1963]. Analysis of Soil and Air Temperatures by Fourier Techniques. *J. Geophys. Res.* **68** (8): 2217–2232. doi:10.1029/JZ068i008p02217.

Celia, M. A., Bouloutas, E. T., and Zarba, R. L. [1990]. A General Mass-Conservative Numerical Solution for the Unsaturated Flow Equation. *Water Resour. Res.* **26** (7): 1483–1496. doi:10.1029/WR026i007p01483.

Çengel, Y. A. [2003]. *Heat Transfer: A Practical Approach*. McGraw-Hill.

Chen, D., Gustavsson, T., and Bogren, J. [1999]. The Applicability of Similarity Theory to a Road Surface. *Meteorol. Appl.* **6** (1): 81–88. doi:10.1017/S1350482799001036.

Chen, Y., Xie, H., Ke, H., and Chen, R. [2009]. An Analytical Solution for One-Dimensional Contaminant Diffusion through Multi-Layered System and Its Applications. *Environ. Geol.* **58** (5): 1083–1094. doi:10.1007/s00254-008-1587-3.

Chuangchid, P. and Krarti, M. [2001]. Foundation Heat Loss from Heated Concrete Slab-on-Grade Floors. *Build. Environ.* **36** (5): 637–655. doi:10.1016/S0360-1323(00)00040-8.

Cinquemani, V., Owenby, J. R., and Baldwin, R. G. [1979]. *Input Data for Solar Systems*. National Climatic Center.

Cleall, P. J. and Li, Y.-C. [2011]. Analytical Solution for Diffusion of VOCs through Composite Landfill Liners. *J. Geotech. Geoenvironmental Eng.* **137** (9): 850–854. doi:10.1061/(ASCE)GT.1943-5606.0000506.

Congedo, P. M., Colangelo, G., and Starace, G. [2012]. CFD Simulations of Horizontal Ground Heat Exchangers: A Comparison among Different Configurations. *Appl. Therm. Eng.* **33–34** (February): 24–32. doi:10.1016/j.applthermaleng.2011.09.005.

Davies, J. H. [2013]. Global Map of Solid Earth Surface Heat Flow. *Geochem. Geophys. Geosystems* **14** (10): 4608–4622. doi:10.1002/ggge.20271.

Deardorff, J. [1978]. Efficient Prediction of Ground Surface-Temperature and Moisture, with Inclusion of a Layer of Vegetation. *J. Geophys. Res.-Oceans Atmospheres* **83** (NC4): 1889–1903. doi:10.1029/JC083iC04p01889.

Deb, S. K., Shukla, M. K., Sharma, P., and Mexal, J. G. [2011]. Coupled Liquid Water, Water Vapor, and Heat Transport Simulations in an Unsaturated Zone of a Sandy Loam Field. *Soil Sci.* **176** (8): 387–398. Scopus. doi:10.1097/SS.0b013e318221f132.

De Vries, D. A. [1958]. Simultaneous Transfer of Heat and Moisture in Porous Media. *Trans. Am. Geophys. Union* **39** (5): 909. doi:10.1029/TR039i005p00909.

De Vries, D. A. [1963]. Thermal Properties of Soils. In , 382. Amsterdam: North-Holland.

Dos Santos, G. H. and Mendes, N. [2006]. Simultaneous Heat and Moisture Transfer in Soils Combined with Building Simulation. *Energy Build.* **38** (4): 303–314. doi:10.1016/j.enbuild.2005.06.011.

Duffie, J. A. and Beckman, W. A. [2006]. *Solar Engineering of Thermal Processes*. 3rd ed. Wiley.

Edinger, J. E., Duttweiler, D. W., and Geyer, J. C. [1968]. The Response of Water Temperatures to Meteorological Conditions. *Water Resour. Res.* **4** (5): 1137–1143. doi:10.1029/WR004i005p01137.

Esen, H., Inalli, M., and Esen, M. [2007]. Numerical and Experimental Analysis of a Horizontal Ground-Coupled Heat Pump System. *Build. Environ.* **42** (3): 1126–1134. doi:10.1016/j.buildenv.2005.11.027.

Farouki, O. [1981]. *Thermal Properties of Soils (CRREL Monograph)*. U.S. Army Corps of Engineers, Cold Regions Research and Engineering Laboratory.

Feddes, R. A., Kabat, P., Van Bakel, P. J. T., Bronswijk, J. J. B., and Halbertsma, J. [1988]. Modelling Soil Water Dynamics in the Unsaturated Zone — State of the Art. *J. Hydrol.* **100** (1–3): 69–111. doi:10.1016/0022-1694(88)90182-5.

Fredlund, D. G. and Rahardjo, H. [1993]. *Soil Mechanics for Unsaturated Soils*. Wiley.

Frouin, R., Lingner, D. W., Gautier, C., Baker, K. S., and Smith, R. C. [1989]. A Simple Analytical Formula to Compute Clear Sky Total and Photosynthetically Available Solar Irradiance at the Ocean Surface. *J. Geophys. Res. Oceans* **94** (C7): 9731–9742. doi:10.1029/JC094iC07p09731.

Fund, S. I. H. and Ångström, A. K. [1915]. *A Study of the Radiation of the Atmosphere Based upon Observations of the Nocturnal Radiation during Expeditions to Algeria and to California*. Washington: Smithsonian Institution.

Gao, Z., Fan, X., and Bian, L. [2003]. An Analytical Solution to One-Dimensional Thermal Conduction-Convection in Soil. *Soil Sci.* **168** (2): 99–107. doi:10.1097/00010694-200302000-00004.

Garratt, J. R. [1994]. *The Atmospheric Boundary Layer*. Cambridge University Press.

Geiger, R. [1950]. *The Climate Near The Ground*. Translated by Milroy N. Stewart. Harvard University Press. http://archive.org/details/climatenearthegr032657mbp.

Grant, S. [2005]. Hydraulic Properties, Temperature Effects. In , 207–211. Oxford: Elsevier. http://www.sciencedirect.com/science/article/B7GG2-4DGTX0B-3X/2/1bf9701d00272ae569b1ffb989d6be1b.

Grifoll, J., Gastó, J. M., and Cohen, Y. [2005]. Non-Isothermal Soil Water Transport and Evaporation. *Adv. Water Resour.* **28** (11): 1254–1266. doi:10.1016/j.advwatres.2005.04.008.

Hagentoft, C. E. [1996a]. Heat Losses and Temperature in the Ground under a Building with and without Ground Water Flow .1. Infinite Ground Water Flow Rate. *Build. Environ.* **31** (1): 3–11.

Hagentoft, C. E. [1996b]. Heat Losses and Temperature in the Ground under a Building with and without Ground Water Flow .2. Finite Ground Water Flow Rate. *Build. Environ.* **31** (1): 13–19.

Haverkamp, R., Bouraoui, F., Zammit, C., and Angulo-Jaramillo, R. [1998]. Soil Properties and Moisture Movement in the Unsaturated Zone. In , edited by J.

Delleur. CRC Press. http://www.crcnetbase.com/doi/abs/10.1201/9781420048582.ch5.

Herb, W. R., Janke, B., Mohseni, O., and Stefan, H. G. [2008]. Ground Surface Temperature Simulation for Different Land Covers. *J. Hydrol.* **356** (3-4): 327–343. doi:10.1016/j.jhydrol.2008.04.020.

Hillel, D. [2003]. Soil Temperature and Heat Flow. In , edited by D. Hillel, 215–233. Burlington: Academic Press. http://www.sciencedirect.com/science/article/pii/B9780123486554500137.

Hillel, D. [2005]. Thermal Properties and Process. In , edited by D. Hillel, 156–163. Oxford: Elsevier. http://www.sciencedirect.com/science/article/pii/B0123485304005233.

Hollmuller, P. and Lachal, B. [2014]. Air–soil Heat Exchangers for Heating and Cooling of Buildings: Design Guidelines, Potentials and Constraints, System Integration and Global Energy Balance. *Appl. Energy* **119** (April): 476–487. doi:10.1016/j.apenergy.2014.01.042.

Huang, R. Q. and Wu, L. Z. [2012]. Analytical Solutions to 1-D Horizontal and Vertical Water Infiltration in Saturated/unsaturated Soils Considering Time-Varying Rainfall. *Comput. Geotech.* **39** (January): 66–72. doi:10.1016/j.compgeo.2011.08.008.

Idso, S. B. and Jackson, R. D. [1969]. Thermal Radiation from the Atmosphere. *J. Geophys. Res.* **74** (23): 5397–5403. doi:10.1029/JC074i023p05397.

İnallı, M. and Esen, H. [2004]. Experimental Thermal Performance Evaluation of a Horizontal Ground-Source Heat Pump System. *Appl. Therm. Eng.* **24** (14–15): 2219–2232. doi:10.1016/j.applthermaleng.2004.01.005.

Iziomon, M. G., Mayer, H., and Matzarakis, A. [2003]. Downward Atmospheric Longwave Irradiance under Clear and Cloudy Skies: Measurement and Parameterization. *J. Atmospheric Sol.-Terr. Phys.* **65** (10): 1107–1116. doi:10.1016/j.jastp.2003.07.007.

Jacovides, C. P., Mihalakakou, G., Santamouris, M., and Lewis, J. O. [1996]. On the Ground Temperature Profile for Passive Cooling Applications in Buildings. *Sol. Energy* **57** (3): 167–175. doi:10.1016/S0038-092X(96)00072-2.

Jansson, C., Almkvist, E., and Jansson, P. [2006]. Heat Balance of an Asphalt Surface: Observations and Physically-Based Simulations. *Meteorol. Appl.* **13** (2): 203–212. doi:10.1017/S1350482706002179.

Kay, B. D. and Groenevelt, P. H. [1974]. On the Interaction of Water and Heat Transport in Frozen and Unfrozen Soils: I. Basic Theory; The Vapor Phase1. *Soil Sci. Soc. Am. J.* **38** (3): 395. doi:10.2136/sssaj1974.03615995003800030011x.

Kondo, J., Saigusa, N., and Sato, T. [1990]. A Parameterization of Evaporation from Bare Soil Surfaces. *J. Appl. Meteorol.* **29** (5): 385–389.

Krarti, M. and Kreider, J. F. [1996]. Analytical Model for Heat Transfer in an Underground Air Tunnel. *Energy Convers. Manag.* **37** (10): 1561–1574.

Kroll, J. A. and Ziegler, F. [2011]. The Use of Ground Heat Storages and Evacuated Tube Solar Collectors for Meeting the Annual Heating Demand of Family-

Sized Houses. *Sol. Energy* **85** (11): 2611–2621. doi:10.1016/j.solener.2011.08.001.

Kubota, A. and Sugita, M. [1994]. Radiometrically Determined Skin Temperature and Scalar Roughness to Estimate Surface Heat Flux. Part I: Parameterization of Radiometric Scalar Roughness. *Bound.-Layer Meteorol.* **69** (4): 397–416. doi:10.1007/BF00718127.

Kupiec, K., Larwa, B., and Gwadera, M. [2015]. Heat Transfer in Horizontal Ground Heat Exchangers. *Appl. Therm. Eng.* **75** (January): 270–276. doi:10.1016/j.applthermaleng.2014.10.003.

Kurylyk, B. L., McKenzie, J. M., MacQuarrie, K. T. B., and Voss, C. I. [2014]. Analytical Solutions for Benchmarking Cold Regions Subsurface Water Flow and Energy Transport Models: One-Dimensional Soil Thaw with Conduction and Advection. *Adv. Water Resour.* **70** (August): 172–184. doi:10.1016/j.advwatres.2014.05.005.

Liu, C., Shi, B., Tang, C., and Gao, L. [2011]. A Numerical and Field Investigation of Underground Temperatures under Urban Heat Island. *Build. Environ.* **46** (5): 1205–1210. doi:10.1016/j.buildenv.2010.12.015.

Li, Y.-C. and Cleall, P. J. [2010]. Analytical Solutions for Contaminant Diffusion in Double-Layered Porous Media. *J. Geotech. Geoenvironmental Eng.* **136** (11): 1542–1554. doi:10.1061/(ASCE)GT.1943-5606.0000365.

Li, Y.-C. and Cleall, P. J. [2011]. Analytical Solutions for Advective–dispersive Solute Transport in Double-Layered Finite Porous Media. *Int. J. Numer. Anal. Methods Geomech.* **35** (4): 438–460. doi:10.1002/nag.903.

Lumb, F. E. [1964]. The Influence of Cloud on Hourly Amounts of Total Solar Radiation at the Sea Surface. *Q. J. R. Meteorol. Soc.* **90** (383): 43–56. doi:10.1002/qj.49709038305.

Mahfouf, J. F. and Noilhan, J. [1991]. Comparative Study of Various Formulations of Evaporations from Bare Soil Using In Situ Data. *J. Appl. Meteorol.* **30** (9): 1354–1365. doi:10.1175/1520-0450(1991)030<1354:CSOVFO>2.0.CO;2.

Maidment, D. [1993]. *Handbook of Hydrology*. 1st ed. McGraw-Hill Professional.

Marinoschi, G. [2006]. *Functional Approach to Nonlinear Models of Water Flow in Soils*. Softcover reprint of hardcover 1st ed. 2006 edition. Vol. 21. Mathematical Modelling: Theory and Applications. Dordrecht; London: Springer.

Marshall, T. J., Holmes, J. W., and Rose, C. W. [1996]. *Soil Physics*. 3 edition. Cambridge England ; New York: Cambridge University Press.

Ma, X., Cheng, B., Liu, W., and Li, J. [2008]. Simulation and Analysis on the Initial Temperature Profiles in Soils. In , 253–256. doi:10.1109/ICSET.2008.4747012.

Michopoulos, A., Papakostas, K. T., Mavrommatis, T., and Kyriakis, N. [2010]. Comparative Assessment of Eight Models Predicting the Ground Temperature. *JP J. Heat Mass Transf.* **4** (2): 119–135.

Mihalakakou, G., Santamouris, M., Lewis, J. O., and Asimakopoulos, D. N. [1997]. On the Application of the Energy Balance Equation to Predict Ground

Temperature Profiles. *Sol. Energy* **60** (3–4): 181–190. doi:10.1016/S0038-092X(97)00012-1.

Monteith, J. L. [1961]. An Empirical Method for Estimating Long-Wave Radiation Exchanges in the British Isles. *Q. J. R. Meteorol. Soc.* **87** (372): 171–179. doi:10.1002/qj.49708737206.

Nabi, M. and Al-Khoury, R. [2012]. An Efficient Finite Volume Model for Shallow Geothermal systems—Part II: Verification, Validation and Grid Convergence. *Comput. Geosci.* **49** (December): 297–307. doi:10.1016/j.cageo.2012.03.023.

Nam, Y., Ooka, R., and Hwang, S. [2008]. Development of a Numerical Model to Predict Heat Exchange Rates for a Ground-Source Heat Pump System. *Energy Build.* **40** (12): 2133–2140. doi:10.1016/j.enbuild.2008.06.004.

National Meteorological Library and Archive. [2014]. Observations: Weather Observations over Land. 17 version 1. Fact Sheets. Meteorological Office. http://www.metoffice.gov.uk/media/pdf/p/6/10_0230_FS_17_Observations.pdf.

Nobre, R. C. M. and Thomson, N. R. [1993]. The Effects of Transient Temperature Gradients on Soil Moisture Dynamics. *J. Hydrol.* **152** (1–4): 57–101. doi:10.1016/0022-1694(93)90141-U.

P.-E. Jansson. [2012]. CoupModel: Model Use, Calibration, and Validation. *Trans. ASABE* **55** (4): 1337–1346. doi:10.13031/2013.42245.

Penman, H. L. [1948]. Natural Evaporation from Open Water, Bare Soil and Grass. *Proc. R. Soc. Lond. Ser. Math. Phys. Sci.* **193** (1032): 120 –145. doi:10.1098/rspa.1948.0037.

Philip, J. R. and de Vries, D. A. [1957]. Moisture Movement in Porous Materials under Temperature Gradients. *Trans. Am. Geophys. Union* **38** (2): 222–232.

Pielke, R. A. [1984]. *Mesoscale Meteorological Modeling*. Academic Press.

P. Koorevaar, G. M. and C. D., ed. [1983]. Heat Transport in Soil. In , Volume 13:193–207. Elements of Soil Physics. Elsevier. http://www.sciencedirect.com/science/article/pii/S0166248108700540.

Qin, Z., Berliner, P., and Karnieli, A. [2002]. Numerical Solution of a Complete Surface Energy Balance Model for Simulation of Heat Fluxes and Surface Temperature under Bare Soil Environment. *Appl. Math. Comput.* **130** (1): 171–200. doi:10.1016/S0096-3003(01)00089-3.

Rajeev, P., Chan, D., and Kodikara, J. [2012]. Ground–atmosphere Interaction Modelling for Long-Term Prediction of Soil Moisture and Temperature. *Can. Geotech. J.* **49** (9): 1059–1073. doi:10.1139/t2012-068.

Rees, S. W., Adjali, M. H., Zhou, Z., Davies, M., and Thomas, H. R. [2000]. Ground Heat Transfer Effects on the Thermal Performance of Earth-Contact Structures. *Renew. Sustain. Energy Rev.* **4** (3): 213–265. doi:10.1016/S1364-0321(99)00018-0.

Rees, S. W., Zhou, Z., and Thomas, H. R. [2007]. Ground Heat Transfer: A Numerical Simulation of a Full-Scale Experiment. *Build. Environ.* **42** (3): 1478–1488.

Reeves, G. M., Sims, I., and Cripps, J. C. [2006]. *Clay Materials Used in Construction*. Geological Society.

Roberson, J. A. and Crowe, C. T. [1989]. *Engineering Fluid Mechanics*. 4Rev e. Houghton Mifflin.

Romero, E., Gens, A., and Lloret, A. [2001]. Temperature Effects on the Hydraulic Behaviour of an Unsaturated Clay. *Geotech. Geol. Eng.* **19** (3-4): 311–332. doi:10.1023/A:1013133809333.

Rumynin, V. G. [2012]. *Subsurface Solute Transport Models and Case Histories: With Applications to Radionuclide Migration*. Springer Science & Business Media.

Ryan, P. J., Harleman, D. R. F., and Stolzenbach, K. D. [1974]. Surface Heat Loss from Cooling Ponds. *Water Resour. Res.* **10** (5): 930–938. doi:10.1029/WR010i005p00930.

Santamouris, M. [2013]. Using Cool Pavements as a Mitigation Strategy to Fight Urban Heat island—A Review of the Actual Developments. *Renew. Sustain. Energy Rev.* **26** (October): 224–240. doi:10.1016/j.rser.2013.05.047.

Sartori, E. [2000]. A Critical Review on Equations Employed for the Calculation of the Evaporation Rate from Free Water Surfaces. *Sol. Energy* **68** (1): 77–89. doi:10.1016/S0038-092X(99)00054-7.

Sauer, T. J. and Horton, R. [2005]. Soil Heat Flux. In , edited by J. L. Hatfield, J. M. Baker, and M. K. Viney, 131–154. http://www.cabdirect.org/abstracts/20073105257.html;jsessionid=FAF31749DB5542E1A7541CBD2B0E829A.

Scholz, M. and Grabowiecki, P. [2007]. Review of Permeable Pavement Systems. *Build. Environ.* **42** (11): 3830–3836. doi:10.1016/j.buildenv.2006.11.016.

Sellers, W. D. [1965]. *Physical Climatology*. Chicago etc.: Univ.Chicago P.

Shang, Y., Li, S., and Li, H. [2011]. Analysis of Geo-Temperature Recovery under Intermittent Operation of Ground-Source Heat Pump. *Energy Build.* **43** (4): 935–943. doi:10.1016/j.enbuild.2010.12.017.

Shao, M., Horton, R., and Jaynes, D. B. [1998]. Analytical Solution for One-Dimensional Heat Conduction-Convection Equation. *Soil Sci. Soc. Am. J.* **62** (1): 123–128.

S. Pal Arya, ed. [1988]. Soil Temperatures and Heat Transfer. In , Volume 42:37–48. Introduction to Micrometeorology. Academic Press. http://www.sciencedirect.com/science/article/pii/S0074614208604192.

Svec, O. J. [1990]. *Spiral Ground Heat Exchangers for Heat Pump Applications*. Canada: Institute for Research in Construction National Research Council of Canada.

Svec, O. J., Goodrich, L. E., and Palmer, J. H. L. [1983]. Heat Transfer Characteristics of in-Ground Heat Exchangers. *Int. J. Energy Res.* **7** (3): 265–278. doi:10.1002/er.4440070307.

Swinbank, W. C. [1963]. Long-Wave Radiation from Clear Skies. *Q. J. R. Meteorol. Soc.* **89** (381): 339–348. doi:10.1002/qj.49708938105.

Thom, A., Stewart, J., Oliver, H., and Gash, J. [1975]. Comparison of Aerodynamic and Energy Budget Estimates of Fluxes Over a Pine Forest. *Q. J. R. Meteorol. Soc.* **101** (427): 93–105. doi:10.1002/qj.49710142708.

Tomasi, C. [1978]. On the Water Vapour Absorption in the 8–13 Mm Spectral Region for Different Atmospheric Conditions. *Pure Appl. Geophys.* **116** (6): 1063–1076. doi:10.1007/BF00874671.

Vasco, D. W. [2010]. On Fluid Flow in a Heterogeneous Medium under Nonisothermal Conditions. *Water Resour. Res.* **46** (12). Scopus. doi:10.1029/2010WR009571.

Vogel, C. A., Baldocchi, D. D., Luhar, A. K., and Rao, K. S. [1995]. A Comparison of a Hierarchy of Models for Determining Energy Balance Components over Vegetation Canopies. *J. Appl. Meteorol.* **34** (10): 2182–2196. doi:10.1175/1520-0450(1995)034<2182:ACOAHO>2.0.CO;2.

Wang, L., Gao, Z., Horton, R., Lenschow, D. H., Meng, K., and Jaynes, D. B. [2012]. An Analytical Solution to the One-Dimensional Heat Conduction–Convection Equation in Soil. *Soil Sci. Soc. Am. J.* **76** (6): 1978–1986. doi:10.2136/sssaj2012.0023N.

Wang, Z.-H. and Bou-Zeid, E. [2012]. A Novel Approach for the Estimation of Soil Ground Heat Flux. *Agric. For. Meteorol.* **154–155** (March): 214–221. doi:10.1016/j.agrformet.2011.12.001.

Winterkorn, H. F. [1962]. Behavior of Moist Soils in a Thermal Energy Field. In , edited by E. Ingerson, 85–103. Pergamon. http://www.sciencedirect.com/science/article/pii/B9781483198422500092.

Wood, C. [2009]. Investigations into Novel Ground Source Heat Pumps. PhD Thesis, Dept. for the Built Environment: University of Nottingham.

Woodside, W. and Messmer, J. H. [1961]. Thermal Conductivity of Porous Media. I. Unconsolidated Sands. *J. Appl. Phys.* **32** (9): 1688–1699. doi:10.1063/1.1728419.

Wu, Y., Gan, G., Verhoef, A., Vidale, P. L., and Gonzalez, R. G. [2010]. Experimental Measurement and Numerical Simulation of Horizontal-Coupled Slinky Ground Source Heat Exchangers. *Appl. Therm. Eng.* **30** (16): 2574–2583. doi:10.1016/j.applthermaleng.2010.07.008.

Xu, J., Wang, R. Z., and Li, Y. [2014]. A Review of Available Technologies for Seasonal Thermal Energy Storage. *Sol. Energy* **103** (May): 610–638. doi:10.1016/j.solener.2013.06.006.

Yumrutaş, R., Kanoğlu, M., Bolatturk, A., and Bedir, M. Ş. [2005]. Computational Model for a Ground Coupled Space Cooling System with an Underground Energy Storage Tank. *Energy Build.* **37** (4): 353–360. doi:10.1016/j.enbuild.2004.07.004.

Zhou, Z., Wang, X., Zhang, X., Chen, G., Zuo, J., and Pullen, S. [2015]. Effectiveness of Pavement-Solar Energy System – An Experimental Study. *Appl. Energy* **138** (January): 1–10. doi:10.1016/j.apenergy.2014.10.045.

Chapter 3 Theoretical framework

3.1 Introduction

In this Chapter governing equations that describe the transfer of heat and mass in soil and the flow of heat within pipe systems are presented. The key assumptions made in the development of these equations are that:

- the soil is non deformable. No change in the volume of the soil is associated with variations of moisture content, implying that a change in the volume of liquid water in a unit volume of soil is directly proportional to a change in the volume of air (and water vapour diffused) per unit volume of soil.
- the air phase is continuous and there are no occluded bubbles. It can be noted that an unsaturated soil with a continuous air phase generally has a degree of saturation less than approximately 80% (Fredlund and Rahardjo, 1993). Occluded air bubbles commonly occur in unsaturated soils having a degree of saturation greater than approximately 90% (Fredlund and Rahardjo, 1993).
- the water inside the pores is incompressible (since there are assumed to be no occluded air bubbles).
- the air phase is at a constant atmospheric pressure. In unsaturated soils the process of moisture transfer usually needs to take into account the diffusion of air in the pores. However, according to Rahardjo (1990), in some cases the pore-air pressure changes can be considered negligible. As a result the variation of pore-air pressure with respect to time can be set to zero and no differential equation for air diffusion needs to be solved. The explanation for this is that in the case of a continuous air phase, the excess pore-air pressures commonly undergo an almost instantaneous dissipation during the consolidation process. In other words, only the water phase undergoes a transient process during consolidation. This behaviour can be attributed to the significantly greater permeability with respect to the air phase than to the water phase. Barden and Pavlakis (1971) reported that the permeability with respect to the air phase can be five to seven orders of magnitude higher than the permeability with respect to the water phase.
- the soil is considered to remain unsaturated.

3.2 Conservation laws

Conservation laws are among the most fundamental principles in physics and appear at the base of many different physical processes. Conservation laws are applicable on closed systems (closed for the physical property under consideration) and generally establish that the amount of energy or matter (interchangeable in a fundamental way) must remain constant over time if it is not added nor removed from the system. This implies that energy or mass cannot be destroyed nor created but it can change its form (physical state, arrangement in space).

The law of conservation of energy, also known as first law of thermodynamics, is useful to describe the variation of temperature on a given region over time. It states that the total internal energy of the system E_i (J/m^3) during a process is equal to the thermal energy q_T (W/m^2) entering or leaving the system during that process (Çengel, 2003). This can be expressed, in a 1-dimensional system as:

$$\frac{\partial E_i}{\partial t} = -\frac{q_T(x+\Delta x) - q_T(x)}{\Delta x} \tag{3-1}$$

Taking the limit $\Delta x \rightarrow 0$

$$\frac{\partial E_i}{\partial t} = -\nabla \cdot q_T \tag{3-2}$$

where ∇ is the differential operator given by:

$$\nabla = \frac{\partial}{\partial x} + \frac{\partial}{\partial y} + \frac{\partial}{\partial z} \tag{3-3}$$

The expressions that define the average rates of heat flow depend on the specific characteristics of the problem and the physical process involved. Fourier's law (discussed below), describes heat conduction in solids but if more process are involved (e.g. internal heat generation, convection, advection) they also need to be considered in the right hand side of equation (3-2).

The law of conservation of mass can be used to develop a relationship between the change in pore-water pressure in a unit volume of soil with the amount of water entering and leaving that same volume. It states that the rate of change in the water content (liquid and vapour) in a closed volume is equal to the rate of change of the

total sum of flows into and out of the volume. The mathematical expression can be derived in a similar way to equation (3-2), it is given as:

$$\rho_w \frac{\partial \theta_w}{\partial t} = -\nabla q_w \qquad (3\text{-}4)$$

where ρ_w (kg/m^3) is the density of liquid water in the soil pore and θ_w is the volumetric moisture content. Equation (3-4) states that the variation in time of the volumetric moisture content is proportional to the divergence of the total moisture flow entering or leaving the system through its surfaces q_w (kg/sm^2). In equation (3-4) q_w and θ_w are assumed to take into account both liquid and vapour forms of moisture.

The specific expressions for the volumetric flow rates are usually defined by Darcy's law, which relates the net volumetric flow of liquid water in a volume of soil with the pressure gradients in it, and by Fick's law (for the case of water vapour) which relates the mass transfer of a diffusing substance across a unit area to the gradient of concentration of the diffusing substance.

Another application of the conservation of energy principle is in the consideration of surface energy balance. A surface does not have volume nor mass, and thus, has no energy but it can be viewed as a fictitious system whose energy content remains constant during a process (Çengel, 2003). In this way it is possible to keep track of the energy interactions at a surface when energy is transferred from one medium to another. The energy balance for a surface (e.g. the soil surface) can be expressed as:

$$q_{ss,in} = q_{ss,\text{out}} \qquad (3\text{-}5)$$

where $q_{ss,in}$ (W/m^2) is the net amount of energy reaching the soil surface and $q_{ss,out}$ (W/m^2) is the net amount of energy leaving it.

3.3 Fourier's law

Fourier's law describes the transfer of thermal energy within a body by conduction. It states that the rate of thermal energy transfer through a material is proportional to the temperature gradient and to the area through which the thermal energy flows. In its differential expression it is given by (per unit area):

$$q_h = -\lambda_b \nabla T \qquad (\mathrm{W/m^2}) \tag{3-6}$$

where T is the temperature of the material (˚C), λ_b (W/m^{2}K) is the bulk thermal conductivity of the material.

The thermal conductivity λ_b defined in equation (3-6) is a material property of the medium through which the thermal energy transfers. It usually depends on several physical parameters and is further discussed in section 3.5.2.

3.4 Darcy's law

Darcy's law is similar in form to Fourier's law and is used to describe the flow of water through a cross-sectional area of soil (porous medium). It states that the total discharge is proportional to the negative of the pressure gradient (i.e. the fluid flows from high pressure to low pressure). It is given by (per unit area):

$$q_w = -\rho_w \nabla K_{w,sat}(h + z) \tag{3-7}$$

where $K_{w,sat}$ (m/s) is the saturated hydraulic conductivity of the medium, h (m) is the pressure head and z (m) is the vertical coordinate and stands for the potential head relative to a datum. The saturated hydraulic conductivity $K_{w,sat}$ is given by:

$$K_{w,sat} = \frac{\kappa_s \rho_w g}{\mu_w(T)} \tag{3-8}$$

where g is the constant acceleration of gravity (m/s^2), μ_w (Pa s) is the viscosity of the liquid water respectively. κ_s (m^2) is the intrinsic permeability of the soil and is a measure of the ability of fluids to flow through it, it is a property of the soil related to its pore structure.

Equation (3-7) is used to calculate the flow of water in saturated soils due to pressure gradients. However, it can also be applied in unsaturated soils. In this case, the hydraulic conductivity $K_{w,}$ varies since part of the available routes for water flow are now occupied by air. In this case the hydraulic conductivity can be expressed as a function of the water content of the soil. Campbell (1974) offers a set of equations that relate the pressure head h, the (unsaturated) hydraulic conductivity K_w:

$$h(\theta_w) = h_{sat}\left(\frac{\theta_w}{\theta_{w,sat}}\right)^{-b} \tag{3-9}$$

$$K_w(\theta_w) = K_{w,sat}\left(\frac{\theta_w}{\theta_{w,sat}}\right)^{2b+3} \tag{3-10}$$

where h_{sat}, $\theta_{w,sat}$ are the values of pressure head and water content corresponding to a fully saturated soil. b is an index parameter which value depends on the type of soil under consideration. Garrat suggest b=11.4 for clay soils. Using K_w, equation (3-7) can be expressed as:

$$q_w = -\rho_w \nabla \cdot \left[K_w(\theta_w)(h+z)\right] \tag{3-11}$$

3.5 Heat and moisture diffusion in soils

The previous Sections discussed conservation principles and flow equations used to describe the transport of heat and moisture within soils. Movement of heat implies non isothermal conditions in the soil which could cause changes in the pore pressure equilibrium of water (Fredlund and Rahardjo, 1993). For example, changes in the temperature of the pore air can change the amount of water vapour that it can hold (this can be represented via consideration of the partial pressure of water vapour). The evaporation or condensation of water modifies the water pore-pressure while at the same time extracts or delivers energy to the soil thereby changing its temperature. These coupled changes in potentials and temperatures can result in moisture, air and water vapour migration and heat transfer within the soil. In addition the physical properties of water are, in principle, dependent on temperature, moisture content and/or pore-pressure (Rees et al., 2000). Soil thermal properties are also dependent on the soil's water content (Rees et al., 2000). Hence, the change in soil moisture content driven by moisture migration can have an impact on the overall thermal properties of the soil.

However, the relative strength of these coupled interdependencies is not equal (as discussed in Chapter 2) for example the variations found in the thermal properties due to changes in the moisture content are more significant than the changes in hydraulic properties due to thermal gradients (Rees et al., 2000). For this reason, a one-way coupling approach is used in this work. In this approach, a partial

differential equation that describes the diffusion of moisture in the soil is written independent of temperature, while the partial differential equation for the diffusion of heat takes into account the changes in the moisture content field through the thermal properties of the soil. Both equations are presented in the following Sections.

3.5.1 Moisture diffusion

Thomas and Rees (1990) used a potential based form of the Richards' equation to describe the process of infiltration into unsaturated clay. Richards' equation is based on the principles of conservation of mass (equation (3-4)) and Darcy's law (equation (3-11)) presented before. It can be expressed as:

$$\frac{\partial \theta_w}{\partial t} = \nabla \cdot \left[K_w(\theta_w) \nabla h \right] + \frac{\partial K_w(\theta_w)}{\partial z} \qquad (3\text{-}12)$$

θ_w can be expressed as a function of h rearranging equation (3-9) and using the chain rule:

$$\frac{\partial \theta_w}{\partial h}\frac{\partial h}{\partial t} = \nabla \cdot \left[K_w(\theta_w) \nabla h \right] + \frac{\partial K_w(\theta_w)}{\partial z} \qquad (3\text{-}13)$$

where $\partial\theta_w/\partial h$ is defined as the specific moisture capacity, i.e. the relationship between the volumetric moisture content and the pressure head. The unsaturated hydraulic conductivity K_w is a function of the moisture content and need to be estimated using equation (3-10).

Equation (3-13) is written in terms of pressure head only and can be used to obtain the pressure head field in the soil that in turn can be used to obtain the moisture content field using equation (3-9). This information can be used to estimate the thermal properties of the soil since, as discussed in Chapter 2, they are in general a function of the moisture content.

3.5.2 Heat diffusion

The partial differential equation for heat flow is obtained using the energy conservation principle given by equation (3-2) and Fourier's law stated by equation (3-6). The bulk volumetric heat content in a volume of soil can be expressed as (using the relations presented in Chapter 2 and assuming a negligible contribution from air) as:

$$E_i = \left[(1-\theta_w)\rho_s c_{p,s} + \theta_w \rho_w c_{p,w} \right] T_{s,K} \quad (3\text{-}14)$$

where ρ_s (kg/m^3) is the soil density and $c_{p,s}$ (J/kgK)and $c_{p,w}$ (J/kgK) are the specific heat capacities of the soil and water respectively. $T_{s,K}$ (K) is the absolute temperature of the soil. Defining the bulk volumetric heat capacity of the soil, $C_{p,b}$ (J/m^{3}K), as:

$$C_{p,b} = (1-\theta_w)\rho_s c_{p,s} + \theta_w \rho_w c_{p,w} \quad (3\text{-}15)$$

Substituting equation (3-14), equation (3-15) and equation into equation (3-6):

$$C_{p,b} \frac{\partial T_s}{\partial t} = \nabla \left(\lambda_b \nabla T_s \right) \quad (3\text{-}16)$$

The soil's bulk thermal conductivity λ_b (as discussed in Chapter 2) is dependent on the soil water content. The use of absolute temperature is no longer required due to the derivation with respect to time.

Equation (3-16) assumes that heat is transferred in the soil only by conduction. As seen in Section 2.2 and 2.6 of Chapter 2, conduction is the dominant heat transfer process in soils and this approach is commonly used (Rees et al., 2007) (as seen in Section 2.6.2 of Chapter 2) to study the heat transfer interactions between the soils and buried thermal devices whenever no significant advection processes are expected to happen in the soil's domain.

3.6 Heat advection

The previous Sections have discussed the process of diffusion of moisture and heat within soils. An additional physical process commonly involved in the interaction between soils and buried thermal devices is advection. Advection is a physical process whereby energy (e.g. heat) or substances (dissolved ions) are transported by means of the bulk motion of a carrier fluid. Examples of this are the transport of pollutants in rivers or heat in pipes (when the fluid is being pumped by an external agent). In this study this physical process is considered in order to describe the transport of thermal energy between a heat exchanger (usually comprised of a set of pipes with a carrier fluid running inside) buried in the ground and an external application. The variation of temperature in a given region due to the advection of thermal energy by movement of a fluid can be expressed as (in one dimension)(Carslaw and Jaeger, 1986; Pérez Guerrero et al., 2009):

$$\rho_f c_{p,f} \left(\frac{\partial T_f}{\partial t} + u_f \frac{\partial T_f}{\partial x} \right) = Q_f \qquad (3\text{-}17)$$

where u_f (m/s) is the velocity vector field that describes the fluid's motion, T_f (˚C), ρ_f (kg/m^3) and $c_{p,f}$ (J/kgK) are its temperature, density and specific heat capacity. Q_f (W/m^3) takes into account heat generation inside the pipes.

It is worth noting that the advection process is assumed to occur only within the pipes constituting a buried heat exchanger while the thermal interaction between these pipes and ground is treated as a boundary condition (for the soil domain) using the transport equations for heat and moisture presented before in Sections 3.5.1 and 3.5.2. This thermal interaction can be treated, for the pipe domain, as an internal heat source using the term Q_f to represent the energy transferred through the pipe's boundaries (W/m^2), integrated on the area of the pipe's element in contact with the soil domain and then distributed on its corresponding volume (W/m^3). This approach is applicable if the relative size between the soil and pipe domains allows the latter to be treated as 1 dimensional. The thermal properties of the fluid inside the pipes are in general a function of its temperature and, together with the fluid's velocity, will affect the amount of energy transferred with the surrounding domain through the pipes boundaries.

Appendix A offers an analysis of the temperature dependence of the physical properties of a common fluid used in thermal engineering applications.

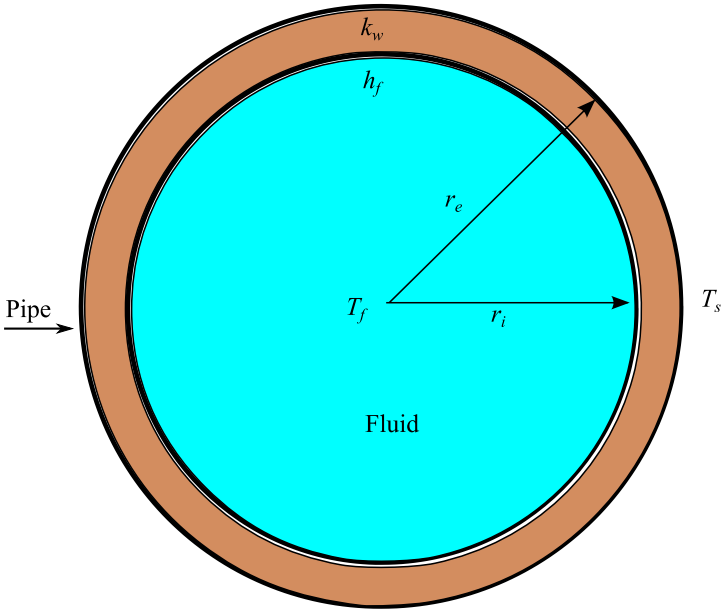

Figure 3-1 - Cross section of one pipe illustrating the main variables involved in heat transfer between surrounding soil and interior fluid

3.6.1 Heat transfer between fluid and solid

Figure 3-1 shows the main variables involved in the heat transfer between the fluid in the interior of the pipes and the surrounding soil. Where r_i (m) is the internal pipe radius, r_e (m) is the external pipe radius, λ_{pw} (W/mK) is the thermal conductivity of the pipe wall, h_f (W/m^{2}K) is the convective heat transfer coefficient between the fluid inside the pipe and the pipe's wall, T_f (˚C) is the fluid temperature at the cross-section and T_s (˚C) is the temperature of the soil directly in contact with the pipes, it is assumed to be equal to the temperature of the exterior pipe walls.

The heat Q_p (W) transferred across the wall of a pipe of length L_p (m) is driven only by conduction (the temperature at the external surface of the wall is assumed to be known and equal to the temperature of the soil directly in contact with it) and is given by (Çengel, 2003):

$$Q_p = 2\pi L_p \lambda_{pw} \frac{T_s - T_{pw}(r_i)}{\ln\left(r_e / r_i\right)} \tag{3-18}$$

where T_{pw} (˚C) is the temperature of the pipe wall. Equation (3-18) is obtained from integrating the Fourier heat equation in cylindrical coordinates across the cylindrical layer of the pipe's wall:

$$Q_p = 2\pi r L_p \lambda_{pw} \frac{dT_{pw}}{dr} \tag{3-19}$$

$$\frac{Q_p}{2\pi r L_p} = \lambda_{pw} \frac{dT_{pw}}{dr} \tag{3-20}$$

$$\int_{r_i}^{r_e} \frac{Q_p}{2\pi r L_p} dr = \int_{T_{pw(r_i)}}^{T_s} \lambda_{pw} dT_{pw} \tag{3-21}$$

The result of the integration of (3-21) is precisely (3-18). Equation (3-18) can be rearranged to resemble Ohm's law for electrical networks:

$$Q_p = \frac{T_s - T_{pw}(r_i)}{\ln\left(r_e / r_i\right) / 2\pi L_p \lambda_{pw}} \tag{3-22}$$

where the denominator corresponds to a thermal resistance, this is, a resistance to the flow of thermal energy across the pipe wall.

The heat transferred between the fluid in the interior of the pipe and its wall is given by forced convection (as the fluid is assumed to be pumped). The temperature profile at the interior of the pipe is neglected and a constant temperature for the cross-section is assumed (although variable along the pipe). The heat transfer is given by:

$$Q_p = 2\pi r_i L_p h_f \left(T_{pw}(r_i) - T_f\right) \tag{3-23}$$

where h_f (W/m^{2}K) is the convective heat transfer coefficient between the fluid and the pipe wall. Equation (3-23) can be rearranged in the same way as (3-22) to give:

$$Q_p = \frac{\left(T_{pw}(r_i) - T_f\right)}{\frac{1}{2\pi r_i L_p h_f}} \tag{3-24}$$

where the denominator in (3-24) has the same physical meaning as in (3-22), this is, a resistance to the flux of thermal energy but in this case in the interface between the pipe wall and the fluid.

Heat transfer in equation (3-22) and equation (3-24) are expressed using the same symbol, Q_p, on purpose since both equations must have the same value (as there are

no thermal sources nor sinks in the pipe wall). Then, following with the electrical network analogy, it is possible to obtain a total resistance by adding up the individual resistances in series. This would be the total resistance to the flux of thermal energy from the fluid inside the pipes to the soil surrounding them. That is:

$$Q_p = \frac{\left(T_s - T_f\right)}{\left(\frac{\ln\left(r_e / r_i\right)}{2\pi L_p \lambda_{pw}}\right) + \left(\frac{1}{2\pi r_i L_p h_f}\right)} \tag{3-25}$$

$$Q_p = \frac{\left(T_s - T_f\right) A_i}{U_p} \tag{3-26}$$

where A_i (m^2) is the pipe internal area defined as $A_i=2\pi r_i L_p$ and U_p (W/m^2K) is the pipe overall heat transfer coefficient defined as:

$$U_p = \left(\frac{r_i \ln\left(r_e / r_i\right)}{\lambda_{pw}}\right) + \left(\frac{1}{h_f}\right) \tag{3-27}$$

It is possible to express equation (3-26) per unit area as:

$$q_p = \frac{Q_p}{A_i} = \frac{\left(T_s - T_f\right)}{U_p} \tag{3-28}$$

All terms in equation (3-28) are known (or assumed to be known) except for h_f, the convective heat transfer coefficient. This coefficient can be calculated from:

$$\mathrm{Nu} = \frac{h_f L_c}{\lambda_f} \tag{3-29}$$

where Nu is the Nusselt number and L_c is the characteristic length of the pipe, in this case, its internal diameter and λ_f (W/mK) is the thermal conductivity of the fluid. The Nusselt number is the dimensionless convection heat transfer coefficient and physically represents the enhancement of heat transfer through a fluid layer as a result of convection relative to conduction across the same fluid layer. The larger the

Nusselt number the more effective the convection is. If this value is known is possible to solve (3-29) for the convective coefficient h_f.

Since there are several relations to calculate Nu (Çengel, 2003) depending on the regime of the fluid (i.e. laminar, transitory or turbulent), it is necessary to determine this regime first. This is given by the Reynolds number:

$$\mathrm{Re} = \frac{\rho_f \upsilon_m L_c}{\mu_f} \tag{3-30}$$

where υ_m (m/s), ρ_f (kg/m^3) and μ_f (kg/ms) are the mean velocity, density and dynamic viscosity of the fluid inside the pipes.

It is important to mention the criteria used to define where the fluid is laminar, transitional or turbulent. For example, Çengel (2003) says that the transitional region is 2300<Re<10000 and that values lower than 2300 assure laminar behaviours while values greater than 10000 assure turbulent ones. However, Roberson and Crowe (1989) mention that although it is possible to maintain laminar regimes at high Reynolds numbers, these regimes are unstable and subjected to become turbulent when there are vibrations present. In most engineering applications there are vibrations involved (as is the case of highways) and it is expected that the transitional region to be narrower. For this reason the limits offered by Roberson and Crowe have been adopted, they define the transitional region as 2000 < Re < 4000 for smooth pipes. A smooth pipe is defined as one where the size of the irregularities on the internal surface relative to the diameter of the pipe is less than 0.00001 (Çengel, 2003).

If the fluid is subjected to a laminar regime, the Nusselt number is constant provided that either constant heat flux (Nu=4.36) or constant temperature (Nu=3.66) can be assumed at the pipe wall (Çengel, 2003). If the fluid is undergoing a turbulent regime the Gnielinski modified equation is suitable to calculate the Nusselt number (Çengel, 2003):

$$\mathrm{Nu} = \frac{\left(\frac{f}{8}\right)(\mathrm{Re}-1000)\,\mathrm{Pr}}{1+12.7\left(\frac{f}{8}\right)^{0.5}\left(\mathrm{Pr}^{0.66}-1\right)} \qquad \begin{pmatrix} 0.5 \le \mathrm{Pr} \le 2000 \\ 3\mathrm{x}10^3 < \mathrm{Re} < 5\mathrm{x}10^6 \end{pmatrix} \tag{3-31}$$

where Pr is the Prandtl number and *f* is the friction factor. The dimensionless Prandtl number describes the relative thickness of the velocity and the thermal boundary layers. It relates the molecular diffusivity of momentum and the molecular diffusivity of heat and is given by (Abu-Hamdeh, 2003):

$$Pr = \frac{\mu_f c_{p,f}}{\lambda_f} \tag{3-32}$$

where $c_{p,f}$ (J/kgK) is the specific heat capacity of the fluid.

f in equation (3-31) is the friction factor and depends on the regime of the fluid and (in case of turbulent regimes) on the level of roughness of the surface in contact with the fluid (Çengel, 2003). The expression for *f* in the laminar regime is given by:

$$f = \frac{64}{\mathrm{Re}} \qquad \mathrm{Re} < 2000 \tag{3-33}$$

Whilst in t turbulent regimes (for smooth surfaces) is given by (Çengel, 2003):

$$f = \left(0.790\ln\left(\mathrm{Re}\right) - 1.64\right)^{-2} \qquad \mathrm{Re} > 4000 \tag{3-34}$$

While in the transitional regime there is no clearly defined expression for the friction factor the behaviour in this region can be assumed to be linear (Roberson and Crowe, 1989) and so it is possible to calculate a linear expression based on the equations for the friction factor on the limits of this region. This expression has the form:

$$f = \frac{\frac{64}{\mathrm{Re}} - \left(0.79\ln\left(\mathrm{Re}\right) - 1.64\right)^{-2}}{2000 - 4000}\left(\mathrm{Re} - 2000\right) + \frac{64}{\mathrm{Re}} \tag{3-35}$$

With equation (3-33), equation (3-34) and equation (3-35) all the possible regimes for the fluid inside the pipe are covered

Finally, with the formulation presented in this Section is possible to solve equation (3-29) and obtain the convective heat transfer coefficient h_f. Appendix B summarizes results for h_f for typical temperatures and mean velocities.

3.6.2 Heat exchangers efficiency

In geotechnical and geo-environmental applications, heat exchangers are devices that facilitate the exchange of heat between a fluid and the surrounding soil. The process of heat transfer in heat exchangers usually involves convection in the fluid flowing through a pipe or duct and conduction through the wall separating the fluid from the soil. In the analysis of heat exchangers, it is convenient to work with an overall heat transfer coefficient U_p (given by equation (3-27)) that accounts for the contribution of these effects on heat transfer. The rate of heat transfer between the fluid and the soil at a location in the pipes comprising the heat exchanger depends on the magnitude of the temperature difference at that location, which varies along the pipe.

There are two main approaches in the analysis of heat exchangers: the logarithmic mean temperature difference (LMTD), which is an equivalent mean temperature difference between the fluid and the surrounding environment for the entire heat exchanger and it is used to dimensioning the heat exchanger when the desired inlet and outlet temperatures are known; and the effectiveness–NTU method, which allows to analyze heat exchangers when the outlet temperature of the fluid is not known. The effectiveness-NTU method enables to determine the heat transfer rate without knowing the outlet temperature of the fluid. It depends on the geometry of the heat exchanger as well as the flow arrangement. Therefore, different types of heat exchangers have different effectiveness relations. The heat transfer effectiveness is defined as:

$$\varepsilon_p = \frac{Q_{real}}{Q_{max}} \tag{3-36}$$

where Q_{real} (W) is the actual heat transfer rate and Q_{max} (W) is the maximum possible heat transfer rate. Q_{real} can be determined from a heat balance on the pipe:

$$Q_{real} = c_{p,f}\dot{m}_f\left(T_{f,o} - T_{f,i}\right) \tag{3-37}$$

where is the $\dot{m}_f$ (kg/s) is the mass flow rate of the fluid flowing through the pipe. Q_{real} will be positive is the fluid is being heated and negative otherwise. $T_{f,i}$ (˚C) and $T_{f,i}$ (˚C) are the temperatures at the inlet and outlet of the pipe respectively.

The maximum possible heat transfer rate, Q_{max}, is proportional to the maximum temperature difference in the heat exchanger. In the context of geo-environmental

thermal applications, the heat exchanger pipes are commonly in contact with soil. If the temperature of soil in contact with a pipe can be considered to remain constant along the direction of the flow in a time step in a transient analysis, then Q_{max} can be expressed as:

$$Q_{max} = c_{p,f}\dot{m}_f\left(T_s - T_{f,i}\right) \tag{3-38}$$

where T_s (˚C) is the temperature of the soil. As can be seen in equation (3-37). The determination of Q_{max} requires the availability of the inlet pipe temperature and its mass flow rate.

The amount of energy being transferred from a differential section of the pipe is proportional to the specific heat capacity of the fluid, the mass flow rate and the change in temperature in the differential section, this is:

$$dQ_p = \dot{m}_f c_{p,f} dT_f \tag{3-39}$$

The energy transferred from the differential section can also be expressed using equation (3-26) as:

$$dQ_p = U_p\left(T_s - T_f\right)dA_i \tag{3-40}$$

Substituting equation (3-40) into equation (3-39) and integrating dT_f from between the pipe inlet and outlet:

$$\ln\left(\frac{T_s - T_{f,o}}{T_s - T_{f,i}}\right) = -\frac{U_p A_i}{\dot{m}_f c_{p,f}} \tag{3-41}$$

Solving equation (3-37) for $T_{f,o}$ and substituting into equation (3-41):

$$\frac{T_s - T_{f,i} - \dfrac{Q_{real}}{\dot{m}_f c_{p,f}}}{T_s - T_{f,i}} = \exp\left(-\frac{U_p A_i}{\dot{m}_f c_{p,f}}\right) \tag{3-42}$$

Using the definition of Q_{max} in equation (3-38) and equation (3-36) it is possible to obtain an expression for the heat transfer effectiveness:

$$\varepsilon_p = 1 - \exp\left(-\frac{U_p A_i}{\dot{m}_f c_{p,f}} \right) \tag{3-43}$$

Using equation (3-43) it is possible to calculate the pipe heat transfer (per square meter) and the outlet temperature from equation (3-40) and equation (3-38) like:

$$q_p = \varepsilon_p \dot{m}_f c_{p,f} \left(T_s - T_{f,i} \right) \tag{3-44}$$

$$T_{f,o} = \frac{q_p}{\dot{m}_f c_{p,f}} + T_{f,i} \tag{3-45}$$

3.7 Energy balance at the soil surface

This Section introduces the general relations that describe thermal energy interactions at the surface of the soil and act as boundary conditions for the moisture and heat transfer equations presented earlier. These interactions are, in the moisture aspect: evaporation and precipitation; and in the thermal: solar radiation, infrared radiation, convection and evaporation.

3.7.1 Solar radiation

The sun emits radiation in several regions of the electromagnetic spectrum. However, the term solar radiation is commonly referred to the radiation located in the visible range (0.4 μm-0.7 μm) (Duffie and Beckman, 2006). The part of the radiation in this region, solar radiation that reaches the Earth and arrives to a surface directly is known as beam radiation. Another part arrives after being scattered by the atmosphere or by other surfaces and is called diffuse radiation. The sum of these two types gives the total solar radiation or global radiation R (W/m^2) which is typically reported in meteorological measurements (Duffie and Beckman, 2006). The amount of this radiation that effectively contributes to the energy balance of a surface is defined by equation (2-8).

When objects in the proximity of a surface are placed in such a way that they have the possibility to block the solar radiation reaching the surface, they cast a shadow and reduce the thermal energy received by it. In general, the shadow cast by an object will move during the day and will vary its position and size through the year due to the seasonal diurnal and seasonal variation of the position of the sun in the sky (Duffie and Beckman, 2006). However, in this work a simplified method to take

into account the shadow cast by near objects over a surface is proposed. This method is expected to be applicable in situations where the detailed seasonal evolution of the shading is not essential. The method involves weighting of the solar radiation calculated with equation (2-8) by a suitable factor:

$$q_{sh} = q_s D_{sh} \tag{3-46}$$

where q_{sh} (W/m^2) is the solar radiation reaching the surface after being blocked (complete or partially) by the object and D_{sh} is the shading factor that takes values between 1 for a complete transparent object and 0 for a fully opaque object.

3.7.2 Infrared radiation

Radiative interaction also occurs in the infrared range of the electromagnetic spectrum. Infrared radiation is generated by the vibration of the molecules present in a body (thermal energy), in this way it is a volumetric radiation, but in general the radiation generated by molecules inside the body are quickly absorbed by the body itself and, so, infrared radiation can be seen as a surface phenomenon. It is proportional to the fourth power of the absolute temperature of the surface, the Stefan-Boltzmann constant, σ (W/m^{2}K^4), and an emissivity factor, ε, that depends on the material and defines the ability of the surface to emit infrared radiation. This heat transfer process takes place between 2 or more surfaces each with its optical properties. The amount of radiation that reaches each surface depends on the view factor, this is a geometrical factor that defines the amount of radiation that can reach a surface in any given arrangement. Beckman (Beckman, 1971) gives a relation to define the net heat transfer, Q_I (W), for any surface in any N-surface arrangement, but in practice, many heat transfer problems involve radiation between two surfaces, for this particular case, the heat transfer process can be defined as (Duffie and Beckman, 2006):

$$Q_{I,1} = -Q_{I,2} = \frac{\sigma(T_{2,\mathrm{K}}^4 - T_{1,\mathrm{K}}^4)}{\frac{1-\varepsilon_1}{\varepsilon_1 A_1} + \frac{1}{A_1 F_{12}} + \frac{1-\varepsilon_2}{\varepsilon_2 A_2}} \tag{3-47}$$

where $Q_{I,1}$ (W) is the heat transferred from surface 1, $Q_{I,2}$ (W) is the heat transferred from surface 2, F_{12} is the total view factor between surfaces 1 and 2 and takes into account the radiation exchange between the surfaces directly and by all possible

specular reflections, A_1 and A_2 (m^2) are the respective areas of surface 1 and 2. A particular case of equation (3-47) of interest in the context of this work is when a relatively small convex object (surface 1) is surrounded by a large enclosure (surface 2). In the context of this work, this case relates to the heat transfer process between the soil (surface 1) and the atmosphere (or sky, surface 2). Under these conditions, the area ratio A_1/A_2 approaches zero, the view factor F_{12} is unity and equation (3-47) can be expressed by equation (2-9) which can be rewritten as:

$$q_I = \varepsilon_{ss}\sigma\left(T_{sky,\mathrm{K}}^4 - T_{ss,\mathrm{K}}^4\right) \tag{3-48}$$

where ε_{ss} is the emissivity of the soil's surface, $T_{ss,K}$ (K) and $T_{sky,K}$ (K) are the absolute temperatures of the soil surface and sky respectively.

The atmosphere is commonly treated as a surface (as if it were a dome) surrounding the soil. However, the atmosphere is actually composed of several layers of gas, each one of them at different temperatures and chemical composition and in continuous movement. These attributes define the radiative characteristics of the atmosphere, in particular the infrared absorption bands of water vapour result in what is termed an 'atmospheric window' between 8 and 14 μm (Duffie and Beckman, 2006; Tomasi, 1978). In this window, the atmosphere is basically transparent to infrared radiation, while outside of it the infrared radiation is mostly absorbed. In conjunction, these properties determine the net incoming long wave radiation from the sky. The atmosphere as a surface is usually treated as a black body at an equivalent sky temperature $T_{sky,\mathrm{K}}$. This model in turn is commonly transformed to a grey surface model (with emissivity different from 1 and possibly wavelength and directionally dependent), where the temperature of the atmosphere is assumed to be equal to some temperature measured at ground level (commonly air temperature), and with an equivalent emissivity ε_{sky} that takes into account the previously mentioned atmospheric complexities. Several relations have been proposed to relate $T_{sky,\mathrm{K}}$ to measured meteorological variables such as vapour pressure and air temperature, as discussed in the literature review of this work (Berdahl and Martin, 1984; Brunt, 1932; Fund and Ångström, 1915; Iziomon et al., 2003; Monteith, 1961; Swinbank, 1963). In general these relations adopt the following form:

$$T_{sky,\mathrm{K}} = \varepsilon_{sky} T_{a,\mathrm{K}}^4 \tag{3-49}$$

where $T_{a,K}$ (K) is the absolute air temperature.

Equation (3-48) depends on the fourth power of the absolute temperature of the surface and its computational implementation would be difficult without using specialized solvers to handle non-linear equations. However, to retain the simplicity of linear equations, a linearization procedure is commonly followed as proposed in (Duffie and Beckman, 2006). In this procedure equation (3-48) can be expressed as:

$$\begin{aligned} q_I &= \sigma\varepsilon_{ss}(T_{sky,\mathrm{K}}^4 - T_{ss,\mathrm{K}}^4) \\ &= \sigma\varepsilon_{ss}(T_{sky,\mathrm{K}}^2 + T_{ss,\mathrm{K}}^2)(T_{sky,\mathrm{K}} + T_{ss,\mathrm{K}})(T_{sky,\mathrm{K}} - T_{ss,\mathrm{K}}) \\ &\approx 4\sigma\varepsilon_{ss}\left(\frac{T_{sky,\mathrm{K}} + T_{ss,\mathrm{K}}}{2}\right)^3\left(T_{sky,\mathrm{K}} - T_{ss,\mathrm{K}}\right) \end{aligned} \tag{3-50}$$

where the following equivalence have been performed (Duffie and Beckman, 2006):

$$\sigma\varepsilon_{ss}(T_{sky,\mathrm{K}}^2 + T_{ss,\mathrm{K}}^2)(T_{sky,\mathrm{K}} + T_{ss,\mathrm{K}}) = 4\sigma\varepsilon_{ss}\left(\frac{T_{sky,\mathrm{K}} + T_{ss,\mathrm{K}}}{2}\right)^3 \tag{3-51}$$

Figure 3-2 shows the comparison of the left hand side (linear coefficient, dotted line) and the right hand side (real coefficient, solid line) of equation (3-51) as a function of the difference in temperature between the sky and the soil surface. It can be seen that both approaches are offer comparable results for differences of up to 50 K.

From equation (3-50), thus, is possible to define an infrared heat transfer coefficient h_{long} (W/m^{2}K) as:

$$\begin{aligned} h_I &= 4\sigma\varepsilon_{ss}\left(\frac{T_{sky,\mathrm{K}} + T_{ss,\mathrm{K}}}{2}\right)^3 \\ &= 4\sigma\varepsilon_{ss}T_*^3 \end{aligned} \tag{3-52}$$

where T_* (K) is the average absolute temperature between $T_{sky,\mathrm{K}}$ and $T_{ss,\mathrm{K}}$. It is not difficult to estimate T_* even without actually knowing both $T_{sky,\mathrm{K}}$ and $T_{ss,\mathrm{K}}$, using for example previous time step value in a numerical solution of a transient initial value problem.

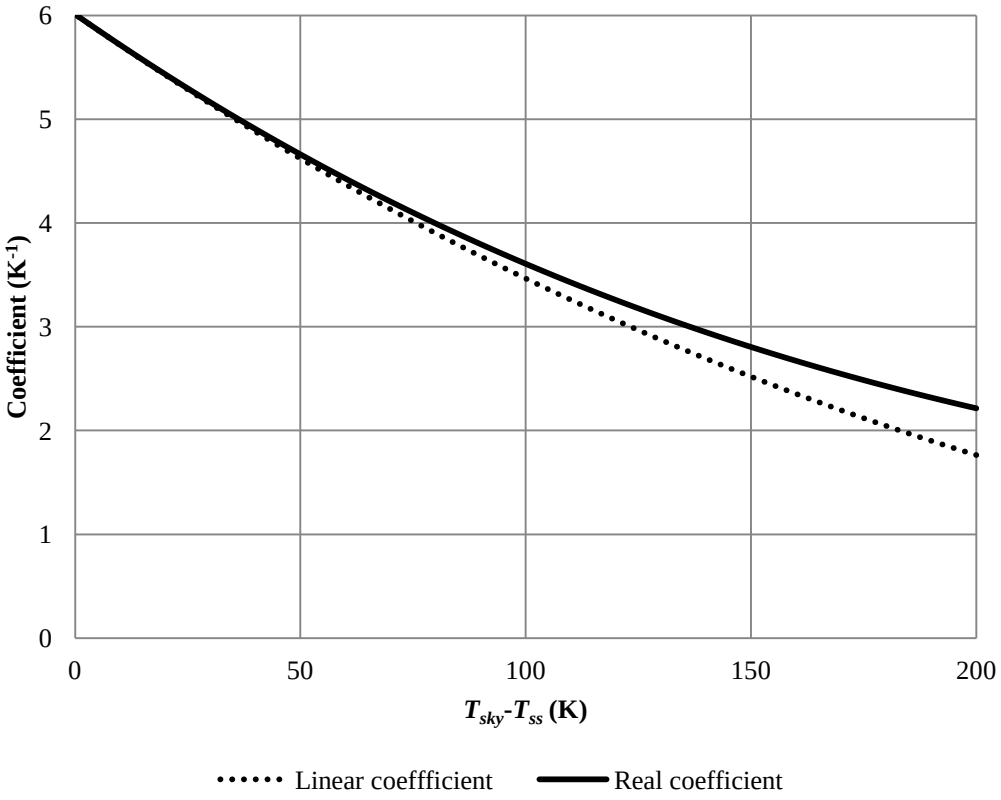

Figure 3-2 - Comparison of the linear and real coefficients for the infrared heat transfer process (assuming ε_{ss}=1).

3.7.3 Air convection

The convective heat flux comes from the interaction of a fluid with a solid, in this case, the atmospheric air and the soil surface. There are two main mechanisms in which convection arise. Forced convection in which the fluid is forced to flow over the surface by external forces; and natural convection in which the movement of the fluid is driven by thermal gradients. In principle, both effects should be taken into account when describing the convective heat flux between the surface of the soil and the atmosphere. However, the relative importance of each process depends on the fluid conditions (i.e. wind speed) and the surface characteristics (e.g. roughness, temperature). In general (Edinger and Brady, 1974; Jansson et al., 2006), the convective heat flux between the soil surface and the atmosphere is commonly expressed using Newton's law of cooling in which the rate of heat transfer per unit area is proportional to the difference between the soil surface temperature and air temperature. Following this approach yields:

$$q_C = h_C \left(T_{ss} - T_a \right) \tag{3-53}$$

where q_c (W/m^2) is the convective heat flux, h_C (W/m^{2}K) is the convective heat transfer coefficient that, as discussed above, is dependent on the fluid characteristics and surface conditions, T_{ss} (˚C) is the soil surface temperature and T_a (˚C) is the temperature of the air.

3.7.4 Evaporation

The evaporation from a soil surface into the atmosphere is usually expressed using Dalton's law of partial pressures (Penman, 1948). In this approach, the evaporation process is driven by the difference between the water vapour pressure on the (saturated) soil surface and the atmospheric saturation water vapour pressure. As discussed in Section 2.4 of Chapter 2, this model was adopted by Penman (1948) who assumed a saturated surface and later by Philip and de Vries (1957) whom introduced a '*soil moisture availability factor*' to take into account the fact that the surface might not be saturated. This factor is equivalent to a relative humidity for the soil surface. In general, the heat flow due to evaporation is given by:

$$q_E = h_E \left(e_a - e_{ss} \right) \tag{3-54}$$

where q_E (W/m^2) is the heat transfer rate per unit area by evaporation, e_a (kPa) is the atmospheric saturation vapour pressure, h_E (W/m^2) is the heat transfer coefficient by evaporation and e_{ss} (kPa) is the water vapour pressure at the saturated soil surface given by (Philip and de Vries, 1957):

$$e_{ss} = \exp\left(-\frac{h_{ss} g}{R_w T_{ss,\mathrm{K}}} \right) e_{ss,sat}(T_{ss}) \tag{3-55}$$

where h_{ss} (m) is the pressure head at the soil surface, g (9.81 m/s^2) is the acceleration due to gravity, R_w (461.5 J/kgK) is the gas constant for water vapour, $e_{ss,sat}$ (kPa) is the saturation vapour pressure at the soil surface. As in the convective heat transfer process, h_E depends on the specific conditions of the fluid and the surface characteristics. The atmospheric saturation water vapour pressure, $e_{a,sat}$, can be calculated according to North and Erukhimova (2009) from the integration of the Clausius-Clapeyron equation (the same equation can be applied for $e_{ss,sat}$):

$$e_{a,sat}(T_a) = e_a(0) \exp\left(\frac{L_{vap}}{R_w} \left(\frac{1}{273.15\mathrm{K}} - \frac{1}{T_{a,\mathrm{K}}} \right) \right) \tag{3-56}$$

where $ea(0)$ is the water vapour pressure at 0 ˚C (0.611 kPa) (North and Erukhimova, 2009), L_{vap} (J/kg) is the latent heat of vaporization of water, R_w (J/kgK) is the gas constant for water vapour.

It can be seen that equation (3-54) is non-linear due to the exponential nature of $e_{a,sat}$ and $e_{ss,sat}$. Deardorff (1978) proposed the following procedure to linearize $e_{a,sat}$:

$$e_{a,sat}(T_a^{n+1}) = e_{a,sat}(T_a^n) + \left(\frac{\partial e_{a,sat}}{\partial T_a}\right)_{T_a^n}\left[T_a^{n+1} - T_a^n\right] \tag{3-57}$$

where the superscripts n and n+1 indicate a previous and a new estimates. A similar procedure can be applied to linearize e_{ss}.

3.7.5 Convective and evaporative heat transfer coefficients

In Chapter 2, three main approaches were discussed for the formulation of convective and evaporative heat transfer coefficients, namely: turbulent, non-turbulent and with the inclusion of a canopy cover. These formulations can be regarded as representative of the main approaches considered in the literature.

3.7.5.1 Turbulent coefficients

This approach is developed from the theory of atmospheric boundary layer and is applicable when the natural convective processes can be neglected due to the characteristics of the flow near the surface of the ground. In this approach the convective and evaporative heat transfer coefficients are given as:

$$h_C = \frac{\rho_a c_{p,a}}{r_a} \tag{3-58}$$

$$h_E = \frac{\rho_a c_{p,a}}{r_a \gamma} \tag{3-59}$$

where ρ_a (kg/m^3) and $c_{p,a}$ (J/kgK) are the density and specific heat capacity of air, γ (kPa/K) is the psychrometric constant. r_a (s/m) is the aerodynamic resistance of the soil surface expressed as:

$$r_a = \frac{1}{\kappa^2 u_s}\ln\left(\frac{z_u}{z_{0m}}\right)\ln\left(\frac{z_T}{z_{0T}}\right) \tag{3-60}$$

where κ is the Von Karman constant, u_s (m/s) is wind speed, z_0 (m) is the dynamic roughness of the soil, z_{0m} (m) is the momentum roughness, z_{0T} (m) is the roughness lengths for sensible heat and z_u (m) and z_T (m) are the reference height at which the measurements of wind speed and temperature are performed respectively.

3.7.5.2 Non-turbulent coefficients

In this study "Non-turbulent " is used to contrast with the heat transfer coefficients present in the previous Sections. The main difference being the inclusion of two terms one which takes into account the effects of natural convections neglected by the previous formulation. They are given by:

$$h_C = \rho_a c_{p,a}(C_{fc}C_{sh}u_s + C_{nc}\Delta\theta_v^{0.33}) \tag{3-61}$$

$$h_E = \rho_a L_V(C_{fc}C_{sh}u_s + C_{nc}\Delta\theta_v^{0.33}) \tag{3-62}$$

where L_v (J/kg) is the latent heat of evaporation, C_{fc}, C_{nc} (m/sK$^{1/3}$) and C_{sh} are coefficients that weight the contribution of forced convection, natural convection and sheltering respectively and take value between 0 and 1, $\Delta\theta_v$ (K) is the difference in virtual temperature between the air and the soil surface. The coefficient of sheltering takes into account the presence of nearby objects that could potentially block the flow of wind over the surface of interest.

3.7.5.3 Canopy cover coefficients

The third formulation considered takes into account the presence of a layer of vegetation on top the soil surface. In this formulation 2 sets of heat transfer coefficients for convection and evaporation are required, one for the soil surface heat balance and a second for the vegetation cover heat balance. The former are identical to the presented in the previous Section and expressed by equation (2-40) and equation (2-41). The latter are given by:

$$h_{C,c} = \frac{\rho_a c_{p,a} \nu}{r_a} \tag{3-63}$$

$$h_{E,c} = \frac{\rho_a L_v \nu}{r_a + r_s} \tag{3-64}$$

where r_{ac} (s/m) is the canopy aerodynamic resistance, and r_s (s/m) is the stomata resistance. v is the density of the canopy cover and takes values between 0 and 1. If v=0 it implies that the soil is completely exposed with no vegetation cover while if v=1 it means that the soil is completely covered by vegetation. These coefficients are defined as:

$$r_a = \frac{1}{c_f u_s} \tag{3-65}$$

$$r_s = 200\left(\frac{R_{max}}{R + 0.03R_{max}} + \left(\frac{\theta_{wp}}{\theta} \right)^2 \right) \tag{3-66}$$

$$c_f = 0.01\left(1 + \frac{0.3}{u_s} \right) \tag{3-67}$$

where c_f is a transfer coefficient, u_s (m/s) is wind speed, R_{max} is the maximum noon solar radiation that can be achieved, θ_w is the soil moisture content and θ_{wp} is the wilting point moisture content.

3.7.6 Evaporation and precipitation (mass transfer)

As long as the soil surface can be considered as unsaturated, the transfer of moisture between the surface and the atmosphere is due mainly to evaporation and precipitation. This flux can be defined as:

$$q_{ep} = \frac{1}{\rho_l}\left(E_v + E_p \right) \tag{3-68}$$

where q_{ep} (m/s) is the volume flow rate per unit area due to evaporation and precipitation, E_v (kg/m^{2}s) is the mass rate per unit area transferred by evaporation and E_p (kg/m^{2}s) is the mass rate per unit area transferred by precipitation. E_v is given by (Jansson et al., 2006):

$$E_v = \frac{q_E}{L_{vap}} \tag{3-69}$$

E_p is usually obtained from meteorological data, although it is commonly reported in (mm) of precipitation in a defined period of time. In principle, precipitation produces an input of sensible heat contained in the arriving volume of moisture, however,

other researchers (Janssen, 2002) have found that its contribution is insignificant and can be neglected and that approach has been adopted in this study.

3.7.7 Overall surface balance equations

Using the previously discussed relations for heat transfer fluxes at the soil surface it is possible to define a surface energy balance equation. As discussed in Section 3.2, a surface does not have volume or mass and, thus, all energy arriving to the surface must leave it in one way or another. The energy that is not reflected back into the atmosphere, is transferred into the soil and is further transported following Fourier's law (equation (3-6)) cast in 1D. In general it is possible to express the energy balance at the soil surface as:

$$-\lambda_b \frac{dT_{ss}}{d\hat{n}} = q_S + q_I + q_C + q_E \tag{3-70}$$

where $\hat{n}$ is the unit vector normal to the surface under consideration.

The specific formulation of equation (3-70) depends on the conditions of the surface. If the surface under consideration is exposed to the atmosphere, equation (3-70) can be expressed as:

$$\begin{aligned} -\lambda_b \frac{dT_{ss}}{d\hat{n}} = {} & (1-\alpha_S)R + \sigma\varepsilon_{ss}\left(\varepsilon_{sky}T_{a,\mathrm{K}}^4 - T_{ss,\mathrm{K}}^4\right) \\ & + h_E(e_a - e_{ss}) + h_C\left(T_a - T_{ss}\right) \end{aligned} \tag{3-71}$$

If the surface is covered by a layer of vegetation two heat balances are required, one for the surface and one for the vegetation cover. The heat balance for the surface is given by:

$$\begin{aligned} -\lambda_b \frac{dT_{ss}}{d\hat{n}} = {} & \left(1-\alpha_S\right)\left(1-\nu\right)R \\ & + \left[\sigma\varepsilon_{ss}\left(\left(1-\nu\right)\varepsilon_{sky}T_{a,\mathrm{K}}^4 - T_{ss,\mathrm{K}}^4\right) + \nu\varepsilon_c\sigma T_{c,\mathrm{K}}^4\right] \\ & + h_E\left(1-C_e\nu\right)\left(e_a - e_{ss}\right) \\ & + h_C\left(1-C_e\nu\right)\left(T_a - T_{ss}\right) \end{aligned} \tag{3-72}$$

where ν, ε_c and $T_{c,\mathrm{K}}$ (K) are the density, emissivity and absolute temperature of the canopy cover. C_e is a constant that establishes the level of soil evaporation for fully

dense canopies, e.g. setting $C_e < 1$ gives non-zero soil evaporation for the full canopy case.

The corresponding mass balance equation at the soil surface is given by:

$$-\rho_w \left(\frac{\partial (K_w h)}{\partial z} + \frac{\partial K_w}{\partial z} \right) \Bigg|_{z=0} = \frac{q_E}{L_{vap}} + E_p \qquad (3\text{-}73)$$

3.8 Boundary conditions applied at the base of a domain

In many geotechnical and geo-environmental initial value and boundary value problems it is necessary to introduce a boundary condition at the bottom boundary of the domain to represent the influence of the strata below the domain on the system. It is common to either fix the temperature on this boundary at an estimated average temperature or assume an insulated (no heat flux) boundary condition. The implication of this last assumption is to neglect any geothermal heat flux. This is typically the case in consideration of the near soil surface (Davies, 2013), however, where this assumption cannot be made, the inclusion of a constant heat flux at the bottom that takes into account this term is not difficult.

When a flux is applied this requires less information about the soil and, provided that the thermal energy and mass transfer interactions at the surface are correctly represented, the calculated temperature of the soil at depth will tend towards a steady state value, which should be representative of the actual temperature. This approach can therefore be used to test how well the surface conditions are being represented if the temperature at the bottom of the soil is known. Under this scenario heat transfer at the bottom of the domain is set to zero.

$$q_T = 0 \qquad (3\text{-}74)$$

3.9 Concluding remarks

In this Chapter, the governing equations of heat and moisture transfer within soils and heat advection within pipe systems are presented. The conservation principles of these equations, the specific laws that define the mass and thermal fluxes within soils and the advective heat transfer process, commonly found in ground thermal devices, are discussed.

Energy and mass balance equations have been used to define the boundary conditions at the soil surface, while the treatment of the boundary conditions applied at the base of a domain have also been discussed. Expressions for the linearization of non-linear relations involved in the soil surface heat and moisture transfer processes have also been provided.

3.10 References

Abu-Hamdeh, N. H. [2003]. Thermal Properties of Soils as Affected by Density and Water Content. *Biosyst. Eng.* **86** (1): 97–102. doi:10.1016/S1537-5110(03)00112-0.

Barden, L. and Pavlakis, G. [1971]. Air and Water Permeability of Compacted Unsaturated Cohesive Soil. *J. Soil Sci.* **22** (3): 302–318. doi:10.1111/j.1365-2389.1971.tb01618.x.

Beckman, W. A. [1971]. Solution of Heat Transfer Problems on a Digital Computer. *Sol Energy* **13**. doi:10.1016/0038-092X(71)90012-0.

Berdahl, P. and Martin, M. [1984]. Emissivity of Clear Skies. *Sol. Energy* **32** (5): 663–664. doi:10.1016/0038-092X(84)90144-0.

Brunt, D. [1932]. Notes on Radiation in the Atmosphere. I. *Q. J. R. Meteorol. Soc.* **58** (247): 389–420. doi:10.1002/qj.49705824704.

Campbell, G. S. [1974]. A Simple Method for Determining Unsaturated Conductivity From Moisture Retention Data. *Soil Science* 117 (6). doi:10.1097/00010694-197406000-00001.

Carslaw, H. S. and Jaeger, J. C. [1986]. *Conduction of Heat in Solids*. Clarendon Press.

Çengel, Y. A. [2003]. *Heat Transfer: A Practical Approach*. McGraw-Hill.

Davies, J. H. [2013]. Global Map of Solid Earth Surface Heat Flow. *Geochem. Geophys. Geosystems* **14** (10): 4608–4622. doi:10.1002/ggge.20271.

Deardorff, J. [1978]. Efficient Prediction of Ground Surface-Temperature and Moisture, with Inclusion of a Layer of Vegetation. *J. Geophys. Res.-Oceans Atmospheres* **83** (NC4): 1889–1903. doi:10.1029/JC083iC04p01889.

Duffie, J. A. and Beckman, W. A. [2006]. *Solar Engineering of Thermal Processes*. 3rd ed. Wiley.

Edinger, J. E. and Brady, D. K. [1974]. *Heat Exchange and Transport in the Environment*. John Hopkins University.

Fredlund, D. G. and Rahardjo, H. [1993]. *Soil Mechanics for Unsaturated Soils*. Wiley.

Fund, S. I. H. and Ångström, A. K. [1915]. *A Study of the Radiation of the Atmosphere Based upon Observations of the Nocturnal Radiation during Expeditions to Algeria and to California*. Washington: Smithsonian Institution.

Garratt, J. R. [1994]. *The Atmospheric Boundary Layer*. Cambridge University Press.

Iziomon, M. G., Mayer, H., and Matzarakis, A. [2003]. Downward Atmospheric Longwave Irradiance under Clear and Cloudy Skies: Measurement and Parameterization. *J. Atmospheric Sol.-Terr. Phys.* **65** (10): 1107–1116. doi:10.1016/j.jastp.2003.07.007.

Janssen, H. [2002]. The Influence of Soil Moisture Transfer on Building Heat Loss via the Ground. PhD Thesis, Belgium: Catholic University of Leuven. http//www.kuleuven.ac.be/ bwf/eng/content/publications 01.htm.

Jansson, C., Almkvist, E., and Jansson, P. [2006]. Heat Balance of an Asphalt Surface: Observations and Physically-Based Simulations. *Meteorol. Appl.* **13** (2): 203–212. doi:10.1017/S1350482706002179.

Monteith, J. L. [1961]. An Empirical Method for Estimating Long-Wave Radiation Exchanges in the British Isles. *Q. J. R. Meteorol. Soc.* **87** (372): 171–179. doi:10.1002/qj.49708737206.

North, G. R. and Erukhimova, T. L. [2009]. *Atmospheric Thermodynamics: Elementary Physics and Chemistry*. Cambridge University Press.

Penman, H. L. [1948]. Natural Evaporation from Open Water, Bare Soil and Grass. *Proc. R. Soc. Lond. Ser. Math. Phys. Sci.* **193** (1032): 120 –145. doi:10.1098/rspa.1948.0037.

Pérez Guerrero, J. S., Pimentel, L. C. G., Skaggs, T. H., and van Genuchten, M. T. [2009]. Analytical Solution of the Advection–diffusion Transport Equation Using a Change-of-Variable and Integral Transform Technique. *Int. J. Heat Mass Transf.* **52** (13–14): 3297–3304. doi:10.1016/j.ijheatmasstransfer.2009.02.002.

Philip, J. R. and de Vries, D. A. [1957]. Moisture Movement in Porous Materials under Temperature Gradients. *Trans. Am. Geophys. Union* **38** (2): 222–232.

Rahardjo, H. [1990]. The Study of Undrained and Drained Behavior of Unsaturated Soils. PhD Thesis, Canada: University of Saskatchewan. http://ecommons.usask.ca/handle/10388/etd-09162010-143302.

Rees, S. W., Adjali, M. H., Zhou, Z., Davies, M., and Thomas, H. R. [2000]. Ground Heat Transfer Effects on the Thermal Performance of Earth-Contact Structures. *Renew. Sustain. Energy Rev.* **4** (3): 213–265. doi:10.1016/S1364-0321(99)00018-0.

Rees, S. W., Zhou, Z., and Thomas, H. R. [2007]. Ground Heat Transfer: A Numerical Simulation of a Full-Scale Experiment. *Build. Environ.* **42** (3): 1478–1488.

Roberson, J. A. and Crowe, C. T. [1989]. *Engineering Fluid Mechanics*. 4Rev e. Houghton Mifflin.

Swinbank, W. C. [1963]. Long-Wave Radiation from Clear Skies. *Q. J. R. Meteorol. Soc.* **89** (381): 339–348. doi:10.1002/qj.49708938105.

Thomas, H. R. and Rees, S. W. [1990]. Modeling Field Infiltration into Unsaturated Clay. *J. Geotech. Eng.* **116** (10): 1483–1500. doi:10.1061/(ASCE)0733-9410(1990)116:10(1483).

Tomasi, C. [1978]. On the Water Vapour Absorption in the 8–13 Mm Spectral Region for Different Atmospheric Conditions. *Pure Appl. Geophys.* **116** (6): 1063–1076. doi:10.1007/BF00874671.

Chapter 4 Numerical solutions

4.1 Introduction

This Chapter presents the numerical solution of the partial differential equations that describe the heat and moisture transfer within soils and the advection of heat by a fluid (as developed in Chapter 3) using the finite element method. The general numerical implementation of different kinds of boundary conditions is also presented.

Since the particular method of discretization adopted allows changes in mesh refinement between time steps in transient simulations, an algorithm for the selection of elements based on the gradient of the independent variable (temperature, pressure head) is also presented.

The numerical approaches adopted in this Chapter are based on the following references: Reddy (2006), Patankar (1980), Baker and Pepper (1990), Thomas and Rees (1990) and Bangerth (2013). This last reference details the Deal.ii library which is used in implementation of the numerical solution.

4.2 Transfer equations

The partial differential equations for heat and moisture transport and for heat advection were presented in Chapter 3. This Section briefly summarizes them.

4.2.1 Moisture diffusion (Richards' equation)

Moisture diffusion in soils is presented in Section 3.5.1. It is given by (equation (3-13)):

$$C_\theta \frac{\partial h}{\partial t} = \nabla \cdot \left[K_w(\theta_w) \nabla h \right] + \nabla K_w(\theta_w) \tag{4-1}$$

where C_θ (1/m) is the specific moisture capacity defined as:

$$C_\theta = \frac{\partial \theta_w}{\partial h} \tag{4-2}$$

An expression that relates the moisture content θ_w to the pressure head h is given by (3-10).

4.2.2 Heat conduction

Heat conduction in soils is presented in Section 3.5.2. It is expressed as (equation (3-16)):

$$C_{p,b}\frac{\partial T_s}{\partial t} = \nabla\left(\lambda_b \nabla T_s\right) \tag{4-3}$$

where $C_{p,b}$ (J/m^{3}K) is the soil's volumetric heat capacity and λ_b (W/mK) is its bulk thermal conductivity.

4.2.3 Heat advection

The advection of heat by a moving fluid is presented in Section 3.6. It is stated as (equation (3-17)):

$$C_f\left(\frac{\partial T_f}{\partial t} + u_f\frac{\partial T_f}{\partial x}\right) = Q_f \tag{4-4}$$

where the velocity of the fluid $u_{f,}$ (m/s) is assumed to be constant, Q_f (W/m^3) is the internal heat generation within the fluid and C_f (J/m^{3}K) is its volumetric heat capacity defined as:

$$C_f = \rho_f c_f \tag{4-5}$$

where ρ_f (kg/m^3) and c_f (J/kgK) are the density and specific heat capacity of the fluid.

4.3 Finite Element Method

The time dependent partial differential equations presented in the previous Section are discretized following Rothe's method. This method involves discretizing first with respect to time, leading to a stationary PDE at each time step which is then solved using standard finite element techniques. The adopted time discretization approach enables, via a parameter, the casting of the solution of the stationary PDE using the implicit, explicit or the Crank-Nicholson schemes depending on the particular equation of interest.

4.3.1 Time discretization

In this Section the temporal discretization procedure is applied in detail to the moisture transport equation. Then, since the same procedure can be applied in a similar manner to the heat transport and heat advection equations, their discretized forms are summarized.

The time discretization for the pressure head field is given by:

$$C_\theta \frac{\partial h}{\partial t} = \nabla \cdot \left(K_w \nabla h \right) + \frac{\partial K_w}{\partial z} \tag{4-6}$$

$$C_\theta^{n+1/2} \frac{h^{n+1} - h^n}{\Delta t} = \nabla \cdot \left[K_w^{n+1/2} \nabla \left(\eta h^{n+1} + (1-\eta) \mathrm{h}^n \right) \right] + \frac{\partial K_w^{n+1/2}}{\partial z} \tag{4-7}$$

$$\begin{aligned} & C_\theta^{n+1/2} h^{n+1} - \eta \Delta t \nabla \cdot \left(K_w^{n+1/2} \nabla h^{n+1} \right) \\ & = C_\theta^{n+1/2} h^n + (1-\eta) \Delta t \nabla \cdot \left(K_w^{n+1/2} \nabla \mathrm{h}^n \right) + \Delta t \frac{\partial K_w^{n+1/2}}{\partial z} \end{aligned} \tag{4-8}$$

where η is a parameter that takes values between 0 and 1. If η=0 the temporal discretization obtained is known as the forward or explicit Euler scheme, on the other hand if η=1 then the backward or implicit Euler method is obtained. A third case would be to set η=1/2, this is known as the Crank-Nicholson method.

When solving (4-6) initially a first solution for time step n+1 is calculated using the solution and physical properties estimated at time step n. Once a first prediction for h^{n+1} is obtained a correction step is formed in which the a second approximation of h^{n+1} is calculated using physical properties estimated at time n+1/2. This method is known a predictor-corrector and is performed for every time step n+1.

As mentioned before, following the same procedure, the time discretization for the heat transport equation is given by:

$$C_{p,b}^{n+1/2} T_s^{n+1} - \eta \Delta t \nabla \left(\lambda_b^{n+1/2} \nabla T_n^{n+1} \right) = C_{p,b}^{n+1/2} T_s^n + (1-\eta) \Delta t \nabla \left(\lambda_b^{n+1/2} \nabla T_s^n \right) \tag{4-9}$$

and for the heat advection equation is given by:

$$\begin{aligned} C_f^{n+1/2} T_f^{n+1} + C_f^{n+1/2} \eta \Delta t u_f \frac{\partial T_f^{n+1}}{\partial x} = {} & C_f^{n+1/2} T_f^n - C_f^{n+1/2} (1-\eta) \Delta t u_f \frac{\partial T_f^n}{\partial x} \\ & + \eta \Delta t Q_f^{n+1} + (1-\eta) \Delta t Q_f^n \end{aligned} \tag{4-10}$$

4.3.2 Spatial discretization

This Section provides the spatial discretization of equation (4-6), equation (4-9) and equation (4-10) using the finite element method, specifically the Galerkin weighted residual method is adopted. As before, the method is performed in detail to obtain the spatial discretization of the moisture transport equation (equation (4-1)) while the

corresponding spatial discretizations for heat conduction and advection equations (equations (4-3) and equation (4-4)) are summarized.

After obtaining the time discretization, the next step to find the approximation of the solution of the desired variable is to derive the weak form of the equation of interest. For example, to approximate the solution of the pressure head *h* it is necessary to obtain the weak form of (4-6) (using an explicit Euler method (η=1) as suggested by Thomas and Rees (1990). This is done by multiplying the equation by a test function ϕ and integrating over the domain of interest denoted as Ω:

$$\int_\Omega \phi C_\theta^{n+1/2} h^{n+1} d\Omega - \Delta t \int_\Omega \phi \nabla \cdot \left(K_w^{n+1/2} \nabla h^{n+1} \right) d\Omega = \int_\Omega \phi C_\theta^{n+1/2} h^n d\Omega + \Delta t \int_\Omega \phi \frac{\partial K_w^{n+1/2}}{\partial z} d\Omega \tag{4-11}$$

Using the divergence theorem it is possible to reduce the order of the second spatial derivatives:

$$\int_\Omega \phi C_\theta^{n+1/2} h^{n+1} d\Omega + \Delta t \int_\Omega K_w^{n+1/2} \nabla \phi \nabla h^{n+1} d\Omega = \int_\Omega \phi C_\theta^{n+1/2} h^n d\Omega + \Delta t \int_\Omega \phi \frac{\partial K_w^{n+1/2}}{\partial z} d\Omega + \Delta t \int_\Omega \nabla \cdot \left(\phi K_w^{n+1/2} \nabla h^{n+1} \right) d\Omega \tag{4-12}$$

The last term in the right hand side of (4-12) can be reformulated in terms of the total potential (*h*+*z*) as

$$\int_\Omega \phi C_\theta^{n+1/2} h^{n+1} d\Omega + \Delta t \int_\Omega K_w^{n+1/2} \nabla \phi \nabla h^{n+1} d\Omega = \int_\Omega \phi C_\theta^{n+1/2} h^n d\Omega + \Delta t \int_\Omega \phi \frac{\partial K_w^{n+1/2}}{\partial z} d\Omega + \Delta t \int_\Omega \nabla \cdot \left(\phi K_w^{n+1/2} \nabla (h+z)^{n+1} \right) d\Omega - \Delta t \int_\Omega K_w^{n+1/2} \frac{\partial \phi}{\partial z} d\Omega - \Delta t \int_\Omega \phi \frac{\partial K_w^{n+1/2}}{\partial z} d\Omega \tag{4-13}$$

where the following relation has been used:

$$\frac{\partial}{\partial z}\left(\phi K_w^{n+1/2}\right) = K_w^{n+1/2}\frac{\partial \phi}{\partial z} + \phi\frac{\partial K_w^{n+1/2}}{\partial z} \tag{4-14}$$

Applying the divergence theorem:

$$\begin{aligned}\int_\Omega \phi C_\theta^{n+1/2} h^{n+1} d\Omega + \Delta t \int_\Omega K_w^{n+1/2}\nabla\phi\nabla h^{n+1} d\Omega = \int_\Omega \phi C_\theta^{n+1/2} h^n d\Omega \\ + \Delta t\int_\Gamma \phi\left(K_w^{n+1/2}\frac{\partial(h^{n+1}+z)}{\partial \hat{n}}\right)d\Gamma \\ - \Delta t\int_\Omega K_w^{n+1/2}\frac{\partial\phi}{\partial z}d\Omega\end{aligned} \tag{4-15}$$

where Γ denotes the boundary of the domain and $\hat{n}$ is a unit vector normal to it.

The next step is to find a function h for which (4-15) is true for all test functions ϕ. This cannot be achieved computationally as a general case, but instead an approximation for h_h is sought:

$$h_h = \sum_j U_j \phi_j(x) \tag{4-16}$$

where U_j are the unknown expansion coefficients that need to be determined and $\phi_j(x)$ are the finite element shape functions that will be used. The typical finite elements used to describe these shape functions are Lagrange elements that define shape functions by interpolation on support points (the simplest use polynomial degree 1 and are denoted as linear). Note additionally that the shape functions are not necessary the same at different time steps. This allows the adaptation of the mesh depending on the behaviour of the main variables. For this reason, in principle, is necessary to mark the use to different shape functions for different time steps:

$$h_h^{n+1} = \sum_j U_j^{n+1}\phi_j^{n+1}(x) \tag{4-17}$$

$$h_h^{n} = \sum_j U_j^{n}\phi_j^{n}(x) \tag{4-18}$$

Using (4-17) and (4-18), and a set of shape functions ϕ_i, the weak form of the discrete problem can be define as:

$$\int_{\Omega} \phi_i^{n+1} C_\theta^{n+1/2} \phi_j^{n+1} d\Omega U_j^{n+1} + \Delta t \int_{\Omega} K_w^{n+1/2} \nabla \phi_i^{n+1} \nabla \phi_j^{n+1} d\Omega U_j^{n+1}$$
$$= \int_{\Omega} \phi_i^{n+1} C_\theta^{n+1/2} \phi_j^{n} d\Omega U_j^{n} + \Delta t \int_{\Gamma} \phi_i^{n+1} \left(K_w^{n+1/2} \frac{\partial (h^{n+1} + z)}{\partial \hat{n}} \right) d\Gamma \qquad (4\text{-}19)$$
$$- \Delta t \int_{\Omega} K_w^{n+1/2} \frac{\partial \phi_i^{n+1}}{\partial z} d\Omega$$

Which can be expressed in matrix form as:

$$\left(\mathbf{M_U^{n+1}} + \Delta t \mathbf{A_U^{n+1}} \right) U^{n+1} = \mathbf{M_U^{n+1,n}} U^n + \Delta t \mathbf{F_U^{n+1}} \qquad (4\text{-}20)$$

where:

$$\mathbf{M_U^{n+1}} = \int_{\Omega} \phi_i^{n+1} C_\theta^{n+1/2} \phi_j^{n+1} d\Omega$$
$$\mathbf{A_U^{n+1}} = \int_{\Omega} K_w^{n+1/2} \nabla \phi_i^{n+1} \nabla \phi_j^{n+1} d\Omega$$
$$\mathbf{M_U^{n+1,n}} = \int_{\Omega} \phi_i^{n+1} C_\theta^{n+1/2} \phi_j^{n} d\Omega \qquad (4\text{-}21)$$
$$\mathbf{F_U^{n+1}} = \int_{\Gamma} \phi_i^{n+1} \left(K_w^{n+1/2} \frac{\partial (h^{n+1} + z)}{\partial \hat{n}} \right) d\Gamma - \int_{\Omega} K_w^{n+1/2} \frac{\partial \phi_i^{n+1}}{\partial z} d\Omega$$

Note that the boundary term defined in matrix $\mathbf{F_U}$ is subjected to change depending on the particular boundary process taking place on the problem. Equation (4-20) is directly applicable for second kind boundary conditions (Neumann). When first (Dirichlet) or third (Robin) boundary conditions need to be applied, additional terms might need to be included in matrix $\mathbf{A_h}$. More discussion on the implementation of boundary conditions is provided in the following Section.

Following a similar procedure, it is possible to define the finite element discretization for the heat conduction equation (using a Crank-Nicholson approach for the time discretization):

$$\int_{\Omega} \phi_i^{n+1} C_{p,b}^{n+1/2} \phi_j^{n+1} d\Omega V_j^{n+1} + \eta \Delta t \int_{\Omega} \lambda_b^{n+1/2} \nabla \phi_i^{n+1} \nabla \phi_j^{n+1} d\Omega V_j^{n+1}$$
$$= \int_{\Omega} \phi_i^{n+1} C_{p,b}^{n+1/2} \phi_i^{n} d\Omega V_j^{n} - (1-\eta) \Delta t \int_{\Omega} \lambda_b^{n+1/2} \nabla \phi_i^{n+1} \nabla \phi_j^{n} d\Omega V_j^{n} \qquad (4\text{-}22)$$
$$+ \eta \Delta t \int_{\Gamma} \phi_i^{n+1} \left(\lambda_b \frac{\partial T_s^{n+1}}{\partial \hat{n}} \right) d\Gamma + (1-\eta) \Delta t \int_{\Gamma} \phi_i^{n+1} \left(\lambda_b \frac{\partial T_s^{n}}{\partial \hat{n}} \right) d\Gamma$$

where U_j are the coefficients to approximate a discrete solution for T_s. In matrix form:

$$\left(\mathbf{M_v^{n+1}} + \eta\Delta t\mathbf{A_v^{n+1}}\right)V^{n+1} = \left(\mathbf{M_v^{n+1,n}} - (1-\eta)\Delta t\mathbf{A_v^{n+1,n}}\right)V^n + \eta\Delta t\mathbf{F_v^{n+1}} + (1-\eta)\Delta t\mathbf{F_v^n} \tag{4-23}$$

where:

$$\begin{aligned}
\mathbf{M_v^{n+1}} &= \int_\Omega \phi_i^{n+1} C_{p,b}^{n+1/2} \phi_j^{n+1} d\Omega \\
\mathbf{A_v^{n+1}} &= \int_\Omega \lambda_b^{n+1/2} \nabla\phi_i^{n+1} \nabla\phi_j^{n+1} d\Omega \\
\mathbf{M_v^{n+1,n}} &= \int_\Omega \phi_i^{n+1} C_{p,b}^{n+1/2} \phi_j^{n} d\Omega \\
\mathbf{A_v^{n+1,n}} &= \int_\Omega \lambda_b^{n+1/2} \nabla\phi_i^{n+1} \nabla\phi_j^{n} d\Omega \\
\mathbf{F_v^{n+1}} &= \int_\Gamma \phi_i^{n+1} \left(\lambda_b \frac{\partial T_s^{n+1}}{\partial \hat{n}}\right) d\Gamma \\
\mathbf{F_v^{n}} &= \int_\Gamma \phi_i^{n+1} \left(\lambda_b \frac{\partial T_s^{n}}{\partial \hat{n}}\right) d\Gamma
\end{aligned} \tag{4-24}$$

In the same way, the finite element approximation for the heat advection equation is given by:

$$\begin{aligned}
&\int_\Omega \phi_i^{n+1} C_f^{n+1/2} \phi_j^{n+1} d\Omega W_j^{n+1} + \eta u_f \Delta t \int_\Omega \phi_i^{n+1} C_f^{n+1/2} \frac{\partial \phi_j^{n+1}}{\partial x} d\Omega W_j^{n+1} \\
&+\eta u_f \Delta t \int_\Gamma \phi_i^{n+1} \phi_j^{n+1} d\Gamma W_j^{n+1} \\
&= \int_\Omega \phi_i^{n+1} C_f^{n+1/2} \phi_i^{n} d\Omega W_j^{n} - (1-\eta)\Delta t u_f \int_\Omega \phi_i^{n+1} C_f^{n+1/2} \frac{\partial \phi_j^{n}}{\partial x} d\Omega W_j^{n} \\
&-(1-\eta) u_f \Delta t \int_\Gamma \phi_i^{n+1} \phi_j^{n} d\Gamma W_j^{n} \\
&+\eta\Delta t \int_\Omega \phi_i^{n+1} Q_f^{n+1} d\Omega + \eta\Delta t \int_\Gamma \phi_i^{n+1} T_{in} d\Gamma \\
&+(1-\eta)\Delta t \int_\Omega \phi_i^{n+1} Q_f^{n} d\Omega + (1-\eta)\Delta t \int_\Gamma \phi_i^{n+1} T_{in} d\Gamma
\end{aligned} \tag{4-25}$$

where W_j are coefficients for the numerical approximation of T_f. Since the boundary condition does not appear naturally in the weak formulation of the heat advection equation, in order to obtain equation (4-25), the following boundary condition

(corresponding to a inflow boundary) has been enforced and added to equation (4-10).

$$T_f = T_{in} \qquad \text{(at inflow boundary)} \tag{4-26}$$

In matrix form, equation (4-25) can be expressed as:

$$\begin{aligned}\left(\mathbf{M_W^{n+1}} + \eta\Delta t\mathbf{A_W^{n+1}}\right)W^{n+1} = \left(\mathbf{M_W^{n+1,n}} - (1-\eta)\Delta t\mathbf{A_W^{n+1,n}}\right)W^{n} \\ +\eta\Delta t\mathbf{F_W^{n+1}} \\ +(1-\eta)\Delta t\mathbf{F_W^{n}}\end{aligned} \tag{4-27}$$

where:

$$\begin{aligned}\mathbf{M_W^{n+1}} &= \int_\Omega \phi_i^{n+1} C_f^{n+1/2} \phi_j^{n+1} d\Omega \\ \mathbf{A_W^{n+1}} &= u_f \int_\Omega \phi_i^{n+1} C_f^{n+1/2} \frac{\partial \phi_j^{n+1}}{\partial x} d\Omega + u_f \int_\Gamma \phi_i^{n+1} \phi_j^{n+1} d\Gamma \\ \mathbf{M_W^{n+1,n}} &= \int_\Omega \phi_i^{n+1} C_f^{n+1/2} \phi_j^{n} d\Omega \\ \mathbf{A_W^{n+1,n}} &= u_f \int_\Omega \phi_i^{n+1} C_f^{n+1/2} \frac{\partial \phi_j^{n}}{\partial x} d\Omega + u_f \int_\Gamma \phi_i^{n+1} \phi_j^{n} d\Gamma \\ \mathbf{F_W^{n+1}} &= u_f \int_\Omega \phi_i^{n+1} Q_f^{n+1} d\Omega + \int_\Gamma \phi_i^{n+1} T_{in}^{n+1} d\Gamma \\ \mathbf{F_W^{n}} &= \int_\Omega \phi_i^{n+1} Q_f^{n} d\Omega + \int_\Gamma \phi_i^{n} T_{in}^{n} d\Gamma\end{aligned} \tag{4-28}$$

4.3.3 Adaptive refinement criteria

In the previous Sections the possibility of changing the mesh refinement from one time step to the next is taken into account. This is desirable when the problem involves time-varying localized gradients of the independent variables (e.g. moving fronts, localized and periodic sink/sources and/or cracks/fractures). In order to select appropriate regions where the re-meshing should performed, a suitable algorithm for the selection of elements must be defined. Since this algorithm can be used to adapt the mesh to the changing conditions of the independent variables it is known as adaptive refinement.

The adaptive refinement approach used in this work and implemented in the finite element library Deal.ii follows the method proposed by Kelly et al. (1983). In this approach an error indicator is calculated and used to sort the refinement priority of

elements. For example, those with the higher values of error indicator can be flagged for further refinement while those with the lowest values can be flagged for coarsening. The error indicator itself is calculated by integration of the change of the gradient of the solution along the faces of each element. Mathematically, for element *K*, it is given by (Ainsworth and Oden 2000):

$$\vartheta_K^2 = \frac{\varsigma}{24}\int_{\partial K}\left(\frac{\partial u_h}{\partial \hat{n}}\right)^2 d\Omega \tag{4-29}$$

where u_h is the discrete approximation of an independent variable u of interest, ς is the size of the mesh element, Ω is domain and $\hat{n}$ is the respective normal faces of the element *K*. The term in brackets denotes the jump of the argument at the face.

4.4 Boundary conditions

Typically three kinds of boundary conditions are encountered in the solution of numerical problems by the finite element method:

- The independent variable is defined at the boundary. Also known as *Fixed, Strong, First kind* or *Dirichlet* boundary condition.
- The normal derivative of the independent variable is defined at the boundary. Also known as *Free, Natural, Second kind* or *Neumann boundary* condition.
- A linear combination of the values of the independent variable and its normal derivative at the boundary is defined. Also known as *Third kind* or *Robin* boundary condition.

One or more of these boundary condition might apply to the physical problem under consideration. Their implementation is performed in the boundary terms that arises after the weak form of the discretized equations is obtained. To illustrate this, different boundary conditions can be assumed and applied in $\mathbf{F_V}$ (evaluated at time step n). This term includes the boundary condition of the heat conduction problem (4-22):

$$\mathsf{F}_{\mathsf{V}}^{\mathsf{n}} = \int_{\Gamma}\phi_i^n\left(\lambda_b\frac{\partial T_s^n}{\partial \hat{n}}\right)d\Gamma \tag{4-30}$$

The following Sections deal with the specific implementation of each type of boundary condition.

4.4.1 Fixed boundary conditions

The implementation of boundary conditions in the finite element method is closely related to the calculus of variations and involves a problem of energy minimization. An energy functional that depends on the independent variable is defined and it needs to be proved that it provides the minimum possible energy for the system for any possible perturbation in the domain including the boundaries. When the value at the boundary is specified, the only possible value for the test function is zero in order to minimize the functional. In this case (4-30) vanishes. This is:

$$\phi_i^n = 0 \tag{4-31}$$

and thus $\mathbf{F_V}$ vanishes as well. Subsequently, after the system has been assembled, the values of the degrees of freedom corresponding to the boundary need to be enforced to the desired fixed value.

4.4.2 Free boundary conditions

In the case of the *free* or *Natural* boundary conditions, the flux normal to the boundary is specified. For example (using Fourier's law):

$$q_T = -\lambda_b \frac{\partial T_s}{\partial \hat{n}} \tag{4-32}$$

The term represented by (4-32) appears naturally in (4-30) (hence *Natural* boundary condition) and can be replaced directly:

$$\mathbf{F}_\mathbf{V}^\mathbf{n} = -\int_\Gamma \phi_i^n q_T d\Gamma \tag{4-33}$$

Equation (4-33) can be added to the right hand side of (4-22) and the problem solved without further modification.

4.4.3 Robin boundary conditions

Robin boundary conditions arise, for example, when the heat flux is dependent on the interaction of the boundary with its environment:

$$\lambda_b \frac{\partial T_s}{\partial \hat{n}} = \xi\left(T_\infty - T_s\right) \tag{4-34}$$

where ξ is a suitable heat transfer coefficient and T_∞ is the temperature of the surrounding environment. In this case (4-30) is transformed into:

$$\begin{aligned}\mathbf{F_V^n} &= -\int_{\Gamma} \phi_i^n \xi \left(T_s^n - T_\infty^n\right) d\Gamma \\ &= -\xi \int_{\Gamma} \phi_i^n T_s^n d\Gamma + \xi \int_{\Gamma} \phi_i^n T_\infty^n d\Gamma\end{aligned} \tag{4-35}$$

It can be seen that the implementation of this type of boundary condition leads to the inclusion of an extra term that depends on the independent variable (T_s in this case) that needs to be included in the in the corresponding matrix $\mathbf{A_V}$ in (4-24).

4.4.4 Mixed boundary conditions

The solution of physical problems by numerical methods usually requires the imposition of more than one kind of boundary condition in the domain. This scenario is known as mixed boundary conditions. If the problem of interest can be represented, for example, with two different boundaries Γ1 and Γ2, where a fixed and free boundary conditions are imposed using (4-31) and (4-33) respectively, (4-30) could be rewritten as:

$$\begin{aligned}\mathbf{F_V^n} &= \int_{\Gamma_1} \phi_i^n \left(\lambda_b \frac{\partial T_s^n}{\partial \hat{n}} \right) d\Gamma_1 + \int_{\Gamma 2} \phi_i^n \left(\lambda_b \frac{\partial T_s^n}{\partial \hat{n}} \right) d\Gamma_2 \\ &= \int_{\Gamma_1} (0) \left(\lambda_b \frac{\partial T_s^n}{\partial \hat{n}} \right) d\Gamma_1 - \int_{\Gamma 2} \phi_i^n q_T d\Gamma_2 \\ &= -\int_{\Gamma 2} \phi_i^n q_T d\Gamma_2\end{aligned} \tag{4-36}$$

This method can be applied to include any number of relevant boundary conditions in the domain.

4.5 Concluding remarks

A time and space discretization approach suited for the basic transport equations of interest in this study has been developed in this Chapter. The approach allows, in principle, the use of adaptive mesh refinement. An algorithm for the selection of elements based on the gradients of the main independent variables has been presented. A general numerical implementation for the relevant boundary conditions present in this work has also been discussed.

4.6 References

Ainsworth, M. and Oden, J. T. [2000]. A Posteriori Error Estimation in Finite Element Analysis. John Wiley & Sons.

Baker, A. J. and Pepper, D. W. [1990]. Finite Elements 1-2-3. New York: Mcgraw-Hill College.

Bangerth, W., Heister, T., Heltai, L., Kanschat, G., Kronbichler, M., Maier, M., Turcksin, B., and Young, T. D. [2013]. The deal.II Library, Version 8.1. ArXiv13122266 Cs Math, December. http://arxiv.org/abs/1312.2266.

Kelly, D. W., De S. R. Gago, J. P., Zienkiewicz, O. C., and Babuska, I. [1983]. A Posteriori Error Analysis and Adaptive Processes in the Finite Element Method: Part I—error Analysis. Int. J. Numer. Methods Eng. 19 (11): 1593–1619. doi:10.1002/nme.1620191103.

Patankar, S. V. [1980]. Numerical Heat Transfer and Fluid Flow. Hemisphere Pub. Corp.

Reddy, J. N. [2006]. An Introduction to the Finite Element Method. McGraw-Hill Higher Education.

Thomas, H. R. and Rees, S. W. [1990]. Modeling Field Infiltration into Unsaturated Clay. J. Geotech. Eng. 116 (10): 1483–1500. doi:10.1061/(ASCE)0733-9410(1990)116:10(1483).

Chapter 5 Full-scale experimental case study

5.1 The TRL Inter-seasonal Heat Transfer Facility (ISHTF)

This Chapter is based on a technical report from UK's Transport Research Laboratory (TRL) (Carder et al. , 2008). TRL is (TRL, 2011) "an internationally recognized centre of excellence providing world class research, consultancy, testing and certification for all aspects of transport in the UK". Under auspices of the British Highways Agency, TRL performed an experimental study about the feasibility of implementing an inter-seasonal heat storage system aimed to provide maintenance to road surfaces by preventing the formation of frost that otherwise would be dangerous for the users. As a result of that work, a report was produced based on the results generated from two experimental configurations put into operation between August 2006 and August 2008. The following Sections provide the relevant data used in this work. For further details the reader is encouraged to read the original report.

5.2 Description of the experiment

The experimental systems are located in an access road near Toddington's motorway service station, 51.952° north, 0.508° west, over the M1 highway between junctions 11 and 12 in England, UK (Figure 5-1). Two configurations were tested, each comprising two sets of pipe arrays that work as heat exchangers. The arrays comprised 10 pipes arranged as shown in Figure 5-2, with a length of 30 m along the direction of the road and 5 m width (the total width of the road). In this study, the pipe arrays are referred to as either collector pipes or storage pipes according to their depth. Collector pipes are those installed at 0.12 m depth directly below the road surface while storage pipes are those installed at 0.875 m depth. The pipes themselves are made of cross-linked polyethylene with 0.025 m diameter with a spacing of 0.25 m between adjacent longitudinal runs. The fluid used as heat carrier is an aqueous solution of water mixed with 10% ethylene-glycol. A polystyrene insulation layer 0.2 m thick is placed on top of the storage pipes in order to minimize heat losses to the soil surface. A pump house was installed in order to pump the fluid through the pipes. The control of the pumping system is discussed in more detail in Section 5.5.

The two experimental systems differ on the location of the storage pipes. One system, referred in this study as System 2, having both the storage pipes and the insulation layer placed directly under the collector pipes, while the other, referred as System 1, had them placed at the same depth, but located next to the road. The motivation for these different configurations arises from practical considerations. The former configuration is expected to be useful when new roads are constructed and is relatively easy to place both heat exchangers under the road. The latter is thought to be suitable for already built roads where it is relatively cheaper to remove only the upper most road layers (due to maintenance for example) to install the collector pipes and excavate next to the road for the installation of the storage pipes. Figure 5-3 shows the general layout of the experimental systems while Figure 5-4 and Figure 5-5 present transverse sections of each system showing the distribution and thickness of the different material layers present in each configuration. The material layers are defined as:

- 1 - Thick wearing course (35 mm)
- 2 - Thick binder course (70 mm)
- 3 - Thick concrete screed (55 mm)
- 4 - Collector pipe array
- 5a - Thick new lean concrete base (165 mm)
- 5b - Thick type 1 granular material (200 mm)
- 5c - Thick existing cement bound material (240 mm)
- 6 - Thick polystyrene insulation (200 mm)
- 7 - Thick sand overlying pipework (150 mm)
- 8 - Store pipe array
- 9 - Backfill from original excavation

It can be observed that the layer of insulation was placed at different levels at both sides of the storage pipes. This is due to the presence of buried services although a minimum overlap of 0.2 m was ensured at all times. In addition, although not shown in Figure 5-4, a slope existed to the west of the road and the insulation layer of System 2 needed to be adjusted properly.

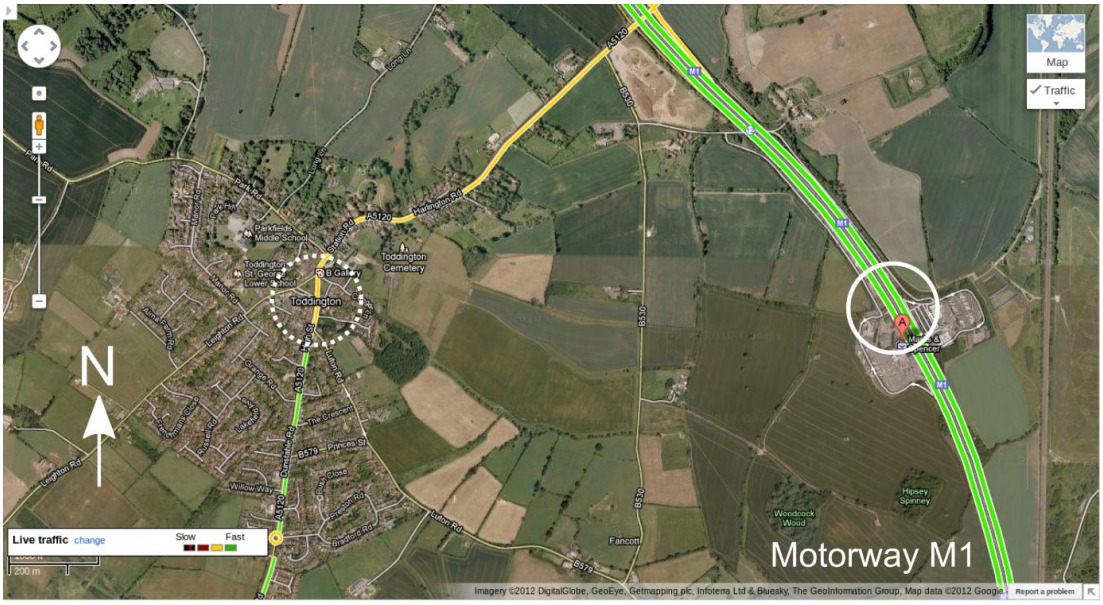

Figure 5-1: Location of Toddington service station (solid line circle). Motorway M1 (highlighted in green) and the location of Toddington (dashed circle) are also shown for reference (Google Maps 2012).

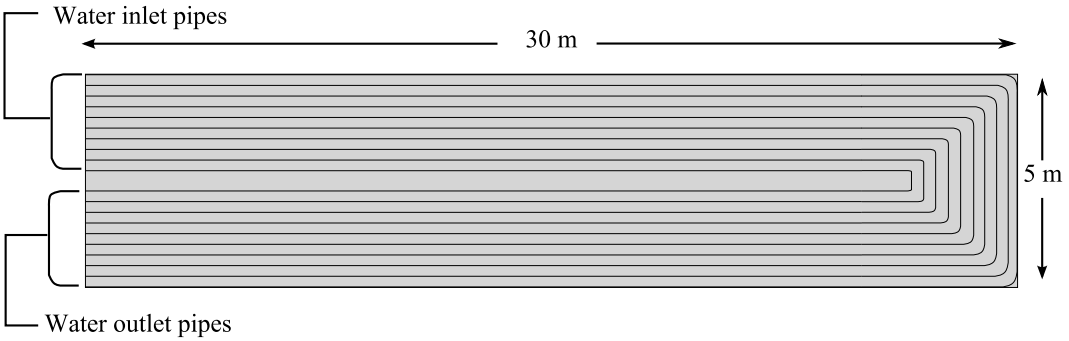

Figure 5-2: Schematic distribution of pipes in the collector and storage arrays. The arrays are 30 m long by 5 m wide (figure not to scale).

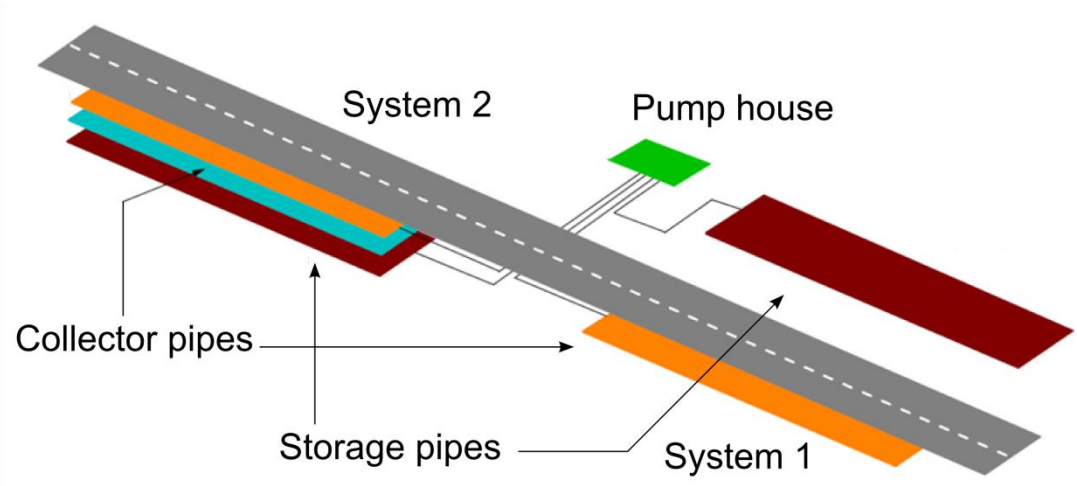

Figure 5-3: Schematic layout of the experimental systems, (Carder et al. 2007).

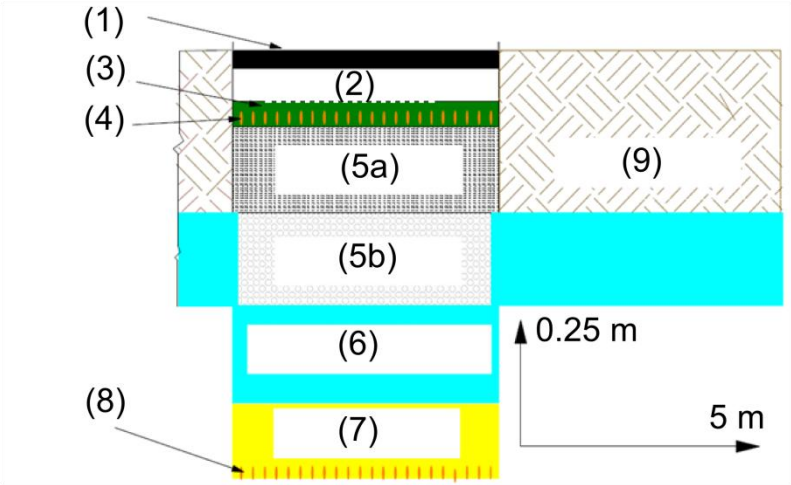

Figure 5-4: Distribution of material layers on experimental System 2 (Carder et al. 2007).

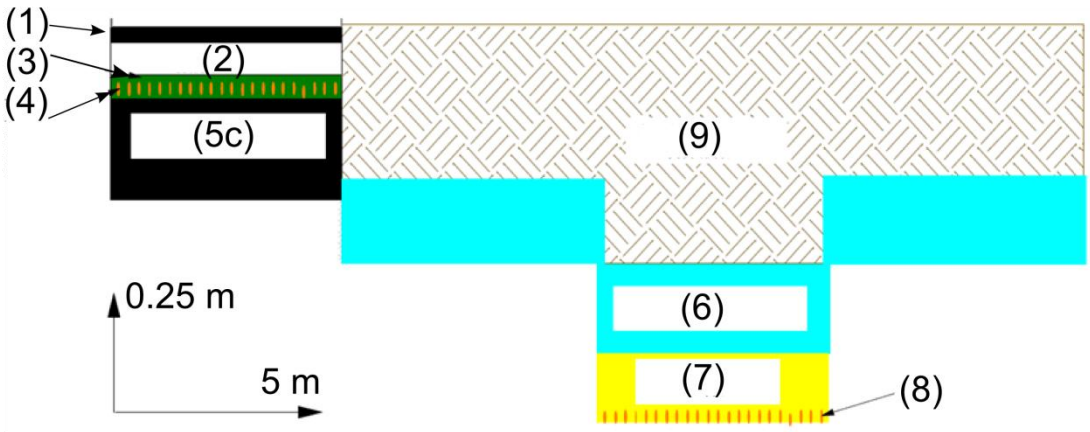

Figure 5-5: Distribution of layers on experimental System 1 (Carder et al. 2007).

5.3 Site layout and instrumentation

For the recovery of data from the experimental systems and surrounding selected locations, several sets of temperature sensors were distributed on the experimental site. To record the unperturbed temperature profile, two control boreholes labelled A and B were drilled to the north and south of the construction zone. In each of these boreholes a set of temperature sensors was distributed at depths of 0.025, 0.125, 0.825, 0.875, 1.025, 1.175, 1.375, 1.875, 3.875, 7.875 and 12.875 m. An additional control borehole was drilled in the middle of the road half way between the experimental systems. This borehole, labelled F, was aim to record the unperturbed temperature variations under the road surface. The temperature sensors were distributed at depths of: 0.875, 0.925, 0.975, 1.025, 1.175, 1.375, 1.875, 2.875, 3.875, 7.875 and 12.875 m. However, the last two sensors were discarded in this borehole due to a drilling ring failure. With the same distribution of sensors, six

additional boreholes were drilled under the locations of the experimental systems, three for each one. The location of these boreholes, labelled C, D, E, G, H, I, and of the control boreholes is shown in Figure 5-6.

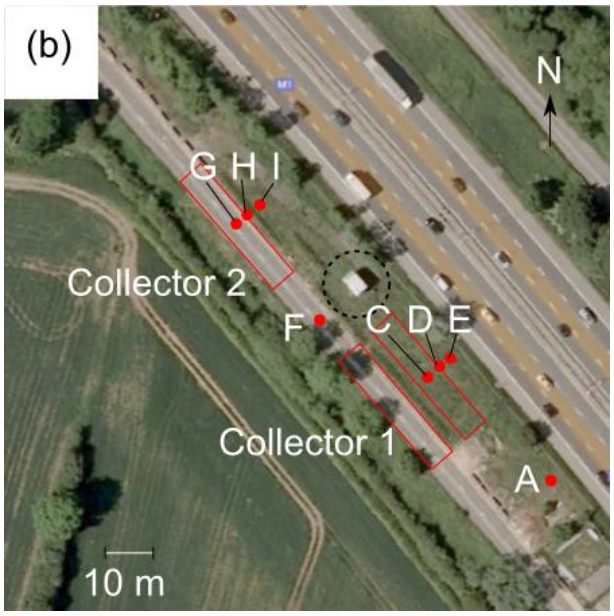

Figure 5-6: Positions of boreholes with temperature sensors on the experimental site (borehole B is not shown). The positions of collector 1 (with storage next to the road) and 2 are included for reference.

Additionally, temperature sensors were placed near the surface of boreholes G and F and at centre of collector 1 at depths of 0.01, 0.025, 0.075 and 0.1 m. These sensors recorded the temperature of the road surface during the execution of the experiment at the centre of each system and at a control zone. Further temperature sensors and strain gauges were distributed in each collector and also flow meter were used to measure the volumetric flow rate in the systems, however these measurements were not used for the purposes of this work.

5.4 Data summary

As mentioned before, TRL placed several temperature sensors through the experimental site to monitor the transient behaviour of the experimental systems during summer and winter modes of operation. In addition to these soil temperature data, a meteorological station was placed on site to record main meteorological variables, namely: air temperature, solar radiation, relative humidity, wind speed and precipitation. TRL, based on literature, also report the main material parameters of

the soil including its thermal properties. The following Sections summarize the relevant data used in this work.

5.4.1 Material properties

Material type	Density (kg/m^3)	Specific heat (J/kgK)	Thermal conductivity (W/mK)
Asphalt	2400	850	0.85
Concrete	2100	840	1.4
Silty clay	1960	840	1.21
Backfill	840	840	1.21
Polystyrene insulation	30	1130	0.034
Sand	2240	840	0.33

Table 5-1: Material parameters reported by TRL and used in their report for numerical analysis purposes.

Internal pipe diameter (m)	0.0227
External pipe diameter (m)	0.0250
Thickness of pipe wall (m)	0.0023
Length of pipes (straight sections) (m)	60
Number of pipes per heat exchanger	10
Pipe thermal conductivity (W/mK)	0.4
Flow rate (l/s)	1.41
Fluid composition	90% water, 10% ethylene glycol

Table 5-2: Pipe system data provided by TRL. The length of the pipes correspond to the straight flow and return sections along the road and need to include curved sections.

Regarding the composition of the soil at the experimental site, Carder et al. (2007). report that the type of soil is composed of stiff grey clay from 3 m to 25 m depth. The Gault Clay is overlain by a layer of firm silty clay at both sides of the road, although a final layer of reworked Gault Clay of 0.8 m existed at the west side of the road.

Table 5-1 shows the material properties given by TRL for the numerical modelling presented in their report. According to TRL these properties were provided the by suppliers (in the case of the polystyrene insulation), calculated from constituents (in the case of the asphalt), obtained from Phoenics 3.5.1 package (in the case of the silty clay, and concrete) and found in the literature (in the case of sand, ASHRAE Fundamentals 2005). Table 5-2 summarizes relevant geometrical and material data of the pipe systems and thermal properties of the fluid used as heat carrier. Note that the pipes were placed in each heat exchanger in a horizontal U-shaped loop. The pipe length reported in Table 5-2 refers to the straight sections of these loops and do not include the curve sections that vary from pipe to pipe.

5.4.2 Meteorological data

In order to monitor accurately the weather variations and to relate them to the transient behaviour of the experimental systems, a weather station was installed on the experimental site. This station recorded air temperature, relative humidity, wind speed (including wind direction and standard deviation of wind direction), solar radiation and rain fall. The data were recorded regularly every five minutes from August 2005 to September 2007. However, during some months at the end of 2006 and during 2007 the data logging system seems to have been stopped or failed since data are not available for those months. Nevertheless, data for most of the relevant periods when the systems were active is available and were used in this work as input for the numerical model proposed.

5.4.3 Temperature data

Similarly, soil temperature data were recorded on the boreholes shown in Figure 5-6. Each borehole being 100 mm in diameter and about 13 m depth with control sensors distributed at the depths mentioned before. After installation of the temperature sensors the boreholes were backfilled with bentonite pellets with the appropriate addition of water. Data is available from August 2005 to September 2007 for all boreholes. The data were recorded regularly every 15 minutes during the whole experiment with the exception of a month during the spring of 2006 where the log system seems to have been stopped or failed. As mentioned before, two temperature sensors at control borehole F (road control borehole) were damaged during installation and data are not available for them. The soil and road temperature data recorded by TRL is used in this work for verification of the numerical model proposed.

5.5 System operation

Regarding the operation of the systems, these are divided into two modes: summer and winter. In summer mode, the heat is transferred from the road surface to the collector pipes and is carried by the fluid to the storage pipes where the soil surrounding them is used as a thermal energy deposit. In winter mode the thermal energy stored in the soil is transferred to the storage pipes, carried to the collector pipes, and then used for heating up the road surface above 0 °C to prevent the formation of frost. In order to minimize the heat losses from the section of the soil used as thermal energy deposit, an insulation layer of 0.2 m thick of expanded

polyethylene was placed over the storage pipes as mentioned before. Although not discussed in the TRL technical report, it is possible that this insulation layer also prevented the normal flow of moisture coming from the surface of the soil.

The experimental project consisted of two periods of heat collection and storage during late summer 2005 and summer 2006 and two periods of road heating during the corresponding winters. This study considers the first storage period from August 23th 2005 to November 13th 2005 and the first heating period. Although the first collection period started at late summer 2005, the placement of insulation was performed in early May 2005. This had an impact on the temperature profiles present on the storage zones at the beginning of the experiment and is briefly discussed in TRL's report.

Regarding the activation of the experimental systems, the pumps were controlled by control temperature sensors located at the centre of each heat exchanger. From experimental measurements reported by TRL, it can be inferred that the pumps were activated when the temperature difference between the control sensors located at the collector and storage was approximately 1.4 ˚C. Once active, the pumps were turned off when the temperature difference dropped to approximately 0.3 ˚C.

5.6 Energy recovered

During the experiment the thermal energy recovered from each heat exchanger was calculated and offers a useful metric to consider the system performance. The recovered energy per pipe, Q_p (W), reported by TRL was determined by measuring the mass flow rate on the pipes and the temperature difference between the inlet and outlet of each heat exchanger using the following equation:

$$Q_p = c_{p,f}\dot{m}_f (T_{f,o} - T_{f,i}) \tag{5.1}$$

where $c_{p,f}$ is the specific heat capacity of the fluid, $\dot{m}_f$ (kg/s) is the mass flow rate, $T_{f,i}$ (˚C) is the inlet pipe temperature and $T_{f,o}$ (˚C) is the outlet pipe temperature.

5.7 Concluding remarks

This Chapter has summarized the work performed by TRL (Carder et al. 2007). The measurements and results reported by them are used as input data and for validation of the numerical model proposed in the current work. Unless otherwise stated, the material, thermal properties and geometric measures used for the simulations performed in this work have been taken from this report.

5.8 References

Carder, D. R., Barker, K. J., Hewitt, M. G., Ritter, D., and Kiff, A. [2007]. Performance of an Interseasonal Heat Transfer Facility for Collection, Storage and Re-Use of Solar Heat from the Road Surface. PPR302. Transport Research Laboratory.

Google Maps. [2012]. Toddington Service Area, Toddington. [Online]. Available at: http://maps.google.co.uk/. [Accessed: 17-Feb-2012].

Chapter 6 Experimental work

6.1 Experimental Investigation of soil properties at the TRL-ISHTF site.

As part of the preliminary work for this research, a site visit was undertaken at the beginning of February 2012 in order to take samples of soil at the experimental site and observe the current state of the surface of the soil. The location of the site has already been presented in Chapter 5. The soil samples were used to investigate the composition of the soil and to determine several relevant physical parameters.

This Chapter provides a brief summary of the information available in the literature regarding the experimental area and also presents the procedures followed for soil sampling. The laboratory tests performed on soil samples obtained from the experimental site and the results obtained are also presented. A summary of the laboratory results is provided at the end of the Chapter.

6.2 Site investigation and sampling

In this Section the main findings of a desk-study research, regarding the identification of the soil type at the experimental site, are presented. The specific locations and procedures for soil sampling are also described.

6.2.1 Soil type

The outcomes of the desk-study performed before the trip to the experimental site are presented below:

i) The soil at the site according to the TRL report is composed mainly of stiff grey Gault clay from 3 m to at least 25 m depth that is overlain by a layer of firm silty clay at the east of the road while to the west the unperturbed Gault clay is overlain by a layer of reworked layer of Gault clay (Carder et al. 2007).

ii) The solid geology around junction 12 is a Gault formation, covered by a layer 4.2 m thick of glacial till and a layer 1.3 m thick of top soil (Highways Agency 2009).

iii) The geological zone between junctions 10 and 13 is a region with a solid geology of Cretaceous Chalk and Gault clay formations covered by Boulder clay and glacial sands, and gravels (Highways Agency 2006).

From the above, it can be concluded that the main type of soil present in the shallow layers of the experimental site is clay or silty-clay, this being formed by 50% silt and 50% clay. Both materials are classified as very fine regarding its particle size (0.0001mm - 0.05mm) according with the U.S. Department of Agriculture (Haverkamp et al. 1998).

6.2.2 Soil sampling

To gather more information about the soil near the surface of the experimental site, soil samples were taken from two drilled boreholes. The locations for soil sampling are shown in Figure 6-1. Two manual augers (Figure 6-2) were used to drill two boreholes (Bh 1 and Bh 2) to a depth of approximately 1 m. In addition, a disturbed sample of soil at the surface of System 2 was taken. As discussed in Chapter 5, the experimental systems use shallow soil as thermal energy deposit and for this reason the main interest is on the properties of the soil near the surface.

The British Standards (British Standards Institute 1990a; British Standards Institute 1990b) make recommendations regarding preservation of undisturbed samples for preventing loss of moisture during transportation, preparation and storage. In the short term it is recommended to wrap the samples in thin plastic 'Clingfilm' followed by aluminium foil, the tests should be carried out as soon as possible after sampling. Regarding long-term storage, if required, samples should be well sealed and stored in a room that is frost-free and not subjected to vibration. Regarding transportation, undisturbed samples should be packed and stored so as to be frost-free and cushioned against jolting and vibration. Regarding preparation for tests, the procedures should be carried out, ideally, in an area maintained at a high relative humidity. The samples recovered are listed in Table 6-1.

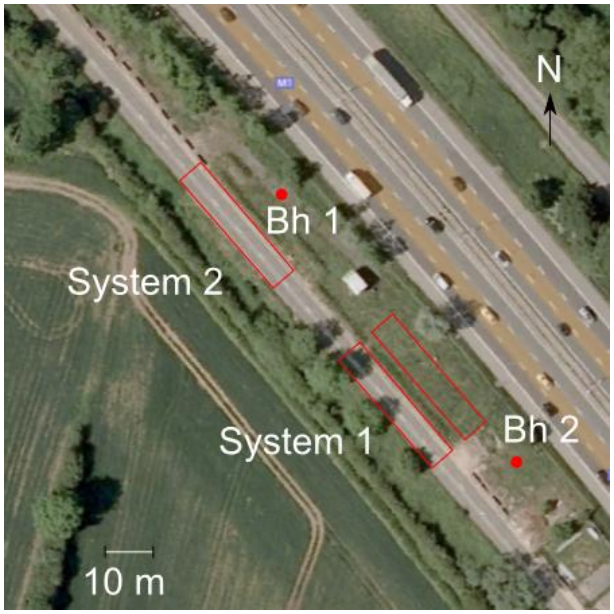

Figure 6-1: Plan view of the experimental site. The locations of the boreholes for soil sampling are labelled as Bh1 and Bh2 and marked in red (Google Maps 2012).

Figure 6-2: Manual augers used for the drilling of shallow boreholes. On the left, 1m non-extensible manual auger; on the right, extensible manual auger with sampling head.

	Depth (m)		
	Borehole 1	Borehole 2	Soil above system 2
Undisturbed samples	0.35	0.45, 0.50, 0.65, 0.75, 0.85, 0.90, 1.07	
Disturbed samples	0.15,0.35	0.15, 0.30, 0.35, 0.60	0.15

Table 6-1: List of disturbed and undisturbed samples taken from borehole 1 and 2 and from the surface of System 2.

6.3 Basic Soil Properties

6.3.1 Laboratory tests

The methods followed for the different laboratory tests performed on the recovered samples from the experimental site are based on the British Standards and on the American Society for Testing and Materials (ASTM) where appropriate. The parameters considered necessary to characterize the soil and to validate the numerical model are:

- Moisture content
- Bulk density
- Particle density
- Mineralogy
- Particle size distribution
- Atterberg limits
- Total suction/moisture content data
- Thermal conductivity

In the following Sections the procedures followed for the determination of each of these properties are described.

6.3.2 Experimental methods

6.3.2.1 Determination of moisture content

The British Standards (British Standards Institute 1990a) specify methods of testing for the determination of basic physical properties including the determination of moisture content. Moisture content is defined as the amount of water, expressed as a proportion by mass of the dry solid particles. The soil is defined as dry when no further water can be removed at a temperature not exceeding 110 °C. The oven-drying method is the definitive procedure used in standard laboratory practice. The weight of the soil sample required for this test is at least 30 g. Three samples from eight different depths from Borehole 2 were tested. Figure 6-3 shows an example of the samples used for the moisture test and Table 6-2 and Figure 6-4 summarize the results obtained.

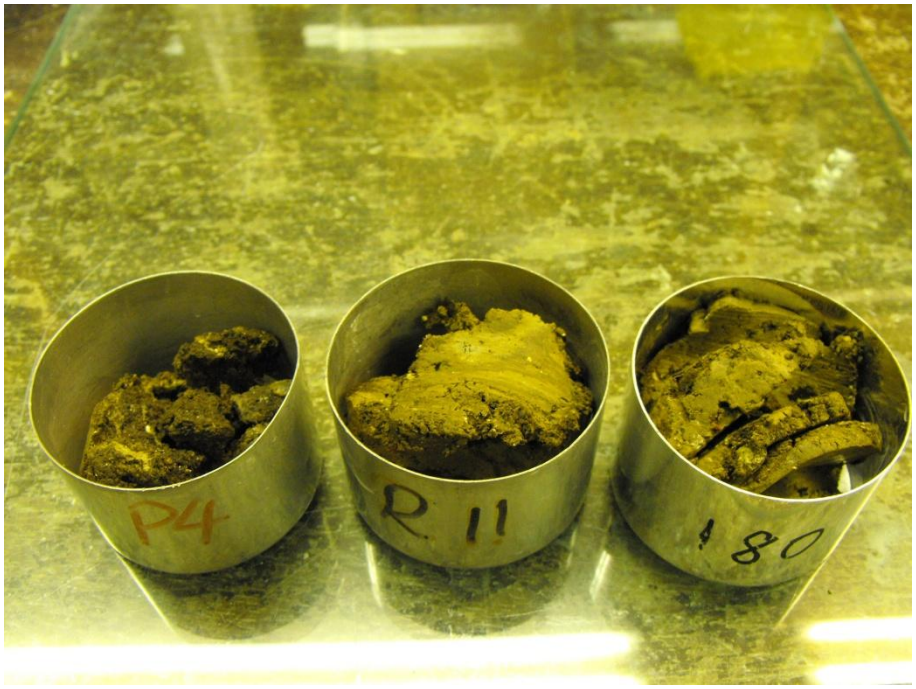

Figure 6-3: The moisture content test requires three samples for each depth. This is an example of how the samples were prepared.

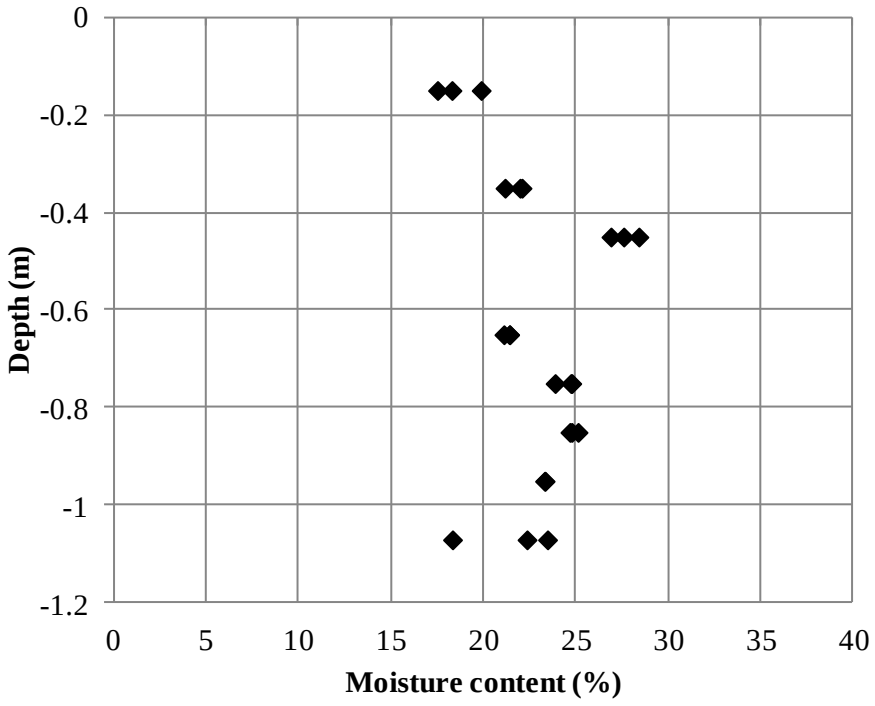

Figure 6-4: Variation with depth of moisture content for samples taken from Borehole 2.

Depth (m)	Moisture Content (%)	Depth (m)	Moisture Content (%)
0.15	19.7	0.75	23.9
0.15	18.3	0.75	24.8
0.15	17.5	0.75	24.7
0.35	22.1	0.85	24.8
0.35	22.0	0.85	25.1
0.35	21.6	0.85	24.7
0.45	28.4	0.95	23.3
0.45	26.9	0.95	23.3
0.45	27.6	1.07	18.3
0.65	21.4	1.07	22.3
0.65	21.4	1.07	23.5
0.65	21.1		

Table 6-2: Experimental data for moisture content test for samples from different depths from Borehole 2.

6.3.2.2 Determination of bulk density

Density or bulk density is defined as the amount of mass per unit volume of soil sample including any water it contains. In the British standards (British Standards Institute 1990b) three methods are specified depending on the cohesive nature of the soil. The method chosen was immersion in water. This method can be employed whenever lumps of material of suitable size can be obtained.

In this method a sample of soil is trimmed and weighed, then it is carefully covered in paraffin wax and weighed again. Then the sample is immersed in water and its apparent mass measured. Next, a portion of the sample, completely free of paraffin wax, is used to determine its moisture content. The volume of the sample is calculated by difference between the mass of the sample plus wax coating and its apparent mass immersed in water, then, the bulk density is calculated using the mass of the sample without wax coating divided by the volume. Finally, the dry density is calculated using the bulk density and the moisture content.

This method was followed for two samples from 0.95 m depth from Borehole 2. Figure 6-5 and Figure 6-6 show the samples used for this test and a sample covered in wax and ready to be immersed in water. Table 6-3 summarizes the results obtained.

Depth (m)	Bulk density (Mg/m^3)	Moisture content (%)	Dry density (Mg/m^3)
0.95	1.99	23.3	1.61
0.95	1.99	23.3	1.61

Table 6-3: Results for the bulk density test. Two samples taken from Borehole 2 at 0.95 m depth were tested.

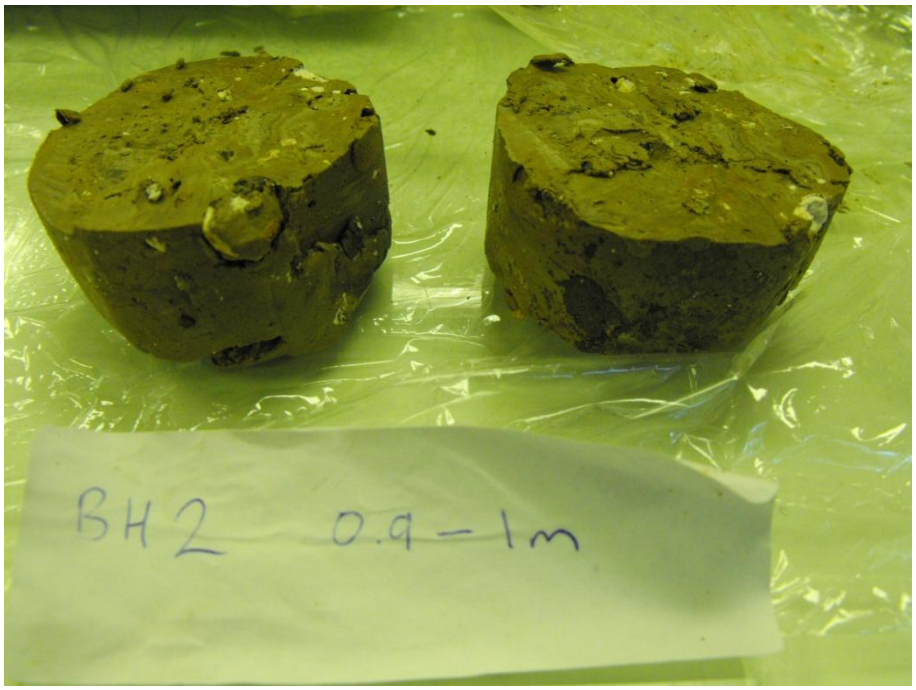

Figure 6-5: Samples used for the bulk density test using the method of immersion in water.

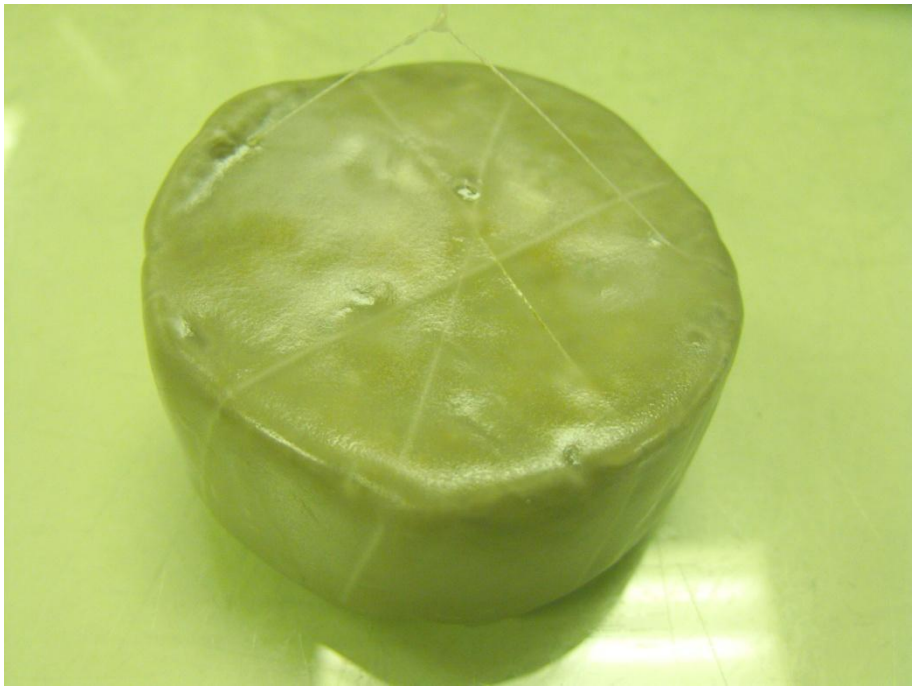

Figure 6-6: Sample covered in wax ready for immersion in water for the bulk density test.

6.3.2.3 Determination of particle density

Particle density also referred as specific gravity, is the density of the solid particles in the soil sample. Three methods are described in the British Standards (British Standards Institute 1990a) for determination of particle density. The method chosen for this test was the small pycnometer method which is the definitive method for soils consisting of clay, silt and sand-sized particles. This method is suitable for soils consisting of particles finer than 2 mm.

The material used for this test was the portion of particles passing the 63 µm sieve in the particle size distribution test using the wet sieving method. The recovered material dissolved in water was oven dried. This procedure hardened the material and additional grinding was required. After the material was ground, it was kept in sealed containers until required. Two samples were tested for each depth using the small pycnometer method. Figure 6-7 shows the pycnometers with soil samples dissolved in water. The pycnometers were surrounded with paper to prevent them from falling due to vibrations and put into a vacuum chamber to extract all the air from the solution as established by the British Standard. The results are summarized in Table 6-4 and Figure 6-8.

Figure 6-7: Pycnometers with soil samples.

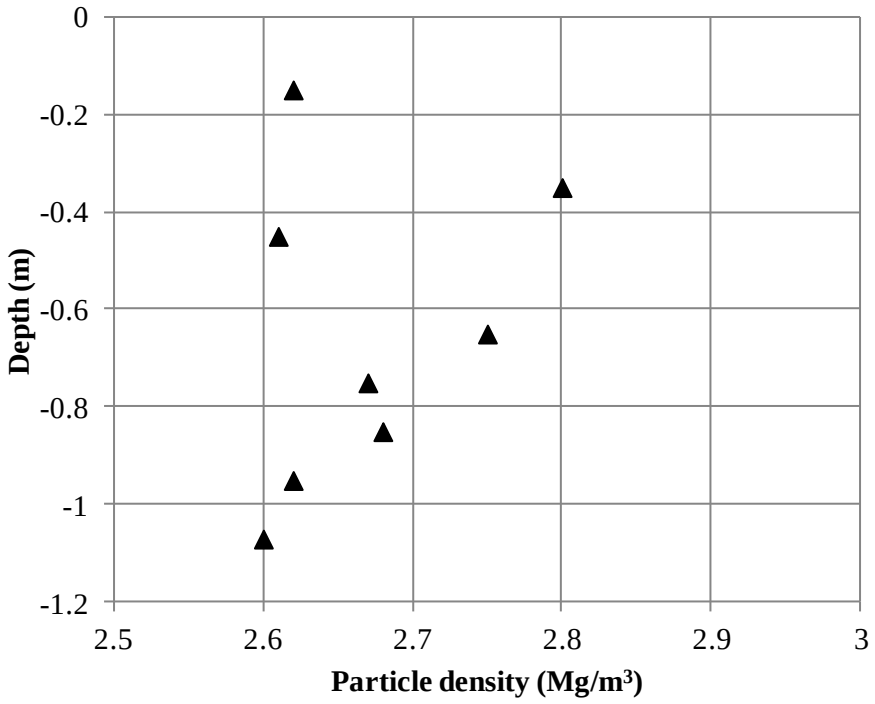

Figure 6-8: Variation with depth of particle density for samples taken from Borehole 2. The plotted points are the average values in Table 6-4.

Depth (m)	Particle density sample 1 (Mg/m^3)	Particle density sample 2 (Mg/m^3)	Average (Mg/m^3)
0.15	2.63	2.61	2.62
0.35	2.81	2.78	2.80
0.45	2.61	2.62	2.61
0.65	2.76	2.75	2.75
0.75	2.68	2.66	2.67
0.85	2.67	2.68	2.68
0.95	2.60	2.64	2.62
1.07	2.58	2.61	2.60

Table 6-4: Results for particle density test.

6.3.2.4 X ray Diffractometer Test

X ray diffraction is a non-destructive technique to identify compounds rather than elements in a sample. X ray wavelength is of the same order of magnitude as the spacing between atoms in a crystal. This allows the radiation to be scattered by atoms in a unique way depending on their crystal structure which in turn is related with a specific compound.

The equipment used is a Phillips PW-1710 Automatic Powder Diffractometer located in the Characterization Laboratory for Environmental Engineering Research

(CLEER) at Cardiff University. The generated results are formed by the intensities of the reflected radiation from the sample as a function of the angle of incidence. This data can later be analysed with its own analytic software than includes a database to compare and identify compounds present in the sample.

The objective of this test was to identify the minerals present in the sample and its relative abundance. The material used for this test was the portion of particles passing the 63 μm sieve in the particle size distribution test using the wet sieving method. The recovered material dissolved in water was oven dried. This procedure, as mentioned before, hardened the material and additional grinding was required. Afterwards, it was kept in sealed containers until required. One test was carried out for each sample. The results from the test showed the presence of four main minerals: Illite, Calcite, Quartz and Kaolinite.

6.3.2.5 Determination of particle size distribution

The determination of the particle size distribution for samples from different depths from Borehole 2 was carried out following specifications from the British Standards (1990b). According to the British Standards (1990b) wet sieving is the definitive method applicable to essentially cohesionless soils with significant quantities of silt and clay. Two sieves were used, 2 mm and 63 μm. The particles that passed the 63 μm sieve were recovered in a bucket for further tests. The masses of particles retained in the 2 mm and 63 μm sieves were determined by direct weighing after oven drying. The mass of particles that passed the 63 μm sieve was determined by difference between the initial mass of the sample and the masses of the particles bigger than 2 mm and the particles between 2 mm and 63 μm as recommended by the standards. Table 6-5 and Figure 6-9 summarize the results from this test.

For the distribution of particles less than 63 μm a particle size analyser was used. The system requires small amounts of fine grained material (< 63 μm), the density of the samples and the identification of the minerals present in them. The minerals are identified from the results of the X ray diffractometer test (Section 6.3.2.4) while the density is obtained from the results of the particle density test (Section 6.3.2.3).

The material used was the recovered from the wet sieving test after oven drying. This procedure hardens the material and further grinding is necessary in order to

obtain powder samples. The powder is kept in sealed containers to keep the samples dry.

The results from the particle size distribution are shown in Figure 6-10. It shows three clearly distinct peaks at 0.8 µm, 5 µm, and 24 µm. According to Reeves et al. (2006) kaolinite has a planar diameter in the range from 0.1 µm to 4 µm and Illite has a planar diameter in the range from 0.1 µm to 2 µm. Calcite particles are generally between 3 and 6 µm. Quartz is generally composed of sand size particles (> 63 µm and < 2 mm) but finer particles might have passed through the 63 µm sieve due to a size smaller than the average and this could explain the peak at 24 µm.

Depth (m)	Particles < 2 mm (%)	2 mm > Particles > 63 µm (%)	Particles < 63 µm (%)
0.15	24.00	49.90	26.60
0.35	5.70	20.00	74.30
0.45	7.60	40.30	52.10
0.65	4.90	26.70	68.40
0.75	3.90	15.60	80.50
0.85	5.00	18.50	76.50
1.07	7.50	26.70	65.80

Table 6-5: Results for particle size distribution test.

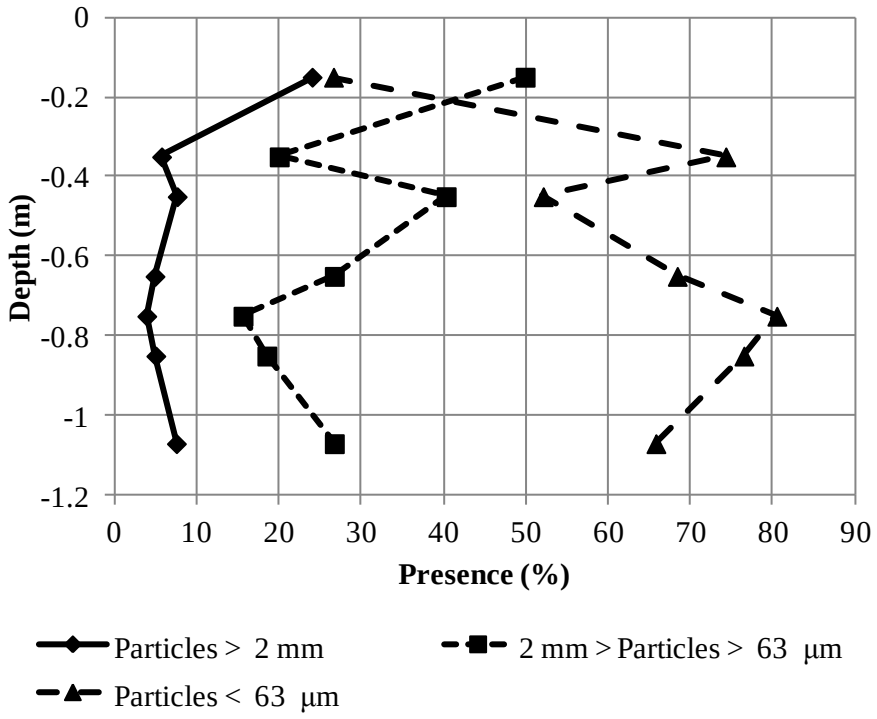

Figure 6-9: Variation with depth of particle size distribution for samples taken from Borehole 2.

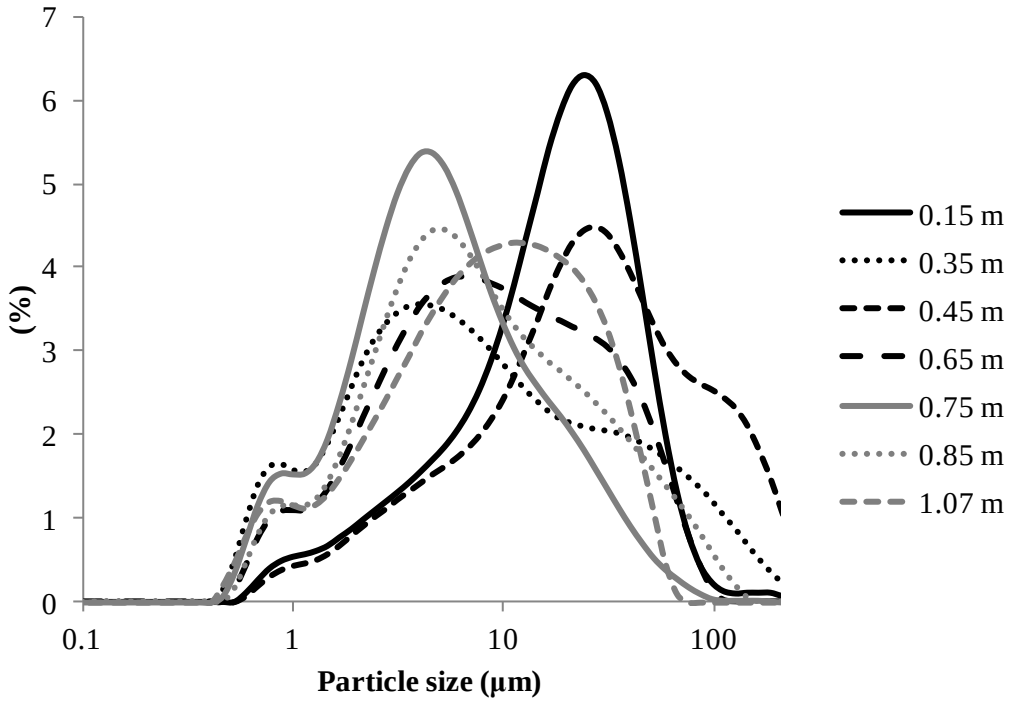

Figure 6-10: Particle size distribution for the fraction of particles that passed the 63 µm sieve corresponding to samples from different depths.

6.3.2.6 Determination of Atterberg limits.

The behaviour and consistency of fine-grained soils can be classified as solid, plastic and liquid depending on its moisture content. These limits are referred to as the Atterberg limits. The shrinkage limit is defined as the limiting moisture content for no change in volume; the plastic limit is defined as the limiting moisture content for plastic behaviour; and the liquid limit is defined as the limiting moisture content for liquid behaviour. These limits are related to other parameters such as: the plasticity index and the liquid index. The plasticity index is the of water contents where the soil exhibits plastic properties, it is defined as the difference between the liquid and plastic limits. The liquidity index measures the degree of liquidity of a soil. It is defined as the ratio of the difference between the natural moisture content and the plastic limit to the difference between the liquid and plastic limits. Others related parameters are: activity, strength, compressibility and volume change.

The liquid and plastic limits; and liquidity and plasticity indexes are determined as indicated in the British standards (1990b) following recommendations made by the ASTM Standards (2010) where appropriate. The Cone Penetration Test was the method preferred to determine the liquid limit as advice by the standard (British

standards, 1990b). Table 6-6 summarizes the results of the Atterberg limits obtained while Figure 6-11 shows the results for the Cone Penetration Test. As indicated in (British standards, 1990b) the liquid limit is reported as that corresponding to a cone penetration of 20 mm. The plastic limit was obtained as suggested in (British standards, 1990b) by taking a sample of about 20 g of moist soil (particles < 425 μm), placing it on a glass mixing plate and mould it with the fingers until it starts to crumble at which point the moisture content is determined. This moisture content marks the plastic limit of the soil sample. Two plastic limit tests were carried out with the following results of moisture content: 18.5 % and 18.1 %.

Liquid limit	50.7
Liquidity index*	0.15
Plastic limit	18.3
Plasticity index	32

Table 6-6: Results for liquid and plastic limits. Derived indexes, plasticity and liquidity, are also included. * The liquidity index reported is an average over the different moisture contents present in each depth.

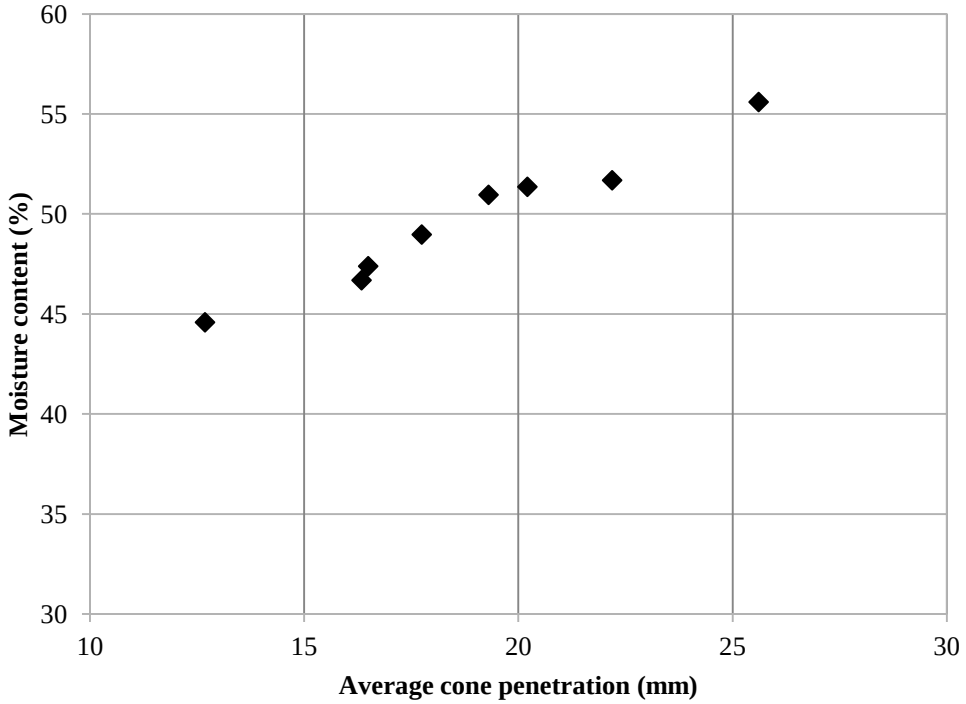

Figure 6-11: Variation of cone penetration with moisture content for liquid limit test.

6.3.2.7 Determination of total suction

The chilled-mirror dew-point technique is used to infer the total suction of the soil under isothermal conditions in a sealed container. The technique is based on equilibrating the liquid phase of the water in a soil sample with the vapour phase of the water in the air space above the sample (Tarantino et al, 2008). The mirror is chilled until dew starts to form on its surface at which the temperature of the mirror is adjusted so that the rate of condensation and evaporation from the mirror surface is in dynamic equilibrium. At this point the temperature of the mirror represents the saturation temperature (dew point) for the water vapour in the air surrounding the soil sample. The chilled-mirror dew-point technique is widely considered to be the most precise method for total suction measurement (Leong et al. 2003). Measurement of the dew point allows determination of the relative humidity which in turn is directly related to the total suction in a soil sample. Total suction is defined as the equivalent suction derived from measurement of the partial pressure of the water vapour in equilibrium with the soil water, relative to the partial pressure of the water vapour in equilibrium with free pure water (Fredlund and Rahardjo 1993). Table 6-7 shows the results for total suction from the chilled-mirror technique and moisture content from two samples from different depths from Borehole 2.

Depth (m)	Moisture content (%)	Total suction (kPa)
0.65	19.0	430
0.95	22.1	460

Table 6-7: Results for total suction obtained with the chilled-mirror dew-point technique for two samples from different depths from Borehole 2. Moisture content for each sample is also include.

6.3.2.8 Determination of heat conductivity

Thermal conductivity is the property of a substance that defines its ability to conduct thermal energy, the higher its value the easier for heat to flow. In experimental measurements it is usually determined as a bulk property, this is, a weighted average of the heat conductivities of all the constituents present on a sample of material. In the case of a soil sample, the constituents are all the minerals in the solid phase and the water and air present on its voids.

This property was determined with the help of the *Centro de Investigaciones Energeticas, Medioambientales y Tecnologicas*, CIEMAT, located in Madrid, Spain. The laboratory uses the transient hot wire method. The method is a transient dynamic

technique based on the measurement of the temperature rise of a linear heat source (hot wire) embedded in the tested material. The minimum size of the soil samples for the determination of thermal conductivity as required by the CIEMAT was 10 cm x 4 cm x 3 cm. Ideally, undisturbed samples should be used, unfortunately, the available undisturbed samples didn't meet the size requirements and new samples were prepared, using the disturbed material, at the same density and water content as the undisturbed samples.

For the preparation of the new samples, a compaction device was constructed by the technical staff at the School of Engineering of Cardiff University. The device consists of a hollow cube made of iron of 10 cm x 10 cm x 10 cm. The cube is partially filled with plastic in order to reduce its interior size to 10 cm x 4 cm. A heavy piece of iron, designed to fit into the empty section of the cube, was used as a piston to compact the soil.

The samples were prepared to have the original bulk and dry density: 1.97×10^3 kg/m^3 and 1.61×10^3 kg/m^3 respectively. However, the objective was to reach three different moisture contents corresponding to degrees of saturation of 100%, 90% and 80%. The degree of saturation is defined as the ratio of volume of water in the soil to the volume of voids for the same volume of soil. The volume of voids is the product of the void ratio times the volume of soil. The void ratio was calculated with the bulk density and particle density for the same depth. It was found to be equal to 0.386. Then, for a sample of 180 cm^3 the volume of voids is 69.5 cm^3 . This is the maximum capacity of water that the soil can hold in its natural state and corresponds to a degree of saturation of 100%. Similarly, a volume of water of 62.5 cm^3 and 55.5 cm^3 corresponds to a degree of saturation of 90% and 80% respectively.

The dimensions of the prepared samples were 10 cm x 4 cm x 4.5 cm in order to leave space to trim any imperfections on the top and bottom of the sample due to the soil sticking to the surface of the apparatus (Figure 6-12).

The material used to prepare each sample was 290 g of oven dried disturbed soil recovered from the drilling of the boreholes mixed with 73 cm^3 , 66 cm^3 and 60 cm^3 of water to reach 100%, 90% and 80% degree of saturation respectively. The soil was mixed inside a plastic bag and left in a fridge overnight to reach equilibrium. The next day a small amount of moist soil was put into the mould and was

hammered with the piston by hand in a consistent manner, then the surface of the compacted soil was scratched to prevent layering and more soil was put into the container and the process was repeated. When the process of compaction was complete, the sample was taken out of the mould carefully. Figure 6-13 shows an example of a reconstituted sample prepared with the mould. Two identical samples were prepared in each case, one was tested to ensure that the requirements were met. The other one was stored for shipping. The shipping samples were wrapped in plastic foil and the samples for testing were sliced in four layers of approximately the same width. Each layer was weighted and prepared to determine its moisture content and dry density. Table 6-8, Table 6-9 and Table 6-10 summarize the results obtained from the tested samples. The samples were wrapped in plastic foil and put into the fridge until shipping. Previous to shipping via courier, the samples were further wrapped with bubble plastic and put into a hard plastic container of a suitable size.

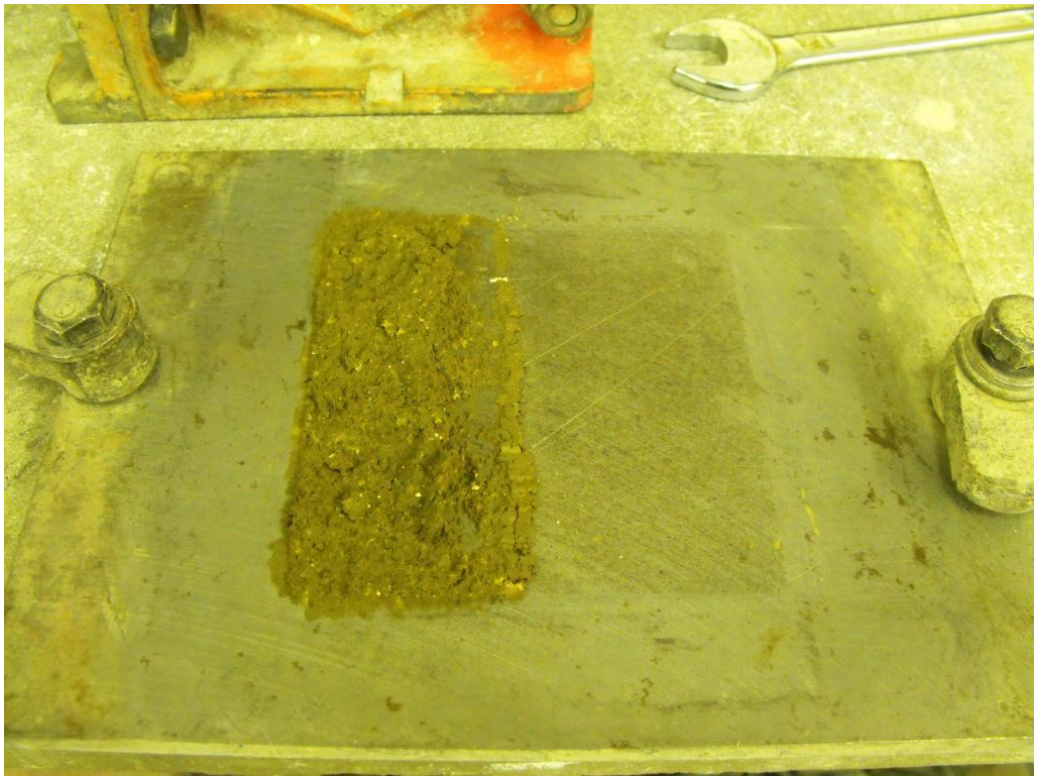

Figure 6-12: Metal base where the samples for the thermal conductivity test were prepared. It can be seen that part of the material stick to the base after preparation. The samples were prepared with additional 1.5 cm height to allow trimming of imperfections at the base.

Figure 6-13: Reconstituted sample prepared with the moulder.

The samples were independently tested by CIEMAT to determine its heat conductivity, moisture content, and dry density. Table 6-11 shows the results from these tests. It can be observed that the moisture contents agree with the intended ones. However, the dry densities are different from the intended values by as much as 7%. The heat conductivity is expected to rise with the moisture content as the voids in the soil fill with water because the water has a higher thermal conductivity than air. The experimental results in Table 6-11 show that the thermal conductivity increments with the dry density despite lower moisture content. This indicates that the dry density has a higher impact on the heat conductivity of the samples than the moisture content. This might be explained since the thermal conductivity of the solid particles is higher than the thermal conductivity of water (Fredlund and Rahardjo, 1993). Since the dry density and moisture content of Sample C is comparable to the dry density and natural moisture content of the soil samples recovered from the experimental site (Table 6-2 and Table 6-3), the thermal conductivity obtained for this sample could be considered representative of the thermal conductivity of the soil in the experimental site.

Sample	Moisture content (%)					Error (%)	
	Expected	Layer 1	Layer 2	Layer 3	Layer 4	Min	Max
A	25.2	23.7	24.7	24.5	24.1	2.0	5.8
B	23.4	22.8	22.6	23.4	22.8	0.1	2.6
C	21.4	21.9	21.8	21.6	22.5	0.9	2.5

Table 6-8: Moisture content data from reconstituted samples prepared for testing. Layers are enumerated from bottom to top.

Sample	Dry density (Mg/m^3)					Error (%)	
	Expected	Layer 1	Layer 2	Layer 3	Layer 4	Min	Max
A	1.61	1.32	1.55	1.64	1.57	1.9	18.2
B	1.61	1.41	1.75	1.56	1.55	3.2	12.5
C	1.61	1.48	1.69	1.73	1.85	5.1	14.6

Table 6-9: Dry density data from test reconstituted samples. Layers are enumerated from bottom to top.

Sample	Moisture content (%)					Error (%)	
	Expected	Layer 1	Layer 2	Layer 3	Layer 4	Min	Max
A	2.0	1.6	1.9	2.1	2.0	1.9	18.7
B	1.9	1.7	2.2	1.9	1.9	3.0	12.6
C	1.9	1.8	2.1	2.1	2.3	5.7	15.9

Table 6-10: Bulk density data from test reconstituted samples. Layers are enumerated from bottom to top.

Sample	Moisture content (%)	Dry density (Mg/m^3)	Heat conductivity (W/mK)
A	25.2	1.50	0.69±0.08
B	22.4	1.57	1.14±0.16
C	21.0	1.61	1.37±0.31

Table 6-11: Laboratory results for moisture content, dry density and heat conductivity for reconstituted samples. The tests were performed independently by the CIEMAT.

6.4 Concluding remarks

This Chapter has presented a set of basic laboratory tests performed on soil samples collected from the experimental site reported by Carder et al. (2007) and summarized in Chapter 5. These tests include: moisture content, bulk density, particle density, mineralogy, particle size distribution, Atterberg limits, total suction/moisture content data and thermal conductivity.

6.5 Bibliography

ASTM Standards. [2010]. Liquid and Plastic Limits as Determined from the Fall Cone and the Casagrande Methods. Technical ASTM D4318-10. West Conshohocken, PA: ASTM International. http://www.astm.org/.

British Standards Institute. [1990a]. *Methods of Test for Soils for Civil Engineering Purposes. Classification Tests*. BS 1377-2:1990. London: British Standards Institute.

British Standards Institute. [1990b]. *Methods of Test for Soils for Civil Engineering Purposes. General Requirements and Sample Preparation*. BS 1377-1:1990. London: British Standards Institute.

Carder, D. R., Barker, K. J., Hewitt, M. G., Ritter, D., and Kiff, A. [2007]. Performance of an Interseasonal Heat Transfer Facility for Collection, Storage and Re-Use of Solar Heat from the Road Surface. PPR302. Transport Research Laboratory.

Fredlund, D. G. and Rahardjo, H. [1993]. *Soil Mechanics for Unsaturated Soils*. Wiley.

Google Maps. [2012]. Toddington Service Area, Toddington. [Online]. Available at: http://maps.google.co.uk/. [Accessed: 17-Feb-2012].

Haverkamp, R., Bouraoui, F., Zammit, C., and Angulo-Jaramillo, R. [1998]. Soil Properties and Moisture Movement in the Unsaturated Zone. In *The Handbook of Groundwater Engineering*, edited by J. Delleur. CRC Press. http://www.crcnetbase.com/doi/abs/10.1201/9781420048582.ch5.

Highways Agency. [2006]. M1 Widening Junctions 10 to 13 - Cultural Heritage Stage 3 Baseline Report. D110842/05/04c. Highways Agency.

Highways Agency. [2009]. M1 Junctions 10 to 13 Improvement – Junctions 11 and 12: Environmental Statement. D123846/5/03. Highways Agency.

Leong, E.-C., Tripathy, S., and Rahardjo, H. [2003]. Total Suction Measurement of Unsaturated Soils with a Device Using the Chilled-Mirror Dew-Point Technique. *Géotechnique* **53** (2): 173–182. doi:10.1680/geot.2003.53.2.173.

Reeves, G. M., Sims, I., and Cripps, J. C. [2006]. *Clay Materials Used in Construction*. Geological Society.

Tarantino, A., Romero, E., and Cui, Y. J. [2008]. Laboratory and Field Testing of Unsaturated Soils. Springer Science & Business Media.

Chapter 7 1D Analytical solutions for ground temperature profiles and stored energy using meteorological data

7.1 Introduction

The estimation of ground temperature profiles is important for several engineering applications that use the soil as a reservoir or source of thermal energy. Examples of these applications are the minimisation of thermal losses and passive heating and cooling of buildings (e.g. Rees et al. 2000; Zoras 2009), ground source heating (e.g. Florides and Kalogirou 2007), shallow energy piles (e.g. Wood et al. 2010) and inter seasonal thermal energy storage (Bobes-Jesus et al. 2013; Pinel et al. 2011). These applications are highly dependent on the amount of energy present in the near-surface region of the soil and its temporal variation. Subsequently one of the first steps in the process of evaluation of their implementation is related with the assessment of ground temperature profiles and overall ground energy storage. To provide sufficient details such assessments are usually performed with the aid of theoretical models solved by numerical methods (Qin et al. 2002; Yumrutaş et al. 2005; Laloui et al. 2006). These numerical methods have the advantage of being able to include a high range of complexities within the domain of interest for example, different physical processes, materials, geometries, boundary conditions, etc. However, if the problem is relatively simple, it can be approached analytically. An analytical solution is usually simpler, easier to implement computationally and offers detailed insight about the underlying physical processes. Also, analytical solutions can be helpful in establishing reasonable initial conditions for more comprehensive numerical simulations when no other information is available.

In this Chapter, the development of a new 1d analytical solution for the transient heat transfer equation is presented. Section 2.6.1 has provided a literature review about the importance and implementation of analytical methods in the prediction of the temperature profile of soils. Special attention was given to the treatment of the boundary condition at the soil surface. Suitable analytical expressions to represent meteorological variables need to be defined in order to consider more realistic boundary conditions at the soil surface. These analytical expressions are developed

here by using *ad-hoc* equations for two main meteorological variables with relatively simple heat transfer coefficients.

Section 7.2 introduces the theoretical formulation for the transient boundary valued problem of heat diffusion. Section 7.3 defines the approach taken for the boundary condition at the soil surface and summarize the required heat transfer coefficients. Section 7.4 provides details for the construction of two analytical expressions to represent diurnal and annual variations in air temperature and solar radiation. Section 7.5 defines and shows the results of a verification exercise to test the numerical model presented in Chapter 4. Section 7.6 shows the results of a validation test for the analytical solution carried out comparing the predicted temperature profiles and energy stored in the soil with experimental measurements provided by TRL (Chapter 5). Finally, Section 7.7 performs a sensitivity analysis on some of the main variables involved in the construction of the analytical model and their impact on the equilibrium temperature of the soil and predicted amount of stored energy.

7.2 Theoretical formulation

7.2.1 General solution

The general form for the one dimensional non-homogeneous transient heat diffusion equation defined in a finite domain of length L_s can be expressed as (based upon equation (3-16), assuming λ_b as constant).

$$\frac{d^2T_s}{dz^2} = \frac{1}{\alpha_b}\frac{dT_s}{dt} \quad \text{in} \quad \begin{matrix} 0 \le z \le L \\ t > 0 \end{matrix} \tag{7-1}$$

where T_s (˚C) is the temperature of the soil and α_b (m^2/s) is the bulk thermal diffusivity defined as:

$$\alpha_b = \frac{\lambda_b}{C_{p,b}} \tag{7-2}$$

where $C_{p,b}$ (J/m^3K) is the bulk volumetric heat capacity of the soil. The solution of this equation can obtained following the approach given in (Özişik 2002) for various boundary conditions using the integral transform technique. The boundary conditions and initial condition considered here are defined as (see Figure 7-1):

$$f_1(t) = -\lambda_b \frac{dT_s}{dz} + h_1 T_s \quad \text{at} \quad z = 0,\ t > 0 \tag{7-3}$$

$$f_2(t) = \lambda_b \frac{dT_s}{dz} + h_2 T_s \quad \text{at} \quad z = L_s,\ t > 0 \tag{7-4}$$

$$T_s = F(z) \quad \text{in} \quad 0 \le z \le L_s,\ t = 0 \tag{7-5}$$

where h_1 (W/m^{2}K) and h_2 (W/m^{2}K) are the heat transfer coefficient at z=0 (soil surface) and z=L_s respectively, and λ_b (W/mK) is the soil thermal conductivity.

In the particular case where a Robin boundary condition $f_1(t)$ is applied at z=0, a zero flux boundary condition is applied at z=L_s and a constant initial condition F_i is used, the solution has the form (Özişik 2002):

$$T_s(z,t) = \sum_{m=1}^{\infty} 2\left(\frac{\beta_m^2 + H_1^2}{L_s(\beta_m^2 + H_1^2) + H_1}\right) e^{-\alpha_b \beta_m^2 t} \cos\beta_m(L_s - z)\left[\frac{F_i \sin(\beta_m L_s)}{\beta_m} + \frac{\alpha_b \cos(\beta_m L_s)}{\lambda_b} \int_{t'=0}^{t} e^{\alpha_b \beta_m^2 t'} f_1(t')dt'\right] \tag{7-6}$$

where H_1=h_1/λ_b and the eigenvalues β_m are the positive roots of (Özişik 2002):

$$\beta \tan\beta = H_1 \tag{7-7}$$

Equation (7-7) is solved iteratively for each m starting with β=0 for m=1 and then using the calculated value for m=2 and so on. For the purpose of this study, the number of terms used in equation (7-6) is 5000.

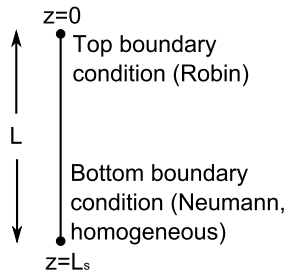

Figure 7-1: 1d domain and boundary conditions considered for the analytical problem.

7.2.2 Energy stored in the soil

The description of the temperature profile of the soil with depth given by equation (7-6) allows the calculation of the energy stored E_s (J/m^2) in a column of soil of depth L_s with reference to the energy present in the soil at an arbitrary reference time as:

$$E_s(z,t) = C_{p,b}\int_0^{L_s}\left[T_s(z,t) - T_s(z,t_{ref})\right]dz \tag{7-8}$$

where $T_s(z,t,)$ is the temperature profile at time t and $T_s(z,t_{ref})$ is the temperature profile at a reference time t_{ref}.

7.3 Boundary condition at the soil surface

The boundary condition at the soil surface (z=0) is based on consideration of the heat energy balance at the surface of the soil and can be defined (as detailed in Section 3.7, equation (3-70) for bare soil) by:

$$\begin{aligned}-\lambda_b\frac{dT_s}{dz} = (1-\alpha_s)R + 4\sigma T_*^3\varepsilon_{ss}\varepsilon_{sky}^{0.25}T_{a,\mathrm{K}} - 4\sigma T_*^3\varepsilon_{ss}T_{s,\mathrm{K}} \\ +h_E(e_a - e_{ss}) + h_C T_a - h_C T_s\end{aligned} \tag{7-9}$$

where α_s is the soil albedo (Garratt 1994), R (W/m^2) is solar radiation, σ (W/m^{2}K^4) is the Steffan-Boltzmann constant, T_a and $T_{a,\mathrm{K}}$ is air temperature in (˚C) and (K) respectively, (variables and constants used to calculate the terms in equation (7-9) are summarized in Table 7-1). T_* (K) is an average temperature that arises from the linearization of the infrared heat transfer equation (Duffie and Beckman 2006) and is defined as:

$$T_* = \left(\frac{\varepsilon_{sky}^{0.25}T_{a,\mathrm{K}} + T_{ss,\mathrm{K}}}{2}\right) \tag{7-10}$$

$T_{ss,\mathrm{K}}$ is the temperature of the soil surface in (K), ε_{ss} is the emissivity of the soil surface (Garratt 1994), ε_{sky} is the sky emissivity (Edinger and Brady 1974; Herb et al. 2008) defined as:

$$\varepsilon_{sky} = N + 0.67(1-N)e_a^{0.08} \tag{7-11}$$

where N is a cloud factor with a non-dimensional value from 0 to 1. N=0 corresponds to clear sky conditions, while N=1 corresponds to fully clouded sky. e_{ss} (kPa) and e_a (kPa) are the vapour pressure for the soil surface and air respectively and are defined as (from eq. (3-55) and (3-56)):

$$e_{ss} = \exp\left(-\frac{h_{ss}g}{R_w T_{ss,\mathrm{K}}}\right)e_{ss}(0)\exp\left(\frac{L_v}{R_w}\left(\frac{1}{273.15\mathrm{K}} - \frac{1}{T_{ss,\mathrm{K}}}\right)\right) \tag{7-12}$$

$$e_a = \left(\frac{H_a}{100}\right) e_a(0) \exp\left(\frac{L_v}{R_w}\left(\frac{1}{273.15\text{K}} - \frac{1}{T_{a,\text{K}}}\right)\right) \tag{7-13}$$

where h_{ss} (m) is the surface water pressure head (the average value of saturation and wilting point for clay provided by Garrat (1994) is used), g (m/s^2) is the acceleration of gravity, R_w (J/kgK) is the gas constant for water vapour, L_v (J/kg) is the latent heat of vaporization of water and H_a (%) is the relative humidity.

The heat transfer coefficients for evaporative (h_E) and convective (h_C) heat flux can be defined following the approach given by Jasson et al. (2006). This approach assumes a turbulent heat transfer process at the surface of bare soils and has the advantage of using relatively simple heat transfer coefficients:

$$h_E = \frac{\rho_a c_{p,a}}{r_a \gamma} \tag{7-14}$$

$$h_C = \frac{\rho_a c_p}{r_a} \tag{7-15}$$

where ρ_a (kg/m^3) is the air density, c_p (J/kgK) is air specific heat capacity, γ (kPa/K) is the psychrometric constant and r_a (s/m) is the aerodynamic resistance defined (for neutral conditions (Garratt 1994)) as:

$$r_a = \frac{\ln\left(\frac{z_u}{z_{0m}}\right)\ln\left(\frac{z_T}{z_{0T}}\right)}{\kappa^2 u_s} \tag{7-16}$$

where u_s (m/s) is the wind velocity, κ is the Von Karman constant, z_u (m) and z_T (m) is the height at which wind speed and air temperature measurements were made respectively, z_{0m} (m) and z_{0T} (m) are the relative roughness for momentum and heat respectively of the soil surface in its interaction with the atmospheric boundary and their values are taken from Garrat (1994) and Kotani and Sugita (2005) respectively.

The psychrometric constant is defined as:

$$\gamma = \frac{c_{p,a} P_a}{0.622 L_v} \tag{7-17}$$

where P_a (kPa) is the atmospheric pressure.

As mentioned in Section 2.4.2, other authors (Edinger and Brady 1974; Herb et al. 2008) use different approaches to define these heat transfer coefficients which are useful for cases were non turbulent processes can be assumed (low wind speeds) that take into account forced and natural convection, however these coefficients are, relatively more complex and not readily amenable for inclusion in the form of analytical solution presented here.

Equation (7-9) can be rewritten in the form of equation (7-3), to subsequently be used in the solution of equation (7-6). Average values for air temperature, wind speed and relative humidity are required to calculate some of these coefficients (namely ε_{sky}, $T_{0,K}$ and e_a) that otherwise would be unsuitable to include in an analytical approach. Also, the evaporative term e_{ss} is dependent on the temperature of the surface of the soil. An average temperature for the soil surface can be estimated by integrating equation (7-9) over a full yearly cycle so as to consider a quasi-equilibrium scenario (i.e. zero net heat flux) after expressions for solar radiation and air temperature have been defined.

ρ_a (kg/m^3)	1.2041	κ	0.41	g (m/s2)	9.8
$c_{p,a}$ (J/kgK)	1012	R_w (J/kgK)	461.5	h_{ss} (m)	-75.2025
L_v (J/kg)	2.45E6	σ (W/m2K4)	5.67E-8	P_a (kPa)	101.325

Table 7-1: Summary of variables and constants used to calculate parameters in equation (7-9).

7.4 Mathematical expressions for meteorological variables

In order to solve equation (7-6) using equation (7-9) as a boundary condition it is necessary to formulate expressions for the meteorological variables required. Mathematical expressions for solar radiation are available in the literature (as noted in Chapter 2). In general these expressions are functions of geographical parameters and provide the amount of radiation between sunrise and sunset, however, they are not suitable for use here because for a continuous analytical solution a function that is applicable during night time is required. In this Chapter it is proposed to develop two simplified mathematical expressions for idealised daily and annual variations of solar radiation and air temperature that can be constructed using widely available averaged meteorological data.

7.4.1 Solar radiation

The expression for solar radiation builds upon an expression for daily variations presented by Lumb (1964). In this thesis, Lumb (1964) expression is expanded to include annual variation as:

$$R(t) = \frac{\pi}{2}\left(\cos^2(\omega_1 t) - \cos(\omega_1 t) + \frac{4-\pi}{2\pi} \right)\left(\mathrm{R}_1 \cos(\omega_2 t) + \mathrm{R}_2 \right) \quad (7\text{-}18)$$

where t is given in seconds taking the origin at midyear (July 1st), ω_2 is the annual period defined as $2\pi/31557600$ s (2π divided by 365.25 days in seconds), and ω_1 is the daily period defined as $2\pi/86400$ s (2π divided by 24 hours in seconds). R_1 and R_2 are coefficients, that can be determined from the meteorological conditions for summer and winter (the summer and winter periods can be arbitrarily defined based on localised conditions). These coefficients are defined as:

$$R_1 = 0.5(A - B) \quad (7\text{-}19)$$

$$R_2 = 0.5(A + B) \quad (7\text{-}20)$$

where A and B are the summer and winter daily average solar radiation respectively.

7.4.2 Air temperature

A similar sinusoidal expression is proposed to represent the diurnal air temperature variation as, in general, air temperature variations correlate to insolation. For simplicity a sinusoidal daily variation with its maximum at midday and the minimum at midnight is assumed. The annual variation is mainly sinusoidal with maxima and minima at summer and winter respectively but incorporates an additional sine term to take into account typically observed slightly higher values in spring and slightly lower values in autumn. The proposed expression is:

$$T_a(t) = T_1\left[\cos(\omega_2 t) + 0.5\sin(\omega_2 t)\right] + T_2 - \left\{T_3\left[\cos(\omega_2 t) + 0.5\sin(\omega_2 t)\right] + T_4\right\}\cos(\omega_1 t) \quad (7\text{-}21)$$

where t is given in seconds taking the origin at midyear (1st July). T_1, T_2, T_3 and T_4 are coefficients determined from the meteorological conditions for mid-summer and mid-winter periods. They are calculated as:

$$T_1 = 0.5(C - D) \quad (7\text{-}22)$$

$$T_2 = 0.5(C + D) \quad (7\text{-}23)$$

$$T_3 = (E - F) \tag{7-24}$$

$$T_4 = 0.5(E + F) \tag{7-25}$$

where coefficients *C*, *D*, *E*, *F* are defined as the mid-summer daily average, mid-winter daily average, mid-summer average amplitude, and mid-winter average amplitude respectively.

The average value for solar radiation and air temperature defined by these mathematical expressions can be calculated by averaging equation (7-18) and equation (7-21) over a suitable period of time (e.g. four years). It can be found that the average value for solar radiation and air temperature is given by R_2 and T_2 respectively.

Due to the relatively random nature of variations in relative humidity and wind speed across an annual time span, mathematical expressions for these variables have not been developed and instead it is proposed that annual averages based on values from meteorological data sets are used.

7.5 Verification of analytical solutions

The analytical solution proposed here is verified via consideration of a hypothetical problem. The results obtained from the analytical solutions are compared with those from a numerical solution using the finite-element method solution for the heat equation (equation (4-22)) presented in Chapter 4. A number of analyses have been undertaken with varying values of material parameter and system coefficients to investigate the uniqueness of the solutions. Results of a typical analysis follow.

Problem statement: A 20 m deep layer of soil is defined with an initially uniform temperature of 14 °C. Hypothetical soil material parameters (λ_b= 1 W/mK, $c_{p,b}$= 800 J/kgK, ρ_b= 2000 kg/m^3), values for the coefficients of equation (7-18) and equation (7-21) (*A*= 250 W/m^2; *B*= 20 W/m^2; *C*= 16 ˚C; *D*= 3.6 ˚C; *E*= 2.5 ˚C; *F*= 5 ˚C), an average value for soil surface temperature of 8.7 ˚C (calculated, as explained before, by integrating equation (7-9) over a full yearly cycle), a cloud factor of 0 and annual averages of relative humidity (80.6 %) and wind speed (1.14 m/s) are assumed. Values of soil surface emissivity (ε_{ss}) and soil surface albedo (α_s) are defined as 0.97 and 0.15 respectively, as proposed by (Garratt 1994). Soil surface roughness for

momentum (z_{0m}) and heat (z_{0T}) are taken as 1E-3. High reference for meteorological measurements (z_u) is taken as 3 m. The finite-element analysis discretised the domain with 512 two-noded equally sized elements and used a constant time step of 1,800 seconds. Comparison of the temperature profiles and energy stored obtained from both the proposed solution and the alternative numerical solution are presented in Figure 7-2 and Figure 7-3 for the 1st, 40th, and 80th year of analysis.

Figure 7-2 presents a comparison of analytical and numerical temperature profiles for 4 sampling dates for 3 different years. The year is taken to comprise 365.25 days and the sampling points have being homogeneously distributed in each year and approximately correspond to calendar dates of 1st July (t1), 1st October (t2), 1st January (t3) and 1st April (t4). It can be seen that the analytical and numerical results are in excellent agreement and that the temperature profiles for the 40th and 80th years are identical implying that a stationary state has been reached.

Figure 7-3 shows the comparison of stored energy, for 40th yearly cycle calculated analytically using equation (7-8) and numerically using:

$$E_{s,h}(z_i, t_j) = C_{p,b} \sum_{i=0}^{m} \left[T_{s,h}(z_i, t_j) - T_s(z_i, t_{ref}) \right] \Delta z_i \qquad (7\text{-}26)$$

where Δz_i is the length of cell i and $E_{s,h}$ (J/m^2) is the numerical approximation of the thermal energy stored the column soil. In both cases, analytical and numerical, a constant reference temperature of 8.7 ˚C (the temperature at the bottom of the domain at year 40th) has been used. The maximum relative error between numerical and analytical is less than 0.1%. Again it can be seen that the analytical and numerical results are in excellent agreement.

In conclusion, the proposed analytical model has been compared and verified using the numerical model presented in Chapter 4. The results of the two approaches are in excellent agreement yielding confidence in both the developed analytical solutions and the proposed numerical model that can be further applied to study 3D problems that might include coupled interactions of heat and moisture transfer.

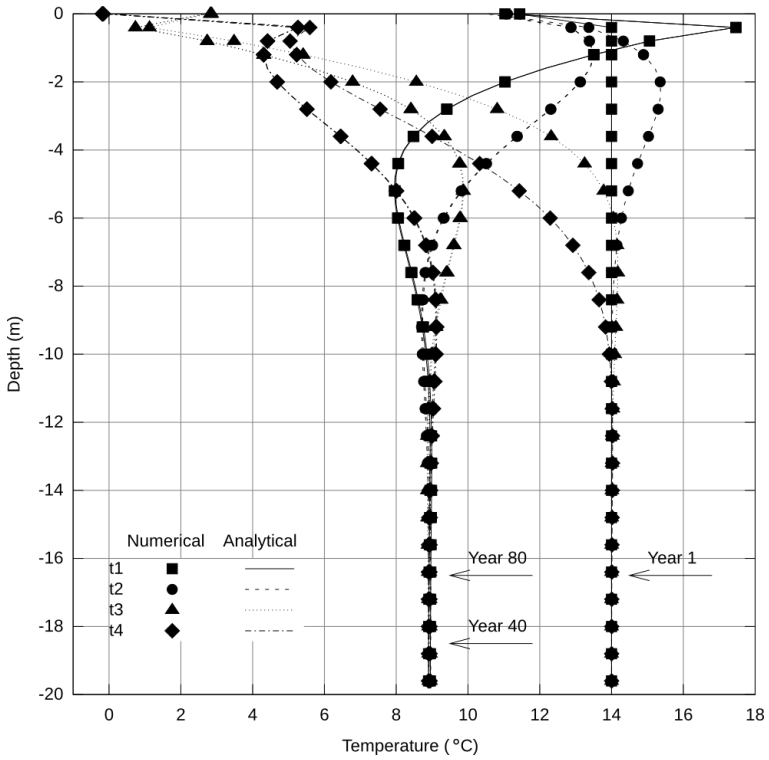

Figure 7-2:Comparison of analytical and numerical results for 4 dates for 3 different yearly cycles (1st, 40th and 80th). 1st July (t1), 1st October (t2), 1st January (t3) and 1st April (t4) yearly cycle.

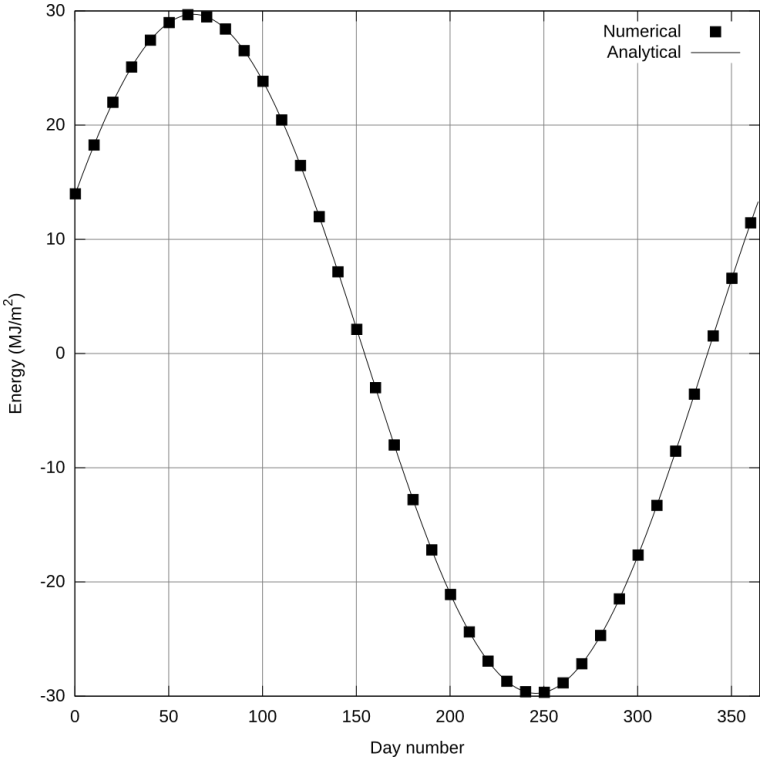

Figure 7-3: Comparison of stored energy calculated analytically using equation (7-8) and numerically using equation (7-26) in a column of soil of 20 m for 40th yearly cycle.

7.6 Validation against field data

The data used in this Chapter for validation is obtained from the experimental project described in Chapter 5. In particular data from a temperature sensor borehole located far from the storage system, which served as control borehole (borehole A), is used. No details regarding regular surface maintenance above this borehole (e.g. grass cutting) are provided in Carder et al. (2007). However site visits (as detailed in Chapter 6) and other photographic records (Google Maps 2012) indicate it is reasonable to assume that the surface was subject to a natural cycle of plant growth (mainly grass).

As mentioned in Chapter 5, TRL set up a meteorological station and took recordings of solar radiation, air temperature, wind speed, relative humidity and precipitation every 15 minutes from July 2005 to May 2007 (Carder et al. 2007). Hourly average values from this station are used in this Chapter to compare against results obtained from the mathematical expressions proposed to describe the meteorological conditions which are based on Met Office data. This approach offers the advantage of testing the ability of the proposed expressions, fitted to readily available long term meteorological data, to represent localised short term measured data.

The proposed mathematical expressions for solar radiation and air temperature have been fitted to meteorological data recordings reported by the British Atmospheric Data Centre (UK Meteorological Office 2012) and the Met Office (UK Meteorological Office 2014) for the period from 1985 to 2004 to investigate their appropriateness and ability to represent realistically the diurnal and seasonal variations. For the purpose of this work, a monitoring station located in Hertfordshire, UK (coordinates 51.8062 latitude, -0.3585 longitude) was selected as it offers daily and hourly meteorological data and is also relatively near (17 km) to the site of the experimental project for which localised meteorological data and soil temperature profiles were also recorded. The variables obtained to allow calculation of the coefficients used in the mathematical expressions for solar radiation, equation (7-18), and air temperature, equation (7-21), are summarized in Table 7-2 and Table 7-3. These variables represent average values for mid-summer and mid-winter periods which in this study are defined respectively as from 25th June to 5th July and from 25th December to 5th January. These periods were chosen since they contained the maximum and minimum values of the variables. Due to data availability, cloud

cover information was obtained from a monitoring station located at Bedford, UK (coordinates 52.2265 latitude, -0.46376 longitude, approx. 31 km from the experimental site). The station has reported hourly cloud cover data from November 2008 allowing the determination of an average cloud factor value of 0.59 for the five year period (2009-2013). It is assumed that this value is representative of the amount of cloud cover present in any other year.

Annual averages of relative humidity (80.6 %) and wind speed (1.14 m/s) based on values recorded during the two-year long (2005-2006) demonstration project are used in the subsequent application of the proposed analytical solution to consider a 20 m deep soil column. The proposed solution also requires a set of material parameters to describe the soil thermal properties, which have been based on those reported in (Carder et al. 2007) and already presented in Chapter 5 for the soil at this site and are summarised in Table 7-4.

A	Mid-summer daily average	204.2 W/m^2
B	Mid-winter daily average	21.3 W/m^2

Table 7-2: Summary of values used to calculate coefficients for the mathematical expression for solar radiation equation (7-18). Based on data from (UK Meteorological Office 2012)

C	Mid-summer daily average	15.4 ˚C
D	Mid-winter daily average	3.6 ˚C
E	Mid-summer average amplitude	2.7 ˚C
F	Mid-winter average amplitude	4.2 ˚C

Table 7-3: Summary of values used to calculate coefficients for the mathematical expression for air temperature equation (7-21). Based on data from (UK Meteorological Office 2012; UK Meteorological Office 2014).

λ_b	Soil thermal conductivity	1.2 W/mK
ρ_b	Soil density	1960 kg/m^3
$c_{p,b}$	Soil specific capacity	840 J/kgK
α_s	Soil thermal diffusivity (= $\lambda_b / \rho_b c_{p,b}$)	
L_s	Depth of the domain	20 m

Table 7-4: Soil material parameters (Carder et al. 2007) and domain depth.

7.6.1 Meteorological data

Figure 7-4 and Figure 7-5 present comparisons of daily average values generated with the proposed mathematical expressions for solar radiation (equation (7-18)) and air temperature (equation (7-21)) with equivalent measured data for the period 1985-2004. In both cases it can observed that the predicted data are constrained by the well defined maximums and minimums. These values, are based on the average values for summer and winter. The data with higher daily average values for solar radiation correspond to summer months while those with lower values correspond to winter

months. It can also be seen that in each month the experimental data tend to have a wider range of lower values this is because the mathematical expression for the predicted data is idealized and in no way takes into account the effect of cloud cover which will decrease the amount of solar radiation that reaches the soil surface. These effects result in the spread of data points displayed in Figure 7-4 having a trapezoidal like shape. As previously mentioned, the data with the higher average values of daily temperature shown in Figure 7-5 correspond to summer months while those with lower values correspond to winter months. It can be seen that the predicted data for air temperature offer a better comparison with the ideal line and offers a slightly better correlation factor than the case for solar radiation (0.67 vs. 0.63). This is probably due to the fact that air temperature is not as highly impacted by the presence of cloud cover. It is noted that if the average value for maximum daily summer temperatures and the average value for minimum daily winter temperatures are used an improved linear fit in Figure 7-5 could be obtained. However daily averages for summer and winter have been used to retain homogeneity with the definition of coefficients for solar radiation. Implementation of averaged values in the proposed solution is trivial (i.e. simply by revising the definition of the coefficients of equation (7-21)) and either approach can be adopted to achieve the best fit with measured data.

Figure 7-6 and Figure 7-7 present comparisons of experimental and predicted daily average values for solar radiation and air temperature respectively for 2005-2006. This permits testing of the proposed expressions for solar radiation and air temperature with an independent subset of data. The experimental values shown are taken from (UK Meteorological Office 2012; UK Meteorological Office 2014). It can be seen that the correlation values are in general similar to those obtained for the period 1985-2004 which was used to establish the coefficients in the expressions.

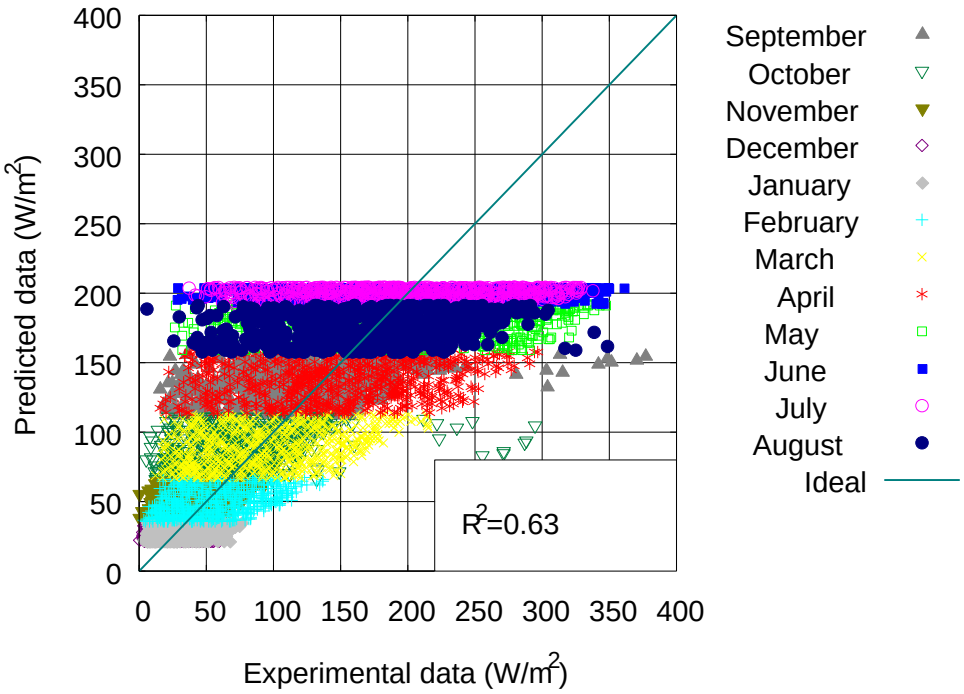

Figure 7-4: Comparison of daily average values for solar radiation predicted with equation (7-18) with data from (UK Meteorological Office 2012) for 1985-2004.

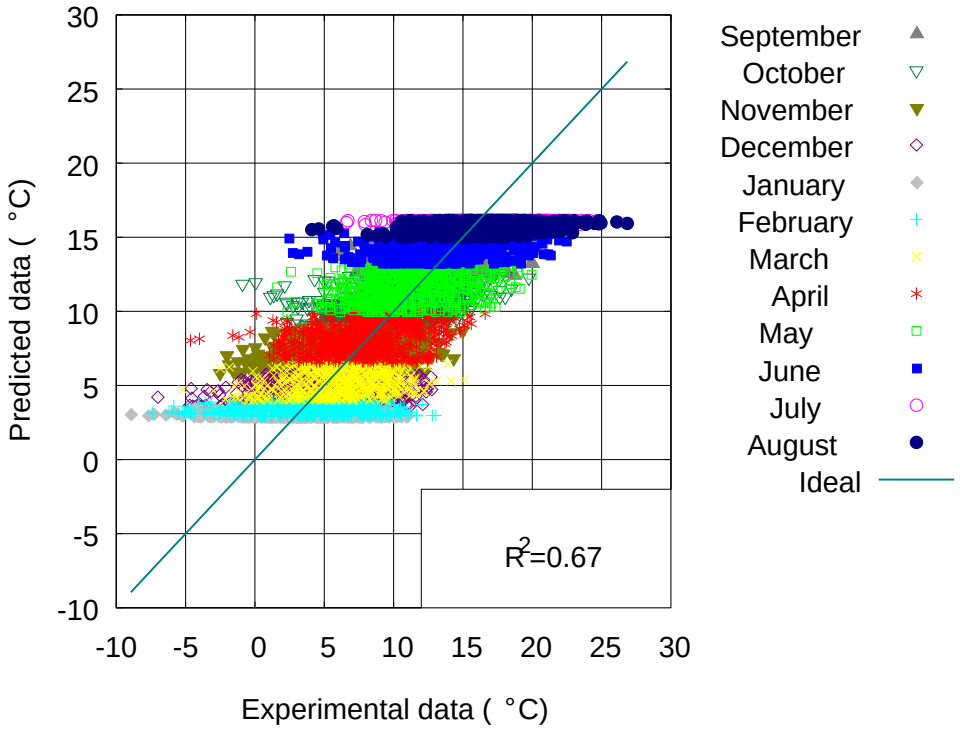

Figure 7-5: Comparison of daily average values for air temperature predicted with equation (7-21) with data from (UK Meteorological Office 2012) for 1985-2004.

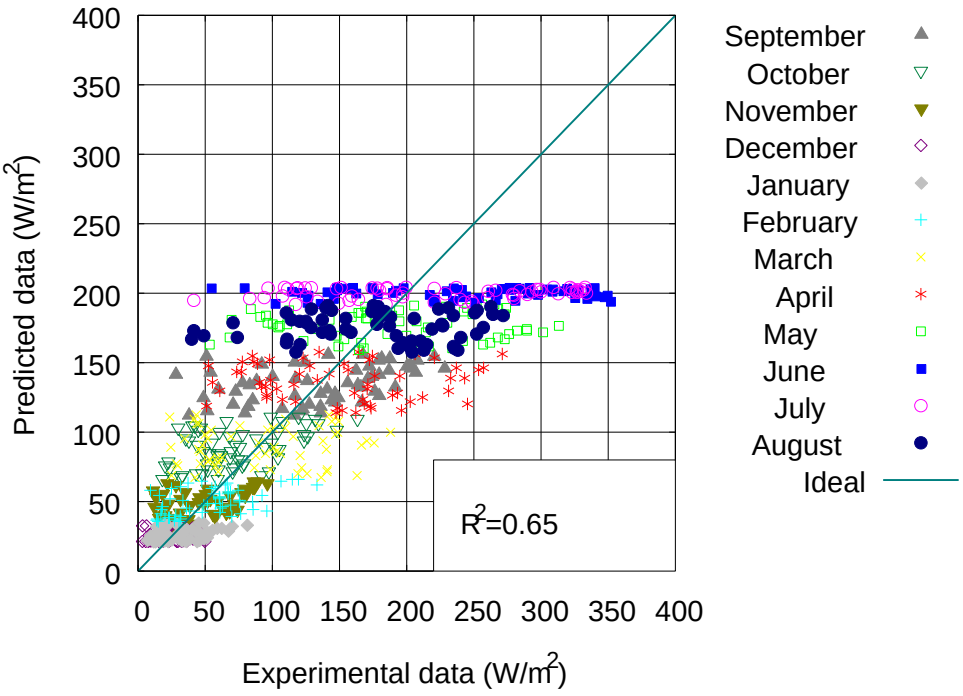

Figure 7-6: Comparison of daily average values for solar radiation predicted with equation (7-18) with data from (UK Meteorological Office 2012) for 2005-2006.

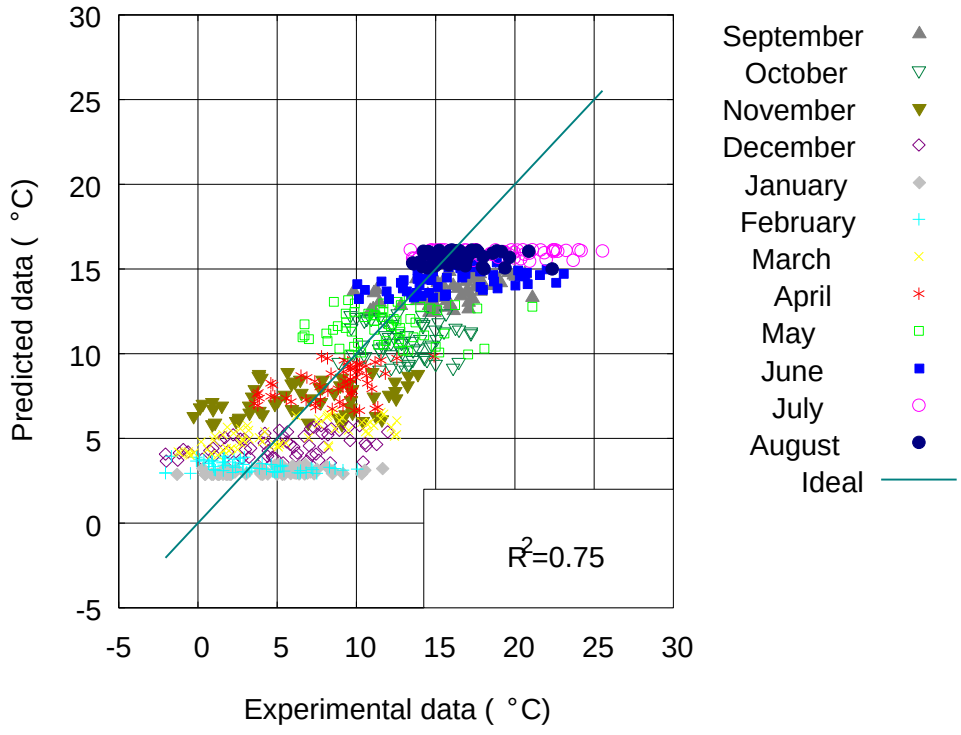

Figure 7-7: Comparison of daily average values for air temperature predicted with equation (7-21) with data from (UK Meteorological Office 2012) for 2005-2006.

Figure 7-8 and Figure 7-9 present comparisons of hourly values of solar radiation and air temperature from the proposed expressions with equivalent data recorded on site by TRL (Carder et al. 2007) from September 2005 to August 2006. In Figure 7-8 a pattern of stratification of the data points can be observed with data points forming horizontal bands. These 'bands' are mostly composed for points belonging to summer months. They arise because as equation (7-18) approaches its maximum in mid-summer it tends to flatten and predict similar values for corresponding hours from mid-May to mid-August while the experimental values are affected by the relatively random presence of clouds.

Figure 7-9 shows experimental and predicted hourly air temperature values. A general trend of underestimation of the predicted temperatures can be observed. It is worth noting that the period considered was warmer (on average by 0.5 °C) than for the previous 20 years. In particular, the average air temperature for the last 20 years was 9.7 °C while the average air temperature for 2005-2006 calculated using TRL data was 10.2 °C. These differences are more marked if they are considered at a monthly level, where the average for July and January for the last 30 years was 16.2 °C and 4.1 °C respectively and 20 °C and 3.4 °C for July 2006 and January 2006 respectively. This in part explains the general under prediction of temperatures seen in Figure 7-9. It can also be observed in Figure 7-8 that a limited number of small negative night time values are given by equation (7-18) due to its sinusoidal and continuous nature, this is illustrated more clearly in Figure 7-10. These unavoidable limitations are acknowledged but it is noted that the overall daily solar radiation is still realistic as seen in Figure 7-4 where the negative values are absent as it is presenting averaged daily values. Figure 7-10 also illustrates the effect of clouds as well as the effect of variation of day length.

7.6.2 Measured data (remote borehole)

Figure 7-11 and Figure 7-12 show the comparison of soil temperatures obtained by applying equations (7-18) and equation (7-21) in equation (7-6) (using the material data provided in Table 7-4 and a domain depth of 20 m) against experimental data from a control borehole of TRL for three different depths. An average cloud factor of 0.59 has been used in equation (7-11) to take into account the effect of clouds in the infrared terms in equation (7-9). Figure 7-11 shows the comparison for the temperature sensor at 0.025 m. Although the correlation factor tends to be low due to

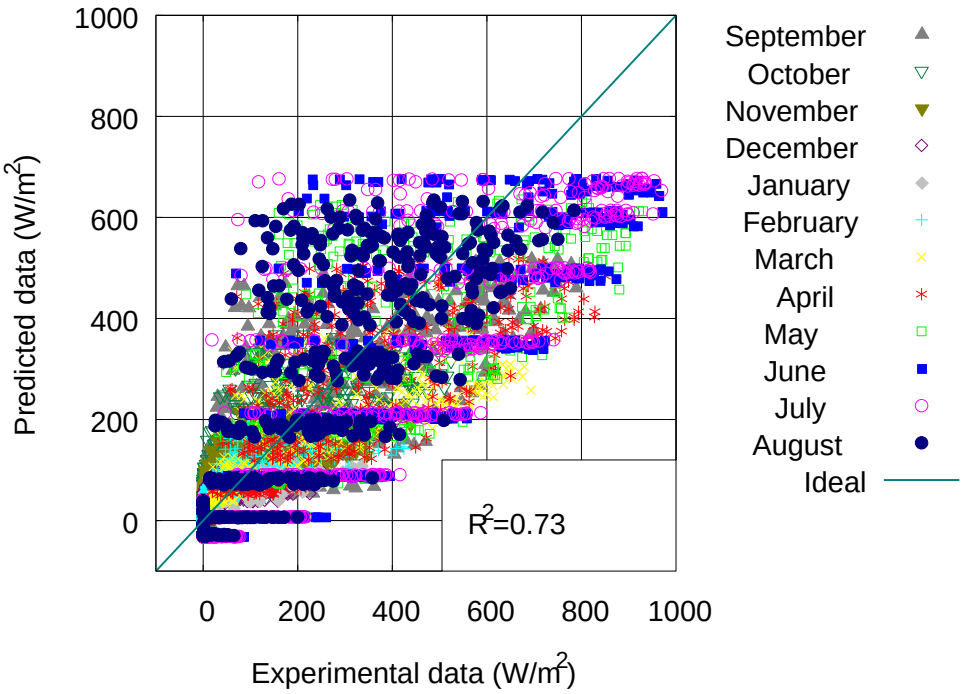

Figure 7-8: Comparison of hourly average values for solar radiation predicted with equation (7-18) with data measured on site provided by (UK Meteorological Office 2014) from September 2005 to August 2006.

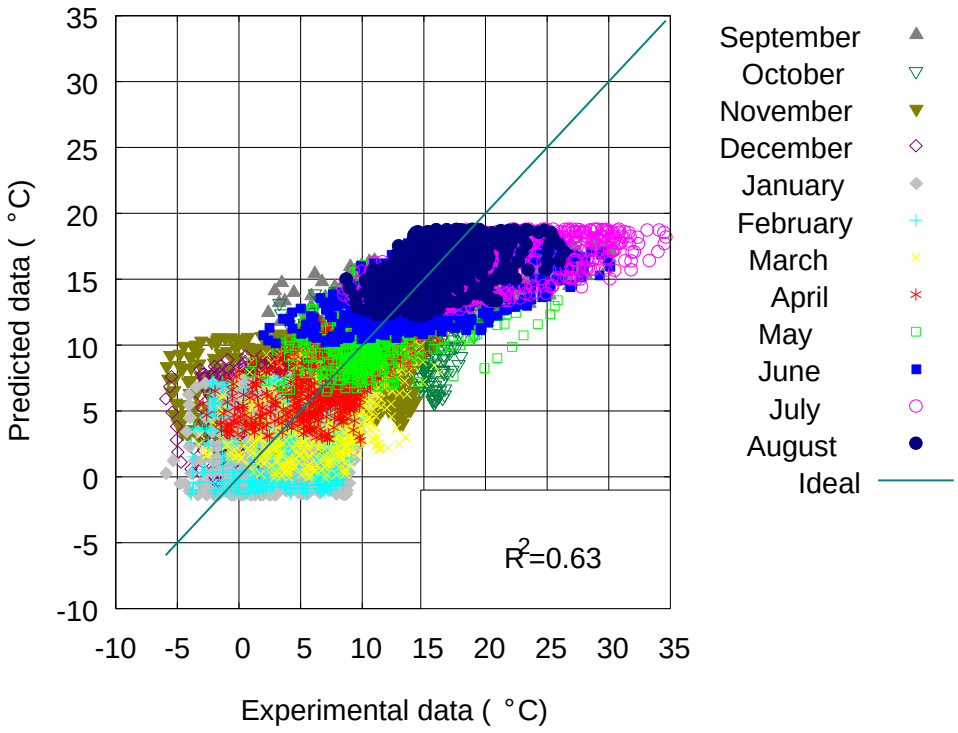

Figure 7-9: Comparison of hourly average values for air temperature predicted with equation (7-21) with data measured on site provided by (UK Meteorological Office 2014) from September 2005 to August 2006.

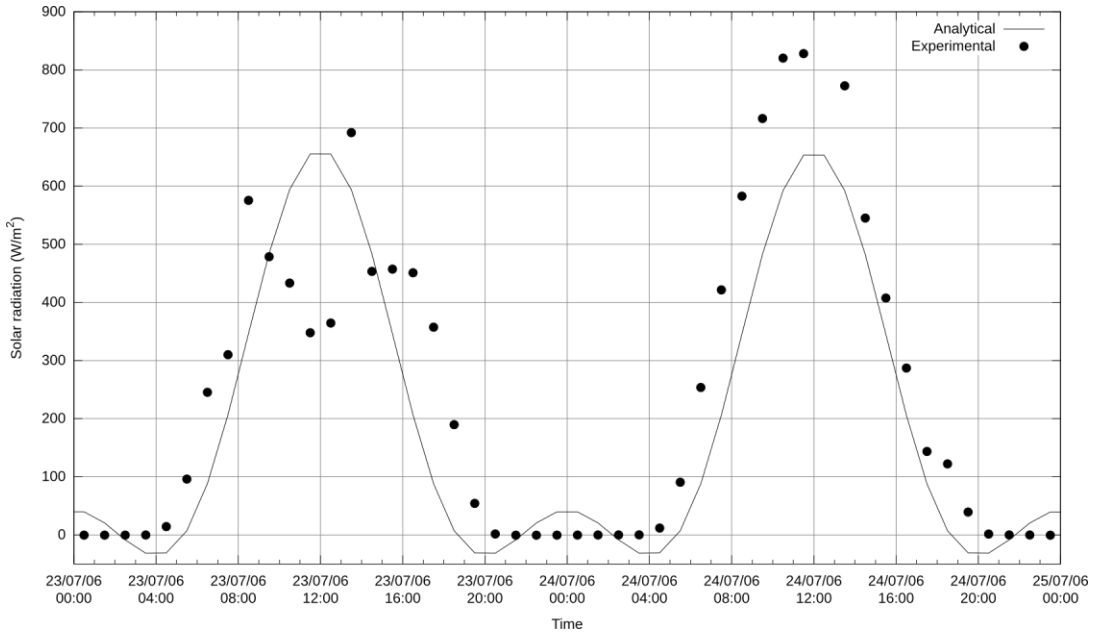

Figure 7-10: Comparison of solar radiation values predicted by equation (7-18) and measured on site by (UK Meteorological Office 2014) for 2 days during summer 2006.

the random nature of the experimental data caused in part by the random nature of the daily meteorological data, it can be seen that the analytical solution offers a reasonable description of the thermal behaviour of the soil.

Figure 7-12 shows the comparison for the temperature sensors located at 1.025 m and 12.875 m. These results, compared with those in Figure 7-11 for 0.025 m depth, indicate that as the depth increases the correlation factor tend to increase (from 0.63 to 0.96). However, for deeper sections of the soil this trend no longer holds, this is due to the fact that the temperature variations in the ground are very small. At depth of 12.875 m, where it would be expected that the soil would maintain at a relatively constant value the analytical solution proposed in this work reasonably predicts the experimental value with a maximum error of 1.3 °C. It is worth noting that the proposed model assumes a homogeneous free flux boundary condition at the bottom of the soil column which is at a depth of 20 m. The advantage of this approach over one that considers a first type (Dirichlet) boundary condition at the base is that no assumption of soil temperature at depth is required.

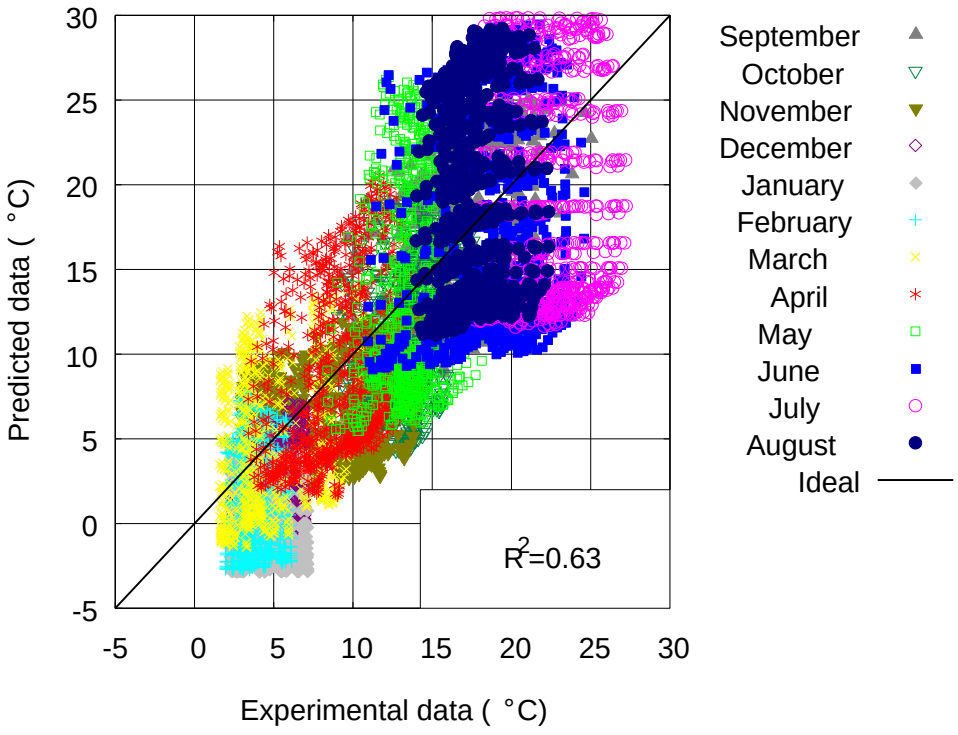

Figure 7-11: Comparison of predicted vs. experimental soil temperatures at 0.025 m depth for the period September 2005 to August 2006.

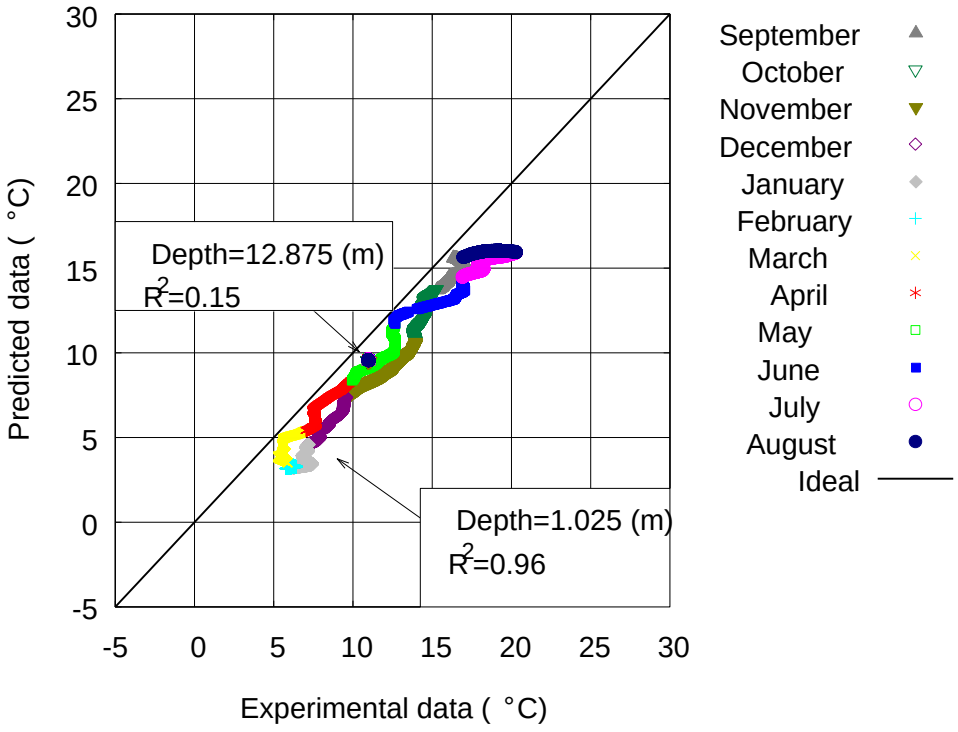

Figure 7-12:Comparison of predicted vs. experimental soil temperatures at 1.025 m and 12.875 m depth for the period September 2005 to August 2006. Note that due to the scale the variations at 12.875 m are restricted to a very small region (pointed with an arrow).

Transient variations in stored energy can be obtained via use of equation (7-8) and consideration of measured temperature profiles. As the experimental temperatures are discrete data, linear interpolation is used to approximate continuous profiles. Figure 7-13 shows comparisons of the calculated and estimated measured stored energy in a column of soil 12.875 m deep. It can be observed that the proposed model is able to offer realistic estimates in the relative change in seasonal energy storage. It is noted that there is a trend of a slight underestimation of energy stored. This is related to the fact that the period compared, as mentioned previously, was slightly warmer than the longer term average of the period used to calibrate equations that represent the surface weather condition.

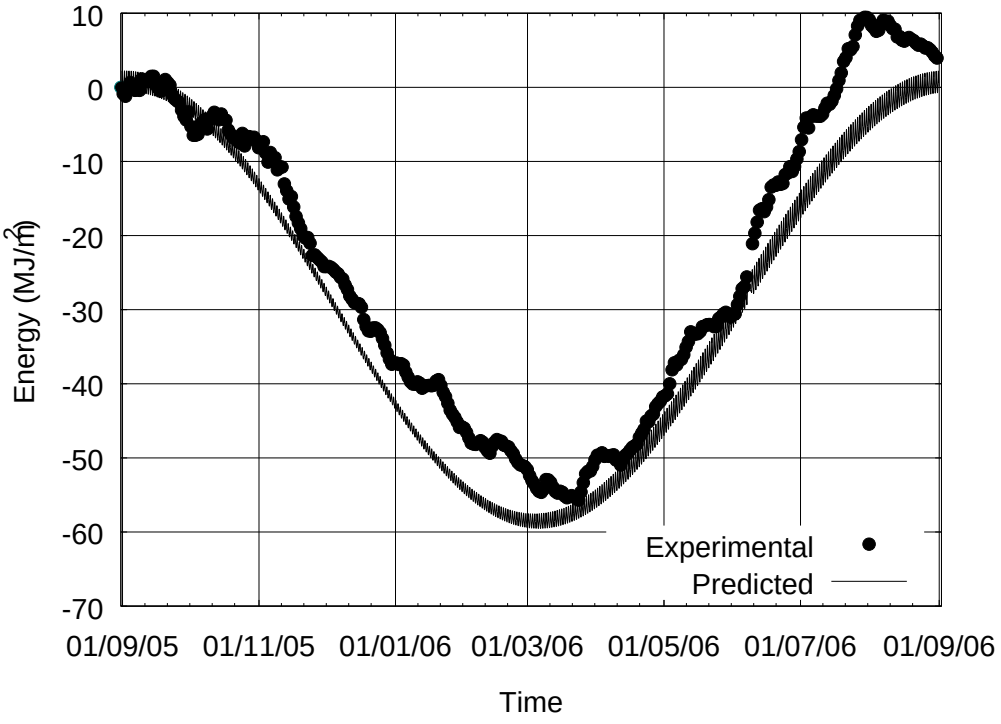

Figure 7-13: Transient variation of stored energy in a column of soil 12.875 m depth for the period September 2005 to August 2006.

7.6.3 Sensitivity study

In this Section a one-at-a-time sensitivity analysis is performed for selected key variables for the analytical model (and for the numerical as well). These variables are: thermal conductivity of the soil (λ_b), the product of soil density (ρ_b) and soil specific heat capacity ($c_{p,b}$), soil surface albedo (α_s), sky emissivity (ε_{sky}), the soil surface water pressure head (h_{ss}), average wind speed (u_s) and average relative humidity (H_a).

The approach selected consists of varying one of the selected variables and observing the change in the value at some key locations or values of the analytical model. In this case the temperature of the soil near the surface (0.025 m depth), near the bottom (12.875 m depth) and the stored energy in a column of soil of 12.875 m , have been selected for this purpose. These values have been chosen to correspond with the presented results in Figure 7-11, Figure 7-12 and Figure 7-13. Furthermore, being a transient model, the sensitivity has been analysed at four points in time, which coincide with those defined in Section 7.5 (1st July (t1), 1st October (t2), 1st January (t3) and 1st April (t4)). The results are expressed as percentage of variation with respect to the baseline model defined in Section 7.5. The percentage of variation is defined as:

$$\Delta(\%) = \frac{U_{\Delta} - U_b}{|\,U_b\,|} \tag{7-27}$$

where U_b is the value at base line, U_{Δ} is the value after the change in the chosen variable.

Table 7-5 shows the results of this analysis for the temperature of the soil at 12.875 m depth. The temperature at this point can be interpreted as the equilibrium temperature of the soil as the seasonal variations are negligible as can be seen in Figure 7-12. It can be seen that variations of +10% and -10% in the values of thermal conductivity λ_b, the product $\rho c_{p,b}$ and soil surface water pressure h_{ss}, produce negligible changes in the temperature at this depth for all four points in time. A variation in solar albedo and average wind speed produce more noticeable variations that behave as expected, an increment in the albedo increases the average temperature of the soil while an increment in the average wind speed decreases it. But the variation in sky emissivity and relative humidity produce particularly high changes in the temperature of the soil at this depth.

	t1		t2		t3		t4	
	+10%	-10%	+10%	-10%	+10%	-10%	+10%	-10%
λ_b	-0.2	0.2	-0.4	0.5	-0.1	0.3	0.1	0.1
$\rho_{cp,b}$	0.2	-0.2	0.4	-0.4	0.2	-0.1	0.03	0.1
α_s	5.3	-5.3	5.3	-5.3	5.3	-5.3	5.3	-5.3
ε_{sky}	12.0	-12.1	12.1	-12.2	12.1	-12.2	12.0	-12.1
h_{ss}	0.1	-0.1	0.1	-0.1	0.1	-0.1	0.1	-0.1
u_s	-1.2	1.4	-1.2	1.4	-1.2	1.4	-1.2	1.4
H_a	14.4	-14.5	14.5	-14.6	14.5	-14.6	14.4	-14.5

Table 7-5: Percentage of variation of temperature of the soil at 12.875 m depth.

Table 2-4 in Chapter 2 presents a range of the variation of thermal properties with water content for clay soils. It can be seen that the thermal conductivity has a range of variation of up to +45% and -77% from the median value (1.1 W/mK) (correspondingly, variation values for specific heat capacity are -23% and +32%, and for density +10% and -10%). On the other hand, Figure 2-4 in Chapter 2 offers a range of variation for sky emissivity for cloudy skies. It can be seen that the variation range is about +10% and -10% from the middle value (0.9). This gives an idea of the possible degree of variation in each variable. With respect to the likeliness of this variation, this is more difficult to assess. For example, while the range of possible values of thermal conductivity is relatively wider than those for sky emissivity, the former correspond to soil conditions that vary from complete dryness to full saturation while the conditions for the sky vary from clear skies to complete cloudiness. The latter variation being more likely to happen perhaps even several times in a single day. However, this of course depends on many climatic factors.

Also it must be noted that the effect due to the change in average relative humidity is due to the impact that this term has in the expression for atmospheric vapour pressure (equation (7-13)) which in turn affects the sky emissivity (equation (7-11)) and the evaporative potential (part of equation (7-9)). From this, it could be said that the parameter with the biggest impact in the analytical model (and possibly in the numerical model too) is the sky emissivity.

Table 7-6 shows the sensitivity analysis results for the amount of energy stored in a column of soil 12.875 m depth. The stored energy is proportional to the average temperature of the soil at any given point in time. It can be seen that an increment in the thermal conductivity of the soil produces an increment of stored energy in t1 and t2 which are in periods of warming, however, at t3 and t4 the stored energy is lower

with increase conductivity. This behaviour is expected since an increment in λ_b reduces the time that the soil takes to respond to changes in the heat fluxes at the surface. The opposite is true for a decrement in λ_b. Also, by comparing with Table 7-5, it can be noted that equivalent variations in λ_b and $\rho c_{p,b}$ produce negligible changes at 12.875 m depth for t1, t2, t3 and t4. This implies that the changes observed in Table 7-6 with the variation of λ_b and $\rho c_{p,b}$ are restricted to the region close to the surface.

Similarly to the results presented in Table 7-5, it can also be seen in Table 7-6 that the higher changes in energy stored are connected to variations in the solar albedo and average wind speed. The most important parameters are relative humidity and sky emissivity, the latter being the variable with the highest impact in the analytical model. The influence of sky emissivity in Table 7-6 is similar to the observed effects in Table 7-5 and could be explained using the same reasoning. Variations of 10% in sky emissivity can produce changes of up to 320% in thermal energy stored that are comparatively higher than those produced in soil temperature (12%) at 12.875 m shown in Table 7-5. However, the energy stored is not proportional to the increment in the equilibrium temperature but to the difference between the average temperature of soil at any point in time and a defined baseline equilibrium temperature (8.7 ˚C which is the average temperature of the soil after 40 yearly cycles for an scenario at as defined in Section 7.5). This is why while the equilibrium temperature of the soil only increments 12% (i.e. from 8.7 ˚C to 9.7 ˚C at the bottom of the domain) for a change in sky emissivity, the difference in stored energy contained in the whole domain can be as high as 320% (from -11MJ/m^2 to -46MJ/m^2 at t3).

Despite the simplicity of the analytical model proposed in this Chapter, it can offer an insight into the impact of the moisture content of the soil. The model includes an evaporative term in equation (7-9) that depends on the water pressure of the soil. This term controls the level of thermal energy lost by evaporation from the soil or gained by condensation of moisture from the atmosphere although admittedly it does not take into account any mass flow. If taken into account, the mass flow would have an effect on the soil's moisture content and its water pressure. It would also have an effect on the bulk density of the soil, the bulk specific heat capacity and thermal conductivity (by filling voids and adding mass per volume). These terms, as

analysed in Table 7-5 and Table 7-6 have a relatively low impact on the temperature of the soil at depth and in the amount of stored energy near the surface when compared with other boundary terms (e.g. sky emissivity). So, as long as the key physical process is restricted to thermal energy diffusion and other processes such as diffusion of contaminants or mechanical deformations (by loads or phase change of water contained in the soil) are not critical the model suggests that moisture diffusion in the soil can be neglected and that attention should be focused on other thermal energy interactions at the surface of the soil (infrared radiation, solar radiation, convection). However, this is a simplified mathematical model and such claims must be confirmed by more comprehensive numerical tests involving coupled interactions of heat and mass transfer.

	t1		t2		t3		t4	
	-10%	+10%	-10%	+10%	-10%	+10%	-10%	+10%
λ_b	-0.01	1.4	-2.4	3.1	11.5	-9.0	7.9	-6.7
$\rho c_{p,b}$	1.8	-0.2	3.5	-2.3	-10.4	10.7	-7.6	7.3
α_s	-107.1	107.1	-58.4	58.4	-132.6	132.6	-58.8	58.8
ε_{sky}	-234.4	231.4	-127.9	126.2	-320.9	316.7	-142.6	140.7
h_{ss}	-1.6	1.6	-0.9	0.9	-2.2	2.2	-1.0	1.0
u_s	31.34	-26.7	17.2	-14.6	31.4	-26.7	13.8	-11.7
H_a	-280.1	278.0	-152.6	151.5	-382.9	380.1	-170.3	169.1

Table 7-6: Percentage of variation of the amount of energy stored in a column of soil 12.875 m deep.

7.7 Concluding remarks

Analytical solutions to estimate the soil temperature with depth and stored energy were presented in this Chapter. The boundary conditions used are of the *second kind* (Neumann) at the bottom and of the *third kind* (Robin) based on a heat balance at the soil surface. In order to describe the soil-atmosphere interactions, mathematical expressions describing the daily and annual variation of solar radiation and air temperature have been proposed. The analytical solutions were shown to correlate well with numerical solutions from a finite-element analysis.

The presented analytical solutions were used to investigate the case study problem presented in Chapter 5. Predicted soil temperature profiles and stored energy transients have been compared against experimental measurements for over one year. Also the predicted meteorological data has been compared against widely available public records and against data recorded on site. The main differences found between the predicted and experimental data are due to the random nature of

certain meteorological variables (e.g. clouds) and the inevitable variability in average data for a particular year in comparison to averages from a longer term data set. The results show that the analytical approach proposed can offer a reasonable estimate of the thermal behaviour of the soil requiring no information from the soil other than its thermal properties. This work provides a useful tool in applications requiring estimations of the soil temperature profiles or in numerical problems where a reasonable initial state can minimise the computational time to reach a convergent steady state.

A sensitivity analysis provided useful information about the impact that variation in key parameters have in the overall thermal response of the soil temperature profile and the stored energy. These results suggest that the main parameters that influence the temperature profile of the soil and the energy stored near the surface are related with the thermal boundary conditions, specifically infrared radiation and solar radiation. Other parameters such as the thermal properties of the soil and the soil water pressure (both related with the moisture content of the soil) seem to have a limited impact in the thermal behaviour of the soil.

7.8 References

Bobes-Jesus, V., Pascual-Muñoz, P., Castro-Fresno, D., and Rodriguez-Hernandez, J. [2013]. Asphalt Solar Collectors: A Literature Review. Applied Energy 102 (February): 962–970. doi:10.1016/j.apenergy.2012.08.050.

Carder, D. R., Barker, K. J., Hewitt, M. G., Ritter, D., and Kiff, A. [2007]. Performance of an Interseasonal Heat Transfer Facility for Collection, Storage and Re-Use of Solar Heat from the Road Surface. PPR302. Transport Research Laboratory.

Duffie, J. A. and Beckman, W. A. [2006]. Solar Engineering of Thermal Processes. 3rd ed. Wiley.

Edinger, J. E. and Brady, D. K. [1974]. Heat Exchange and Transport in the Environment. John Hopkins University.

Florides, G. and Kalogirou, S. [2007]. Ground Heat exchangers—A Review of Systems, Models and Applications. Renewable Energy 32 (15): 2461–2478. doi:10.1016/j.renene.2006.12.014.

Garratt, J. R. [1994]. The Atmospheric Boundary Layer. Cambridge University Press.

Google Maps. [2012]. Toddington Service Area, Toddington. [Online]. Available at: http://maps.google.co.uk/. [Accessed: 17-Feb-2012].

Herb, W. R., Janke, B., Mohseni, O., and Stefan, H. G. [2008]. Ground Surface Temperature Simulation for Different Land Covers. Journal of Hydrology 356 (3-4): 327–343. doi:10.1016/j.jhydrol.2008.04.020.

Jansson, C., Almkvist, E., and Jansson, P. [2006]. Heat Balance of an Asphalt Surface: Observations and Physically-Based Simulations. Meteorological Applications 13 (2): 203–212. doi:10.1017/S1350482706002179.

Kotani, A. and Sugita, M. [2005]. Seasonal Variation of Surface Fluxes and Scalar Roughness of Suburban Land Covers. Agricultural and Forest Meteorology 135 (1–4): 1–21. doi:10.1016/j.agrformet.2005.09.012.

Laloui, L., Nuth, M., and Vulliet, L. [2006]. Experimental and Numerical Investigations of the Behaviour of a Heat Exchanger Pile. International Journal for Numerical and Analytical Methods in Geomechanics 30 (8): 763–781. doi:10.1002/nag.499.

Lumb, F. E. [1964]. The Influence of Cloud on Hourly Amounts of Total Solar Radiation at the Sea Surface. Quarterly Journal of the Royal Meteorological Society 90 (383): 43–56. doi:10.1002/qj.49709038305.

Özişik, N. [2002]. Boundary Value Problems of Heat Conduction. Dover Publications, Incorporated.

Pinel, P., Cruickshank, C. A., Beausoleil-Morrison, I., and Wills, A. [2011]. A Review of Available Methods for Seasonal Storage of Solar Thermal Energy in Residential Applications. Renewable and Sustainable Energy Reviews 15 (7): 3341–3359. doi:10.1016/j.rser.2011.04.013.

Qin, Z., Berliner, P., and Karnieli, A. [2002]. Numerical Solution of a Complete Surface Energy Balance Model for Simulation of Heat Fluxes and Surface

Temperature under Bare Soil Environment. Applied Mathematics and Computation 130 (1): 171–200. doi:10.1016/S0096-3003(01)00089-3.

Rees, S. W., Adjali, M. H., Zhou, Z., Davies, M., and Thomas, H. R. [2000]. Ground Heat Transfer Effects on the Thermal Performance of Earth-Contact Structures. Renewable and Sustainable Energy Reviews 4 (3): 213–265. doi:10.1016/S1364-0321(99)00018-0.

UK Meteorological Office. [2012]. Met Office Integrated Data Archive System (MIDAS) Land and Marine Surface Stations Data (1853-Current). NCAS British Atmospheric Data Centre. [Online]. Available at: http://badc.nerc.ac.uk/view/badc.nerc.ac.uk__ATOM__dataent_ukmo-midas. [Accessed: 03-Apr-2014].

UK Meteorological Office. [2014]. Met Office: UK Climate Summaries. [Online]. Available at: http://www.metoffice.gov.uk/climate/uk/index.html. [Accessed: 04-Apr-2014].

Wood, C. J., Liu, H., and Riffat, S. B. [2010]. An Investigation of the Heat Pump Performance and Ground Temperature of a Piled Foundation Heat Exchanger System for a Residential Building. Energy 35 (12). The 3rd International Conference on Sustainable Energy and Environmental Protection, SEEP 2009: 4932–4940. doi:10.1016/j.energy.2010.08.032.

Yumrutaş, R., Kanoğlu, M., Bolatturk, A., and Bedir, M. Ş. [2005]. Computational Model for a Ground Coupled Space Cooling System with an Underground Energy Storage Tank. Energy and Buildings 37 (4): 353–360. doi:10.1016/j.enbuild.2004.07.004.

Zoras, S. [2009]. A Review of Building Earth-Contact Heat Transfer. Advances in Building Energy Research 3 (1): 289–314. doi:doi:10.3763/aber.2009.0312.

Chapter 8 1D soil column analysis: investigation of initial and boundary conditions

This chapter presents 1D analyses of measured field data from soil columns to provide both partial validation of the model presented in Chapter 3 and Chapter 4 and to investigate methods of defining appropriate initial and boundary conditions. The following aspects are considered in detail:

- Boundary conditions at the top of the domain.
- Boundary conditions at the bottom of the domain.
- Initial conditions.
- Use of different sources of meteorological data.
- Thermal energy stored in the domain.
- Variation of thermal properties with moisture content.

The chapter is divided in sections detailing approaches taken for each of these aspects and the numerical features of the simulations undertaken.

i) Section 8.1 specifies the source of experimental data used in this Chapter to compare against the proposed numerical model in 1D.

ii) Section 8.2 describes three scenarios considered in this study to specify the initial temperature of domain.

iii) Section 8.3 provides the description of the boundary conditions considered for the soil surface and at the far-field (lower) boundary of the domain. In particular, three heat transfer formulations are considered for the soil surface boundary condition while two cases (free and fixed) are considered for the boundary condition at the bottom of the domain.

iv) Section 8.4 presents three sources of meteorological data used as input for the numerical model proposed in this Chapter.

v) Section 8.5 shows the discretized domain considered in this study.

vi) Section 8.6 states the discretized equation, temporal resolution and time span considered for the numerical analysis.

vii) Section 8.7 analyses the results obtained. The analysis is focused in three aspects of the problem: soil temperature profiles near the bottom of the soil column, soil temperature profiles at the soil surface, thermal energy stored in the soil and the effects of coupled heat and moisture transfer considerations.

viii) Section 8.8 presents the final conclusions for the Chapter

8.1 Experimental data – control boreholes

In order to validate the numerical model proposed in Chapter 4, hourly measurements of soil temperature provided by the case study presented in Chapter 5 spanning from September 2005 to August 2006 are used in this Chapter. Specifically, experimental data measured at control borehole A (figure 5.6) are used. It can be seen that this borehole is located in the south east area of the experimental site. It is worth noting, based on a site visit and photographic evidence, that the soil surface at this location is subjected to normal seasonal vegetation growth and decay although no particular measurements of this are reported by Carder et al (2007). Details on the depths of the temperature sensors are provided in Chapter 5.

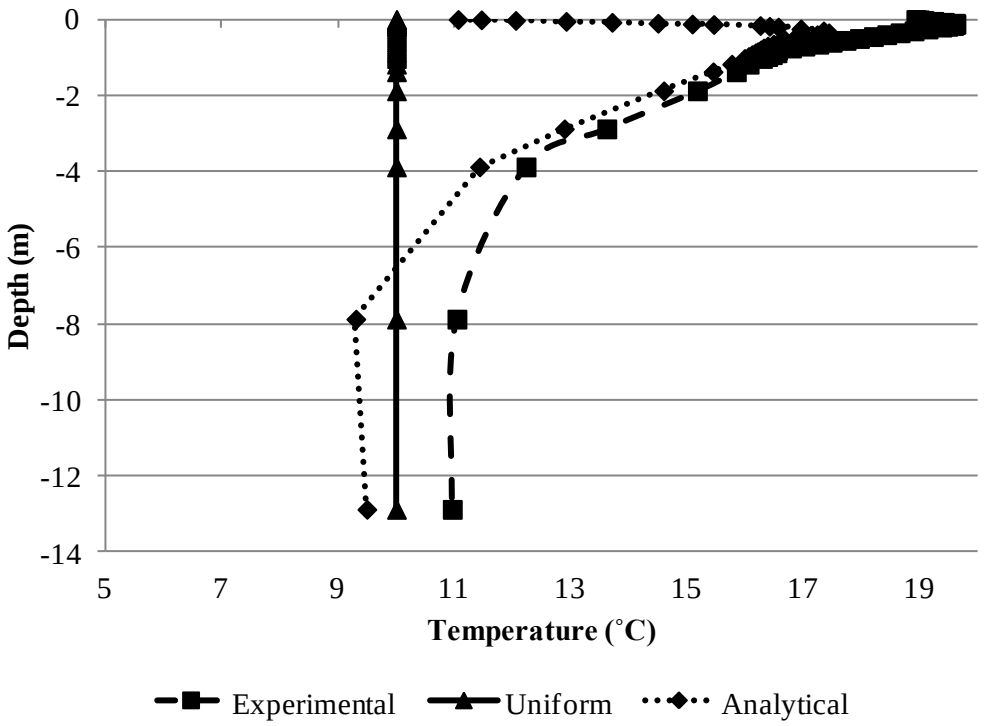

Figure 8-1 - Temperature profiles considered in this study as initial conditions for a 1D domain.

8.2 Initial conditions

Three approaches to specify the initial temperature for the domain are considered, namely:

- Uniform: Uniform temperature thorough the domain equal to the annual average ambient air temperature calculated from the meteorological data provided by TRL (Carder et al, 2008) corresponding to the period between September 2005 and August 2006.
- Experimental: A temperature profile linearly interpolated from experimental measurements reported by TRL and taken from borehole A at a selected initial date (1st September 2005).
- Analytical: A temperature profile generated with the analytical equation proposed and described in Chapter 7 and again corresponding to a selected initial date (1st September 2005).

The three profiles obtained are shown in Figure 8-1

8.3 Boundary Conditions

8.3.1 Soil surface

One of the main objectives of this chapter is to study the effect that different formulations for the boundary condition at the top of the domain have on the prediction of its temperature profile and thermal energy stored in the soil column. In general, this boundary condition is assumed have the form given by equation (3-70). The specific expressions for the different heat fluxes depend on the assumptions made for the interactions between the soil surface and the atmosphere. In Section 3.7.5, three main approaches were discussed: turbulent, non-turbulent and canopy cover inclusion. These formulations can be regarded as representative of the main approaches considered in the literature. In this chapter, they are compared using suitable physical parameters found in the literature.

- Turbulent: This approach assumes turbulent wind flow conditions over the soil surface that influence the heat transfer processes of convection and evaporation. Specific equations for this approach are presented in 3.7.5.1.

Suitable parameters values are taken from the literature as presented in Section 2.4 (Jansson et al. 2006; Alvenäs and Jansson 1997; Garratt 1994).

- Non-turbulent: This approach takes into account heat transfer processes driven by natural convection that implies the absence of turbulent conditions. The specific formulation for this approach is given in Section 3.7.5.2. Suitable parameters are taken from the literature as given in Section 2.4 (Herb et al. 2008).
- Canopy Cover: This approach considers the presence of a layer of vegetation covering the soil surface and its impact on the heat transfer interactions between soil and atmosphere. Section 3.7.5.3 presents the specific formulation for this approach. Suitable parameters taken from the literature are given in Section 2.4 (Herb et al. 2008; Best 1998; Deardorff 1978).

Additional required parameters in the Non-turbulent and Canopy Cover approaches in equations (3-61), (3-62) and (3-72) are: C_e=0, C_{fc}=0.0015, C_{nc}=0.0015, C_{sh}=1, z_u=3, z_h=3, ν=0.85-0.95. C_e defines the level of convection and evaporation between the soil and the atmosphere. C_e=0 implies that the vegetation layer is considered *transparent* to evaporative and convective interactions. C_{nc} and C_{fc} are coefficients defining the level of natural and forced convection respectively. C_{sh} is a sheltering coefficient that takes into account the effects of trees buildings and topographical features on surface wind velocity. C_{sh}=1 implies that no effect from these objects is being taken into account since, in the current study, there is no data to estimate it. These values for these parameters are based on those proposed by Herb (2008) for tall grass canopy covers. z_u and z_h are the heights to which wind speed and temperature are measured respectively. The canopy density ν is set to 0.85 between April and December and 0.95 between November and March based on seasonal density values provided by Herb (2008) and others (Deardorff 1978; Geiger 1950) for tall grass and to an expected process of seasonal growth and decay of vegetation on the experimental site. Experimental data provided by TRL also suggests this seasonal behaviour on the vegetation cover.

The infrared radiation formulation chosen for all approaches is given in Table 2-3 (Edinger et al. 1968). It takes into account cloudy skies via a cloud factor *N* that is set to 0.59 as explained in Chapter 7.

8.3.2 Far-field (lower) boundary

Besides the boundary condition at the surface of the domain, the boundary condition at the bottom of the domain is also analysed. Two approaches are considered:

- Fixed temperature equal to the yearly average temperature recorded by the deepest temperature sensor at control borehole A (12.875 m).
- Free boundary condition. No assumption is made upon the temperature at the bottom of the domain.

8.4 Source of meteorological data

The effect of the using different sources for meteorological data is analyzed. The main sources considered are:

- *Meteorological data recorded on site by TRL* (Section 5.4.2). Several meteorological variables (solar radiation, air temperature, wind speed, relative humidity) were measured for the duration of the experiment.
- *Meteorological Office data*. As mentioned in Chapter 7, meteorological data from the British Atmospheric Data Centre (UK Meteorological Office 2012) and the Met Office (UK Meteorological Office 2014) corresponding to a monitoring station located in Hertfordshire, UK (17 km from the experimental site).
- *Analytical expressions*. Additionally, the analytical expressions defined in Chapter 7 for air temperature (7-21) and solar radiation (7-18) are also used for comparison.

8.5 Discretization

For the purpose of this study, the 1D domain has been discretized using 17 elements distributed as shown in Figure 8-2.

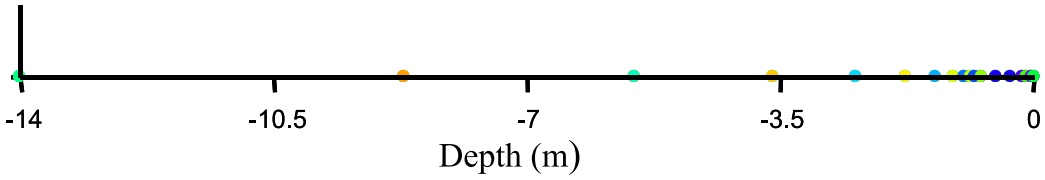

Figure 8-2 - 1D domain discretization used in this study.

This discretization approach has been compared with homogeneous refinements of 1024 and 2048 elements and has been found to yield converged results.

8.6 Numerical Investigation

The numerical solution for the heat transfer equation (4-22) (formulated in 1D) is applied to investigate the uncoupled transient diffusion of heat in a column of soil 14 m deep using the mesh shown in Figure 8-2. The initial condition for the transient simulation corresponds to the date 1st September 2005 at 0 h. The numerical analysis comprises 11 yearly cycles using hourly time steps and different combinations of the settings presented in the previous sections for boundary conditions, initial conditions and meteorological data. The column of soil is considered to be composed of silty clay with homogeneous material properties presented in Table 8-1. Thermal conductivity and density are based on laboratory tests described in Chapter 6 and on material data shown in Table 5-1 provided by Carder et al (2007) for the experimental case study presented in Chapter 5. Specific heat capacity is taken from Garrat (1994) assuming a homogeneous moisture content of 23%. Evaporative terms in all boundary formulations listed in Section 8.3 require an estimation of pressure head at the soil surface. This value is set at -75.2025 m as the average of saturation and wilting point values for clay soils (Garratt 1994).

Thermal conductivity	1.21 W/mK
Density	1960 kg/m^3
Specific heat capacity	1227 J/kgK
Surface pressure head	-75.2025 m

Table 8-1 - Material properties of silty clay used in the numerical solution of the uncoupled 1D heat transfer equation.

8.6.1 Coupled numerical problem

In this study the coupled heat and moisture transfer numerical problem defined by equations (4-19) and (4-22) is compared with the uncoupled numerical problem of transient heat transfer defined using only equation (4-22). The analysis is focused on the variations in the thermal properties of the soil under these different settings to explore the necessity of a full coupled model.

In the coupled problem, the initial and boundary conditions for the heat transfer equation are chosen from those presented in the previous sections. Specific initial and boundary conditions and material parameters for heat and moisture equations are provided in Section 8.7.4 devoted to discuss the outcome of the coupled analysis.

8.7 Results

In the following Section results of the various analyses undertaken are presented and discussed. Initially the representation of temperatures at some depth (>12m) are considered, followed by analysis of the transient variations of soil temperatures close to the surface, after this results for annual variations in the predicted thermal energy storage are shown, and finally comparisons in temperature profiles and thermal properties between coupled and uncoupled equations for heat and moisture transfer are presented.

8.7.1 Temperature below 12 m

Figure 8-3 shows the variation of temperature at a depth of 12.875 m on September 1st at 0 h during each of the 11 yearly cycles using a fixed boundary condition equal to 10.9 ˚C at 14 m depth and using meteorological data provided by TRL. The 9 sets of data plotted correspond to the 9 different combinations of the 3 initial conditions (Analytical, Experimental and Uniform) and 3 formulations for the boundary condition at the surface of the soil (Turbulent, Non-turbulent and Canopy Cover) detailed in Section 8.2 and Section 8.3 respectively. It can be seen that the domain reaches a steady state near the bottom of the domain in the first yearly cycle independent of the initial condition or boundary formulation at the surface. This is expected since the imposed fixed boundary condition is close to the location of the point being analysed.

Similarly, Figure 8-4 shows the variation of temperature at 12.875 m on September 1st at 0 h during each of the 11 yearly cycles using a free boundary condition at 14 m depth and using meteorological data provided by TRL. The data plotted again corresponds to the 9 different combinations of the 3 initial conditions (Analytical, Experimental and Uniform) and 3 formulations for the boundary condition at the soil's surface (Turbulent, Non-turbulent and Canopy Cover) described earlier. It can be seen that after 10 yearly cycles all 9 test cases are approaching a steady state. However, it can also be seen that they reach different temperatures depending on the surface boundary formulation used, with the turbulent formulation being the one that better represents the experimental average temperature of the soil at this point (10.9 ˚C). The canopy cover formulation is slightly below this value (10.4 ˚C) and the non-turbulent formulation above it (12.1 ˚C). It is worth noting that the rate at which the

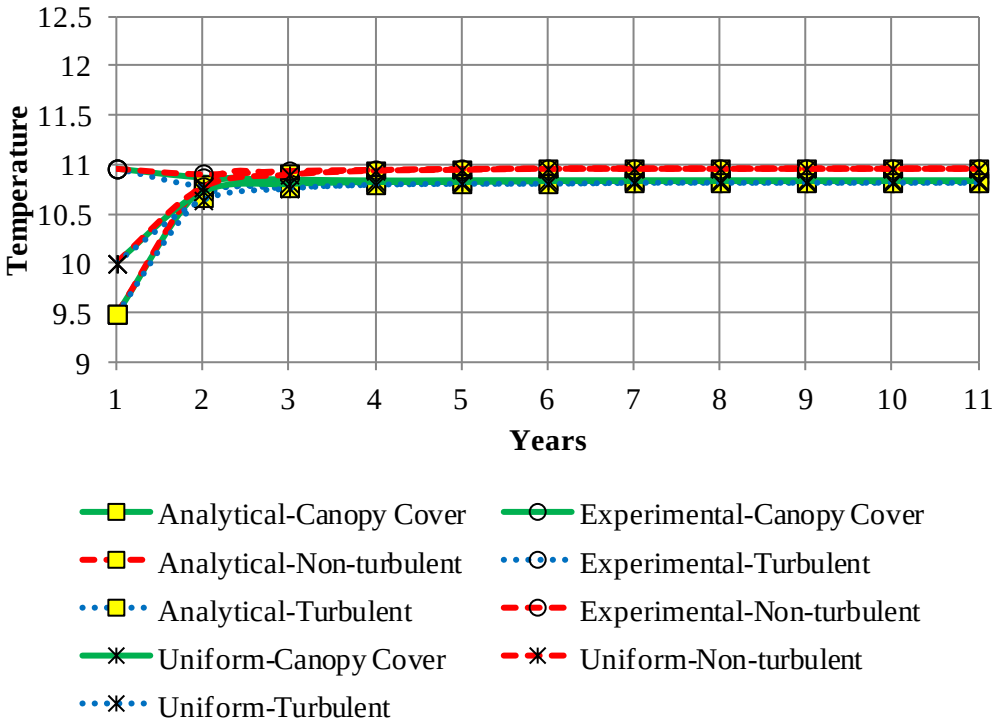

Figure 8-3 - Soil temperature at 12.875 m on September 1st for 11 yearly cycles assuming a fixed bottom boundary condition and using 9 combinations of initial conditions and soil surface boundary formulations.

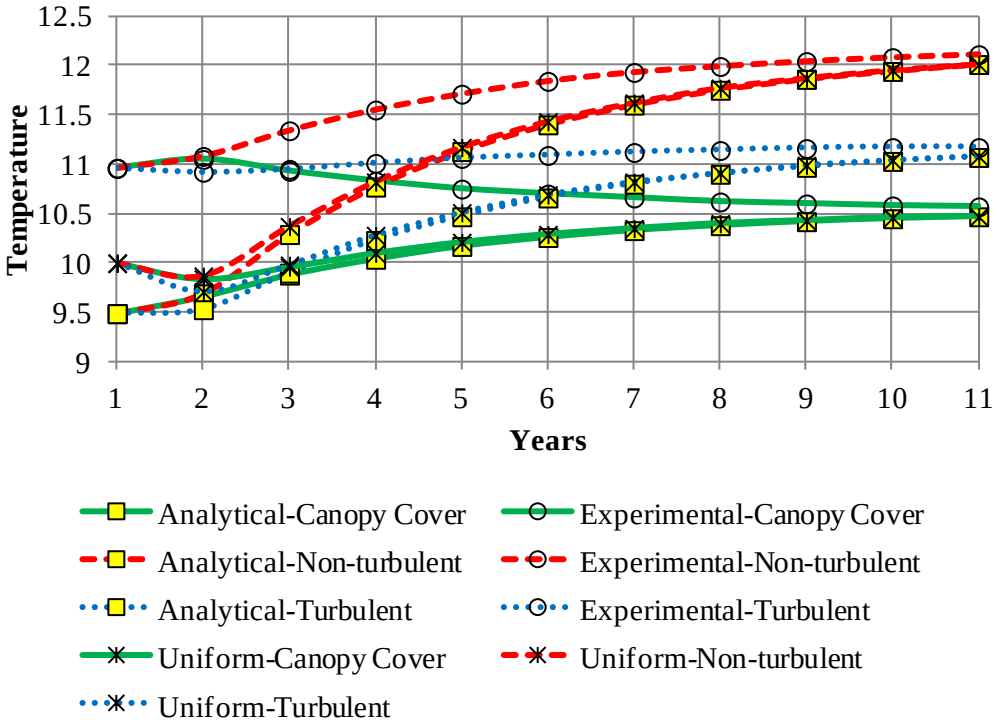

Figure 8-4 - Soil temperature at 12.875 m on September 1st for 11 yearly cycles assuming a free bottom boundary condition and using 9 combinations of initial conditions and soil surface boundary formulations.

domain reaches a steady state at this depth is practically independent of the initial state used for the canopy cover formulation. However this is not the case for turbulent and non-turbulent formulations which converge faster under experimental initial conditions. This implies that the rate of convergence towards a steady state is not only dependent on the initial condition of the system but also on the boundary formulation used at the surface.

8.7.2 Temperature close to soil surface

The following figures show comparisons between the experimental and predicted temperature of the soil at 0.025 m for the 11^{th} yearly cycles using a free boundary condition at the bottom of the domain and homogenous initial condition. The corresponding results for a fixed boundary condition at the bottom and experimental and analytical initial conditions are very similar and so for the sake of clarity are omitted. The meteorological data used in each set of figures and boundary surface formulations is as follows:

- Figure 8-5, Figure 8-6 and Figure 8-7 use meteorological data provided by TRL and Turbulent, Non-turbulent and Canopy Cover boundary formulations for the surface respectively. Due to missing solar radiation data in February 2006 and the three first weeks of March 2006, data from 2007 is used for these periods.
- Figure 8-8, Figure 8-9 and Figure 8-10 use meteorological data obtained from BADC and the Meteorological Office using Turbulent, Non-turbulent and Canopy Cover boundary formulations for the surface respectively.
- Figure 8-11, Figure 8-12 and Figure 8-13 use analytical meteorological data generated with equations (7-18) and (7-21) (as presented in Chapter 7) using Turbulent, Non-turbulent and Canopy Cover boundary formulations for the surface respectively.

From Figure 8-5 to Figure 8-13 it can be clearly observed that a Turbulent approach tends to overestimate the soil surface temperatures close to the surface in summer and to underestimate them in winter. This is due to the turbulent nature of the heat transfer coefficients that this formulation uses. From equations (3-58),(3-59) and (3-60) it can be seen that the convective and evaporative heat transfer coefficients are directly proportional to the wind speed. If the wind speed falls close to zero (as

was the case upon close examination of the experimental data), this formulation tends to over predict temperatures at the surface. However, as seen in Figure 8-4, the predicted temperature near the bottom of the domain is close to the experimental measurements. This implies that this formulation, although overestimating seasonal variations in temperature, could be useful for annual average values required in macro scale approaches (e.g. weather prediction). On the other hand, the use of a Non-turbulent formulation offers an improvement in the prediction of the temperatures near the surface that is related to the inclusion of a natural convection term in the convective and evaporative heat transfer coefficients (equations (3-61) and (3-62)) that keep the temperature of the surface close to the ambient temperature even when low wind speeds are present. However, as shown in Figure 8-4, the Non-turbulent formulation overestimates the temperature of the soil near the bottom by about 1.2 ˚C. This overestimation is explained in contrast with the use of a formulation that takes into account a layer of vegetation. The canopy cover formulation is based on the Non-turbulent formulation by adding consideration of a canopy cover that in fact reduces the exposure of the soil surface to solar radiation and infrared radiation while allowing the independent variation of the level of convection and evaporation by modifying a single parameter (C_e) in equation (3-72). If C_e is equal to zero (as assumed in this study) the vegetation layer is considered as transparent to evaporative and convective interactions between the soil and the atmosphere. Hence, the improvement provided by the use of this formulation on the soil surface temperature and the temperature near the bottom over the non-turbulent formulation is solely due to the reduction in exposure to solar radiation and infrared radiation.

Note that figures from Figure 8-5 to Figure 8-13 include the coefficient of determination R^2 which indicates how well data fits a proposed model. Ideally, R^2=1 indicating a perfect fit. It can be seen that in general, the canopy cover formulation offers higher values for the determination coefficient for any source of meteorological data. However, it can also be seen that the turbulent formulation offers a higher value of R^2 compared to with the non-turbulent one. This may seem odd since the figures show that the non-turbulent formulation is closer to the ideal behaviour (marked by a diagonal line in each figure) than the turbulent. The reason is that R^2 in effect measures how often predicted high values correspond to measured

high values and vice versa for low values. In the non-turbulent formulation, although providing a better overall fit, high predicted values are not necessarily corresponding to high measured values.

With regard to the use of different sources of meteorological data it can be seen that the results from the analysis using analytical meteorological data and a turbulent boundary formulation at the surface, shown in Figure 8-11, are very similar to those presented in Figure 7-11. This is expected given that the description of the problem given in Section 8.6 is similar to the one presented in Section 7.6. The discussion of the analysis presented in Section 7.6.2 also applies in this case. The same trend of overestimation, although to a lesser degree, in summer and underestimation in winter due to the turbulent formulation can be appreciated and similar improvements are noted with use of non-turbulent and canopy cover formulations.

The predictions using meteorological data measured on site are very similar to those obtained by using data obtained from public meteorological stations near the experimental site. However, there is a notable difference corresponding to March that can be observed in Figure 8-5, Figure 8-6 and Figure 8-7 that indicate an over prediction of temperatures in this month that does not correlate with those shown in Figure 8-8, Figure 8-9 and Figure 8-10. The reason for this over prediction of temperatures during March is that the meteorological data provided by TRL was incomplete. The last week of February 2006 and the three first weeks of March 2006 were missing. In the analysis meteorological data for this period was defined by using corresponding meteorological data from 2007 as shown in Figure 8-14. Figure 8-15 shows data provided by BADC for the equivalent period. By comparing Figure 8-14 and Figure 8-15 it can be seen that the last two weeks of March 2007 were particularly sunny in contrast with the corresponding period from 2006. However, it can be argued that, although significant in the predictions of soil surface temperature, the impact of the method adopted to replace this range of dates has a minimal effect on the overall temperature profile of the soil.

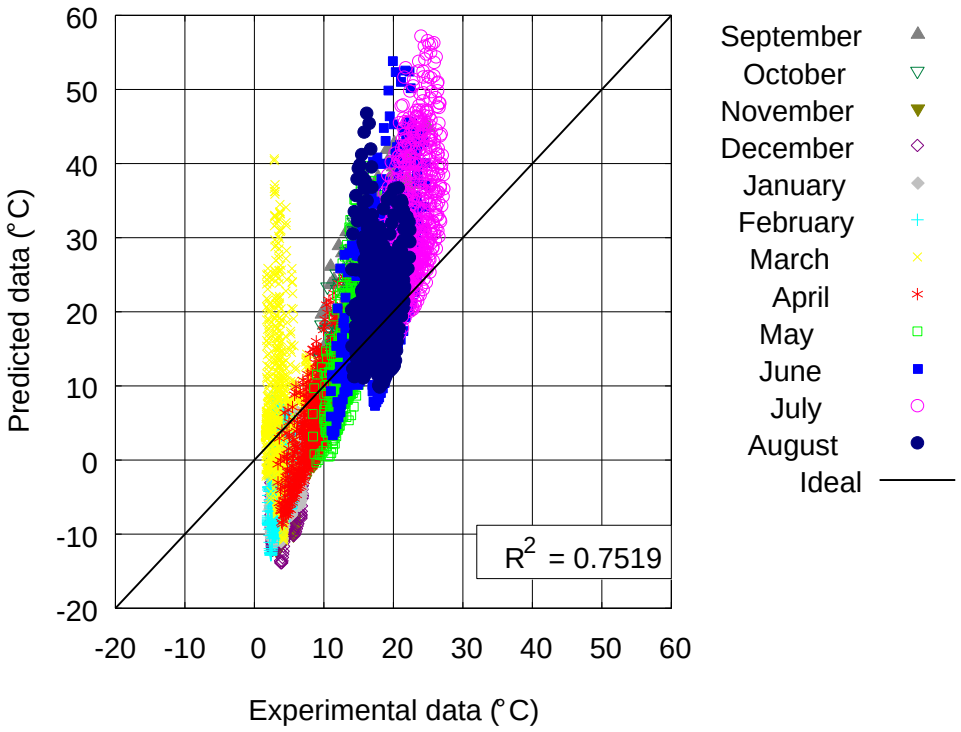

Figure 8-5 - Experimental vs predicted soil temperature at 0.025 m using a Turbulent surface boundary formulation and meteorological data provided by TRL.

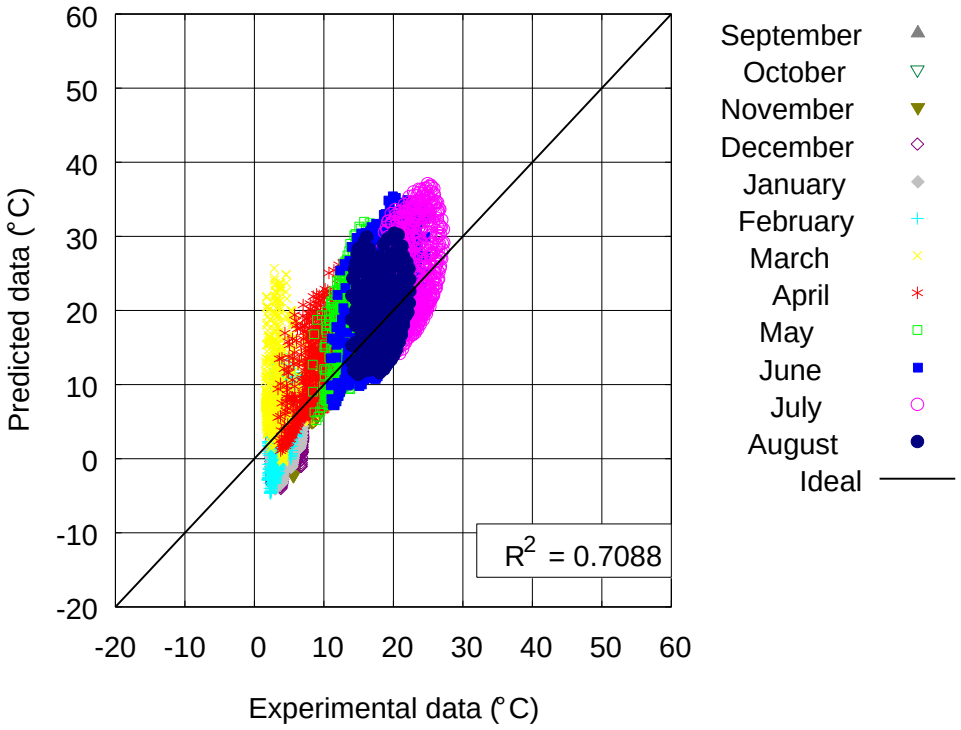

Figure 8-6 - Experimental vs predicted soil temperature at 0.025 m using a Non-turbulent surface boundary formulation and meteorological data provided by TRL.

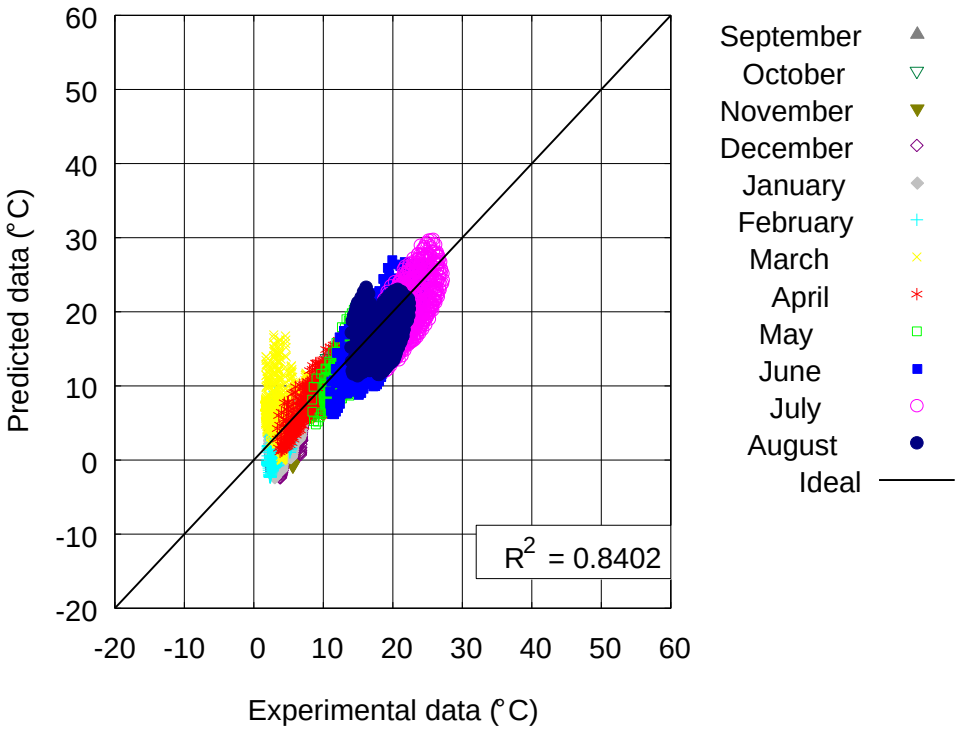

Figure 8-7 - Experimental vs predicted soil temperature at 0.025 m using a Canopy Cover surface boundary formulation and meteorological data provided by TRL.

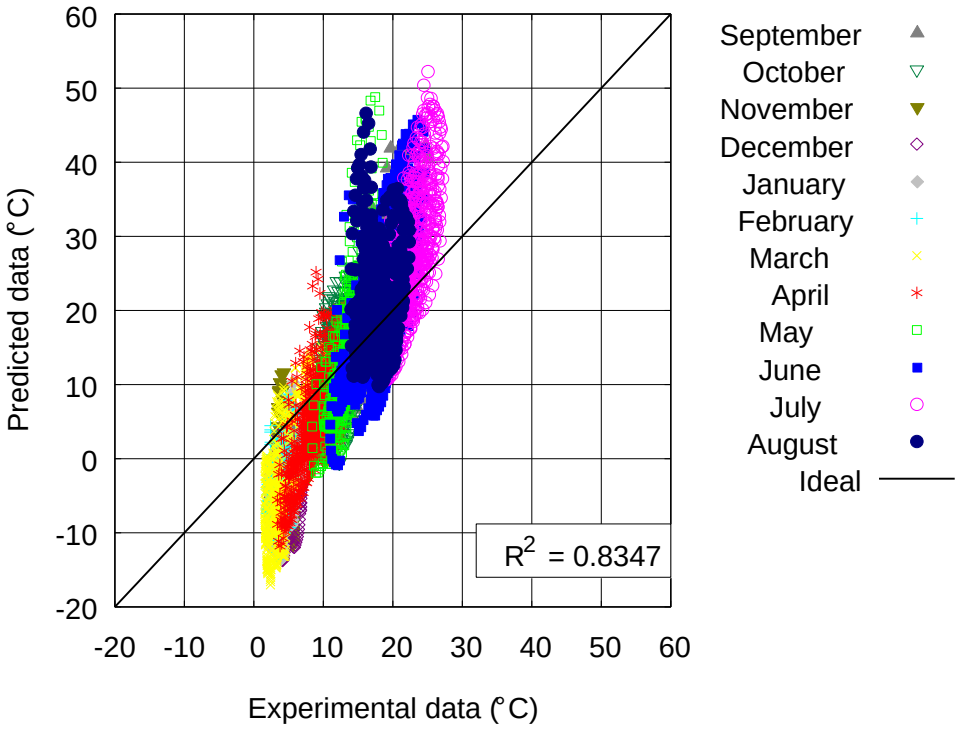

Figure 8-8 - Experimental vs predicted soil temperature at 0.025 m using a Turbulent surface boundary formulation and meteorological data provided by BADC and the Meteorological Office.

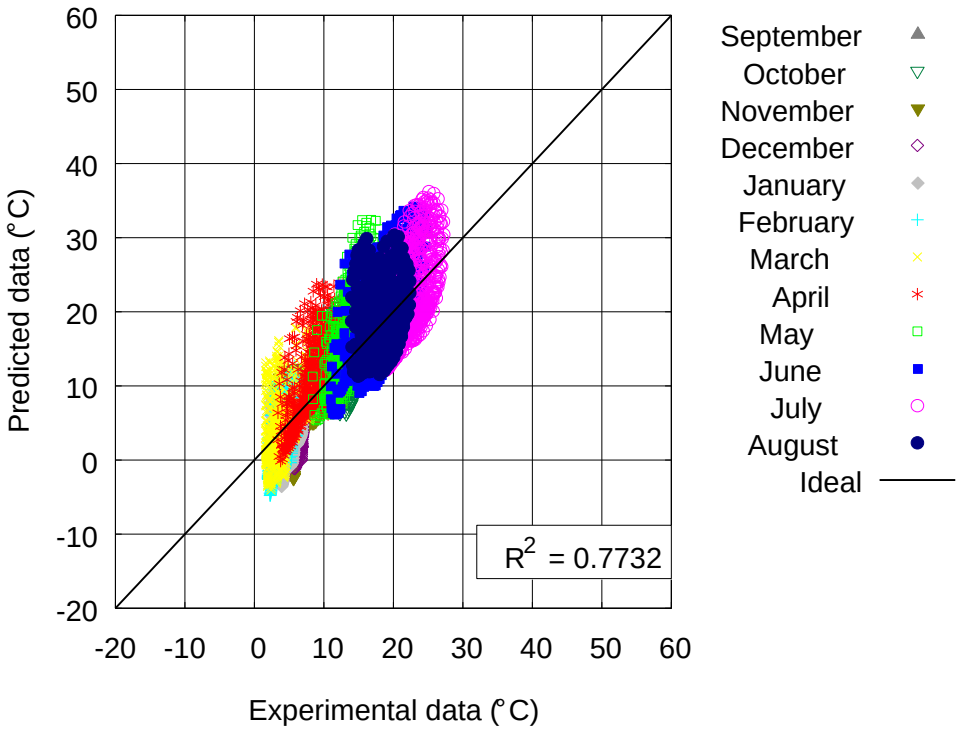

Figure 8-9 - Experimental vs predicted soil temperature at 0.025 m using a Non-turbulent surface boundary formulation and meteorological data provided by BADC and the Meteorological Office.

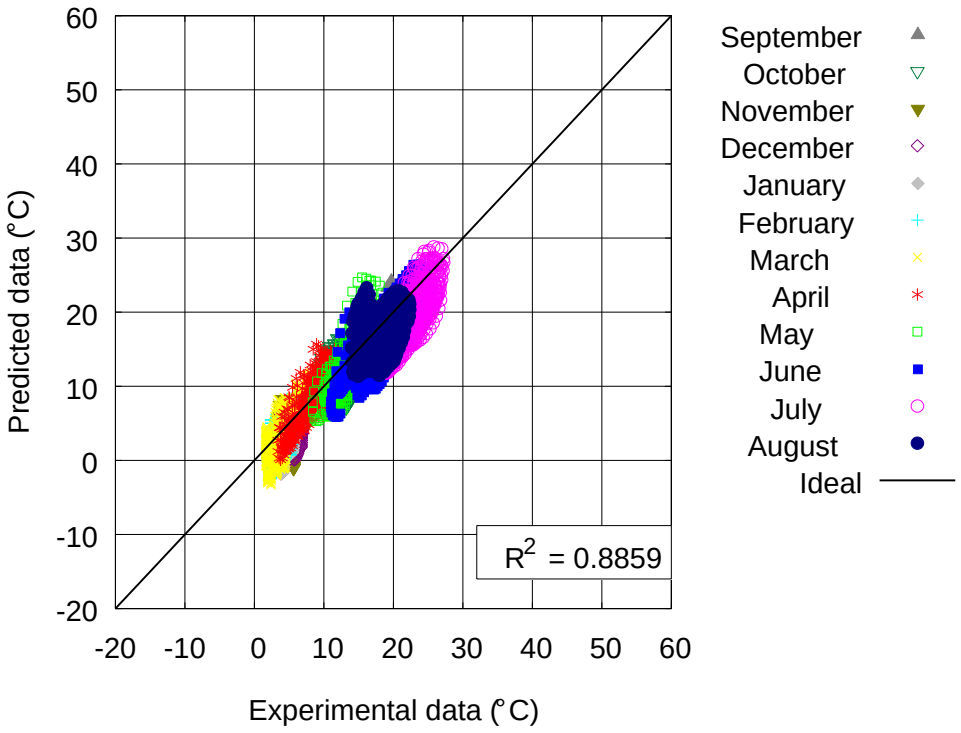

Figure 8-10 - Experimental vs predicted soil temperature at 0.025 m using a Canopy Cover surface boundary formulation and meteorological data provided by BADC and the Meteorological Office.

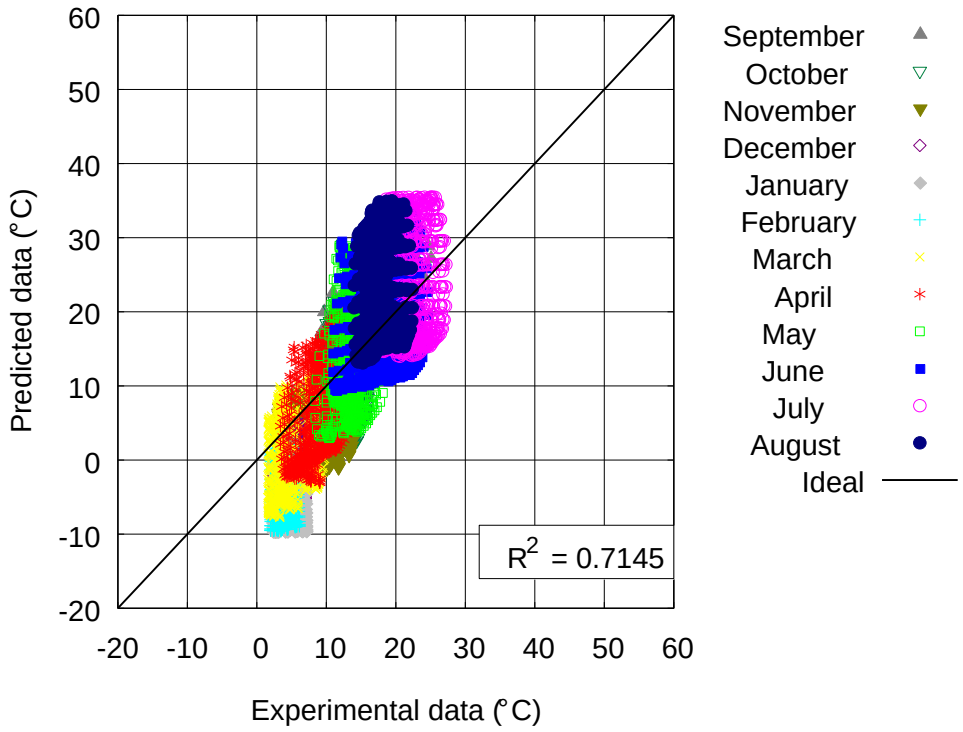

Figure 8-11 - Experimental vs predicted soil temperature at 0.025 m using a Turbulent surface boundary formulation and meteorological data provided by the analytical approach presented in Chapter 7.

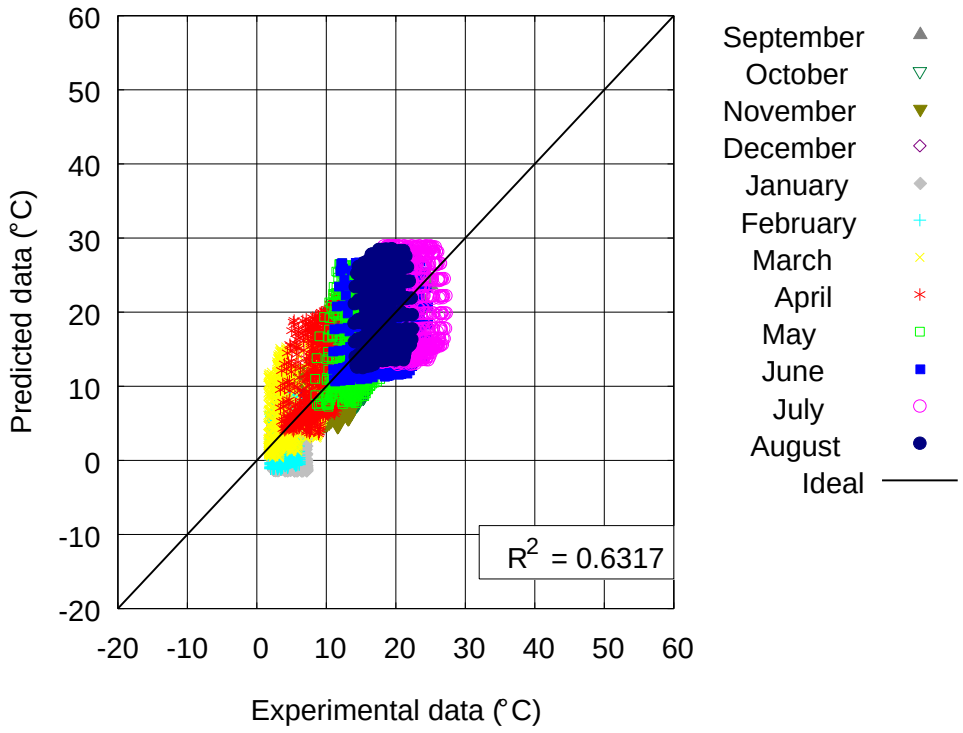

Figure 8-12 - Experimental vs predicted soil temperature at 0.025 m using a Non-turbulent surface boundary formulation and meteorological data provided by the analytical approach.

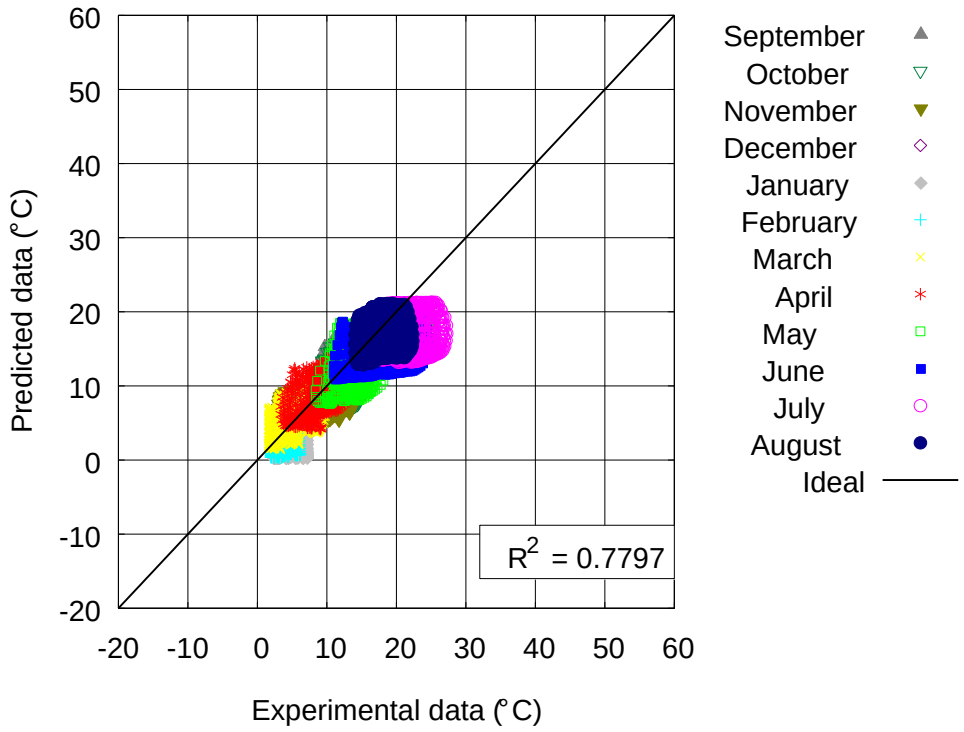

Figure 8-13 - Experimental vs predicted soil temperature at 0.025 m using a Canopy Cover surface boundary formulation and meteorological data provided by the analytical approach.

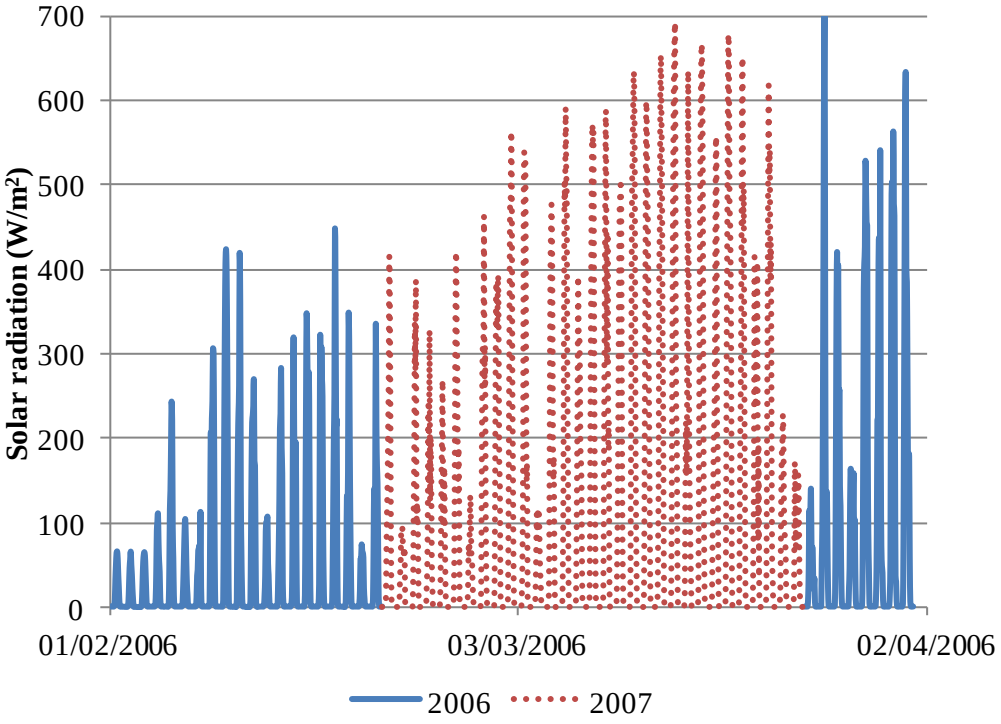

Figure 8-14 - Solar radiation measured on site by TRL in Febuary and March 2006 and 2007.

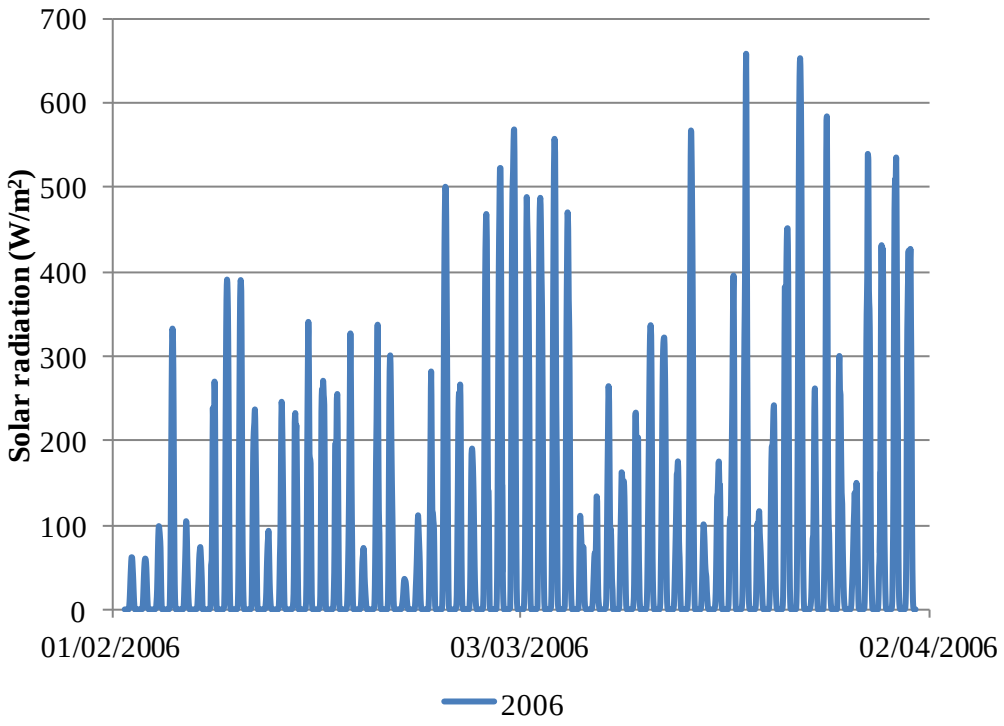

Figure 8-15 - Solar radiation provided by BADC for the period Febuary to March 2006.

8.7.3 Stored thermal energy

Figure 8-16, Figure 8-17 and Figure 8-18 show annual variations of total thermal energy stored in the soil domain for the 11th yearly cycle assuming a free boundary condition at the bottom of the domain and a uniform initial condition. Similarly to Section 8.7.2, the corresponding results in this Section for a fixed boundary condition at the bottom and experimental and analytical initial conditions are not appreciably different and are not shown. The stored thermal energy is calculated in a similar manner as discussed in Section 7.5. In the calculation temperature profiles are obtained by linear interpolation from a discrete set of points that match the position of the temperature sensors. The temperatures at these points are obtained both from the numerical model and from the experimental measurements. The amount of energy stored at any given point in time is obtained from the difference between its temperature profile and a reference temperature profile (defined as that corresponding to September 1st of yearly cycle 11) integrated over the total depth of the soil column times the density and specific heat capacity of the soil. Figure 8-16 shows the annual variation in total thermal energy predicted using meteorological data provided by TRL while Figure 8-17 show corresponding results using meteorological data provided by BADC and the Meteorological Office and Figure

8-18 shows results using the analytic expressions (equations (7-21) and (7-18)) proposed in Chapter 7. It can be seen that, in general, the Turbulent approach over estimates the annual variation in soil energy while the Canopy Cover formulation offers the best match for the experimental data.

Figure 8-16 presents the effect in the total thermal energy stored in the soil of the sunny weeks from March 2007 but used in March 2006 as discussed before. The Turbulent formulation shows a clear peak of thermal energy gained in this period. A more subtle peak (marked with a circle in Figure 8-16 and correspondingly in Figure 8-17) is observed in the Non-turbulent formulation while a discrete change in slope is perceived using the Canopy Cover formulation. However, it can be seen that in all cases the impact of the disturbance reduces with time and the general trend becomes increasingly comparable to the results obtained using meteorological data from public sources shown in Figure 8-17. This seems to imply that any excess thermal energy gained in this period is confined to the shallow regions of the ground and that it is quickly released (via infrared radiation and convection due to the higher surface temperatures).

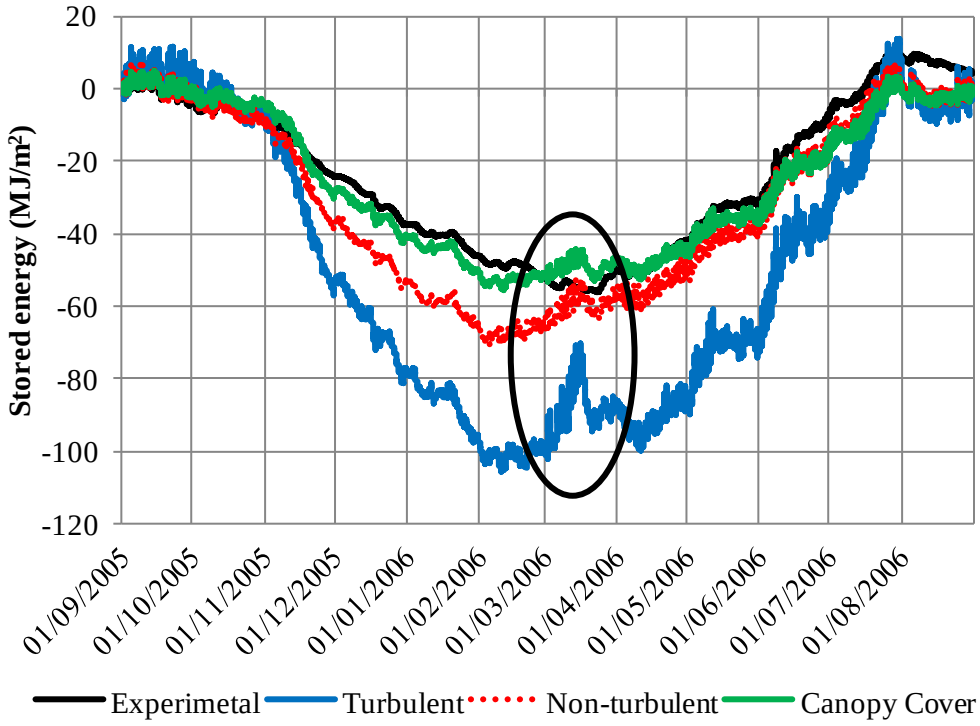

Figure 8-16 -Annual variation of total thermal energy stored in the soil domain using meteorological data provided by TRL.

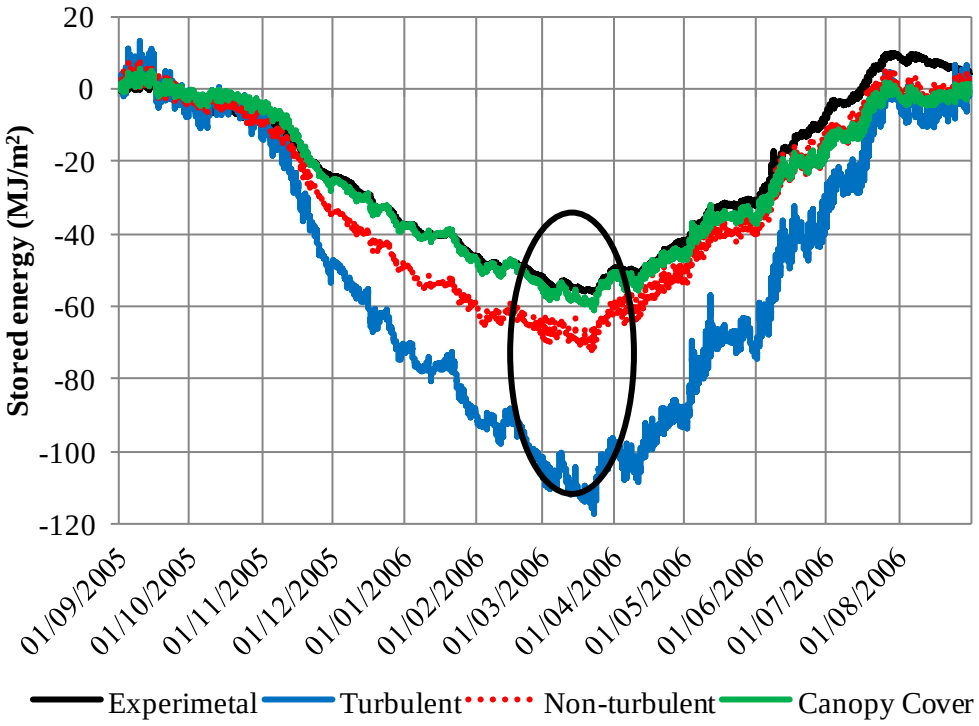

Figure 8-17 -Annual variation of total thermal energy stored in the soil domain using meteorological data provided by BADC and the Meteorological Office.

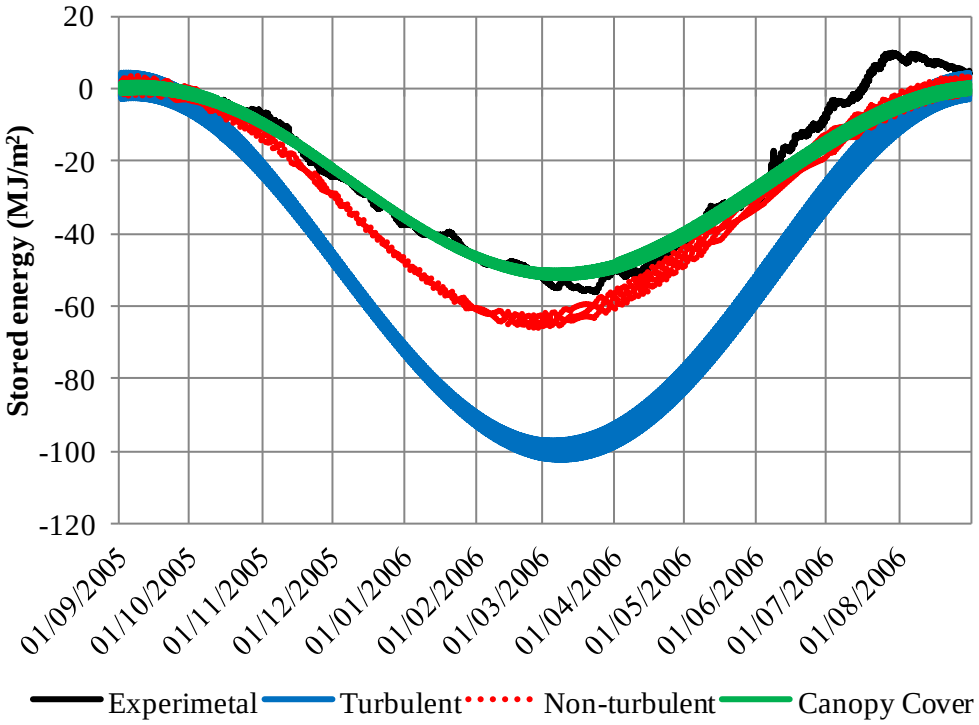

Figure 8-18 - Annual variation of total thermal energy stored in the soil domain using meteorological data generated using the analytical approach proposed in Chapter 7.

8.7.4 Coupled analysis

The results presented in Sections 8.7.1, 8.7.2 and 8.7.3 have been obtained using an uncoupled numerical solution for the heat transfer equation. A coupled analysis comprising 11 yearly cycles has also been performed using homogeneous initial conditions for temperature (10˚C) and pressure head (-10 m), free boundary condition at the bottom of the domain for both variables. Based on the earlier results a Canopy Cover surface boundary formulation has been used for the surface thermal fluxes (using meteorological data provided by TRL). For the pressure head domain the boundary condition at the surface is implemented as follows: a fixed boundary condition equal to -150 m is enforced whenever the pressure head reaches the wilting point (-150 m), this condition remains active while there is no moisture flux entering the domain through condensation or precipitation; a fixed boundary condition equal to (-10 m) is enforced whenever the pressure head reaches this value at the surface, this condition is maintained while there is no moisture flux leaving the domain (through evaporation); if the surface pressure head is located between these two points, a Neumann boundary condition is implemented as described in Section 3.7. Thermal properties as a function of moisture content are interpolated from the values shown in Table 2-4 (Garratt 1994). Water retention curve and hydraulic conductivity relations are defined by equations (3-9) and (3-10). The results of this analysis are presented in Figure 8-19, Figure 8-20 and Figure 8-21.

Figure 8-19 compares the profile of soil thermal conductivity for an uncoupled (constant thermal conductivity) and a coupled problem on 1st September of the 11th yearly cycle. Typical minimum and maximum values for thermal conductivity for clay soils have been added for reference (Pielke 1984). Similarly, Figure 8-20 compares the volumetric heat capacities for the uncoupled and coupled problems. Figure 8-21 shows a comparison between the coupled and uncoupled temperature profiles corresponding to September 1st at 12:00:00 for the 11th yearly cycle. From these figures it can be seen that the higher variations in thermal properties are localized at the bottom of the domain (as would be expected due to higher moisture content in this region due to gravitational forces) while at surface these variation do not exceed a 10% of the range of defined by the minimum and maximum values. Moreover, the comparison of temperature profiles reveal that these variations have negligible impact in the prediction of the thermal behaviour of the soil. The

implication of this is that it is unnecessary to undertake a coupled analysis in this particular case.

θ_w	λ_b (W/mK)	$c_{p,b}$ (J/kgK)	ρ_b (kg/m^3)	α_b (m^2/s)
0	0.25	890	1600	0.18
0.2	1.1	1170	1800	0.52
0.4	1.6	1550	2000	0.52

Table 8-2: Variation of thermal properties with water content for clay soils (Garratt 1994).

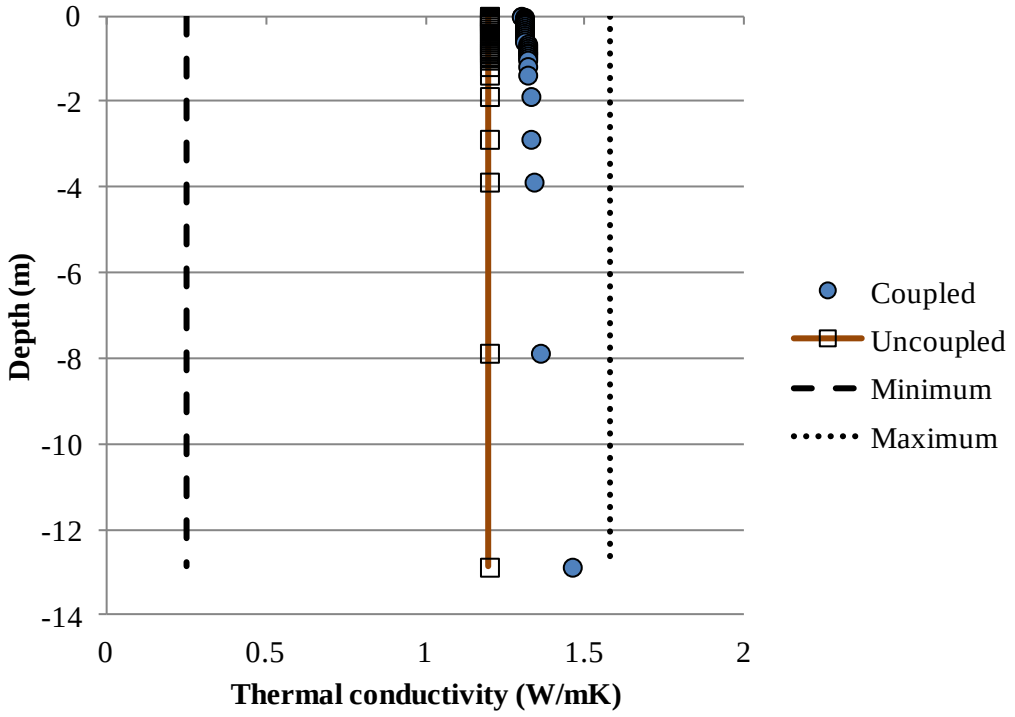

Figure 8-19 - Comparison of thermal conductivities (on for September 1st , 11th yearly cycle) for a coupled and uncoupled problem.

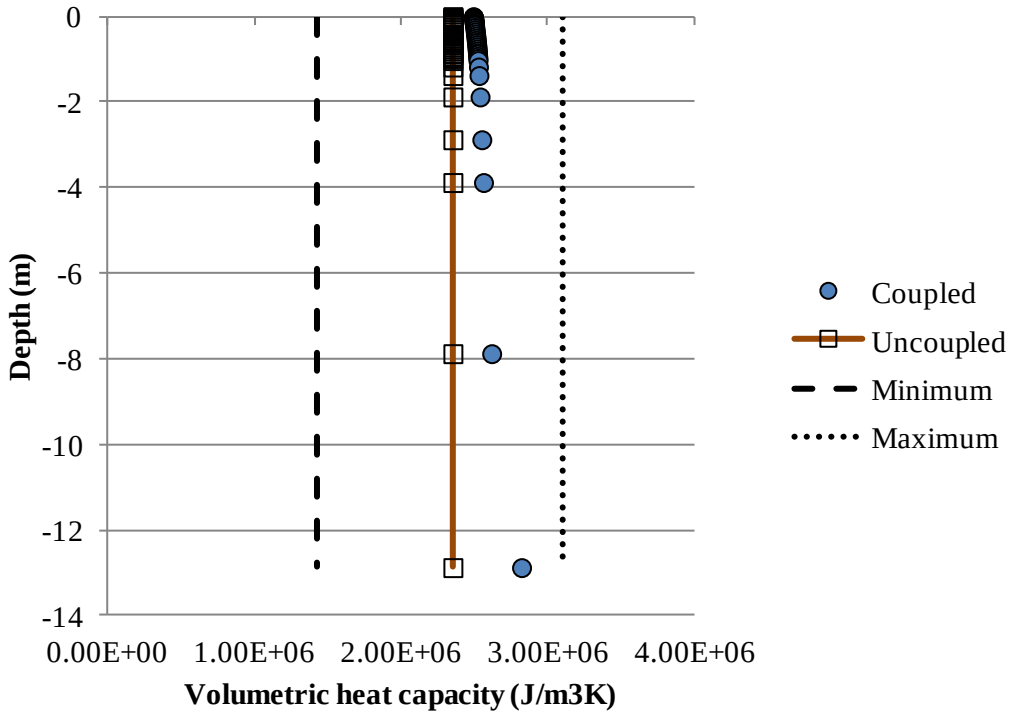

Figure 8-20 - Comparison of volumetric heat capacities (on September 1st , 11th yearly cycle) for a coupled and uncoupled problem.

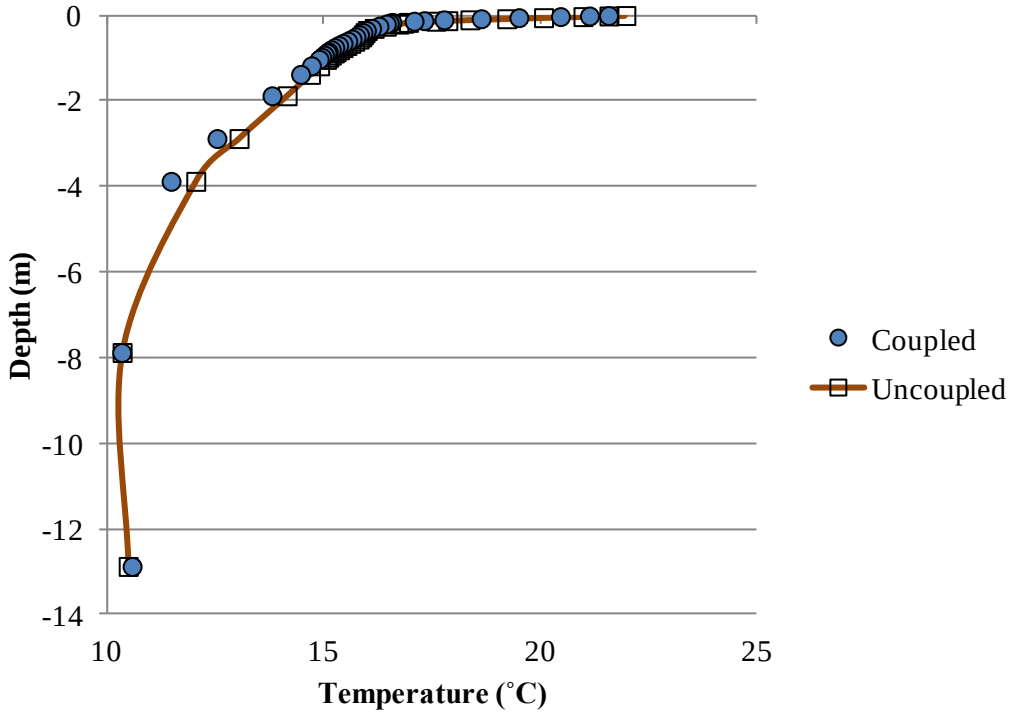

Figure 8-21 - Comparison of temperature profiles (on September 1st , 11th yearly cycle) for a coupled and uncoupled problem.

8.8 Concluding remarks

This Chapter has presented a 1D analysis of the heat transfer process in a column of soil. The impact of different assumptions for the initial conditions, surface boundary formulations, far-field (lower) boundary conditions and sources of meteorological data have been explored.

Three initial conditions (homogeneous, experimental and analytical) have been analyzed. It has been found that the initial condition for the problem may have an impact on the number or yearly cycles required for the domain to reach a steady state, but this needs to be considered along with the formulation used to define the heat flux at the surface of the domain. For example, if a Canopy Cover formulation is used, there is no significant difference in the time taken to reach a steady state between the three different initial conditions considered.

In terms of the formulations used to define the boundary conditions at the surface of domain it has been found that the formulation that best predicts the temperature of the soil near the surface and the total thermal energy stored (Figure 8-16, Figure 8-17 and Figure 8-18) is the Canopy Cover formulation. However, although the Turbulent approach in general overestimates both temperatures near the surface

and thermal energy stored, it offers good estimates of the temperature at the bottom of the domain.

Regarding the boundary condition at the bottom of the domain, it was found that both assumptions (fixed and free) offer comparable results, the main difference being in the number of yearly cycles required to reach a steady stated. However it is noted that whilst a fixed approach requires considerably less iterations than a free approach it does require a priori knowledge of the soil temperature at depth.

The use of meteorological data obtained from different sources has also been studied. It has been found that the use of meteorological data recorded on site is comparable to the use of data obtained from public meteorological stations located near the experimental site. Although the latter could offer the additional advantage of a more robust database (since more than one station could be located near the experimental site) it has been found that errors introduced by replacing short periods

of missing data on the on-site measurements by equivalent periods of contiguous years is minimal.

A coupled analysis of heat and moisture transfer has been performed to compare the variations on thermal properties and temperature profiles with respect to the assumptions and predictions made in an uncoupled analysis of heat transfer. It has been demonstrated that the variations in thermal properties are minimal and that the impact that they have in the prediction of the soil's temperature profile is, in this case, negligible.

8.9 Bibliography

Alvenäs, G. and Jansson, P.-E. [1997]. Model for Evaporation, Moisture and Temperature of Bare Soil: Calibration and Sensitivity Analysis. *Agricultural and Forest Meteorology* **88** (1–4): 47–56. doi:10.1016/S0168-1923(97)00052-X.

Best, M. J. [1998]. A Model to Predict Surface Temperatures. *Boundary-Layer Meteorology* **88** (2): 279–306. doi:10.1023/A:1001151927113.

Carder, D. R., Barker, K. J., Hewitt, M. G., Ritter, D., and Kiff, A. [2007]. Performance of an Interseasonal Heat Transfer Facility for Collection, Storage and Re-Use of Solar Heat from the Road Surface. PPR302. Transport Research Laboratory.

Deardorff, J. [1978]. Efficient Prediction of Ground Surface-Temperature and Moisture, with Inclusion of a Layer of Vegetation. *Journal of Geophysical Research-Oceans and Atmospheres* **83** (NC4): 1889–1903. doi:10.1029/JC083iC04p01889.

Edinger, J. E., Duttweiler, D. W., and Geyer, J. C. [1968]. The Response of Water Temperatures to Meteorological Conditions. *Water Resources Research* **4** (5): 1137–1143. doi:10.1029/WR004i005p01137.

Garratt, J. R. [1994]. *The Atmospheric Boundary Layer*. Cambridge University Press.

Geiger, R. [1950]. *The Climate Near The Ground*. Translated by Milroy N. Stewart. Harvard University Press.

Herb, W. R., Janke, B., Mohseni, O., and Stefan, H. G. [2008]. Ground Surface Temperature Simulation for Different Land Covers. *Journal of Hydrology* **356** (3-4): 327–343. doi:10.1016/j.jhydrol.2008.04.020.

Jansson, C., Almkvist, E., and Jansson, P. [2006]. Heat Balance of an Asphalt Surface: Observations and Physically-Based Simulations. *Meteorological Applications* **13** (2): 203–212. doi:10.1017/S1350482706002179.

Pielke, R. A. [1984]. *Mesoscale Meteorological Modeling*. Academic Press.

UK Meteorological Office. [2012]. Met Office Integrated Data Archive System (MIDAS) Land and Marine Surface Stations Data (1853-Current). *NCAS British Atmospheric Data Centre*. [Online]. Available at: http://badc.nerc.ac.uk/view/badc.nerc.ac.uk__ATOM__dataent_ukmo-midas. [Accessed: 03-Apr-2014].

UK Meteorological Office. [2014]. Met Office: UK Climate Summaries. [Online]. Available at: http://www.metoffice.gov.uk/climate/uk/index.html. [Accessed: 04-Apr-2014].

Chapter 9 Inter-seasonal heat transfer system and shading impact: 2D Numerical Simulations

9.1 Introduction

In this Chapter the numerical model for transient heat transfer presented in Chapter 3 are applied to the development of a 2D model able to represent the process of ground thermal energy storage carried out by buried engineering geo-environmental devices. This includes the process of heat collection from external sources and the storage in the soil mass; and the extraction of heat from the soil mass to be delivered to external applications. For this, a 2D algorithm able to represent the performance of geo-environmental devices composed by pipe heat exchangers is developed.

The proposed numerical model is applied to investigate the experimental case study presented in Chapter 5. In particular, System 2 has been chosen due to its more complex geometrical configuration, having all collection and storage components located under the road surface, offering a more challenging problem in terms of model validation.

Detailed examination of the data set provided by Carder et al (2007), and on site observations, indicate the presence of shaded areas over the regions where the experimental system were placed. The impact of this shading is further considered and investigated with the proposed numerical model via suitable modifications on the formulation used to represent the soil surface heat interactions with the atmosphere.

The objectives of this Chapter are:

- to develop a 2D numerical model to represent the process of heat collection and storage in soil.
- to propose and validate a 2D algorithm to represent the operational geo-environmental buried devices composed of pipe heat exchangers.
- to assess the impact that shading cast by adjacent objects has on the thermal performance of a ground storage device.

The Chapter is divided in the following sections:

i) Section 9.2 presents preliminary numerical considerations and material properties used in this Chapter. It also introduces the proposed numerical algorithm to represent in 2D the behaviour of a buried heat exchanger system.

ii) Section 9.3 describes the domain under consideration and shows its discretized representation.

iii) Section 9.4 lists the initial and boundary conditions used to solve the numerical problem.

iv) Section 9.5 presents temperature variations near the soil and road surfaces for a selected period of time that shows the influence of shading by nearby trees.

v) Section 9.6 lists the different period of analysis in which the study of the experimental case is divided.

vi) Section 9.7 discusses the results obtained for each of periods of analysis.

9.2 Numerical approach

The results obtained in Chapter 8 have shown that a coupled analysis of heat and moisture transfer was unnecessary to study the thermal performance of soil under the conditions described in Chapter 5 for control borehole A. Furthermore, since the current analysis is focused in a section of soil that includes an impermeable insulation layer near the surface of the ground (see Figure 5-3 and Figure 5-4), it is expected that the variations of moisture in the domain to be even less significant. For these reasons, an uncoupled numerical analysis using the heat transfer equation presented in Section 4.3 has been performed.

The soil surrounding System 2 is considered to be composed of silty clay based on laboratory tests described in Chapter 6. The material properties of the soil are assumed to be homogeneous and are presented, along with those of the different layers composing System 2, in Table 9-1 (‘Code’ refers to the numbering shown in Figure 5-4, detailing the relative position of the constitutive layers). Thermal conductivity and density of soil are based on material data provided by Carder et al (2007), which agree with material properties for this type of soil available in the literature (Garratt 1994). The specific heat capacity is based on the data presented in Appendix 4 of (Garrat,1994) for clay soil assuming a homogeneous moisture

content of 23%. Evaporative terms for the soil boundary formulation require an estimation of pressure head at the soil surface. This value is set at -75.2025 m as the average of saturation and wilting point values for clay soils (Garratt 1994).

Code	Material type	Density (kg/m^3)	Specific heat (J/kgK)	Thermal conductivity (W/mK)
1	Wearing course	2400	850	0.85
2	Binder course	2400	850	0.85
3	Concrete screed	2100	840	1.4
5a	New lean concrete base	2100	840	1.4
5b	Type 1 granular material	2100	840	1.4
6	Polystyrene insulation	30	1130	0.034
8	Sand	2240	840	0.33
9	Soil	1960	1227	1.21

Table 9-1 - Material parameters used in this study to investigate the experimental test case presented in Chapter 5.

9.2.1 2D representation of ground heat exchanger

The inter seasonal heat transfer system described in Chapter 5 is composed of two sets of 10 pipes placed near the surface of the ground which act like heat exchangers. The pipes are arranged in a U-loop running 30 m back and forth along the road as shown in Figure 5-2. The geometrical dimensions of the pipe arrays and fluid composition is summarized in Table 5-2.

For the purpose of modelling, 3D pipes in collector and storage arrays are idealized as shown in Figure 9-1. Each consisting of a flow and return section. In the case of a collector pipe $T_{cf,i}$ and $T_{cf,o}$ correspond to inlet and outlet temperatures in the flow section while $T_{cr,i}$ and $T_{cr,o}$ correspond to inlet and outlet temperatures in the return section. Note that in a 3D scheme, $T_{cf,o}=T_{cr,i}$. The heat flux rate from the flow and return sections are referred as q_{cf} (W/m^2) and q_{cr} (W/m^2) respectively. A similar nomenclature convention is used for each storage pipe.

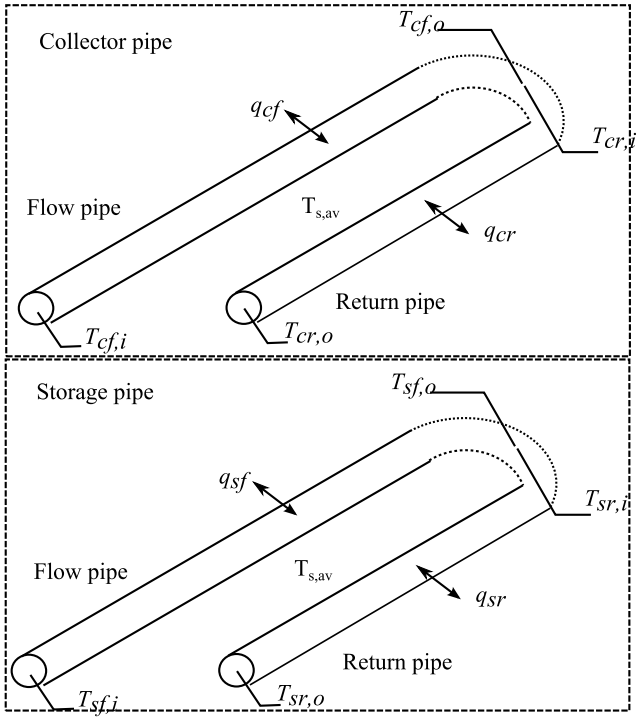

Figure 9-1 - Idealization of 3D pipe for 2D modelling.

In order to solve the 2D numerical problem, suitable values for the heat fluxes on the flow and return sections of the pipes need to be estimated. With this purpose, the following assumptions and simplifications are made:

- In each time step, there are two possible states for the system: ON and OFF. These states depend on activation criteria defined in Section 9.6.
- If the system is OFF, then the numerical problem is solved setting the boundary values at the soil-pipes boundaries, q_{cf}, q_{cr}, q_{sf}, and q_{sr}, to 0.
- If the system is ON, then q_{cf}, q_{cr}, q_{sf}, and q_{sr} need to be estimated. Under this scenario, the following additional considerations are taken into account:
    - the soil in direct contact with the pipes is considered to be at constant temperature $T_{s,av}$, during the time step, equal to the average between the previous time step and the current estimation of the current time step.
    - The fluid flowing through the pipes is considered to complete a certain number of flow cycles, F_c, in the system (collector and storage pipes) as shown in Figure 9-2 in each time step defined by the flow velocity and the length of the pipes.

- No heat losses are considered in the transit section between collector and storage arrays.

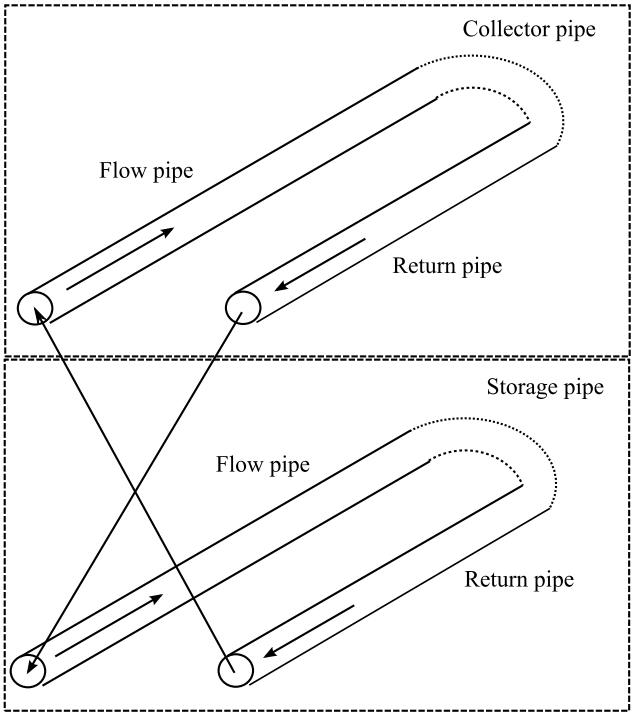

Figure 9-2 - Flow direction in an idealized system.

The following algorithm is proposed to represent the system in 2D under ON conditions:

1. Initial state. If the system was OFF during the previous time step, then $T_{cf,i}$, $T_{cf,o}$, $T_{cr,i}$, $T_{cr,o}$, $T_{sf,i}$, $T_{sf,o}$, $T_{sf,i}$ and $T_{sf,o}$ are assumed to be equal to $T_{s,av}$. If the system was ON then $T_{cf,i}$, $T_{cf,o}$, $T_{cr,i}$, $T_{cr,o}$, $T_{sf,i}$, $T_{sf,o}$, $T_{sf,i}$ and $T_{sf,o}$ are assumed to be equal to the corresponding values for the previous time step. In both cases q_{cf}, q_{cr}, q_{sf}, and q_{sr} are initialized to 0.
2. Pipe outlet temperatures: $T_{cf,o}$, $T_{cr,o}$, $T_{sf,o}$ and $T_{sf,o}$ are calculated using the overall pipe heat transfer coefficient U_p presented in Section 3.6.
3. Pipe heat fluxes: q_{cf}, q_{cr}, q_{sf}, and q_{sr} are calculated using the pipe effectiveness ε_p presented in Section 3.6.
4. Pipe inlet temperatures: as mentioned before, based on the geometry shown in Figure 9-1, the following consideration is made: $T_{cr,i}$.=$T_{cf,o}$ and $T_{sr,i}$.=$T_{sf,o}$ Regarding $T_{cf,i}$ and $T_{sf,i}$, these are equal to $T_{cr,o}$ and $T_{sr,o}$ or to the averages of the corresponding temperatures in a pipe arrangement (i.e. the fluid is mixed at the inlet of the heat exchanger).

5. Steps 1-4 are repeated until the required number of flow cycles is achieved. Corresponding pipe heat fluxes are added to q_{cf}, q_{cr}, q_{sf}, and q_{sr}.

When the required number of flow cycles F_c is completed, the heat fluxes are averaged by F_c. Averaged values for q_{cf}, q_{cr}, q_{sf}, and q_{sr} are used as boundary conditions at the soil-pipes boundaries and the numerical problem is solved and a new estimation for $T_{s,av}$ is obtained. The previous algorithm is repeated until the difference between the current and previous estimation for $T_{s,av}$ is less that a suitable convergence criteria δ.

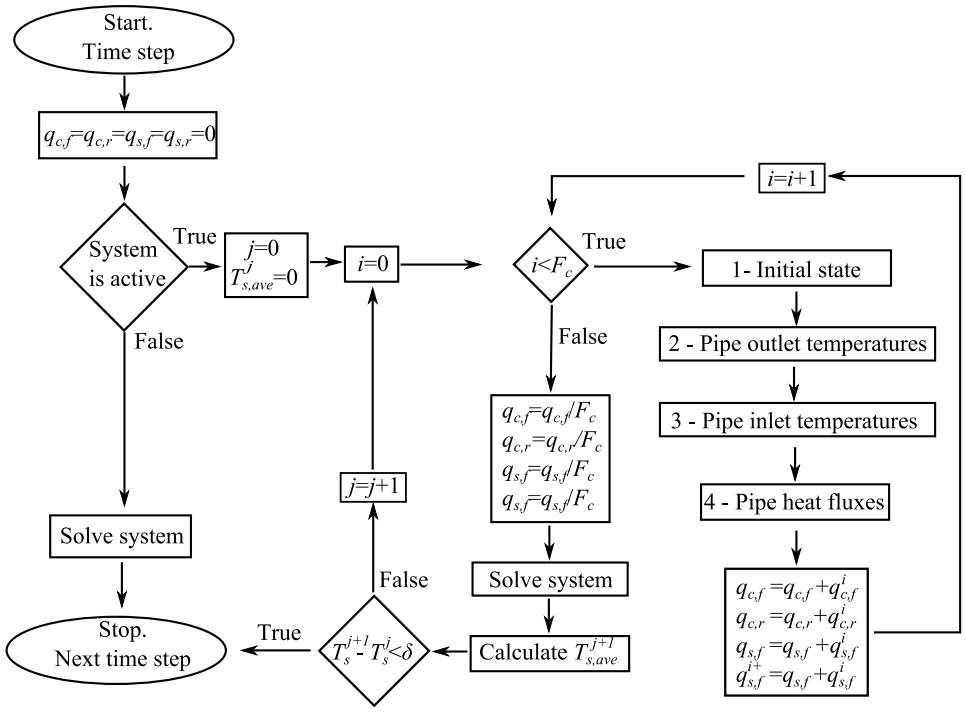

Figure 9-3 - Flow diagram of proposed algorithm to calculate pipe heat exchanger heat fluxes.

9.3 Domain and discretization

Figure 33-4 shows the 2D domain under consideration composed by 2452 quadrangular elements. The domain represents a 2 dimensional section of soil 14 m deep by 27.6 m wide containing the road material layers and heat exchangers near its centre. The slope next to the road is considered in order to correctly model the heat transfer flow in the soil domain, specifically under the insulation layer. The position of boreholes A and F/G are shown for reference. Notice that boreholes F and G are both positioned in the middle of the road (Figure 9-5). The use of either F or G nomenclature depends on the period of simulation and will be discussed in the following sections.

9.4 Initial and Boundary Conditions

Initial and boundary conditions are set as:

- Surface boundary condition - Soil. Based on the results from Chapter 8 the formulation including a canopy layer (Section 3.7) is applied as it has been found to be suitable for the representation of thermal fluxes at the soil surface.
- Surface boundary condition - Pavement. An initial analysis considering Turbulent and Non-turbulent boundary formulations (Section 3.7) is performed for the pre system activation period and the 1st activation period (see Section 9.6). The more suitable formulation is used to continue the analysis on the remaining activation periods.
- Free flux boundary condition is used at the bottom of the domain. After the analysis performed in Chapter 8 it was concluded that, with the correct representation of heat transfer processes at the boundary, the boundary condition at the bottom of the domain has a minimal impact in the prediction of the temperature profile of the soil.
- Free flux boundary conditions are used on the vertical far-field boundaries of the domain.
- Initial condition. A uniform value of 10 ˚C is used as the initial condition for the domain. This value is calculated from the average air temperature measured on the experimental site by TRL (Carder et al. 2007) for the period September 2005 to August 2006. The domain is then subjected to a pre system activation analysis consisting of 8 yearly cycles using meteorological data provided by Carder et al (2007) for the period September 2005 to August 2006, reaching a temperature profile equivalent to that presented in Figure 8-21. This allows the initial thermal condition of the domain, which is consistent with the applied boundary conditions, to be established before the simulation of the system activation period is commenced.

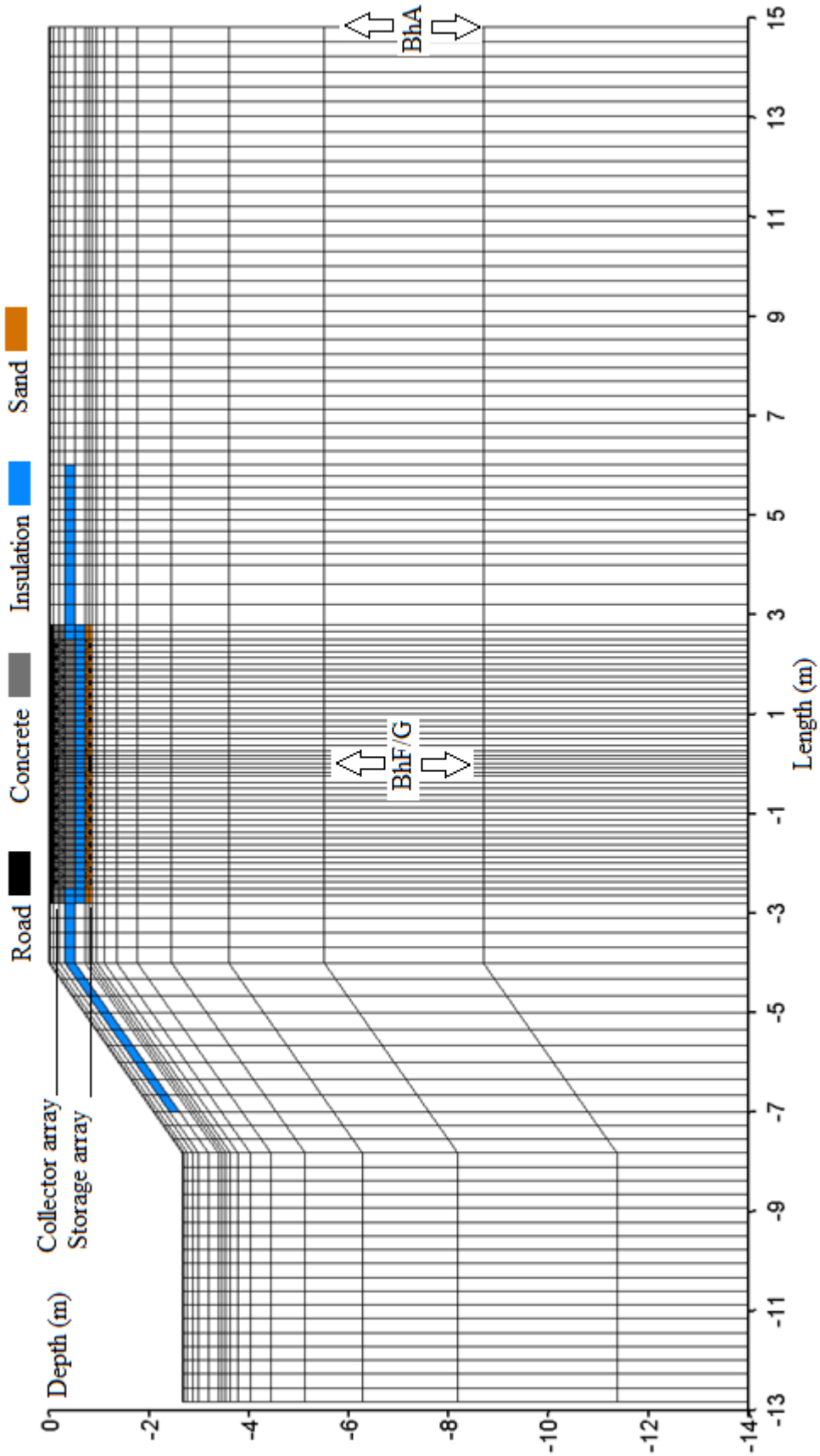

Figure 9-4 - 2D domain considered in this study. Main materials are indicated by colour. Positions of collector and storage arrays are indicated. For a detailed arrangement of material layers see Figure 5-4.

9.5 Shading

Analysis of the experimental measurements reported by Carder et al (2007) indicates that sections of the surface of the road were exposed to periods of shading during the operation of the collection system. Figure 9-5 shows a plan view of the experimental site described in Chapter 5 with the position of the two heat collectors and three boreholes corresponding to control borehole A (soil), control borehole F (pavement), and borehole G (middle of System 2). The presence of a line of trees next to collector 1 and close to the position of boreholes F can be observed.

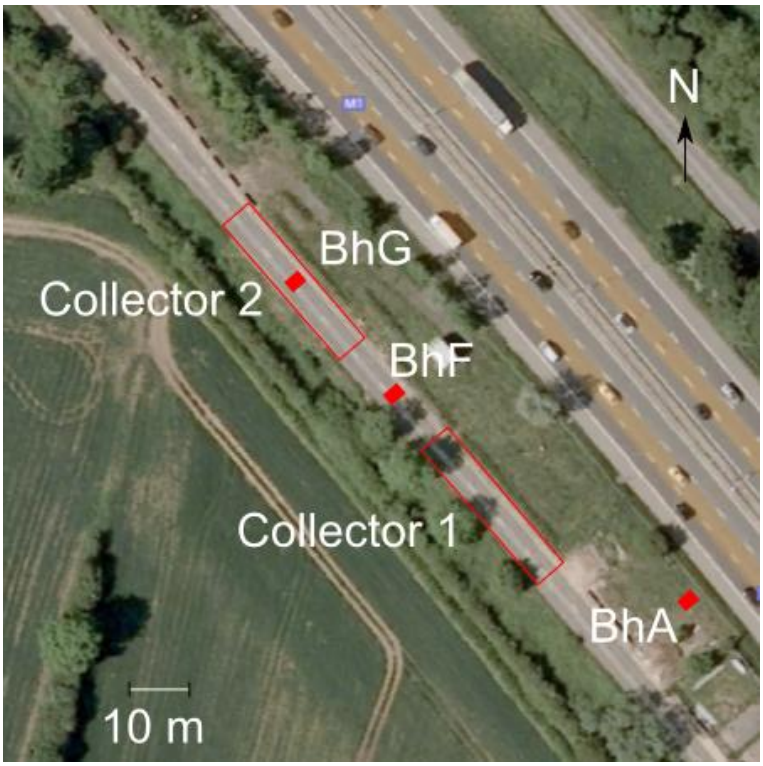

Figure 9-5-Plan view of experimental site. Positions of heat collectors and boreholes considered in this study are indicated.

Figure 9-6 shows an example of the measurements recorded from the temperature sensors located at 0.025 m depth corresponding to control boreholes F (dashed line) and A (dotted line) for the period 13th September 2005 to 16th September 2005. Besides the obvious difference in temperature due to the different surface properties, a temperature drop in the data for the pavement surface, that is not present in the data for the soil surface, between approximately 12:00 h and 15:00 h can be seen. It is believed that this effect is related to diurnal shading.

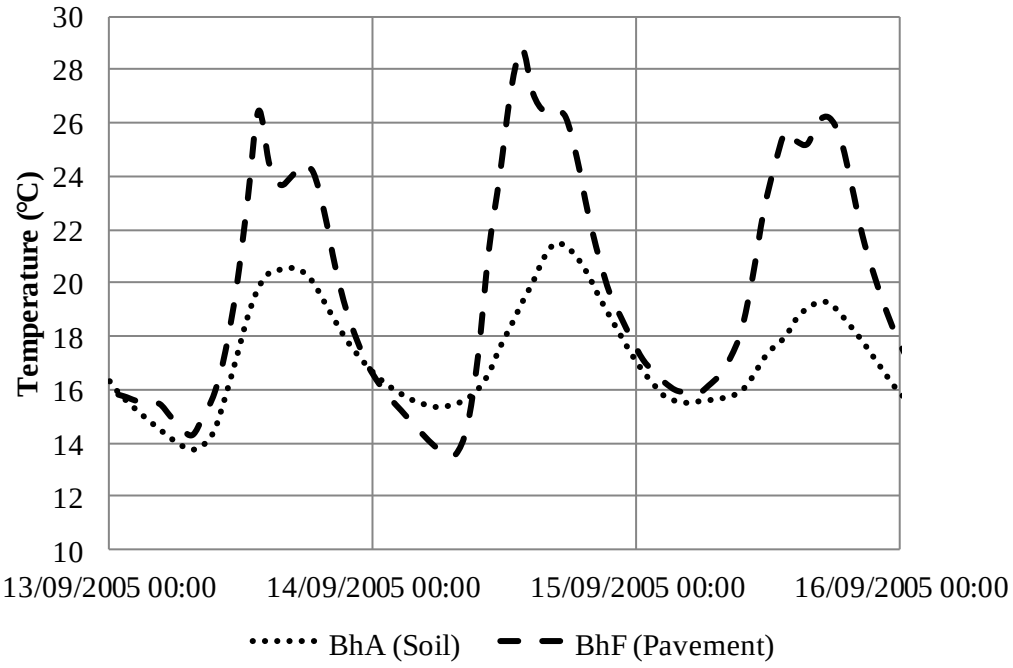

Figure 9-6 - Temperatures at 0.025 m for soil (BhA) and pavement (BhF), data from Carder et al (2007) .

From Figure 9-5 and Figure 9-6 it can be concluded that borehole F and System 1 were highly influence by shading. In the case of System 2, this is not obvious, Figure 9-5 might suggest that it was not exposed to shading, however, in photographic records (Figure 9-7) obtained after a visit to the experimental site on early February 2011 it can be observed the presence of trees with scarce treetops (although this expect to vary seasonally) and growing vegetation next to the road. Figure 9-8 shows a comparison of temperature profiles measured at 0.01 m depth at the centres of collector 1 and collector 2, and borehole F during the first week of April 2006 (during the second insulation period and therefore without influence of the systems being active, see Section 9.6). It can be observed the influence of shading on borehole F during the day. However, effect of shading on collector 2 and collector 1 is more subtle. In particular, during the 4^{th}, 5^{th} and 9^{th} shading can be observed in borehole F (implying a decreased effect of cloud cover) while the temperatures at collector 1 and collector 2 do not show this effect. For this reason, in the absence of more detailed shading measurements on the surface of collector 2, it is assumed that it was influenced to some degree by the cast projected by nearby trees. Simulations with varying degrees of shading were performed to try to assess the impact of this variable. The results are presented in Section 9.7.

Figure 9-7 - State of location of System 2 on early February 2011. It can be observed the presence of trees with scarce treetops at this date and growing vegetation next to the road.

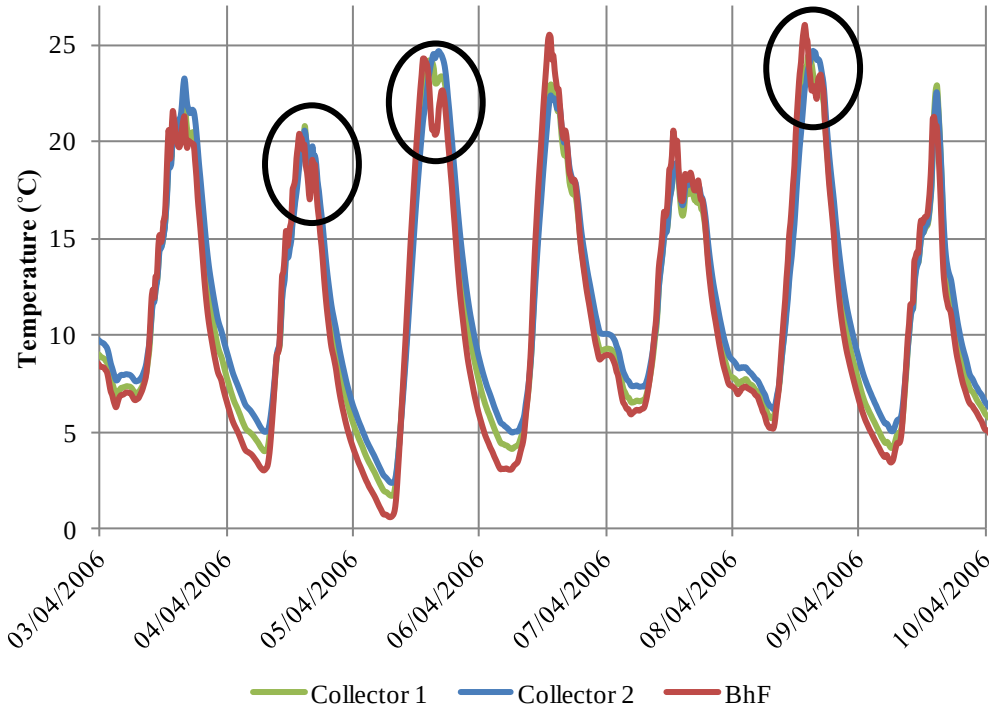

Figure 9-8 - Comparison of temperatures measured at 0.01 m from borehole F, and from the centres of collector 1 and collector 2.

A detailed analysis of the shade being cast over the paved surface is in general dependent on the season, time of the day, number and, strictly speaking, the age of the trees or vegetation surrounding the surface. Given these complications, a simplified approach is proposed instead to assess the impact of shade over collector 2. The approach proposed to represent the impact of shading is as follows:

- Shade is considered to be cast only on the road surface between 12:00 h and 17:00 h every day, without seasonal variation. The solar radiation is calculated using equation (3-46).
- In a first analysis, two limit cases are considered during the pre warming period. 0% shade, corresponding to a scenario where no objects that could potentially cast shade are located in the neighbourhood of the surface of interest; and 100% shade, corresponding to a cover of trees blocking completely the solar radiation in the period of time defined before (this is the case assumed for borehole F).
- A second analysis is performed in the first period of analysis (see section 9.6) to assess the shade levels on the performance of the inter-seasonal heat storage system. Three levels of shade are considered based on the results of the previous analysis: 25%, 40% and 50%.
- This shading description is not applied to the soil surface since the boundary formulation used (Canopy Cover) already takes into account the presence of vegetation.

9.6 Periods of analysis

The numerical analyses presented in this Chapter are divided into considering 7 periods (including pre system activation) based on the experiment description provided by Carder et al (2007). These periods are summarized as follow:

- Pre system activation period: based in the results obtained in Chapter 8, a period of 8 yearly cycles is considered suitable for this period of analysis. During this period the layers corresponding to insulation and sand are replaced by soil in the analysis.
- First insulation period: the installation of the experimental system was performed in early May 2005 (actual date is not specified, here is assumed to be on 1st May 2005). However the system was not activated until 23rd August

2005. During the period ranging from 1st May 2005 to 22nd August 2005, the soil under the insulation layer was prevented from normally heating up. The output of this period is the initial condition for the first activation period. During this period and the following the distribution of material layers is as described in Chapter 5 (including the insulation and sand layers) For this period only two experimental data points are available: 9th May 2005 at 12:30h and 15th July 2005 at 14:00 h.

- First activation period: the experimental system was activated on the 23rd August 2005. During this period ranging until the 13th November 2005, the system was operated under collection settings. The fluid in the heat exchangers was pumped when the temperature difference between the temperature sensor located at the middle of the collection pipes and that located at the middle of the storage pipes was approximately 1.4 ˚C. Once active, the pumps were turned off when the temperature difference dropped to approximately 0.3 ˚C.
- Second activation period: from 14th November 2005 to 20th February 2006. The experimental system was operated under usage settings. The pumps were activated when the road surface fell below 2˚C for more than 15 min and were turned off when the surface temperature rose above 2 ˚C for more than 15 min.
- Second insulation period: from 21st February 2006 to 26th April 2006. The system is put into a pause until the Third activation period begins. The soil in the storage region is prevented from being heated normally due to the presence of the insulation layer.
- Third activation period: from 27th April 2006 to 31st October 2006. The system was operated under collection settings as described for the First activation period.
- Fourth activation period: from 1st November 2006 to 1st March 2007. The system was operated under usage settings as described for the Second activation period.

9.7 Results

Before presenting the results obtained it is worth remarking that in a 2D domain borehole F and G (Figure 9-5) correspond to the same position (middle of the road). The temperature profiles referred as control borehole F are those obtained from the pre system activation period (before any insulation layer is put into place or the system is activated). Temperature profiles referred as borehole G are those obtained from the first insulation period onwards. This convention is to facilitate comparison with 3D results in Chapter 10.

Section 9.7.1 compares experimental and numerical temperature profiles corresponding to borehole F (pre activation period) using Turbulent and Non-turbulent boundary formulations for the road surface.

Section 9.7.2 presents numerical transient variations of temperature corresponding to borehole G for the first period of insulation at 0.875 m depth (under insulation layer). Three levels of shade are compared: 0%, 50% and 100%. Corresponding temperature variations are included from borehole F (pre system activation without insulation) for reference.

Section 9.7.3 compares experimental and numerical transient variations of temperature corresponding to borehole G at two selected depths, 0.1325 m (collector depth) and 0.8475 m (storage depth), for the first activation period for three levels of shading, 25%, 40% and 50%. A similar analysis is performed using Turbulent and Non-turbulent boundary formulations for the road surface with a level of shading of 50%. Based on results from this section and section 9.7.1 a suitable boundary formulation for the road surface is chosen for the subsequent analyses.

Section 9.7.4, Section 9.7.5, Section 9.7.6, Section 9.7.7 compare experimental and numerical transient variations of temperature corresponding to borehole G at two selected depths, 0.1325 m (collector depth) and 0.8475 m (storage depth) for the second activation period, second insulation period and third and fourth activation periods respectively using the results from the previous sections to select a suitable level of shade and boundary formulation at the road surface.

Section 9.7.8 shows the amount of thermal energy being collected and extracted from the ground in comparison with the electrical energy required to run the pump

system. It offers a coefficient of performance based on the useful thermal energy extracted in winter 2006-2007 and the total amount of electrical energy required in the collection and usage periods.

9.7.1 Pre system activation period: Pavement control temperatures

Figure 9-9 shows a comparison on 15th July at 14:00 h (during the 1st insulation period) of experimental measurements corresponding to control borehole F located between System 1 and 2 (see Figure 5-6) with temperatures predicted by the numerical model in 2D using a Non-turbulent boundary formulation on the road surface and shading levels of 0%, 50% and 100% for the period between 12:00 h to 17:00 h. Experimental measurements for borehole F are available only up to 4 m depth. It can be seen that the temperature profile corresponding to total shading are in better agreement with the experimental measurements while the scenario without shade over estimates the temperatures of the domain (by 0.8 ˚C at the bottom). The case with 50% shading is located between these two limits as would be expected.

Figure 9-10 shows an amplification of Figure 9-9 corresponding to the region near the surface (up to 3 m depth). In Figure 9-10 it is possible to appreciate the impact of shading in the region directly under the paved surface. It can be seen that under the assumption of 0% shading the temperatures at the surface reach levels higher than 53.5 ˚C at 0.01 m depth while the experimental measurements at the same depth are 36.5 ˚C while a situation with 100% shading predicts a temperature of 26 ˚C at this depth. In comparison, the case with 50% shade estimates a temperature of 41 ˚C for this depth.

A similar analysis has been performed using a Turbulent formulation for the paved surface. The results presented in Figure 9-11 and Figure 9-12 are restricted to a level of shading of 50% for clarity. It can be seen that the Turbulent formulation agrees better with the experimental data for depths below 3 m. However, for the region near the soil surface it can be observed that the Non-turbulent formulation describes better the thermal behaviour of the soil. These results agree with those obtained in Chapter 8 for soil where it was noticed that a Turbulent formulation offer better predictions of the temperature of the soil near the bottom of the domain.

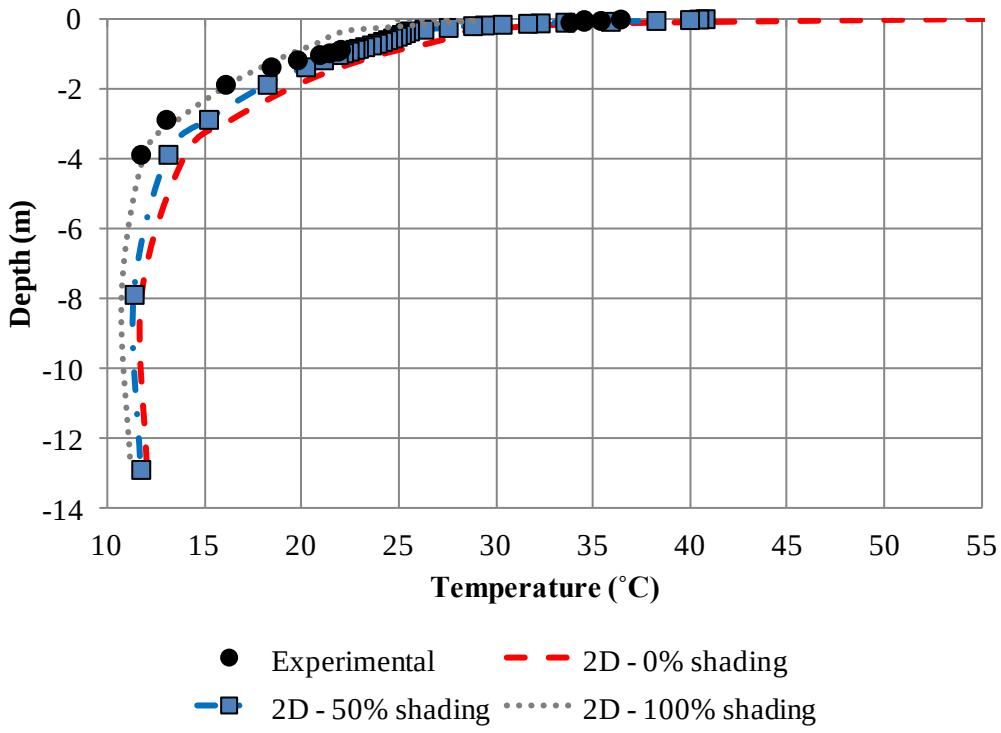

Figure 9-9 - Experimental and numerical (non turbulent) soil temperature profiles corresponding to control borehole F (pavement) for 15th July 2005 at 14:00 h.

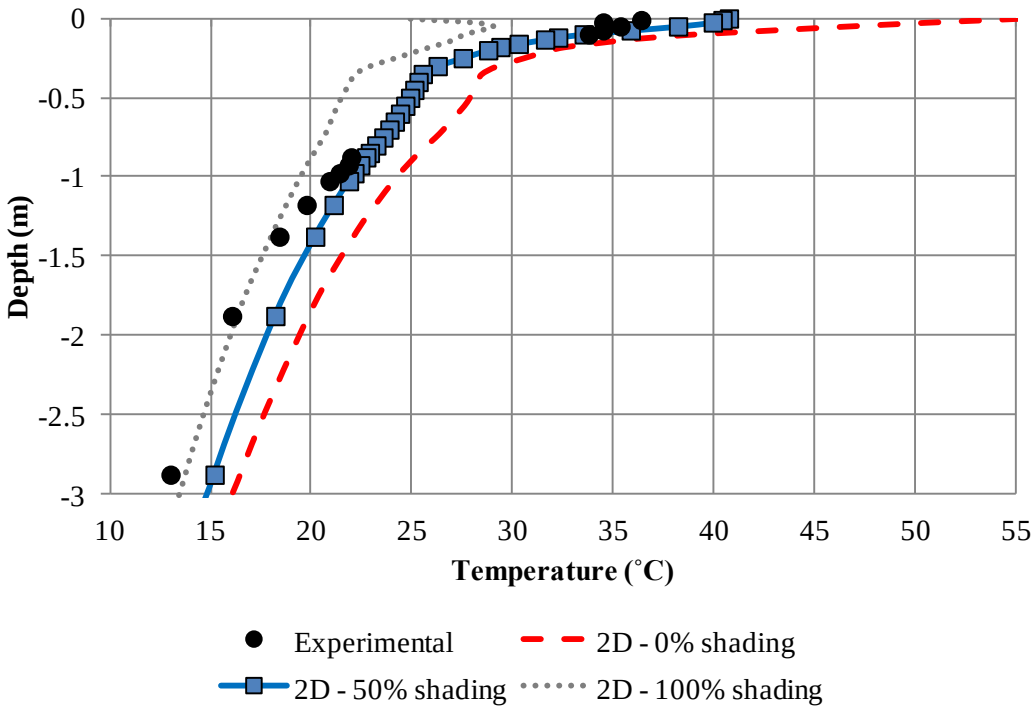

Figure 9-10 - Experimental and numerical soil temperature profiles corresponding to the region near the surface of control borehole F (pavement) for 15th July 2005 at 14:00 h.

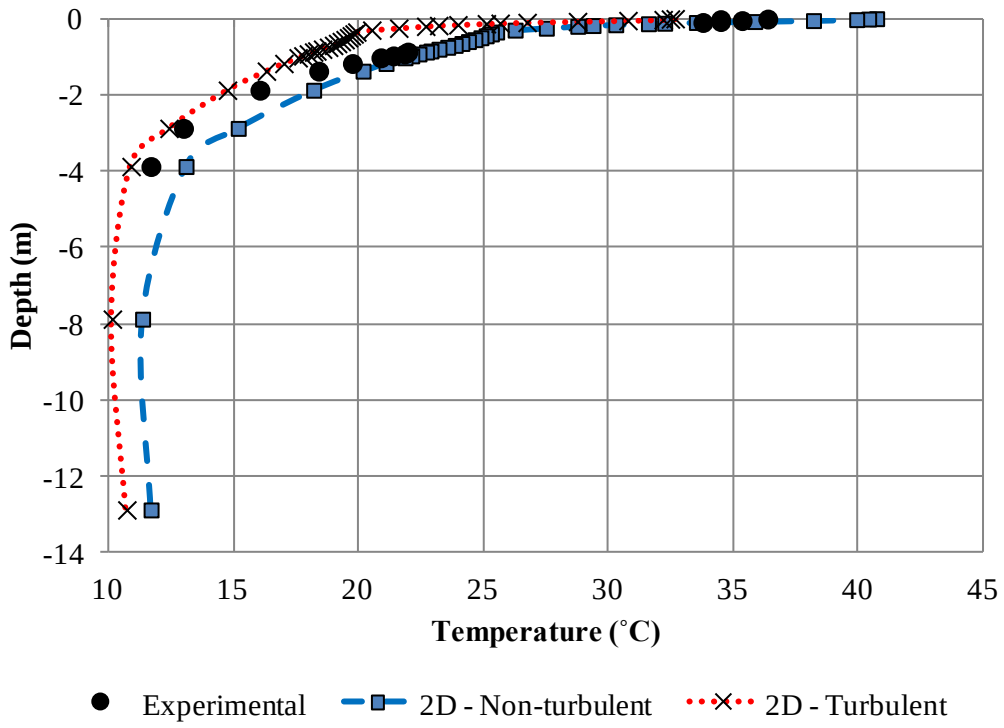

Figure 9-11 - Experimental and numerical soil temperature profiles corresponding to control borehole F (pavement) for 15th July 2005 at 14:00 h using Turbulent and Non-turbulent boundary formulations and 50% level of shade.

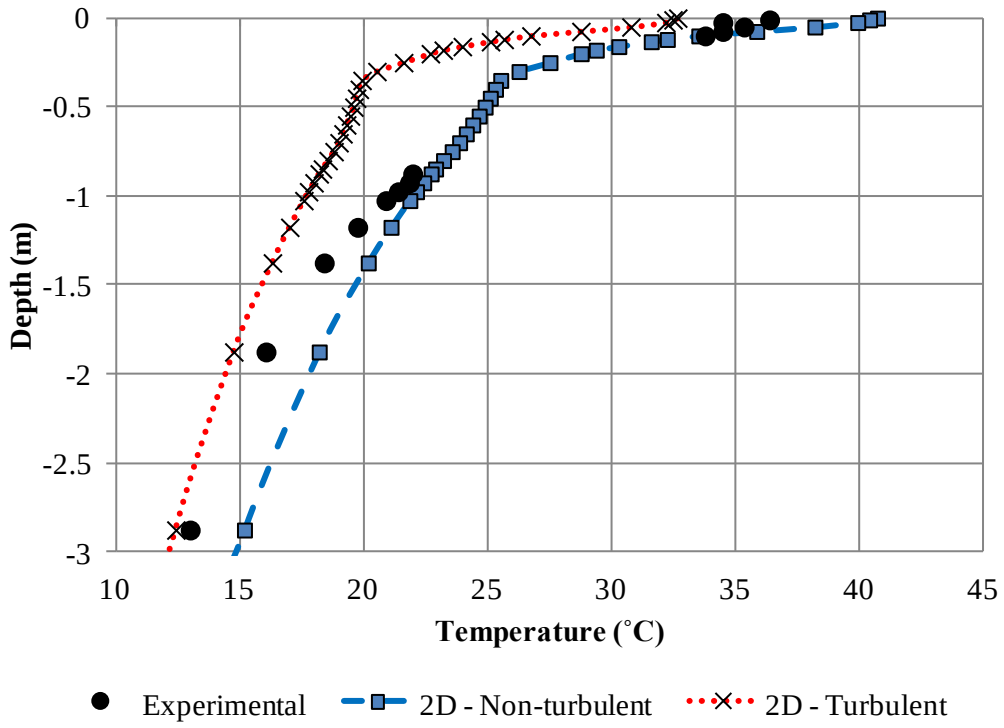

Figure 9-12 - Experimental and numerical soil temperature profiles corresponding to the region near the surface of control borehole F (pavement) for 15th July 2005 at 14:00 h using Turbulent and Non-turbulent boundary formulations and 50% level of shade.

9.7.2 First insulation period May 1st May 2005 - 22nd August 2005

Figure 9-13 shows the comparison of the transient variations of the temperature of the soil at borehole G (System 2, under insulation layer at pipe storage depth) at 0.8475 m depth for three levels of shading (0%, 50% and 100%). Experimental measurements are only available for 9th May 2005 at 12:30h and 15th July 2005 at 14:00 h during this period, however, note that the first experimental measurement is likely to be disturbed due to the installation process. The corresponding profiles for the previous yearly cycle (part of the pre system activation period) are shown for reference (in gray). It can be seen that, compared to the previous yearly cycle (normal soil heating), the temperature variations during this period are notably damped with only a small increment of approximately 2 ˚C at the end of July and then slowly decreasing towards the end of August. This behaviour is expected from a region of soil located under a layer of material insulating it from the atmospheric interactions at the surface. Note also that the temperature difference between the 0% and 100% shade tend to decrease from approximately 4 ˚C to 2 ˚C. This behaviour is also expected since an insulation layer decreases the impact at this depth of the level of radiation received at the surface of the road. It can be observed that the numerical results for 50 and 100% shading lie either side of the experimental values.

Figure 9-14 shows the temperature profile in the region of soil near the road surface at the end of the 1st insulation period. The effect of the insulation layer above the storage pipes can be clearly seen in the temperature gradient near the surface, falling from temperatures above 16 ˚C to approximately 13˚C under the road and from 15 ˚C to 13 ˚C under the soil surface. The region of soil under the insulation layer, being less exposed to temperature variations from the surface tends to have a layered temperature distribution. This is the thermal state of the ground when the system is switched on for the first time.

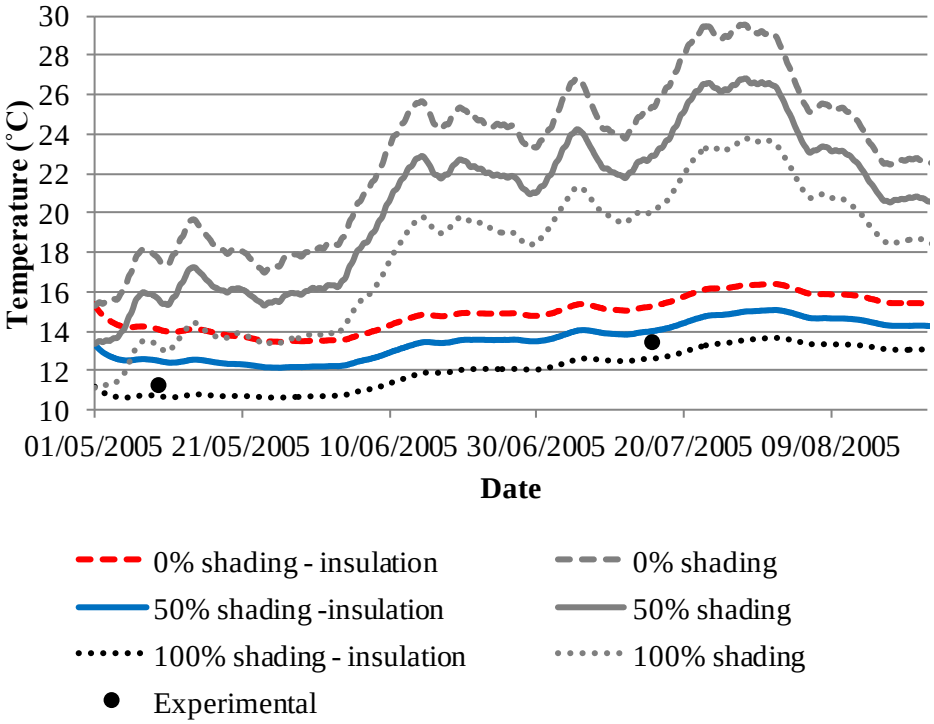

Figure 9-13 - Comparison of numerical predictions under different levels of shading for the first insulation period at 0.8475 m depth. Numerical results for the same period from previous yearly cycle (without insulation) are added in grey for reference.

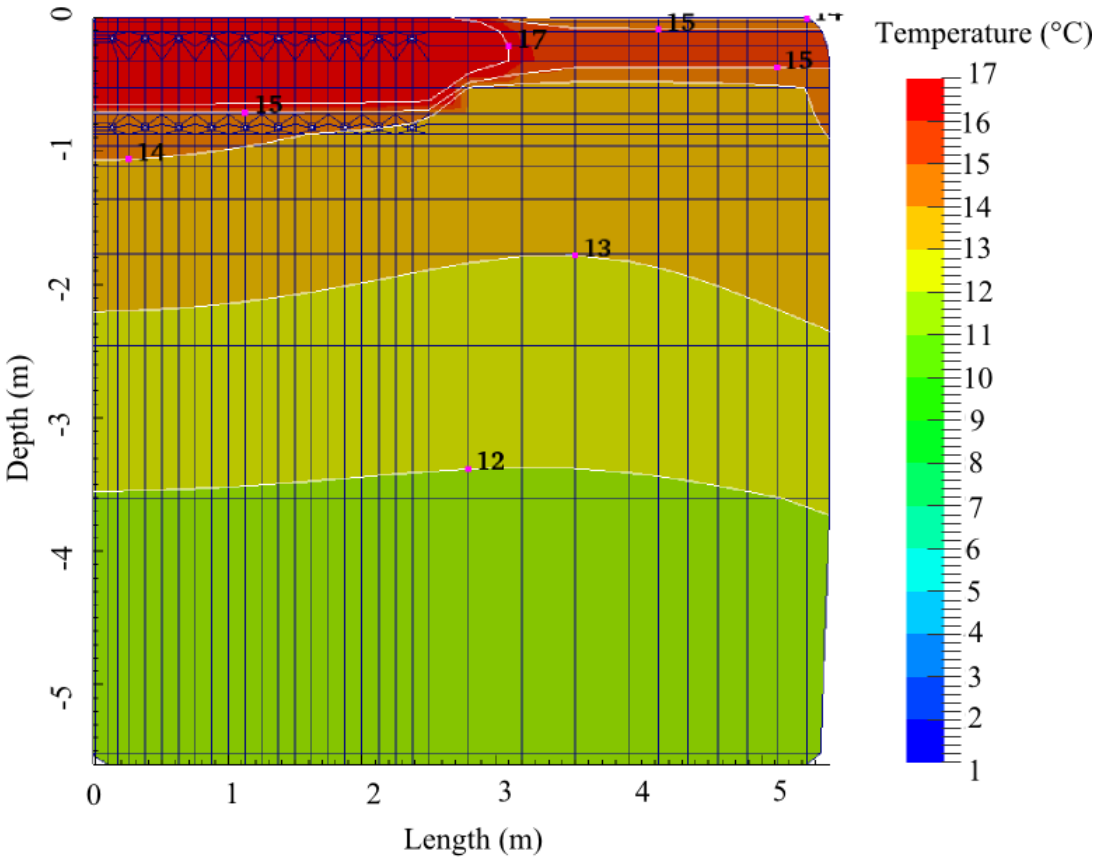

Figure 9-14 - 2D contour temperature profile near the road surface corresponding to the end of the 1st insulation period (22nd August 2005).

9.7.3 First activation period: 23rd August 2005 - 13th November 2005 (collection)

Figure 9-15 shows the comparison of numerical results and experimental measurements for the transient variations of soil temperature at borehole G at 0.1325 m depth (System 2, under road at collector pipes depth) for the three levels of shading (25%, 40% and 50%). While Figure 9-16 shows the corresponding comparisons at 0.8475 m depth (storage pipes depth). This collection period begins at the end of summer 2005, after the insulation period presented in the previous section. The periods when the system is switched on are clearly visible as peaks in Figure 9-16. During the first month the system is switched on relatively often compared with the rest of the period. This correspond to an increment in the temperature at the storage region of up to 6 ˚C during the first month of operation followed by a slow decrease in temperature as the thermal energy in this region is conducted away from the region closest to the pipes, and with the slow decrease in the temperatures at the collector depth (Figure 9-15) due to seasonal weather conditions.

It can be seen that in general the three considered shade scenarios match the trend of daily variations found in the experimental data at collector and storage depths. However, it can also be noticed that they tend to overestimate them. The case with 50% shade offers the best prediction for the experimental measurements with a maximum difference of 1 ˚C at the beginning of September and 0.2 ˚C at the end of this activation period.

A similar analysis has been performed using a Turbulent formulation for the paved surface. Figure 9-17 and Figure 9-18 compare the temperature profiles corresponding to borehole G at 0.1325 m and 0.8475 m obtained with a Turbulent and a Non-turbulent boundary formulation on the road surface using 50% shade for the first activation period. Notice that the temperature of the road surface in both cases is being underestimated by the Turbulent formulation. The opposite was found in Chapter 8 (Figure 8-5 and Figure 8-6). The reason of this behaviour could be that under lower levels of radiation, the turbulent heat transfer coefficients in the Turbulent formulation tend to bring the surface temperature closer to the ambient temperature. This could explain why in Figure 9-18 the temperature in the storage region is being significantly underestimated. For these reasons all the subsequent analyses are performed using a Non-turbulent formulation.

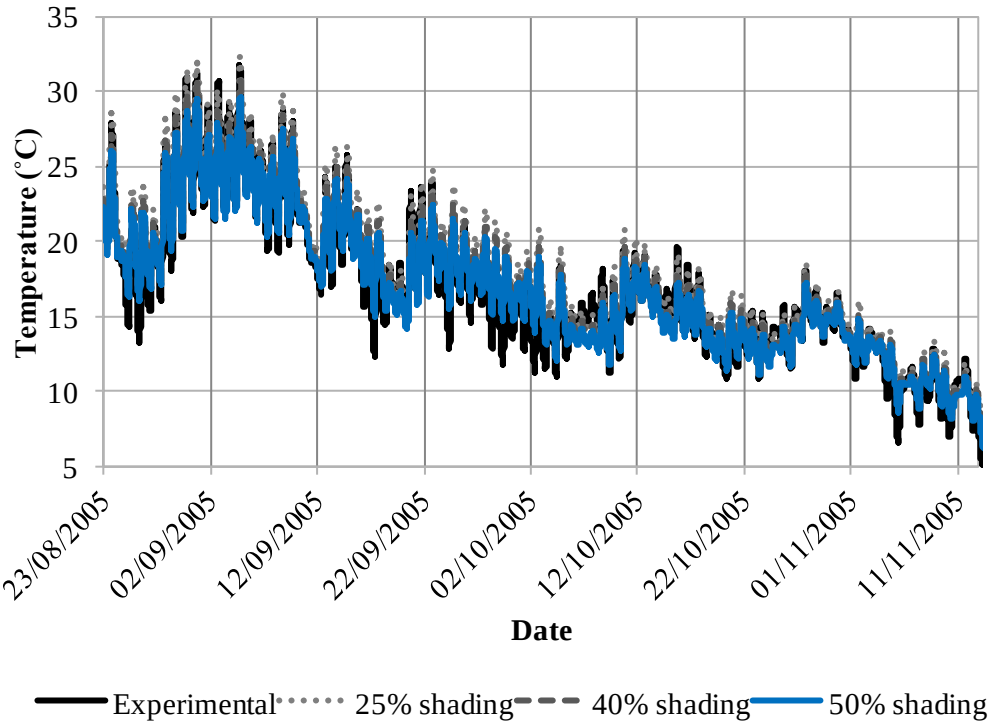

Figure 9-15 - Transient variations of soil temperature at borehole G at 0.1325 m (collector depth) for the first activation period (collection).

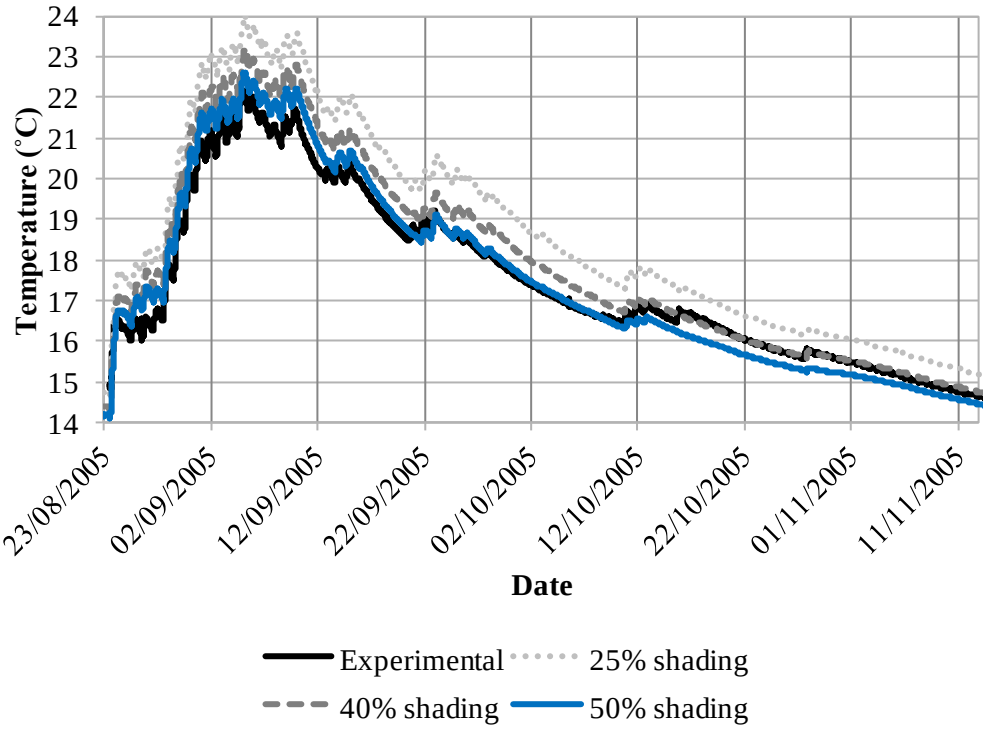

Figure 9-16 -Transient variations of soil temperature at borehole G at 0.8475 m (storage depth) for the first activation period (collection).

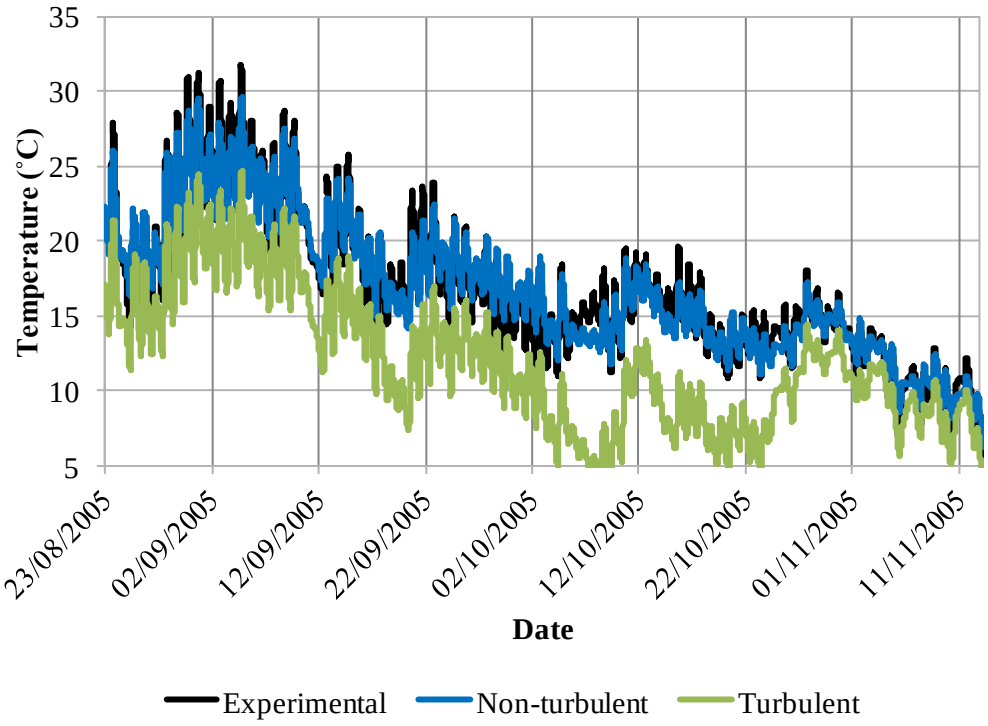

Figure 9-17 - Transient variations of soil temperature at borehole G at 0.1325 m (collector depth) for the first activation period (collection) using Turbulent and Non-turbulent boundary formulations.

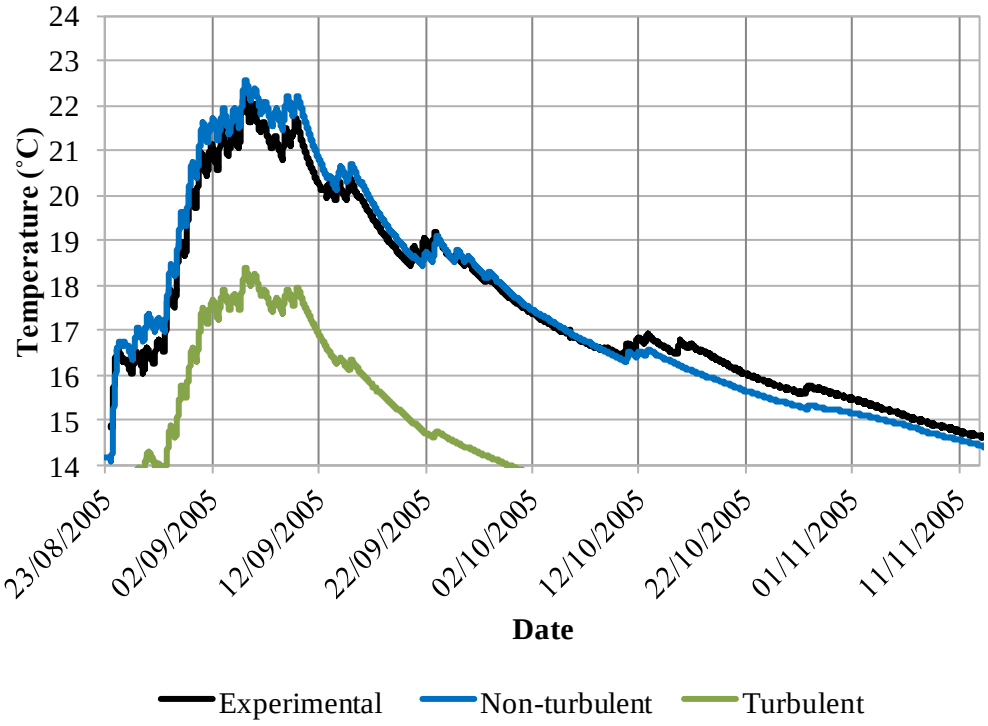

Figure 9-18 - Transient variations of soil temperature at borehole G at 0.8475 m (storage depth) for the first activation period (collection) using Turbulent and Non-turbulent boundary formulations.

Figure 9-19 shows the temperature profile in the region of the soil near the road surface at the end of this period. A marked increase in temperature under the insulation layer can be seen. This is thermal state of the soil at the beginning the second activation period (winter 2005-2006)

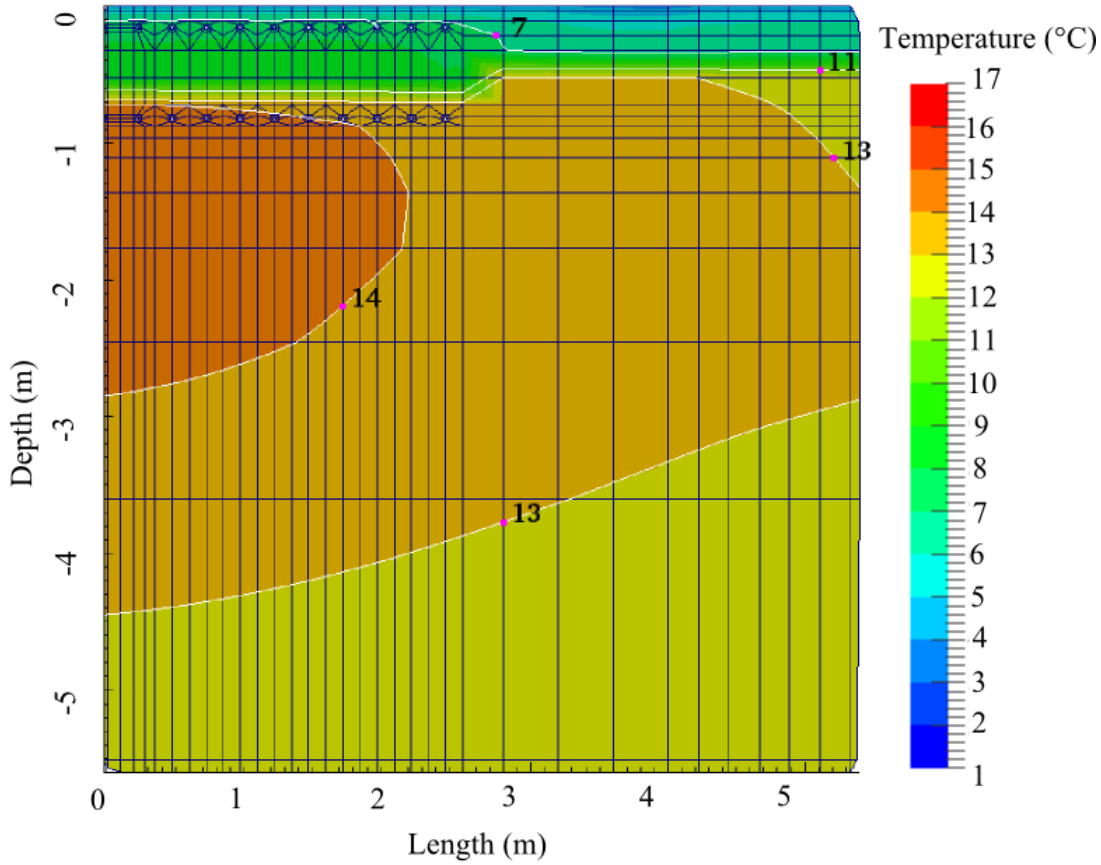

Figure 9-19 - 2D contour temperature profile near the road surface corresponding to the end of the 1st activation period (collection, 13th November 2005)).

9.7.4 Second activation period: 14th November 2005 - 20th February 2006 (usage)

Figure 9-20 shows the comparison of numerical results and experimental measurements for the transient variations of soil temperature at borehole G at 0.1325 m depth (System 2, under road at collector pipes depth) for a degree of shading of 50% corresponding to the second activation period. While Figure 9-21 shows the corresponding comparisons at 0.8475 m depth (storage pipes depth). It can be seen that the numerical results in general follow the trend of the experimental measurements. However, during the first and second weeks of January 2006 and the second week of February 2006 there are three periods where it can be seen how the numerical predictions deviate from the experimental measurements for up to 4 ˚C

both in collector and storage. These deviations are believed to be related with periods of snow fall where a certain amount of snow could have been accumulated on the road surface. Unfortunately the meteorological data provided by TRL does not include a measure of snow fall nor does the data obtained from the Meteorological Office. However, TRL reports a detailed account of snowfall and salting periods on the nearby M1 highway (Figure 5-1) for the winter 2006-2007 where similar numerical results were obtained (see section 9.7.8, corresponding to fourth activation period). The similarity between the results corresponding to deviations periods for the winter 2006-2007 (related with snowfall) and winter 2005-2006 suggest that the deviations found in the latter are due in fact to snowfall events.

Figure 9-22 shows the temperature profile in the region of the soil near the road surface at the end of this period. A reduction in temperature under the insulation layer due to the thermal energy extraction process can be seen. This is the thermal state of the soil at the beginning the second insulation period.

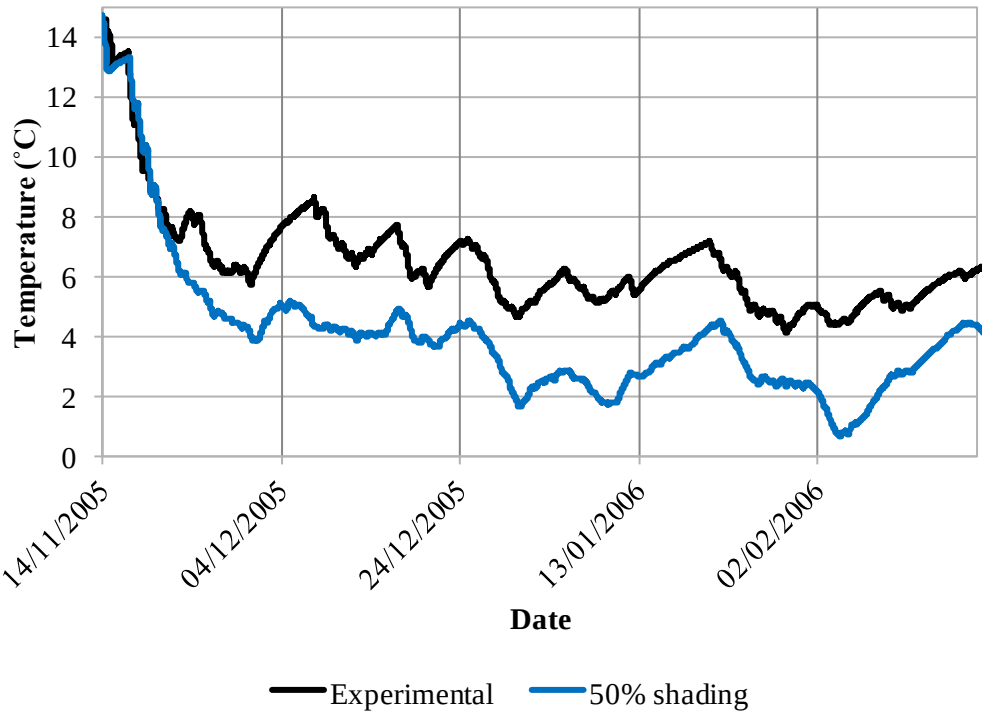

Figure 9-20 - Transient variations of soil temperature at borehole G at 0.1325 m (collector depth) for the second activation period (usage).

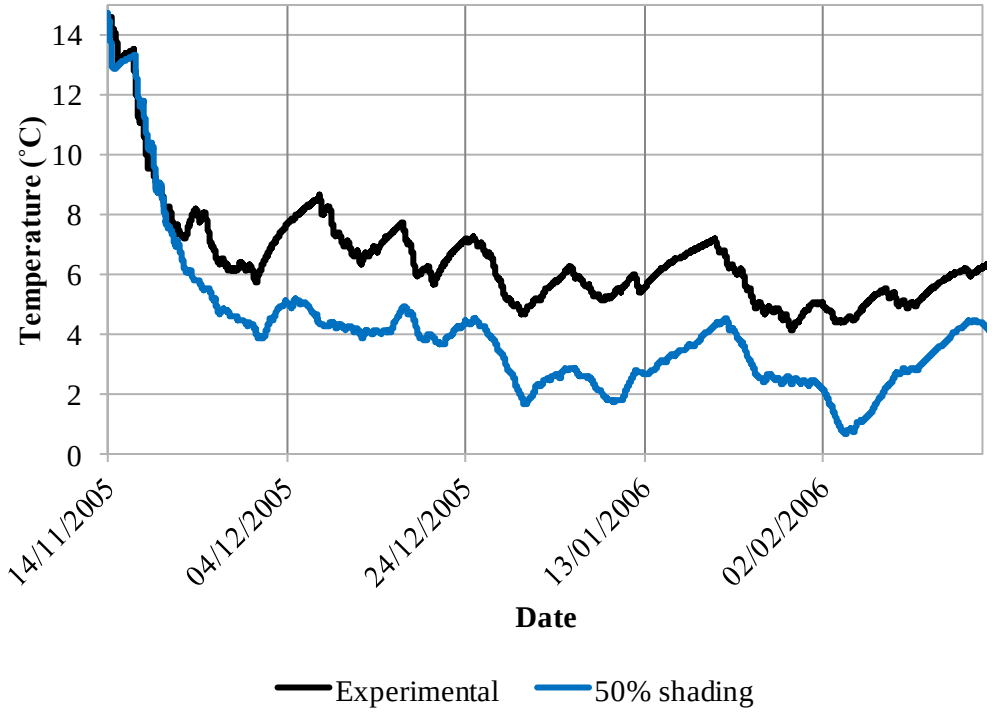

Figure 9-21 - Transient variations of soil temperature at borehole G at 0.8475 m (storage depth) for the second activation period (usage).

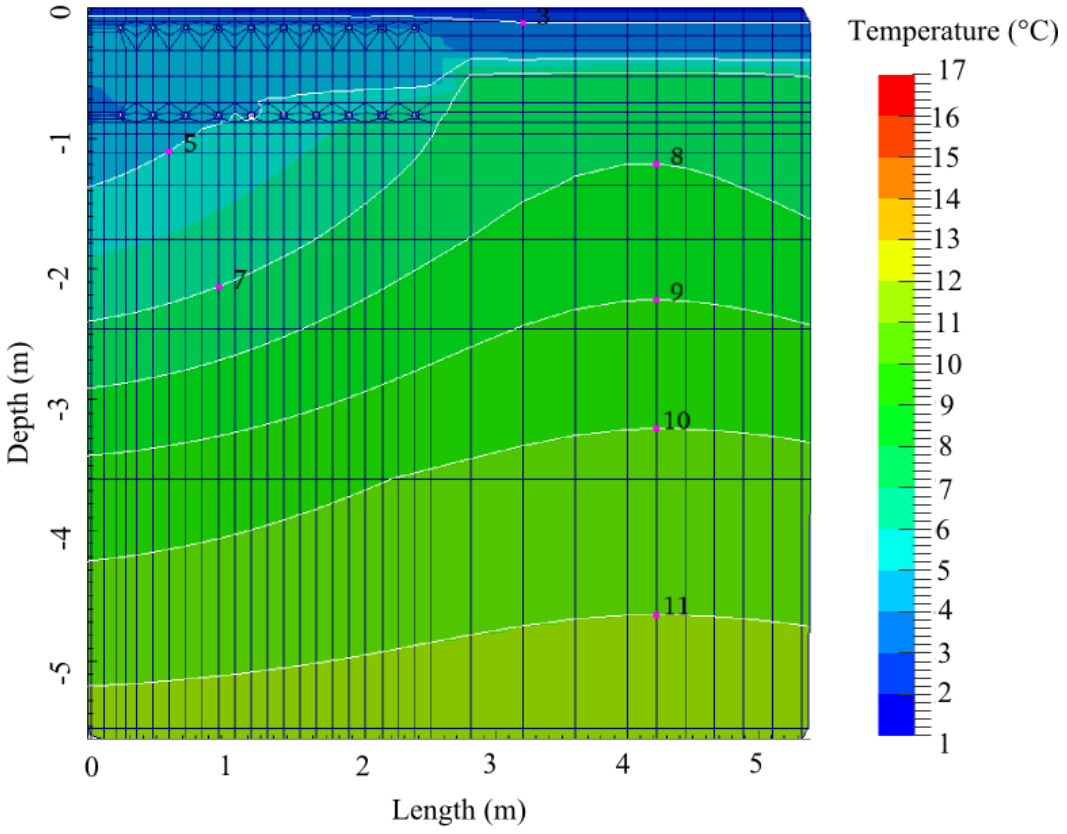

Figure 9-22 - 2D contour temperature profile near the road surface corresponding to the end of the 2nd activation period (usage, 20th February 2005).

9.7.5 Second insulation period: From 21st February 2006 to 26th April 2006.

During the period between 21st February 2006 and 26th April 2006 the system was switched off manually for maintenance. No heat collection or usage was carried out. Figure 9-23 shows the comparison of numerical results and experimental measurements for the transient variations of soil temperature at borehole G at 0.1325 m depth (System 2, under road at collector pipes depth) for a degree of shading of 50%. While Figure 9-24 shows the corresponding comparisons for the transient variations of soil temperature at borehole G at 0.8475 m depth (storage pipes depth). It can be seen that even when the system was turned off the temperatures at storage depth show a slow increment of about 4 ˚C while the temperatures at collector depth slowly rose 10 ˚C. The difference between the increments at collector and storage depth are in part due to the insulation layer preventing the soil underneath from heating normally.

The deviation of the numerical results from the experimental data in Figure 9-23 is due to the usage of meteorological data corresponding to late February 2007 and March 2007 into the corresponding months of 2006 due to the absence of these periods on the experimental weather data as discussed in the results section of Chapter 8. However, it can be seen that after this period, the numerical results are in very good agreement with the experimental measurements. The abnormal behaviour of the experimental measurements around 23rd March 2006 is not commented on by Carder et al (2007) and is believed to be due to a temporary glitch in the experimental system.

Figure 9-25 shows the temperature profile in the region of the soil near the road surface at the end of this period. It can be noticed that the temperature under the insulation layer is almost homogeneous and similar to the temperature at -3 m and -4 m shown in Figure 9-24. This suggest that the soil has reached a thermal equilibrium using in part thermal energy stored at these depths.

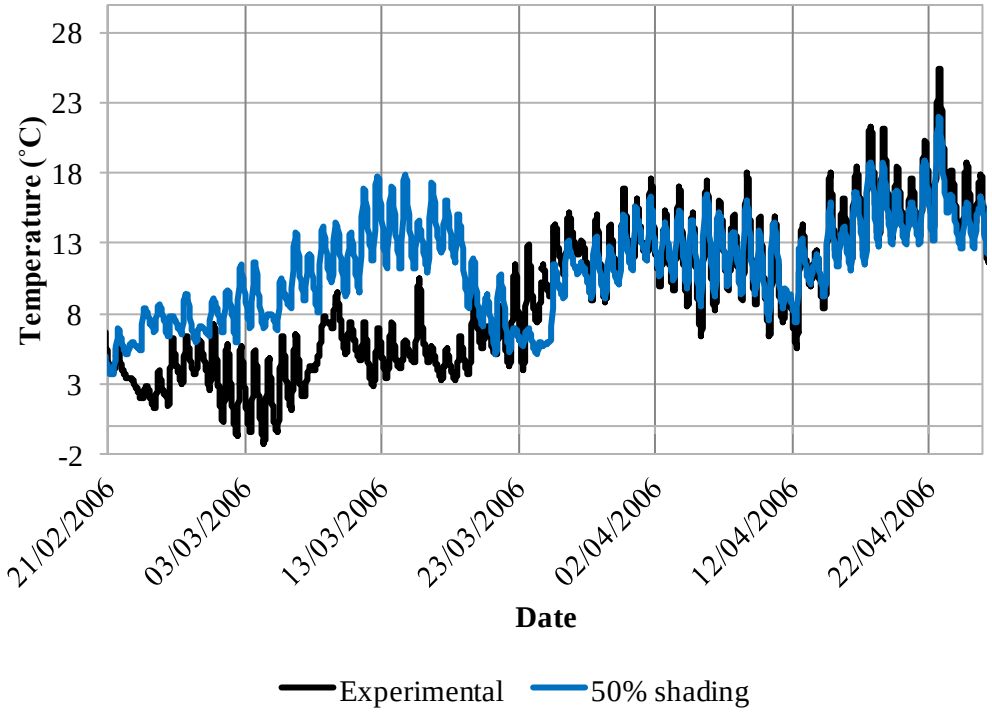

Figure 9-23 - Transient variations of soil temperature at borehole G at 0.1325 m (collector depth) for the second insulation period.

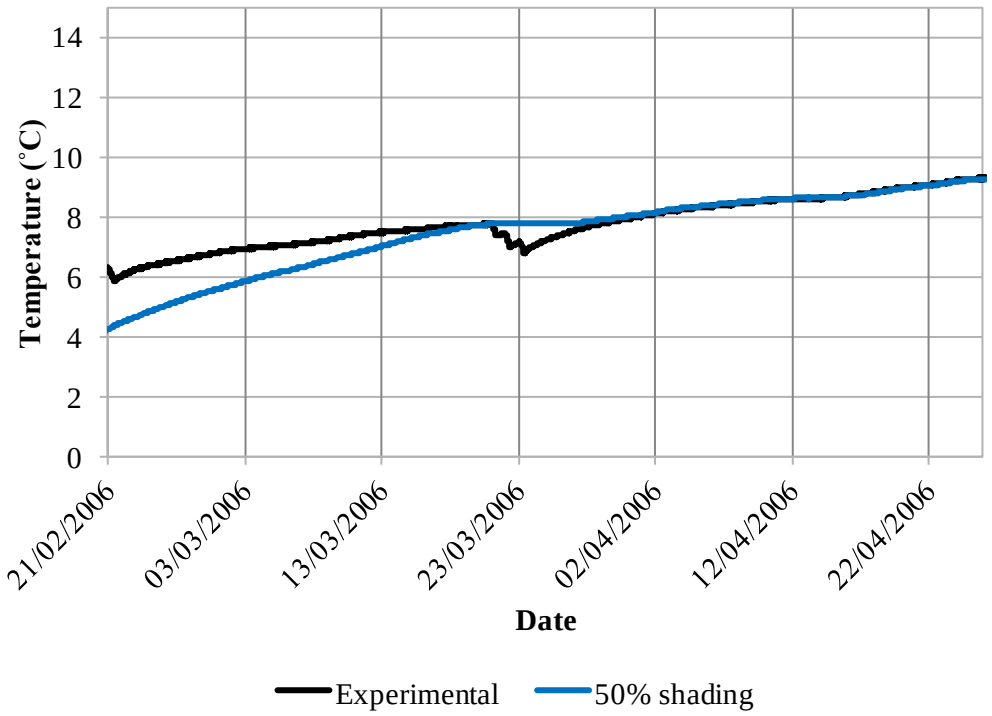

Figure 9-24 - Transient variations of soil temperature at borehole G at 0.8475 m (storage depth) for the second insulation period.

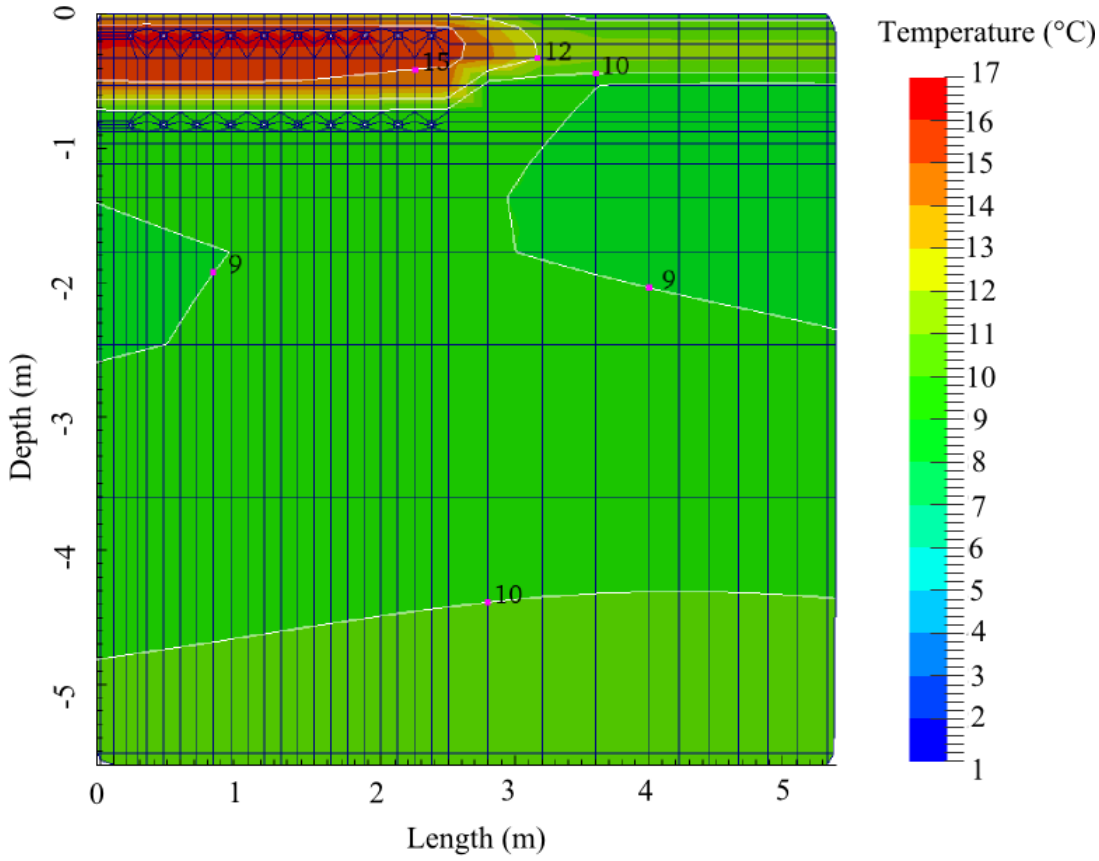

Figure 9-25 - 2D contour temperature profile near the road surface corresponding to the end of the 2nd insulation period (26th April 2006).

9.7.6 Third activation period: From 27th April 2006 to 31st October 2006

Figure 9-26 shows the comparison of numerical results and experimental measurements for the transient variations of soil temperature at borehole G at 0.1325 m depth (System 2, under road at collector pipes depth) for a degree of shading of 50% for the third activation period. While Figure 9-27 shows the corresponding comparisons for the transient variations of soil temperature at borehole G at 0.8475 m depth (storage pipes depth). Experimental data for this period is available until the 6th September 2006. In general a good agreement between experimental measurements and numerical predictions for both depths can be observed. According to Carder et al (2007) the collection process was interrupted between 18th May 2006 and 7th June 2006 due to significant airlocks preventing operation. This interruption is enforced in the numerical simulation by overriding the automatic activation of the system and forcing it to remain switched off.

The comparison between the third activation period and the first activation period shows that higher temperatures were achieved in the former both at collector and

storage depths. This is expected because the third activation period was performed for a full summer (approx. 5 months), while the first activation period was operated at the end of summer 2006 (approx. 1.5 months). This agrees with the temperature profile shown in Figure 9-28 where a marked increment in temperature can be clearly observed, compared with the temperature profile shown in Figure 9-19, in the region under the road surface and that extends further into the ground. This is the thermal state at the beginning of the 4th activation period (winter 2006-2007).

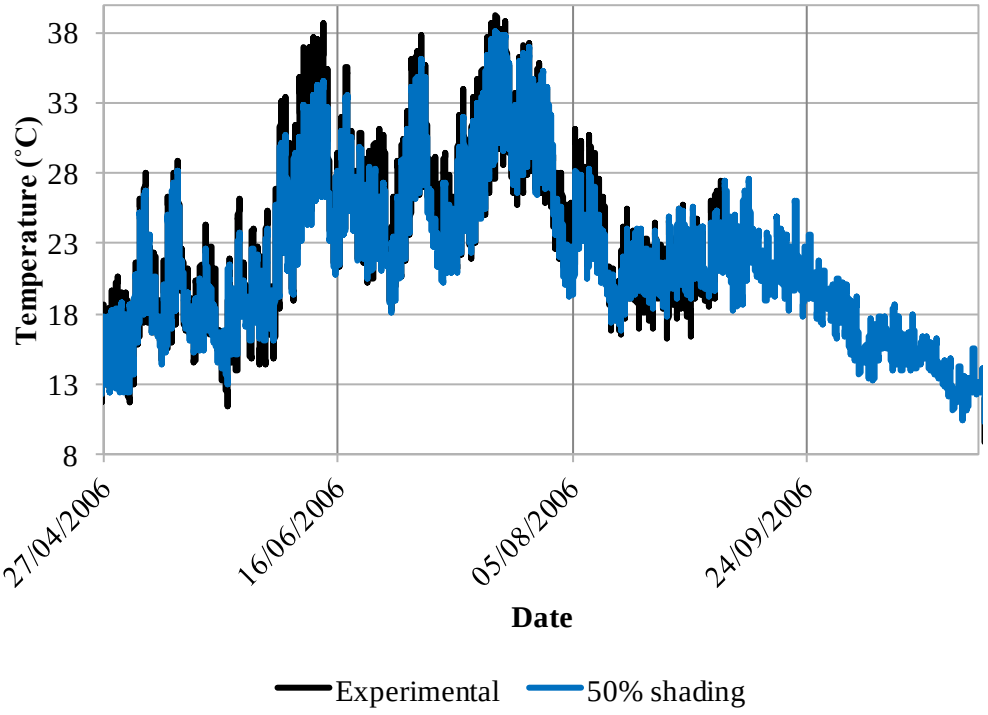

Figure 9-26 - Transient variations of soil temperature at borehole G at 0.1325 m (collector depth) for the third activation period (collection).

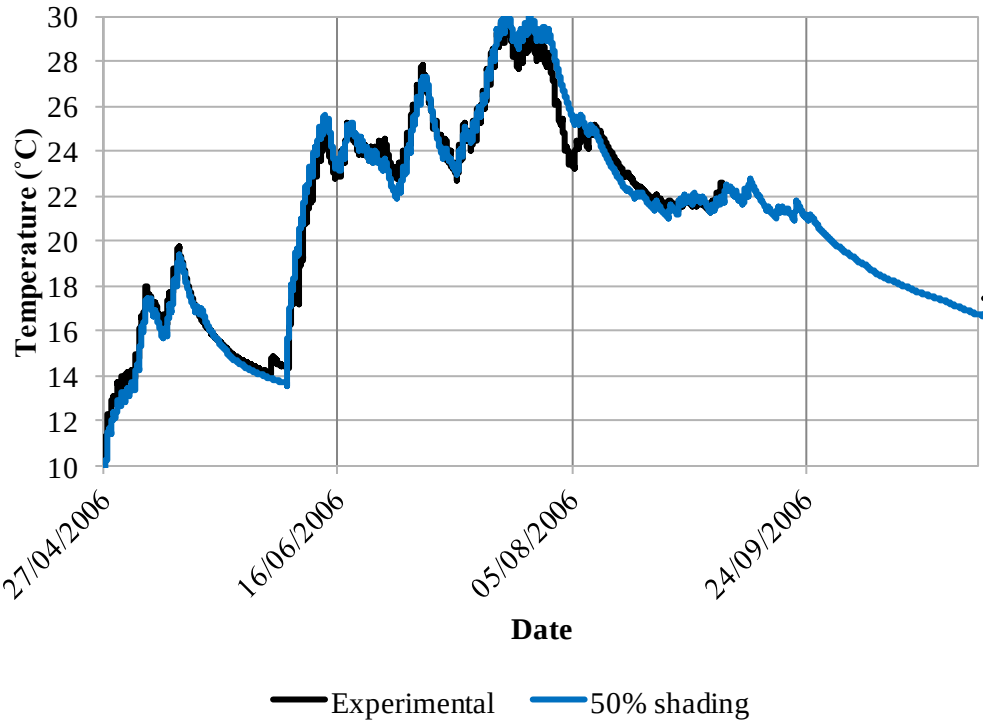

Figure 9-27 - Transient variations of soil temperature at borehole G at 0.8475 m (storage depth) for the third activation period (collection).

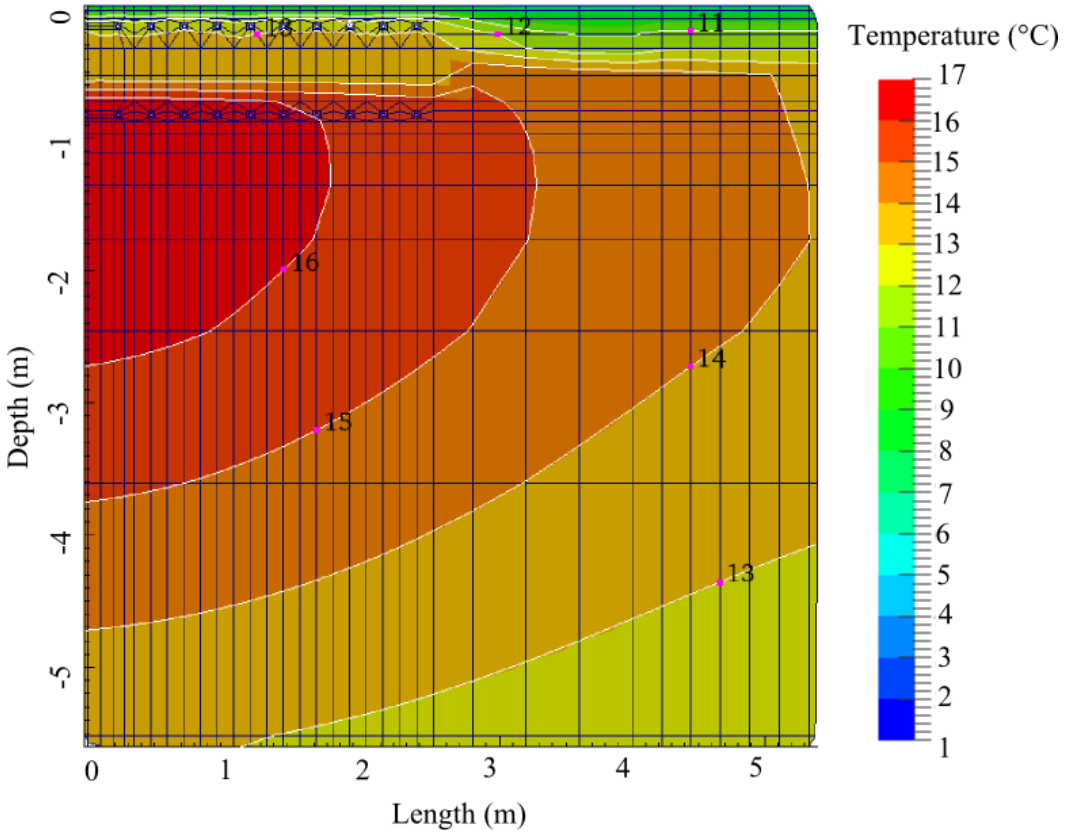

Figure 9-28 - 2D contour temperature profile near the road surface corresponding to the end of the 3rd activation period (collection, 31st October 2006).

9.7.7 Fourth activation period: From 1st November 2006 to 1st March 2007 (usage)

Figure 9-29 shows the comparison of numerical results and experimental measurements for the transient variations of soil temperature at borehole G at 0.1325 m depth (System 2, under road at collector pipes depth) for a degree of shading of 50% for the fourth activation period. While Figure 9-30 shows the corresponding comparisons at borehole G at 0.8475 m depth (storage pipes depth). In general it can be observed a good agreement between experimental measurements and numerical predictions for both depths except during two periods during the third week of December 2006 and the first week of February 2007. The deviations from the experimental measurements (of up to 5 ˚C) during the last week of December 2006 are similar to those observed during the winter 2005-2006 during the second activation period. Carder et al (2007) reported a detailed relation of periods where salt spreading took place at the nearby highway M1 (Figure 5-1). Salt spreading commonly takes place to prevent the formation of ice or snow settling on the paved surfaces when the weather conditions are such that frost or snowfall might occur. In this relation it is stated that salting took place from the 8th December 2006 to 22th December 2006 on a daily basis, including the 19th when salt spreading took place on two occasions; and from 3rd February 2007 to 9th February 2007 on a daily basis including the 7th and 8th where salting took place on 2 and 6 occasions respectively. These periods correspond with the observed deviations in the numerical predictions. The first one occurring on the afternoon of 20th December 2006 and lasting until the morning of the next day. This particular period produced a deviation of 2 ˚C at collector depth from the experimental data that remained during the following days. The numerical model then follows the experimental trend and approaches to the reported experimental temperatures until early February where the numerical predictions deviate again. Carder et al (2007) specifically reports extreme weather conditions during this period and the settlement of snow on the road surface. From these observations it can be said that the deviations found during the second activation period are likely to be related with snowfall events. The effect of a snow cover seems to be to insulate the surface of the road from the extreme weather conditions. The numerical model, not considering snow settlement and thawing processes, assumes that the road surface is exposed to these weather conditions and

overestimates heat losses at the surface and consequently the thermal energy required to maintain the surface above 2 ˚C.

Figure 9-31 shows the temperature profile of the ground near the road surface at the end of this period. It can be observed the effect of temperature reduction due to the extraction process performed during this period as compared with the final state of the third activation period (Figure 9-28). However, the temperatures are comparatively higher that at the end of the second activation period shown in Figure 9-22. This seems to imply that not all the thermal energy being collected during the summer is being used in the thermal maintenance of the road surface and that part of it remains in the ground and could possibly be used for other applications.

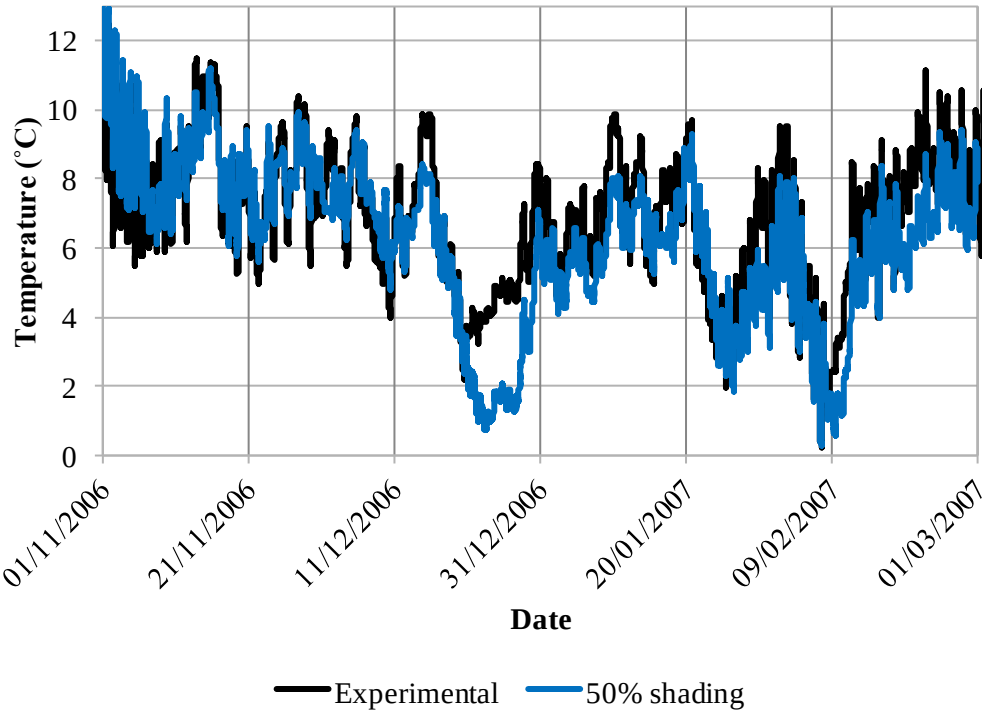

Figure 9-29 - Transient variations of soil temperature at borehole G at 0.1325 m (collector depth) for the fourth activation period (usage).

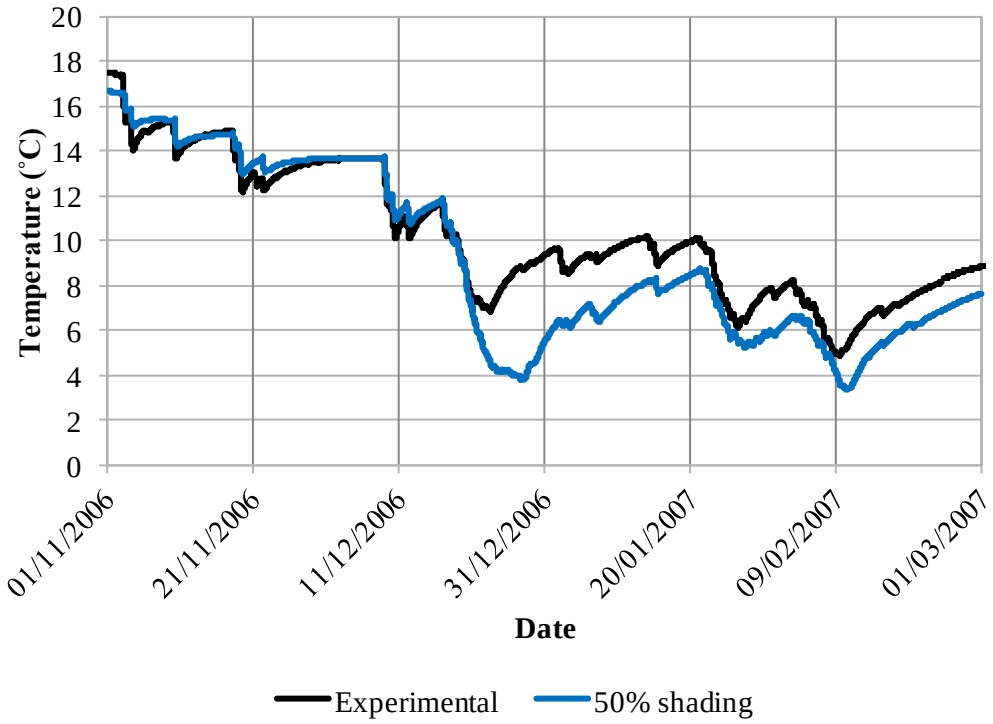

Figure 9-30 - Transient variations of soil temperature at borehole G at 0.8475 m (storage depth) for the fourth activation period (usage).

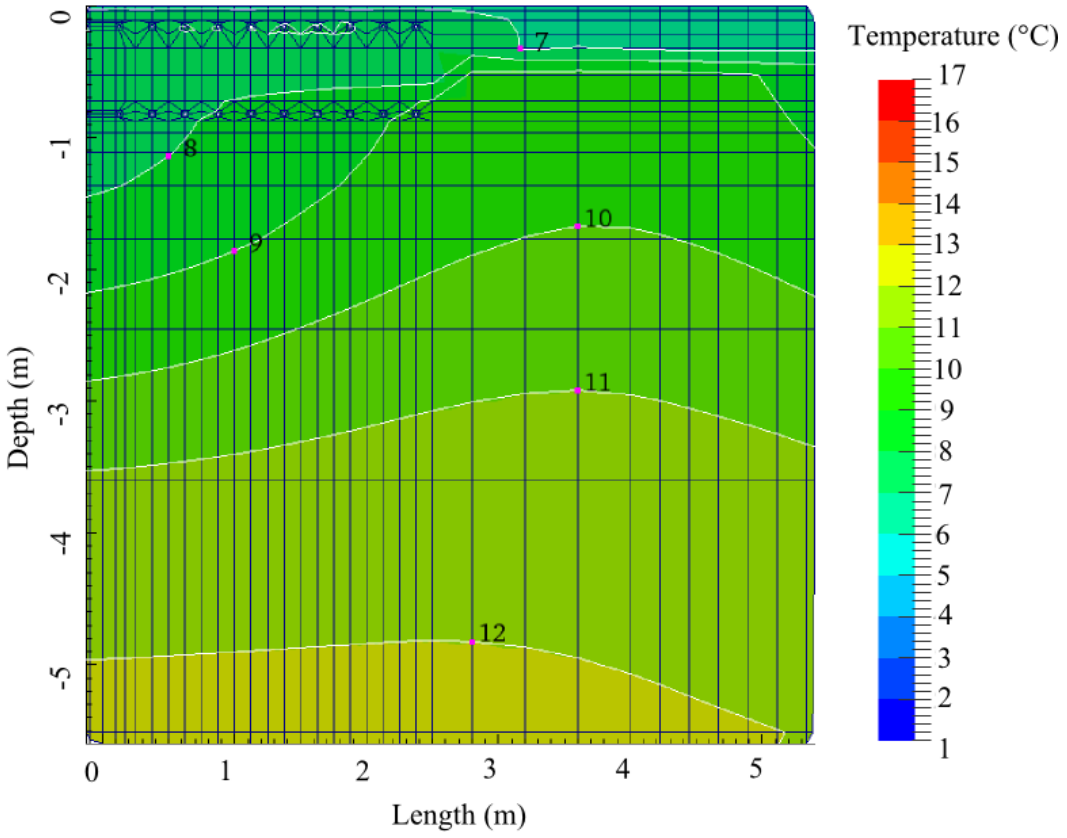

Figure 9-31 - 2D contour temperature profile near the road surface corresponding to the end of the 4th activation period (usage, 1st March 2007).

9.7.8 Thermal energy collection and storage and electrical energy usage

Figure 9-32 and Figure 9-33 present the numerical predictions of thermal energy stored during the third activation period (summer 2006) and the thermal energy recovered during the fourth activation period (winter 2006-2007) respectively compared against the experimental measurements of electrical energy used in the pumping system. Thermal energy is calculated as explained in Section 9.2.1. The objective is to estimate a coefficient of performance for the inter-seasonal heat storage system analysed in this Chapter.

It can be seen that in general the thermal energy collected or recovered is one order of magnitude higher than the electrical energy required to activate the pumping system. Thermal energy collected in summer 2006 is approximately 13000 MJ while the electrical energy required to activate the pumping system during the same period is approximately 800 MJ. In comparison, the thermal energy recovered from the soil during winter 2006-2007 is approximately 5500 MJ while the electrical energy required is 330 MJ. It can be seen that about one third of the thermal energy collected during summer is used in winter for thermal maintenance of the road surface. The remaining thermal energy could potentially being used in other applications (e.g. heating of buildings). In total, the system requires about 1130 MJ to operate the pumping system during the collection and usage periods while the useful energy being extracted is about 5500 MJ. This gives a coefficient of performance of 4.8.

Figure 9-32 the impact of the period of maintenance during which the system was switched off (late May 2006 and early June 2006) can be seen. In Figure 9-33 the impact of the periods of snow fall discussed before (late December 2006 and early February 2007) can be observed. The numerical model over predicts the thermal energy required during these periods while the electrical measurements indicate that the experimental system was active fewer times probably due to the presence of a cover of snow insulating the road from the extreme weather conditions. This means that the model in fact is overestimating the coefficient of performance presented before since it is predicting higher levels of thermal extraction. However, it also indicates that in fact the system has the potential to deliver higher levels of thermal energy.

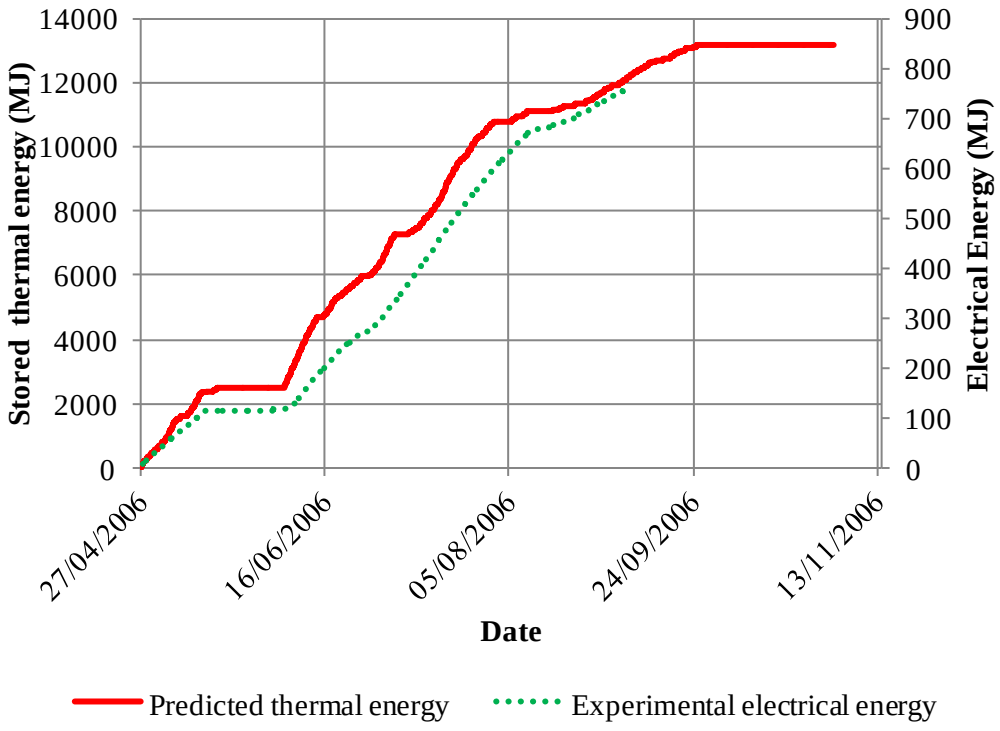

Figure 9-32 - Comparison of predicted thermal energy collection during the third activation period (summer 2006) with experimental measurements of electrical energy required for the pumping system.

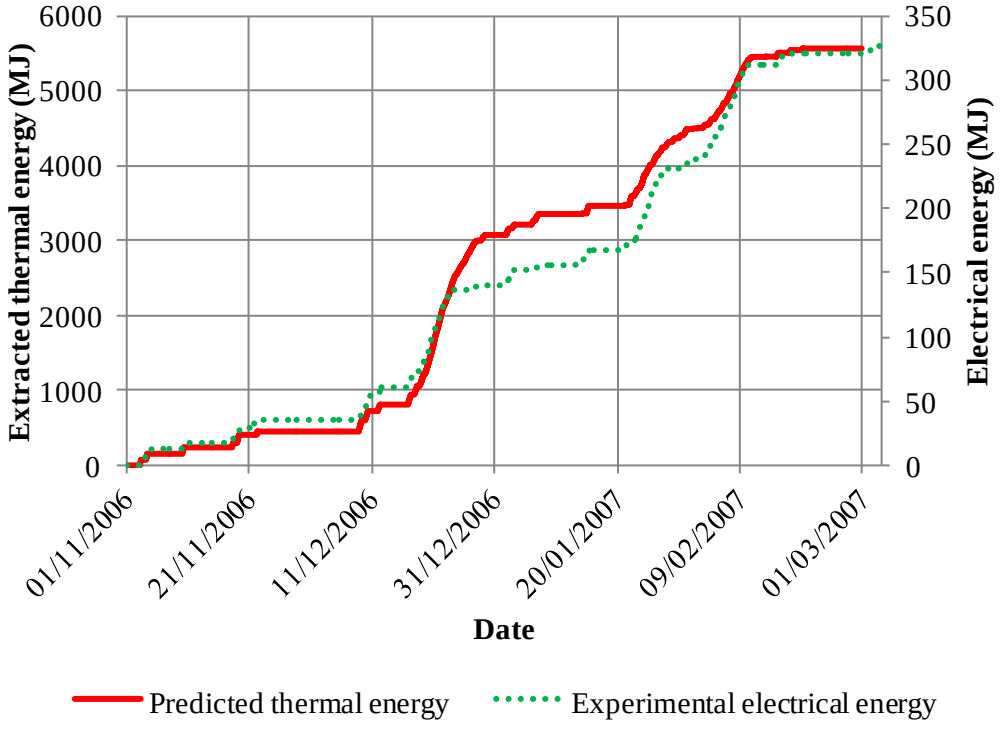

Figure 9-33 - Comparison of predicted thermal energy recovered during the fourth activation period (winter 2006-2007) with experimental measurements of electrical energy required for the pumping system.

9.8 Concluding remarks

This Chapter has presented the development of a 2D numerical model capable of represent the process of ground thermal energy storage carried out by buried engineering geo-environmental devices via the use of pipe heat exchangers. It has also been proposed an algorithm able to represent the 3D behaviour of pipe heat exchangers in 2D.

The proposed numerical model has been applied to investigate the case study presented in Chapter 5 that deals with the application of an inter-seasonal heat storage system during a consecutive period of 2 years divided in 2 periods of insulation, 2 periods of thermal energy collection (summer 2005, summer 2006) and two periods of thermal energy extraction (winter 2005-2006, winter 2006-2007).

After analysing the different periods where the system was active (under collection or usage settings) including idle periods, the proposed 2D numerical model has proved to be able to represent successfully the behaviour of inter-seasonal thermal storage devices. It was found that:

i) a suitable thermal boundary formulation for the soil surface is defined by the Non-turbulent formulation presented in Section 3.7.

ii) a free boundary condition at the far-field (lower) of the soil domain is able to represent the thermal behaviour of the soil for the investigation of active engineering thermal devices located near the soil surface. This minimizes the amount of data required to predict the performance of such devices.

iii) it is necessary to take into account the presence of nearby objects that might prevent the collection surfaces of the system from receiving optimal amounts of solar radiation and in turn reduce the thermal potential of the system.

iv) it is possible to represent the behaviour of a 3D pipe heat exchanger system in a 2D model and potentially reduce the computational effort to represent geo-environmental devices that make use of them.

v) the thermal energy required to provide thermal maintenance to a road surface is lower than the amount of thermal energy that an inter-seasonal heat storage device

has the potential to collect. This difference could be used in turn in other applications that require thermal energy in winters (e.g. building heating).

The main limitation found was the model inability to deal with snow events. The model is capable of predicting the thermal behaviour of a road surface being heated under winter conditions except during heavy snowfalls during which the model overestimates the amount of thermal energy demanded by the road. However, it has been shown that these are localized events and that in general the model is able to estimate the amount of thermal energy being collected and extracted from the ground by this kind of geo-environmental devices.

9.9 References

Carder, D. R., Barker, K. J., Hewitt, M. G., Ritter, D., and Kiff, A. [2007]. Performance of an Interseasonal Heat Transfer Facility for Collection, Storage and Re-Use of Solar Heat from the Road Surface. PPR302. Transport Research Laboratory.

Garratt, J. R. [1994]. *The Atmospheric Boundary Layer*. Cambridge University Press.

Chapter 10 Inter-seasonal heat transfer system: 3D Numerical Simulations

10.1 Introduction

This Chapter develops a 3D numerical model based on the numerical equations for transient heat transfer and heat advection presented in Chapter 3 for the representation of ground thermal energy storage processes carried out by buried engineering geo-environmental devices. In particular, the model is developed for engineering applications that make use of pipe heat exchangers in order to deliver or extract thermal energy from the soil mass.

The proposed 3D numerical model is applied to investigate System 2 in the experimental case study presented in Chapter 5 (due to its complexity, with all system components located under the road offering a more challenging problem in terms of model validation.), in a similar manner as presented in Chapter 9 for the case of a 2D numerical model. The analysis of the case study is divided into a number of time periods following the same logic as presented in Chapter 9. The 3D numerical results from this Chapter are compared against corresponding results in 2D from Chapter 9 and experimental measurements provided by Carder et al (2007) at selected dates and depths.

The findings of Chapter 8 and Chapter 9 are used in this Chapter with respect to the selection of suitable boundary conditions for the soil domain and a suitable level of shading on the road surface.

The objectives of this chapter are:

- to develop a 3D numerical model to represent the process of heat collection and storage in soil.
- to apply the proposed model for the study and analysis of an experimental inter-seasonal heat storage facility developed by others.
- to compare the results obtained from the proposed 3D model with results obtained from the 2D numerical model presented in Chapter 9.

The Chapter is divided in the following Sections:

i) Section 10.2 presents numerical considerations and material properties used in this Chapter for the solution of the numerical equations for heat transfer and heat advection.

ii) Section 10.3 describes the domain under consideration and presents its discretized representation.

iii) Section 10.4 lists the initial and boundary conditions used to solve the numerical problem.

iv) Section 10.5 lists the different period of analysis in which the study of the experimental case is divided and gives further details on material properties and time steps used in each period.

v) Section 10.6 discusses the results obtained on each of periods of analysis.

10.2 Numerical approach

Results obtained from Chapter 8 suggest that a coupled analysis of heat and moisture transfer in the soil domain is unnecessary to study the thermal behaviour of soil in the far field and at the vicinity of an inter-seasonal thermal storage device covered by an insulation layer such as the one described in Chapter 5. This is further confirmed by the results obtained in Chapter 9 that are in good agreement with the experimental measurements from the case study.

Likewise, Chapter 8 and Chapter 9 have shown that the optimal heat transfer boundary formulations for soil and pavement, in the study of an inter-seasonal heat storage facility like the one presented in Chapter 5, are Canopy Cover and Non-turbulent respectively. These formulations are discussed in Section 3.7.5. Similarly, the far-field (bottom) boundary condition is chosen as a free-flux based on previous results.

The 3D domain is assumed to be composed by the same materials as the 2D domain described in Chapter 9 with thermal properties listed in Table 9-1. As mentioned in Chapter 9, the soil surrounding System 2 is considered to be composed of silty clay based on laboratory tests described in Chapter 6.

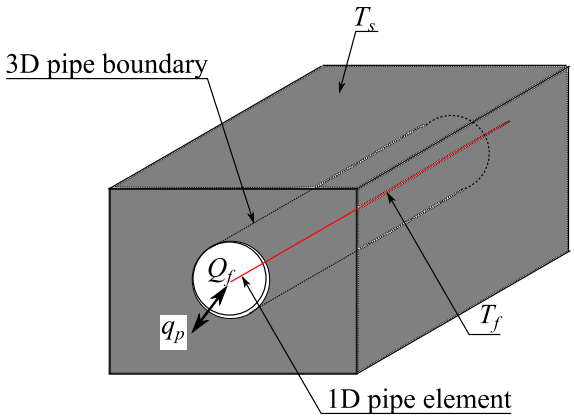

Figure 10-1 - Simplified schematic representation of a 3D element including a pipe boundary and its equivalent 1D representation.

10.2.1 3D representation of ground heat exchanger

The inter seasonal heat transfer system described in Chapter 5 is composed of two sets of 10 pipes placed near the surface of the ground which act like heat exchangers. The pipes are arranged in a U-loop running 30 m back and forth along the road as shown in Figure 5-2. The geometrical dimensions of the pipe arrays and fluid composition is summarized in Table 5-2.

In Chapter 9, the pipe heat exchangers were represented via a 2D numerical algorithm. In this Chapter this is accomplish by modelling each pipe in the heat exchangers as 1D domains and coupling them with the 3D domain via heat flux interactions at the soil-pipe boundaries. This is done, as explained in Section 3.6, in the following way (Figure 10-1):

- The heat rate per unit area q_p (W/m^2) transferred in a pipe segment in 3D is given by equation (3-28) that relates the temperature difference between the fluid inside the pipe (T_f) and the temperature of the surrounding soil (T_s). The total heat rate (W) transferred through the boundary of the pipe segment in 3D can be obtained by integrating equation (3-28). This total heat rate can be divided by the volume of the pipe segment in 3D in order to estimate an internal heat generation rate Q_f (W/m^3) that can be applied in the solution (in 1D) of the heat advection equation with internal heat generation given by eq. (4-25).
- The solution of the heat advection equation defines a new temperature profile along the pipe (T_f) that can be used to calculate a new value for q_p (using equation (3-28)) that in turn defines a new boundary condition at the

pipe boundary of the 3D domain. The solution of the 3D problem delivers a new soil temperature profile T_s.

The previous steps are repeated until the variation of the calculated heat fluxes is lower than a suitable convergence criteria.

In order to apply the previous $p_r$ocedure the followin_g assumptions and simplifications are ma_de:

- The fluid inside the pipes is considered to be an aqueous solution of water with 10% ethylene-glycol with temperature dependent thermal properties.
- The pipes can be treated as 1D domains in relation with the soil domain.
- No heat losses are considered in the transit section between heat exchangers.

10.3 Domain and discretization

10.3.1 Spatial discretization

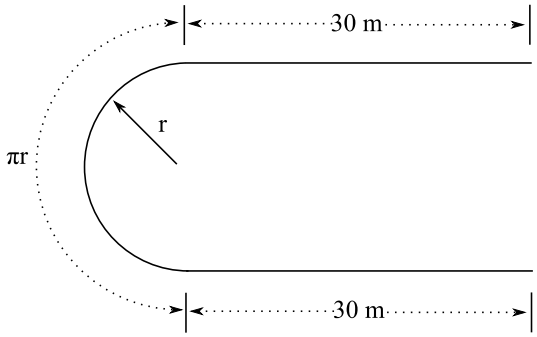

Figure 10-2 -Size of 1D pipe domain.

The 3D volume of soil under study spans a region 14 m depth by 27.6 m wide by 54 m long containing the road material layers and heat exchangers near its centre and is discretized with 154256 hexahedral linear finite elements. Figure 10-3 shows the representation of the 3D domain considered, the positions of boreholes A, F and G, and the main components of the experimental system. Three planes of interest are also shown: y=0 m, y=25 m and x = 0 m. Plane y=25 m corresponds to the equivalent position of the 2D domain presented in Chapter 9.

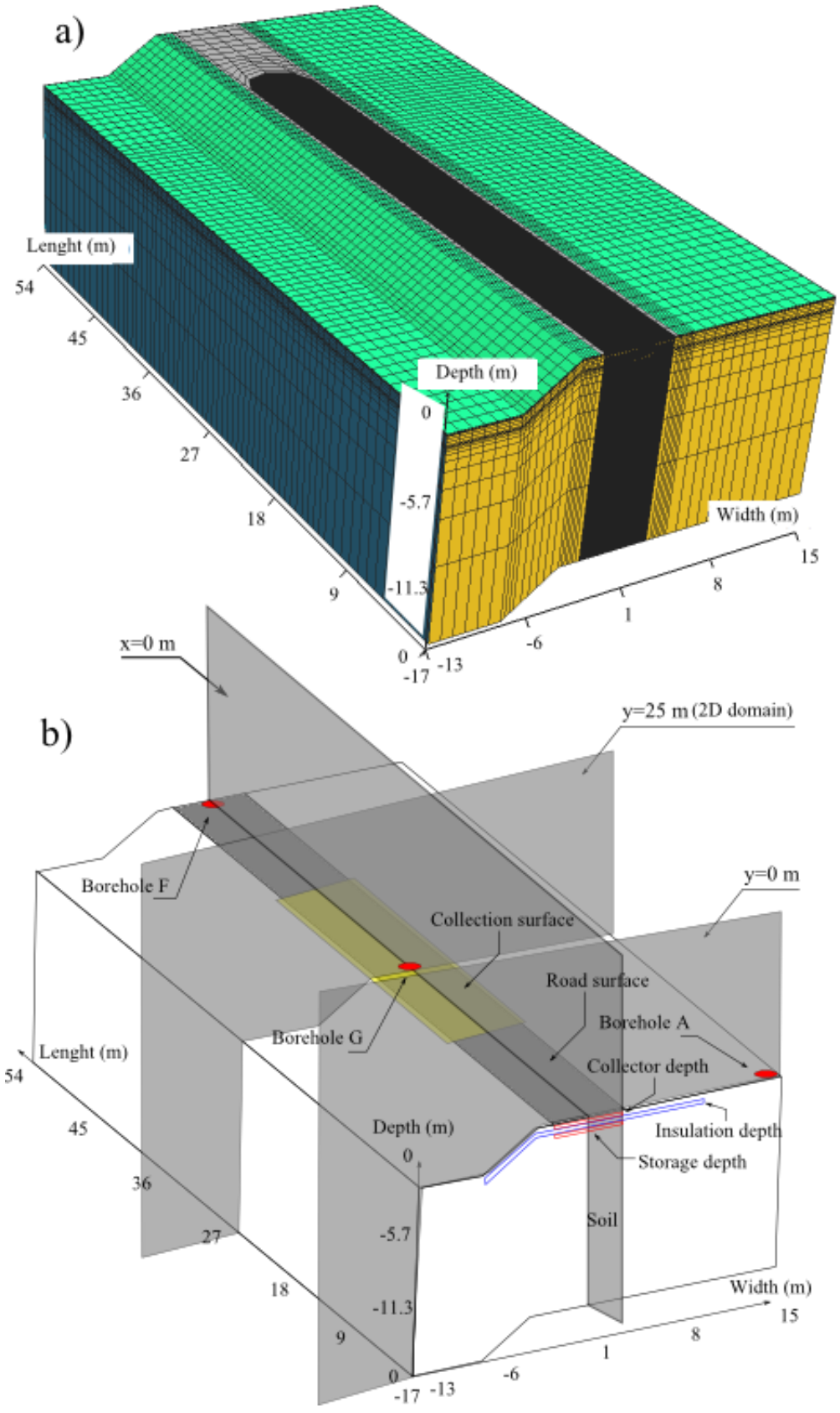

Figure 10-3 - Three dimensional domain. a) Mesh representation. b) Position of main components and planes of reference.

As mentioned before, each pipe in the heat exchangers is considered as a 1D domain with a total length dependent on its position in the array. The difference in distance arise from the curvature of the pipes in the U-loop as shown in . The total distance for each pipe is given as 60 m + πr, where r is the radius of curvature. It is obvious that those pipes located near the centre of the array are shorter than those at the edges. The 1D domain shown in is homogeneously discretized using 1024 linear finite elements.

10.3.2 Temporal discretization

The 3D problem is solved using a Crank-Nicholson time scheme with time steps depending on the period of simulation under consideration (See section 10.4). Two time steps are used: Hourly (3600 s) time steps for the pre system activation period and insulation periods and 15 min (900 s) for the activation periods. Hourly time steps are chosen based on previous analysis in order to optimize numerical accuracy and computational effort. 15 min time steps are chosen due to the temporal resolution of the problem under study indicating that the system could be switched on and off within this period of time.

The heat advection equation (equation (4-25)) is solved using a Crank-Nicholson time scheme with time steps of 60 s based on the time that the fluid inside the pipes takes to run through collector and storage heat exchangers (~1 min) without including the run through the pump system.

Each of these time step sizes have been checked to ensure numerical convergence.

10.4 Initial and Boundary Conditions

Initial and boundary conditions in the 3D domain are set as:

- Surface boundary condition - Soil. A formulation including a canopy layer (Section 3.7.5.3) has been found suitable for the soil surface based on the results from Chapter 8.
- Surface boundary condition - Pavement. A non-turbulent formulation (Section 3.7.5.2) has been found suitable for the road surface based on the results from Chapter 9. From the same results, a 50% level of uniform shading over the entire road surface is considered between 12 h and 17 h without seasonal variation. It is recognised that this is a limitation of the

current work but unfortunately was beyond the scope of this study to consider the 2D variation of shading on the road surface.

- A free flux boundary condition is used at the bottom of the domain. Following the analyses performed in Chapter 8 and Chapter 9 it was concluded that, with the correct representation of heat transfer processes at the surface boundaries, the boundary condition at the bottom of the domain has a minimal impact in the prediction of the temperature profile of the soil.
- Free flux boundary conditions are used at the vertical far-field boundaries of the domain.
- Initial condition. A uniform value of 10.9 ˚C is used as initial condition for the domain. This value is calculated from the average air temperature measured on the experimental site by TRL (Carder et al. 2007) for the period September 2005 to August 2006. The domain is then subjected to a pre system activation analysis of 8 yearly cycles using meteorological data provided by Carder et al (2007). This allows the initial thermal condition of the domain, which is consistent with the applied boundary conditions, to be established before the simulation of the system activation period is commenced.

For the solution of the heat advection equation in the heat exchanger 1D pipes:

- Initial condition: If the system is switched on due to the fulfilment of activation criteria (see section 10.5), the temperature profile is assumed to be equal to the temperature of the surrounding soil.
- Boundary condition: The temperatures at the inlets are the only required boundary condition in this case. They are assumed to be equal to the average outlet temperatures of the second heat exchanger (e.g. inlet collector temperatures are equal to the average outlet storage temperatures).

10.5 Periods of analysis

Following a similar approach as in Chapter 9, the numerical analysis presented in this Chapter is divided in 7 periods (including pre system activation) based on the experiment description provided by Carder et al (2007). In all cases a 50% level of uniform shading on the road surface between 12 h and 17 h has been applied based on the results from Chapter 9. These periods are summarized as follow:

- Pre system activation period. Based in the results obtained in Chapter 8, a period of 8 yearly cycles is considered suitable for this period of analysis. During this period the layers corresponding to insulation and sand are replaced by soil.
- First insulation period. The installation of the experimental system was performed on early May 2005 (actual date is not specified, here is assumed to be on 1st May 2005). However the system was not activated until 23rd August 2005. During the period ranging from 1st May 2005 to 22nd August 2005 the distribution of material layers is as described in Chapter 5 (inclusion of insulation layer and sand layer). For this period only two experimental data points are available: 9th May 2005 at 12:30h and 15th July 2005 at 14:00 h.
- First activation period. The experimental system was activated on the 23rd August 2005. During this period ranging until the 13th November 2005, the system was operated under collection settings. The fluid in the heat exchangers was pumped when the temperature difference between the temperature sensor located at the middle of the collection pipes and that located at the middle of the storage pipes was approximately 1.4 ˚C. Once active, the pumps were turned off when the temperature difference dropped to approximately 0.3 ˚C.
- Second activation period. From 14th November 2005 to 20th February 2006. The experimental system was operated under usage settings. The pumps were activated when the road surface fell below 2˚C for more than 15 min and were turned off when the surface temperature rose above 2 ˚C for more than 15 min.
- Second insulation period. From 21st February 2006 to 26th April 2006. The system is put into a pause until the Third activation period begins. The soil in the storage region is prevented from being heated normally due to the presence of the insulation layer.
- Third activation period. From 27th April 2006 to 31st October 2006. The system was operated under collection settings as described for the First activation period.

- Fourth activation period. From 1st November 2006 to 1st March 2007. The system was operated under usage settings as described for the Second activation period.

10.6 Results

The results presented in this section are grouped by periods of analysis as listed in Section 10.5 and as presented in Chapter 9. Where possible, comparisons are made with numerical results obtained in Chapter 9. As mentioned there, in a 2D domain borehole F and G correspond to the same position (middle of the road) while in a 3D domain they are located in their correct position as shown in Figure 10-3. For this reason, 2D the temperature profiles referred as borehole F are those obtained from the pre system activation period (before any insulation layer is put into place or the system is activated) while 2D temperature profiles referred as borehole G are those obtained from the first insulation period onwards.

Section 10.6.1 compares experimental and numerical temperature profiles in 2D and 3D corresponding to the boreholes located under the road surface (F and G) for three selected dates.

Section 10.6.2, Section 10.6.3, Section 10.6.4 and Section 0 presents numerical transient variations of temperature corresponding to borehole G for the first and second periods of insulation and for the first and second periods of activation at two selected depths: 0.1325 m (collector pipes depth) and 0.875 m depth (storage pipes depth). These sections also show contour temperature profiles for plane y=25 m corresponding to the end of each period.

Section 10.6.5 and Section 10.6.6 compares experimental measurements with numerical 3D and 2D transient variations of temperature corresponding to borehole G for the third and fourth periods of activation at two selected depths: 0.1325 m (collector pipes depth) and 0.875 m (storage pipes depth). These sections also show contour temperature profiles for plane y=25 m and y=0m corresponding to the end of the third and fourth activation periods. Additionally, Section 10.6.7 shows a contour temperature profile of plane x=0 for the same dates.

10.6.1 Pavement temperatures: borehole F and borehole G

This section presents comparisons of experimental and numerical (2D and 3D) soil temperatures for borehole F and G on three selected dates: 9th May 2005 (first experimental measurement after installation of experimental systems), 15th July 2005 (at the middle of the first insulation period) and 15th October 2005 (at the middle of 1st activation period). In all cases, Canopy Cover and Non-turbulent boundary formulations have been used for soil and road surfaces respectively. A 50% level of uniform shading is assumed on the road surface.

Figure 10-4 and Figure 10-5 show results for the 9th May 2005 at 12:30 h corresponding to borehole F and borehole G respectively. 2D numerical soil temperatures are included in Figure 10-5 for comparison. Although, both numerical models offer in general a good match for the experimental measurements in borehole F and G, the 3D model predicts slightly lower temperatures that are in better agreement. Two observation can be made from these figures: first, in Figure 10-4 the temperatures under 0.875 m depth (marked with a horizontal dashed line) are higher than those from Figure 10-5, conversely, the temperature above this depth are lower in Figure 10-4. This is due to the first effects of the insulation layer (assumed in the numerical models to be placed on the 1st May 2005) preventing thermal energy from flowing into the ground and raising the temperature of the region above this layer. Second, it can be seen that the experimental measurements in Figure 10-5 appear to be disturbed near the surface. It is not completely understood the reason of this behaviour, however, Carder et al. (2007) report that the excavation process to place the insulation layer was carried out at the beginning of May, the disturbance of the soil due to this procedure might be related with the observed temperatures.

Figure 10-6 and Figure 10-7 show results for 15th July 2005 at 14:00 h corresponding to borehole F and borehole G respectively. The temperatures under the insulation layer (borehole G) are clearly lower than those at the same depth of borehole F. As before it can be seen that both 2D and 3D numerical models offer a good match with the experimental measurements and that the 3D model predicts slightly lower temperatures that seems to be in better agreement with the experimental measurements.

Figure 10-8 (borehole F) and Figure 10-9 (borehole G) show results for the 15th October 2005 at 0 h. These figures show a smaller temperature range (since the results correspond to midnight and the high surface temperatures are avoided) in which is possible to appreciate that the order or the error between the numerical models and the experimental measurements is of about 2 ˚C near the surface of borehole F and of about 0.4 ˚C near the bottom of borehole G. Note, however, that the error of 2 ˚C observed in borehole F is restricted to a few centimetres under the surface and that in decreases with depth, being of about 1 ˚C at 1 m depth. This difference is not observed in borehole G, this could be due to the presence of the insulation layer, that prevents temperature variations from propagating into the ground. However, notice that these figures correspond to the middle of the 1st activation period and that the temperature at this depth in borehole G is influenced by temperatures at the surface via the active pipe heat exchangers. It is believed that the difference observed in borehole F is due to a non-uniform level of shading on the road surface being perhaps more pronounced on its neighbourhood.

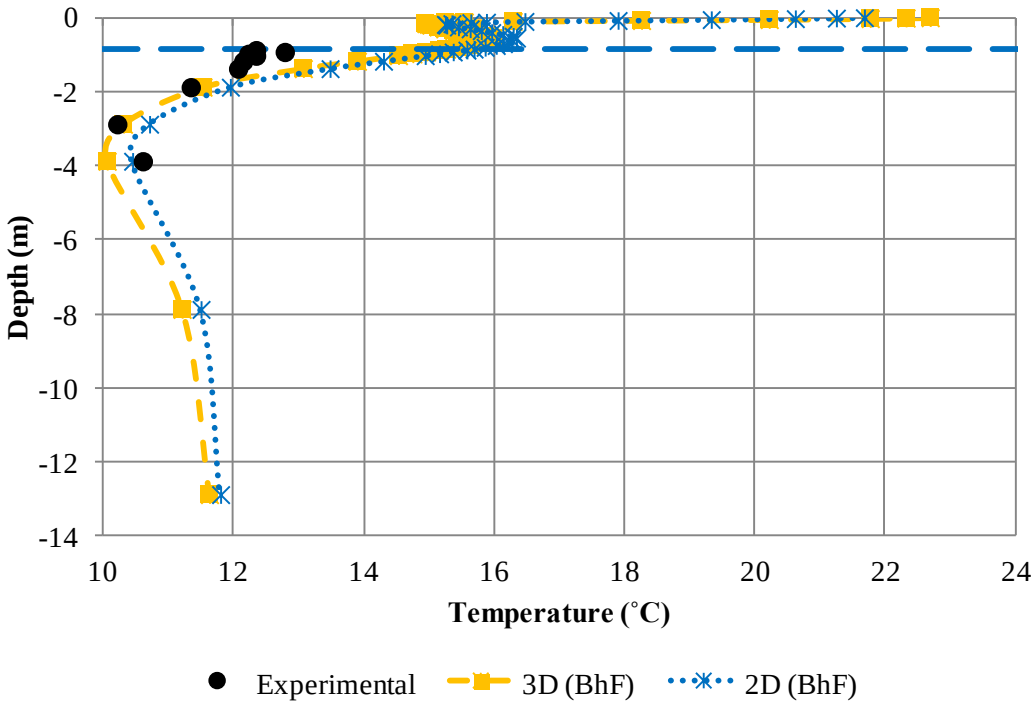

Figure 10-4 - Soil temperature profile at borehole F on the 9th May 2005 at 12:30 h. Insulation depth (0.0875 m, blue dashed line) is shown for reference.

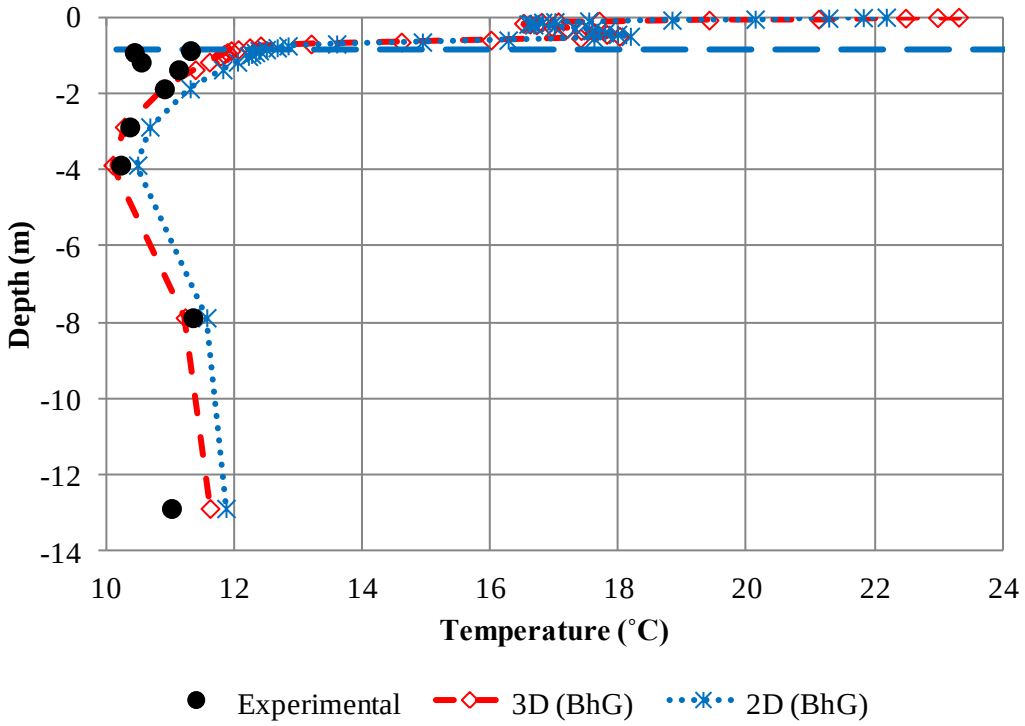

Figure 10-5 - Soil temperature profile at borehole G on the 9th May 2005 at 12:30 h. Insulation depth (0.0875 m, blue dashed line) is shown for reference

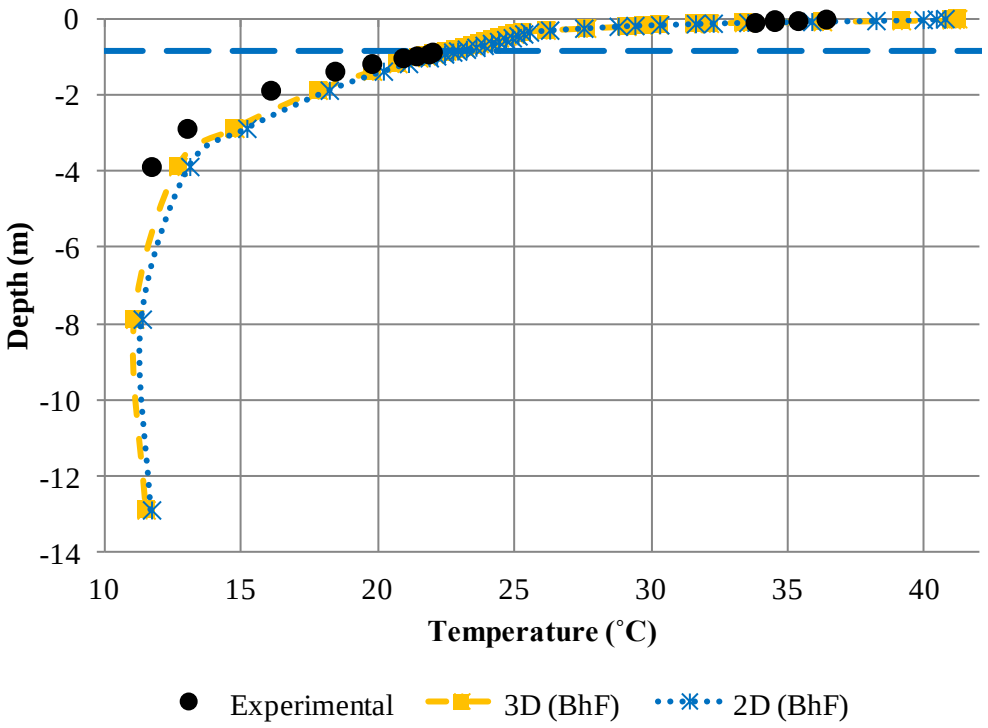

Figure 10-6 - Soil temperature profile at control borehole F on the 15th July 2005 at 14:00 h. Insulation depth (0.0875 m, blue dashed line) is shown for reference

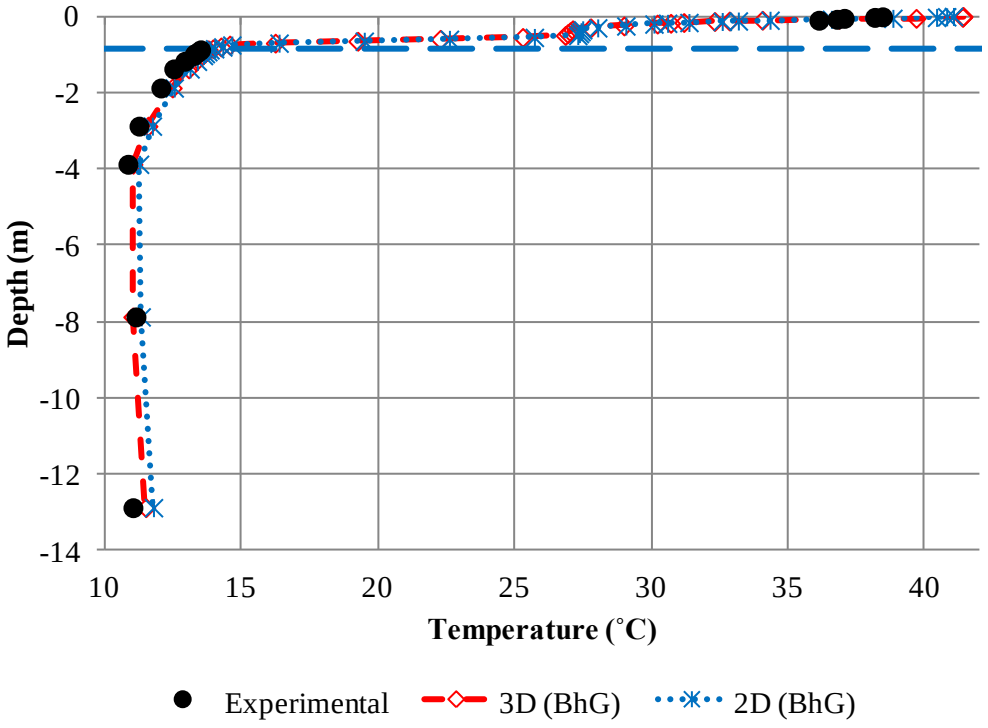

Figure 10-7 - Soil temperature profile at borehole G on the 15th July at 14:00 h. Insulation depth (0.0875 m, blue dashed line) is shown for reference

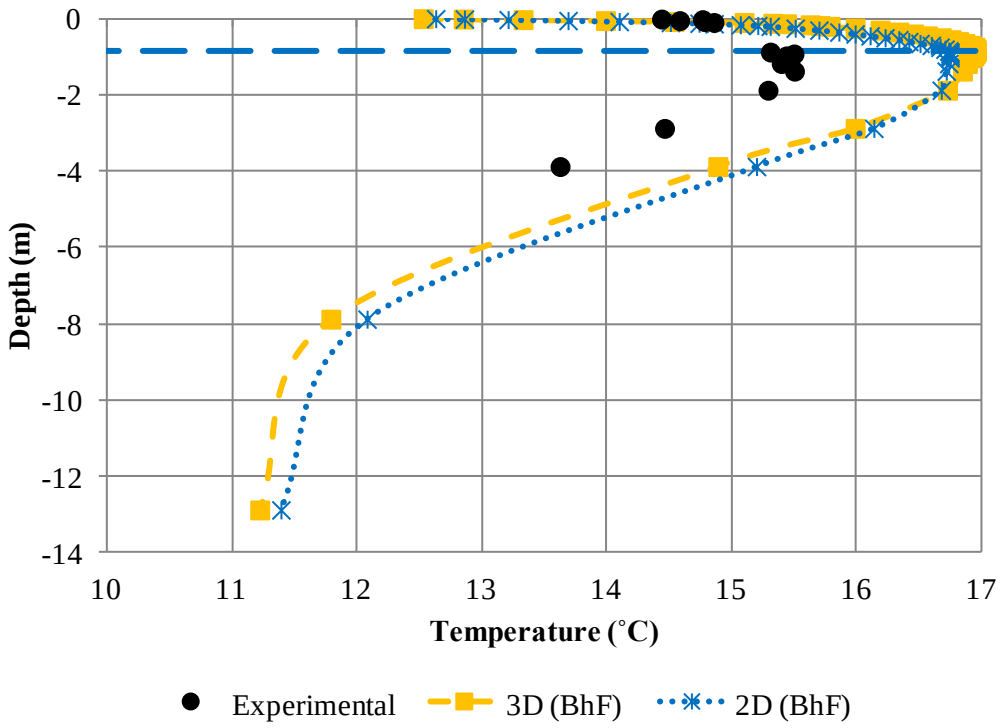

Figure 10-8 - Soil temperature profile at borehole F on the 15th October 2005 at 00:00 h. Insulation depth (0.0875 m, blue dashed line) is shown for reference

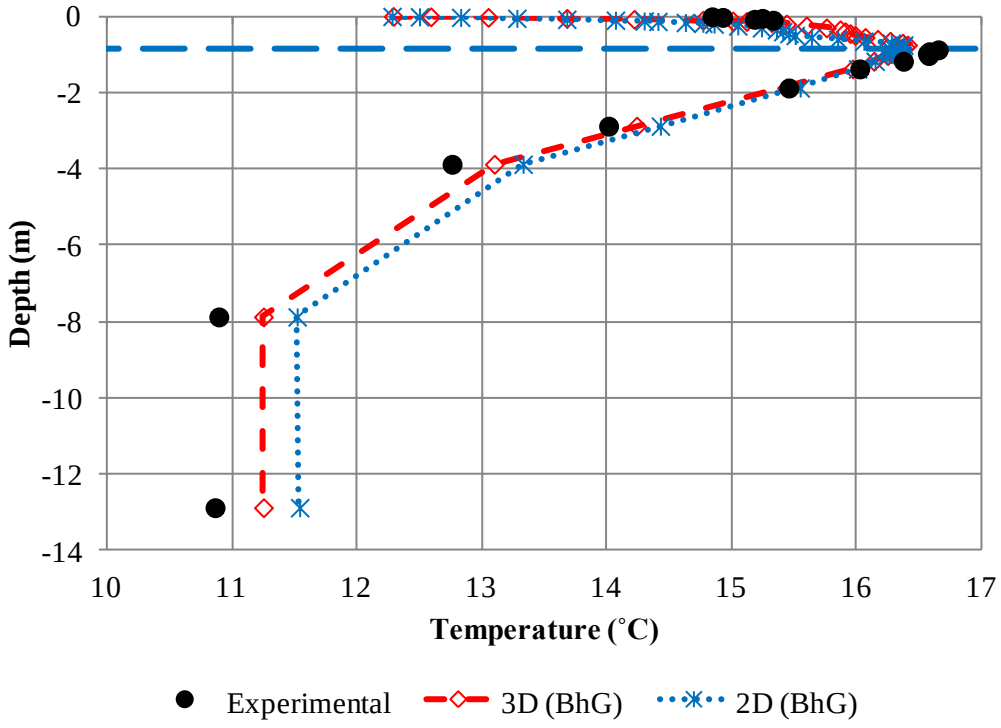

Figure 10-9 - Soil temperature profile at borehole G on the 15th October 2005 at 00:00 h. Insulation depth (0.0875 m, blue dashed line) is shown for reference.

10.6.2 First insulation period May 1st May 2005 - 22nd September 2005

Figure 10-10 shows comparison of predicted transient variations of soil temperatures in 3D and 2D at borehole F and G. Two available experimental measurements for 9th May 2005 and 15th July 2005 are included for reference. Corresponding temperature profiles for the previous yearly cycle (part of the pre warming period) are also shown for reference. It can be seen that the predictions at this depth from the 2D and 3D models are very similar for this period. As discussed in Chapter 9, the results show that the temperatures under the insulation layer are drastically damped compared to the previous yearly cycle (normal soil heating), with only a small increment of approximately 2 ˚C at the end of July and then slowly decreasing towards the end of August. The corresponding temperatures for borehole F during the first insulation period are equal to the temperatures from borehole G for the pre warming period. This might indicate (in the absence of any other source of error) that no disturbance is propagated into borehole F (at least above 0.8475 m depth) due to the presence of the insulation layer on borehole G. Figure 10-11 shows a contour temperature profile of a section of soil located near the road surface at the plane y=25 m in Figure 10-3 at the end of this period and corresponding to the equivalent 2D domain in Chapter 9 (Figure 9-14). The main difference being the temperature profile in the regions near the edge of the domain in 3D under the insulation layer. In the rest of the domain, however, it can be seen that both models predict similar temperature patterns for this period.

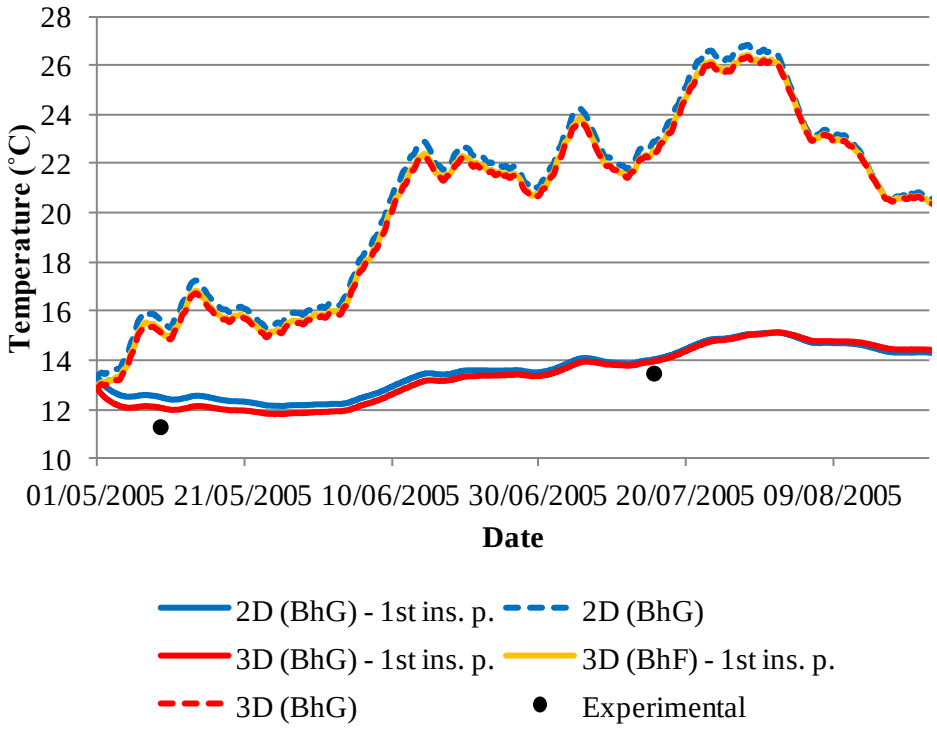

Figure 10-10 - Comparison of numerical predictions in 2D and 3D for the first insulation period. Numerical results for the same period from previous yearly cycle (without insulation) are added for reference. Note that "3D (BhF) - 1st ins. p." coincides with "3D (BhG)".

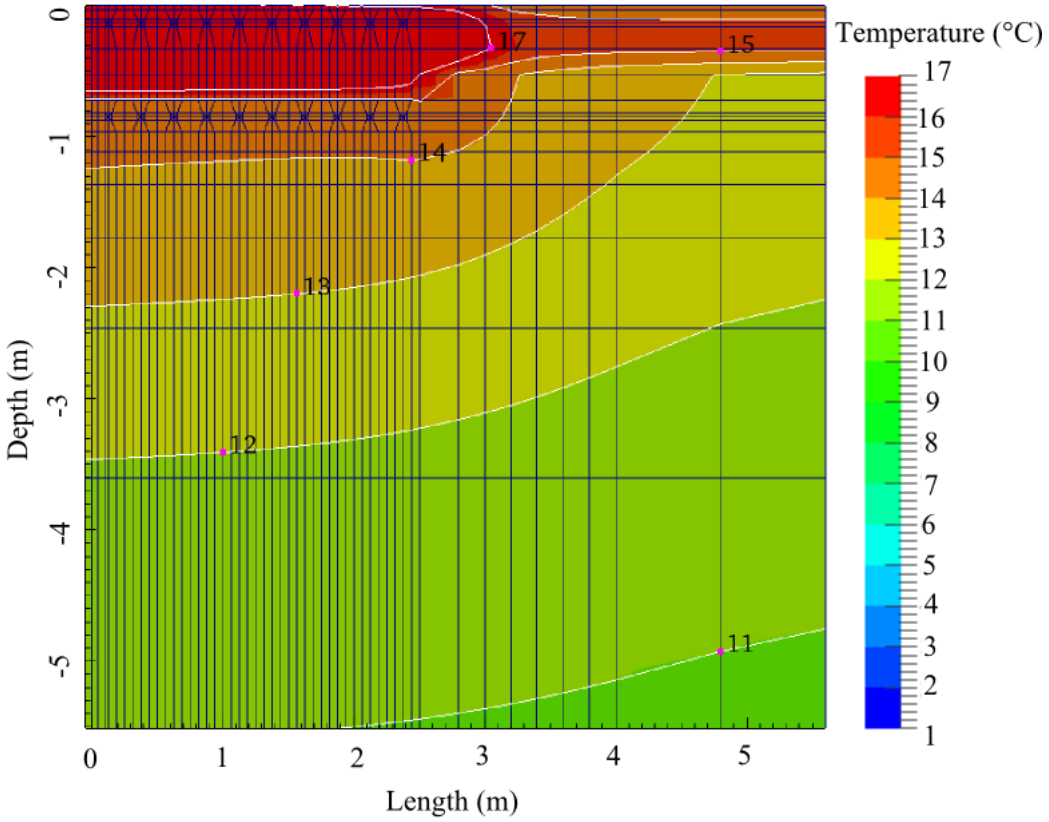

Figure 10-11 - Contour temperature profile near the road surface at y=25 m (Figure 10-3) corresponding to the end of the 1st insulation period (22nd August 2005).

10.6.3 First activation period: 23rd August 2005 - 13th November 2005 (collection)

Figure 10-12 shows the comparison of numerical results and experimental measurements for the transient variations of soil temperature at borehole G at 0.1325 m depth (System 2, under road at collector pipes depth). Figure 10-13 shows the corresponding comparisons at 0.8475 m depth (storage pipes depth). It can be seen that the match with the experimental measurements of the numerical predictions from the 2D and 3D models seems to be very similar at collector depth. At the storage depth the 2D model seems to offer better predictions while the 3D model underestimates the temperatures at this depth. However, at the end of the activation period both models tend to reach the same temperature.

Figure 10-14 and Figure 10-15 show the temperature profiles at collector and storage depth respectively for the first week of September 2005. Notice that, although in Figure 10-12 both models seem to predict very similar temperatures at collector depth, a closer look shows that in fact the difference is about 2 ˚C, the same difference observed at storage depth. The 3D model is predicting lower temperatures compared with the 2D model. This is believed to be related with the assumption of homogeneous shading being cast on the road surface. While a 50% level of homogeneous shading was considered appropriate for 2D simulations based on the results presented in Section 9.7, it might not be completely suitable for a 3D domain where, given the uneven distribution of shade cast by trees, some regions might be receiving more radiation than others.

Figure 10-16 shows a contour temperature profile of a section of soil located near the road surface at the plane y=25 m in Figure 10-3 at the end of this period and corresponding to the equivalent 2D domain in Chapter 9. The temperature profile predicted by 3D model is very similar to the corresponding predictions in 2D shown in Figure 9-19. In particular, both models predicts almost the same temperature profiles with depth. However, the region with temperatures higher than 13 ˚C is wider in the 2D model than in the 3D model. This might be due to the higher temperatures predicted by the 2D model as shown in Figure 10-13 particularly during the month of September.

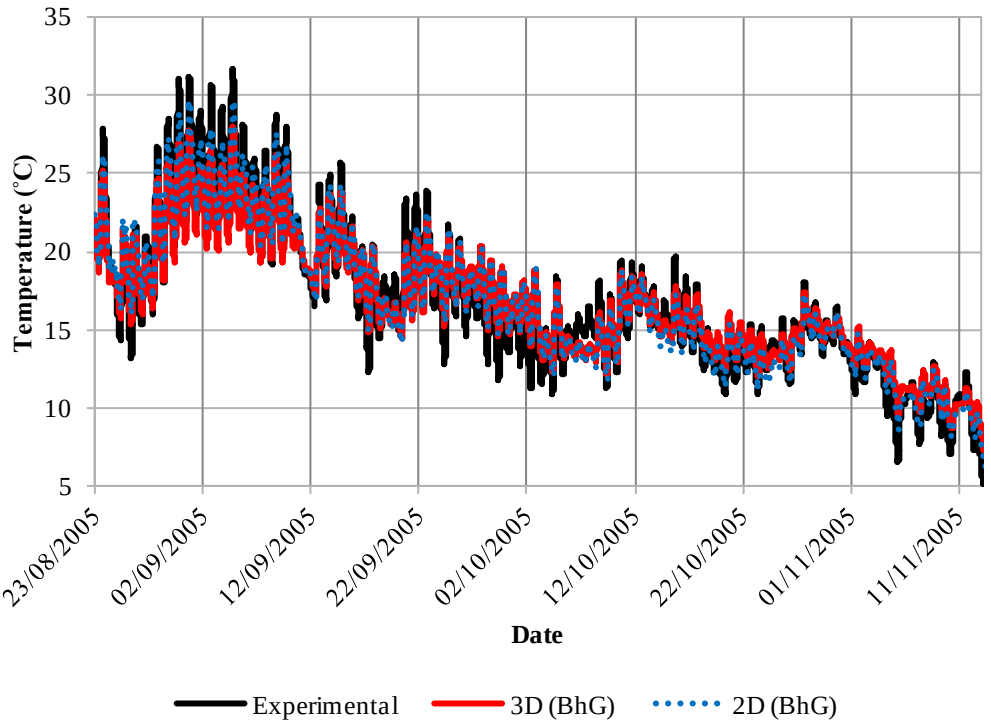

Figure 10-12 - Transient variations in 3D of soil temperature at borehole G at 0.1325 m (collector depth) for the first activation period (collection).

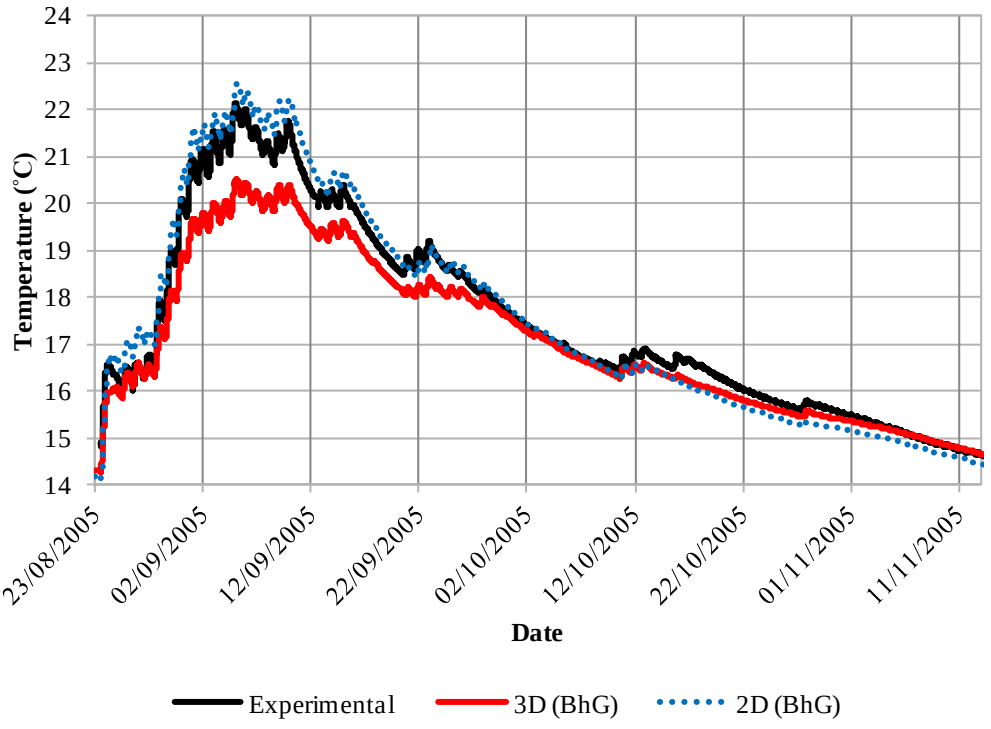

Figure 10-13 - Transient variations in 3D of soil temperature at borehole G at 0.8475 m (storage depth) for the first activation period (collection).

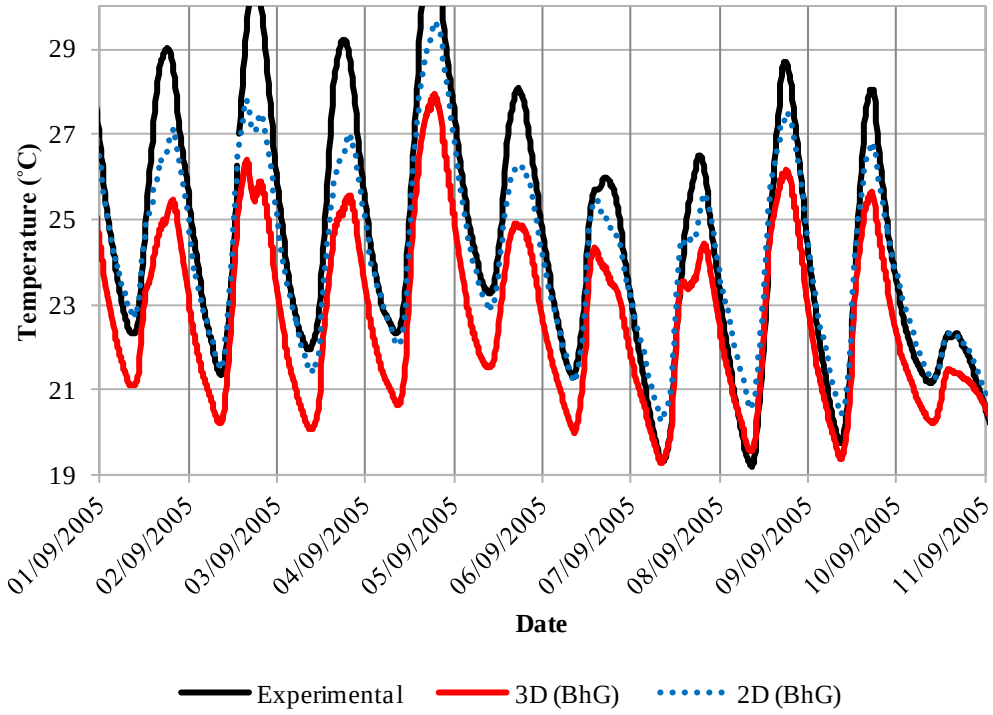

Figure 10-14 - Detail of Figure 10-12 showing the temperature profile for the first week of September at borehole G at collector depth. Notice the difference between 2D and 3D predictions.

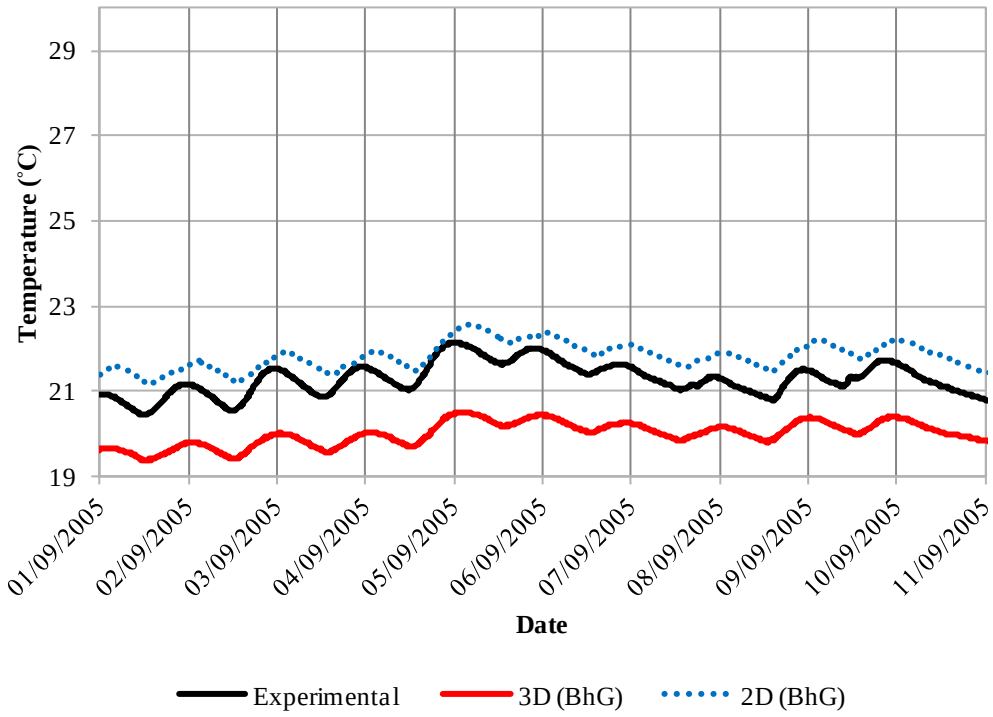

Figure 10-15 - Detail of Figure 10-13 showing the temperature profile for the first week of September at borehole G at storage depth. Notice the difference between 2D and 3D predictions.

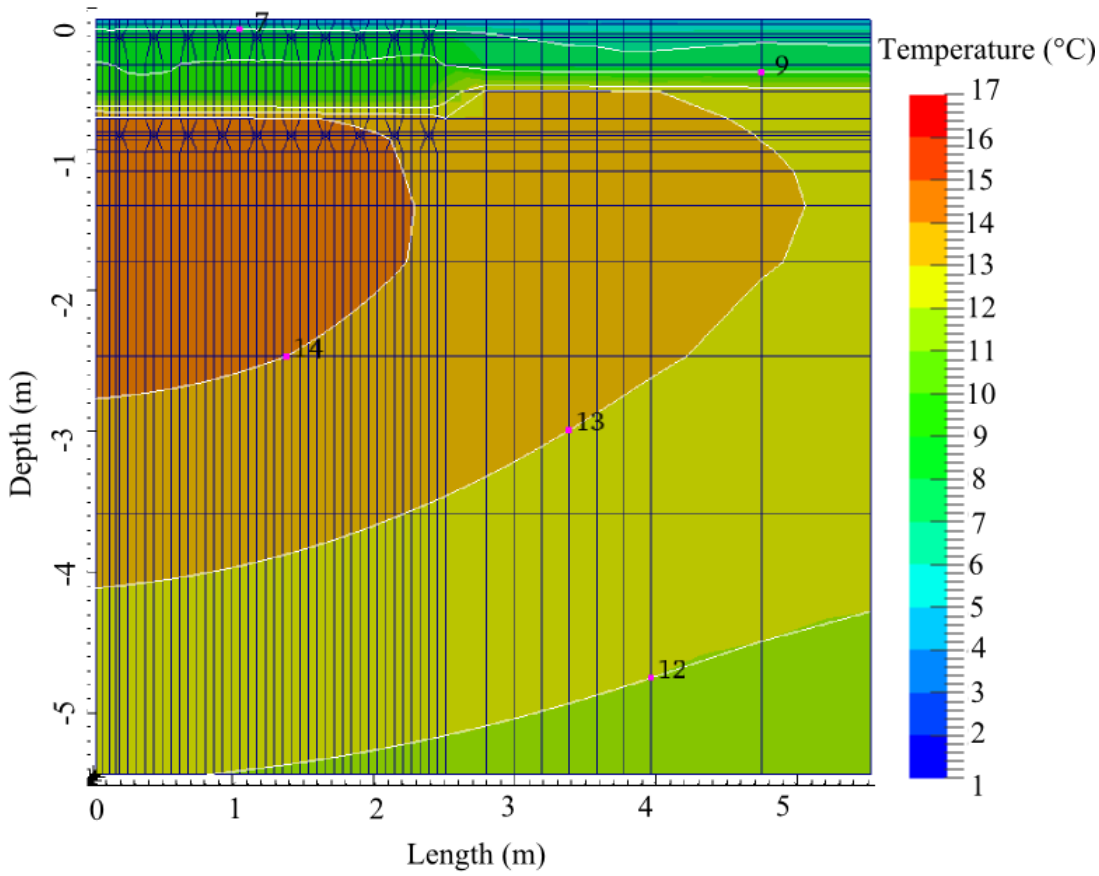

Figure 10-16 - Contour temperature profile near the road surface at y=25 m (Figure 10-3) corresponding to the end of the first activation period (13th November 2005).

10.6.4 Second activation period: 14th November 2005 - 20th February 2006 (usage)

Figure 10-17 shows the comparison of numerical results and experimental measurements for the transient variations of soil temperature at borehole G at 0.1325 m depth (System 2, under road at collector pipes depth) corresponding to the second activation period. While Figure 10-18 shows the corresponding comparisons at 0.8475 m depth (storage pipes depth). Again it can be seen that the numerical predictions in 2D and 3D seem very similar and that in general follow the trend of the experimental measurements at collector and storage depth. At collector depth, although not visible, differences are present between 2D and 3D models of about 0.5 ˚C, while at storage depth these differences are in general of about 1 ˚C, being in both cases the 2D predictions lower in comparison with the 3D. The apparent better performance of the 3D model as compared with the 2D model during this period (winter, where shading has a decreased impact) is believed to be related with the simplifications used to estimate the heat fluxes in the 2D model that might be

overestimating these fluxes and predicting slightly higher temperatures in summer (see Section 10.6.3) and lower in winter as compared with the 3D model.

In Figure 10-17 and Figure 10-18 it can be seen that there are at least three periods, during the first and second weeks of January 2006 and the second week of February 2006, where it can be seen how the numerical predictions in 2D and 3D deviate from the experimental measurements for up to 4 ˚C. From the results presented in Chapter 9, it was concluded that these deviations are likely to be related with periods of snow fall where a certain amount of snow was accumulated on the road surface.

Figure 10-19 shows a contour temperature profile of a section of soil located near the road surface at the plane y=25 m in Figure 10-3 at the end of this period and corresponding to the equivalent 2D domain in Chapter 9. Again the temperature profile predicted by 3D model is very similar to the corresponding predictions in 2D shown in Figure 9-22 with the main differences restricted to the region next to the road and under the insulation layer. It can also be seen that the 3D temperatures around the storage area are slightly higher than those predicted by the 2D model. This agrees with the temperature profiles shown in Figure 10-18.

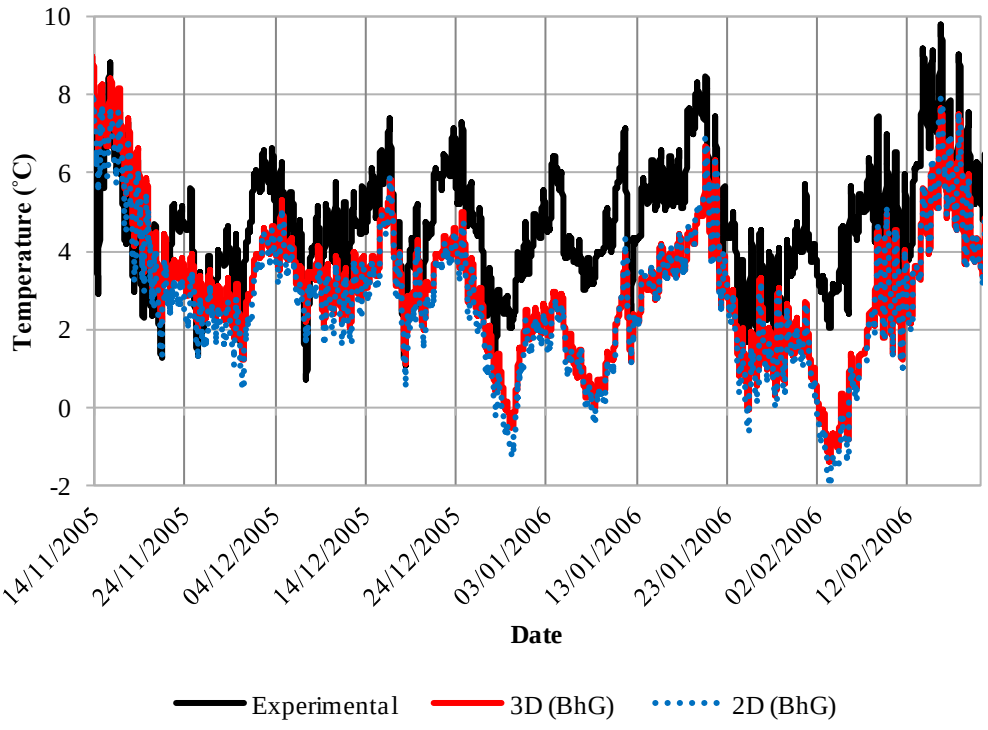

Figure 10-17 - Transient variations in 3D of soil temperature at borehole G at 0.1325 m (collector depth) for the second activation period (usage).

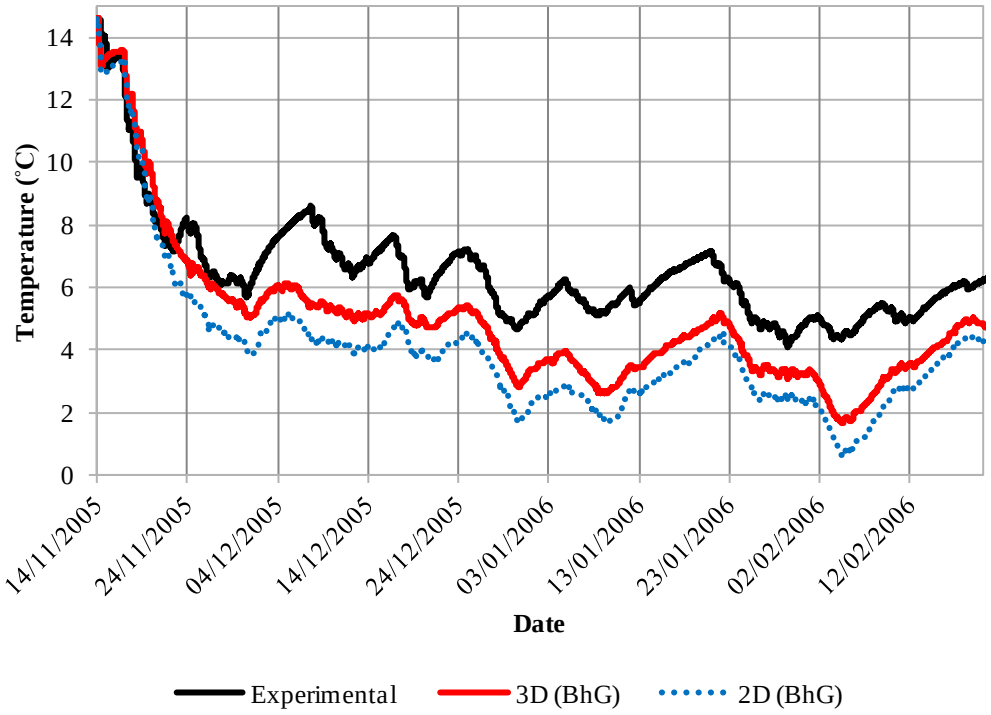

Figure 10-18 - Transient variations in 3D of soil temperature at borehole G at 0.8475 m (storage depth) for the second activation period (usage).

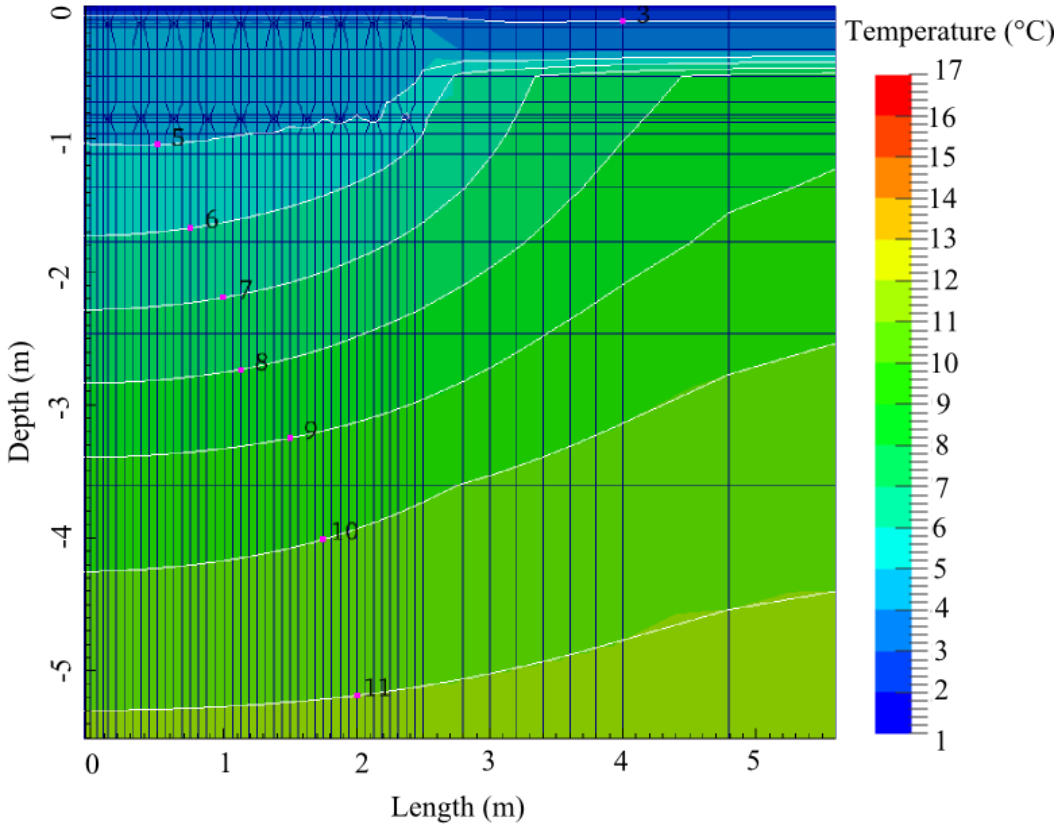

Figure 10-19 - Contour temperature profile near the road surface at y=25 m (Figure 10-3) corresponding to the end of the second activation period (20th February 2006).

10.6.5 Second insulation period: From 21st February 2006 to 26th April 2006.

As mentioned in Chapter 9, during the period between 21st February 2006 and 26th April 2006 the system was switched off manually. No heat collection or usage was carried out. Figure 10-20 shows the comparison of numerical results and experimental measurements for the transient variations of soil temperature at borehole G at 0.1325 m depth (System 2, under road at collector pipes depth). While Figure 10-21 shows the corresponding comparisons at 0.8475 m depth (storage pipes depth). It can be seen that 2D and 3D numerical model predict essentially the same thermal behaviour at these depths during this period. At storage depth the temperatures show a slow increment of about 4 ˚C while the temperatures at collector depth slowly rose by 10 ˚C. As explained in Chapter 9, these differences are in part due to the insulation layer preventing the soil underneath from heating normally.

As discussed in Chapter 8, meteorological data corresponding to late February 2007 and March 2007 were used into the corresponding months of 2006 due to the absence of these periods on the experimental weather data provided by Carder et al (2007). This is reason of the deviation observed in the numerical results from the experimental data during this period. As mentioned in Chapter 9, The abnormal behaviour of the experimental measurements around 23rd March 2006 is not commented on by Carder et al (2007) and is believed to be due to a temporary glitch in the experimental system.

Figure 10-22 shows a contour temperature profile of a section of soil located near the road surface at the plane y=25 m in Figure 10-3 at the end of this period and corresponding to the equivalent 2D domain in Chapter 9. It can be seen that the temperature profiles predicted by the 3D model is almost identical to the temperature profile predicted by the 2D model and shown in Figure 9-25. This seems to imply that the differences observed in the previous activation periods are due mainly to the performance of the pipe heat exchangers in 2D and 3D.

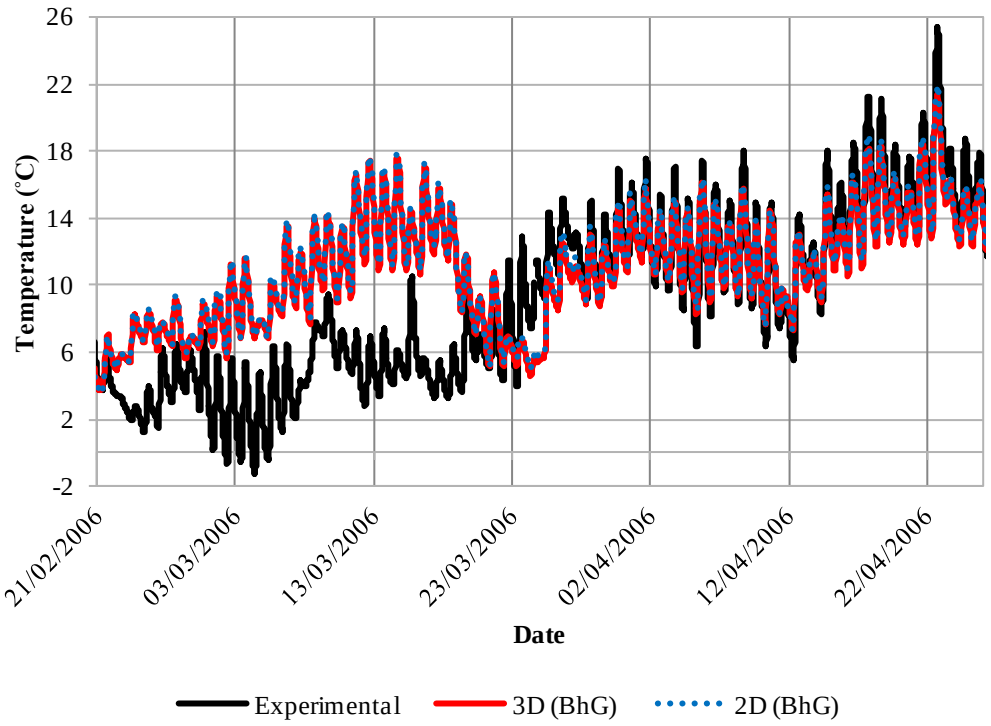

Figure 10-20 - Transient variations in 3D of soil temperature at borehole G at 0.1325 m (collector depth) for the second insulation period.

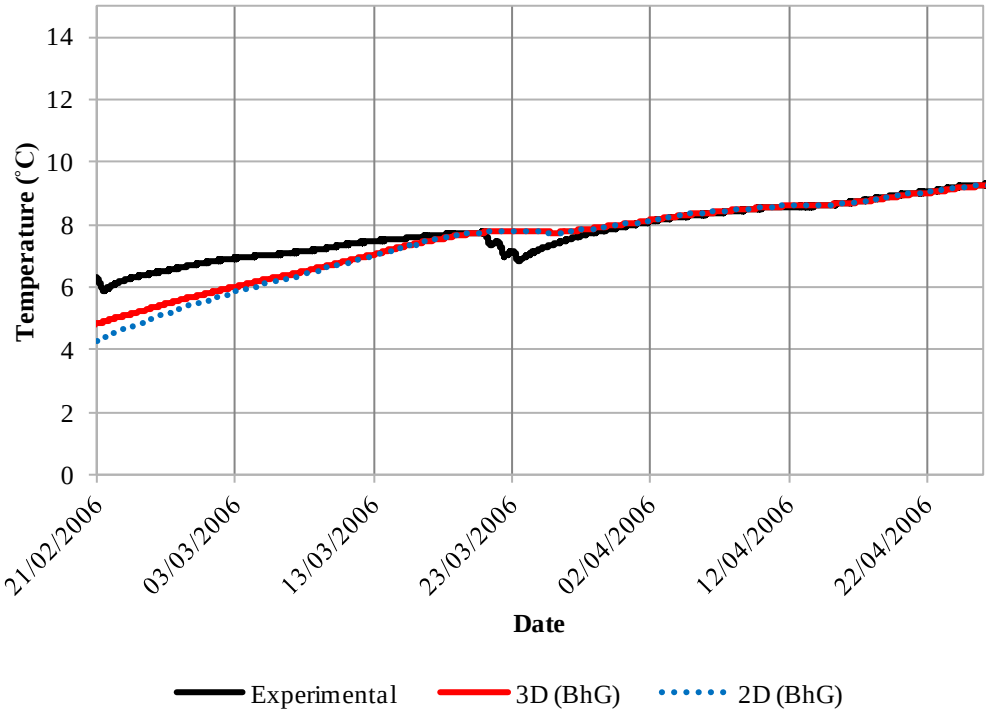

Figure 10-21 - Transient variations in 3D of soil temperature at borehole G at 0.8475 m (storage depth) for the second insulation period.

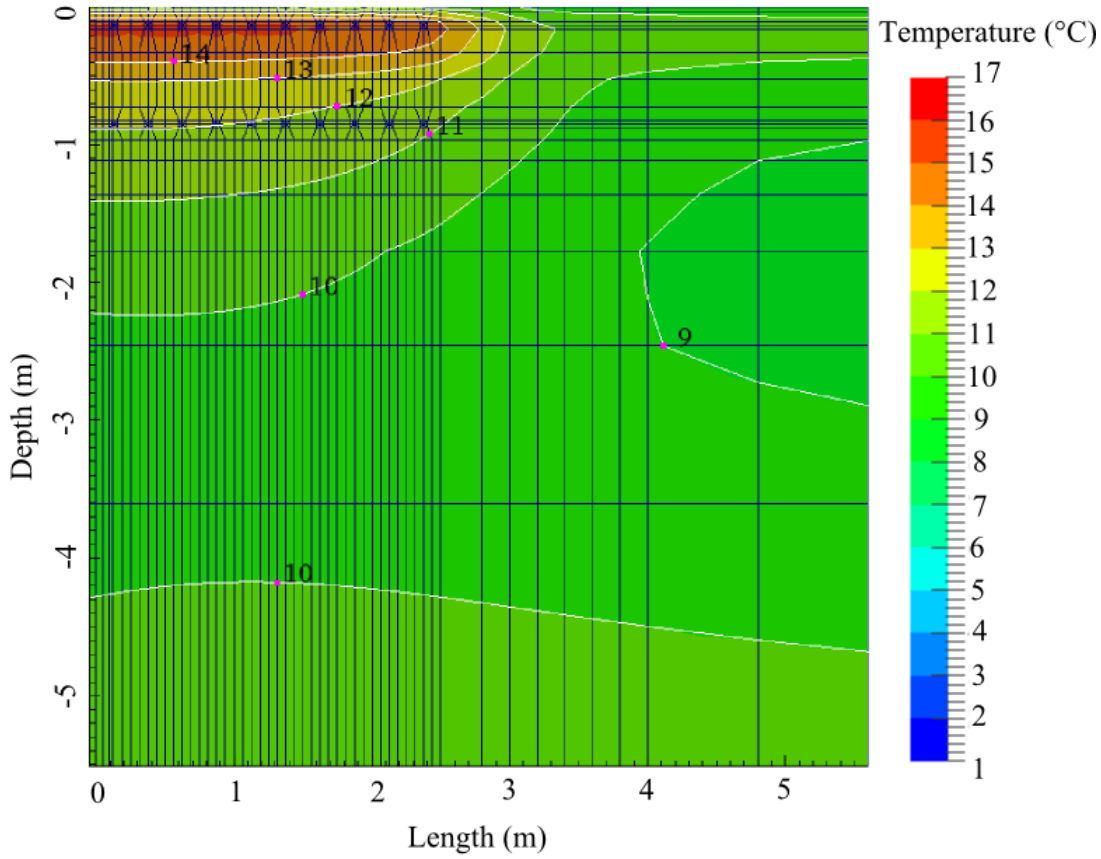

Figure 10-22 - Contour temperature profile near the road surface at y=25 m (Figure 10-3) corresponding to the end of the second insulation period (20th February 2006).

10.6.6 Third activation period: From 27th April 2006 to 31st October 2006

Figure 10-23 shows the comparison of numerical results and experimental measurements for the transient variations of soil temperature at borehole G at 0.1325 m depth (System 2, under road at collector pipes depth) for the third activation period. While Figure 10-24 shows the corresponding comparisons at 0.8475 m depth (storage pipes depth). Experimental data for this period is available until the 6th September 2006. The collection process was interrupted between 18th May 2006 and 7th June 2006 due to significant airlocks preventing operation according to Carder et al (2007). This interruption is enforced in the numerical simulation by overriding the automatic activation of the system and forcing it to remain switched off.

The numerical predictions in 3D show a similar level of agreement with the experimental measurements as the 2D predictions at collector depth and storage depth with differences in the order of 2 ˚C as shown in Section 10.6.3. It can be seen that again the 3D model and 2D model reach the same level of temperature at the end of this period. Figure 10-25 shows that although the predicted region with

temperatures higher than 16 ˚C is wider in the 3D model compared with the corresponding region predicted by the 2D model (Figure 9-28), in the 2D model the regions with temperatures of 14 ˚C and 15 ˚C extend further in the domain. This suggest that the higher temperatures predicted by the 2D model in the storage region (Figure 10-24), have diffused more rapidly (due to the higher gradient) into the ground by the end of the collection period.

Figure 10-26 shows a contour temperature profile of the region near the road surface located at plane y=0 m in Figure 10-3. It can be seen that under 3 m depth the temperature profile at this plane is similar to that at y=25 m shown in Figure 10-25. This seems to imply that the thermal depth of influence of the system if about 3 m. However this might vary if the system operates under several yearly cycles and if inequalities exist in the inputs and outputs of thermal energy. Notice that although the region with temperatures of 14 ˚C is wider in the plane y=0 m (due to summer warming through the soil surface in addition to the pavement surface), the region with temperatures higher than 16 ˚C is broader in the plane y=25 m and that the effect of thermal containment by the insulation layer is clearly visible.

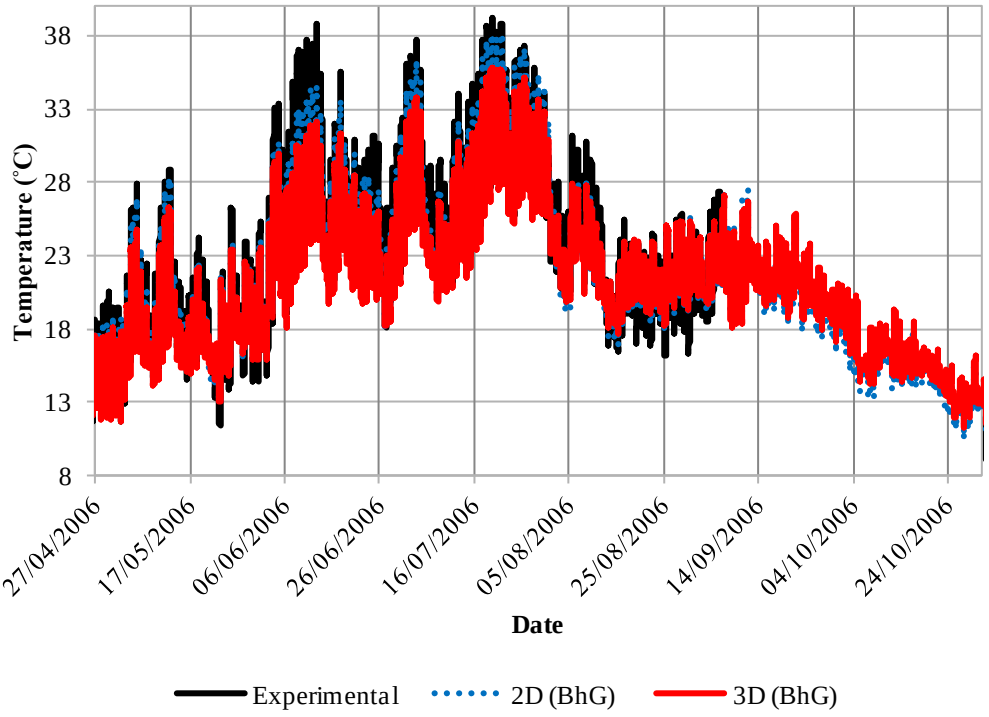

Figure 10-23 - Transient variations in 3D of soil temperature at borehole G at 0.1325 m (collector depth) for the third activation period.

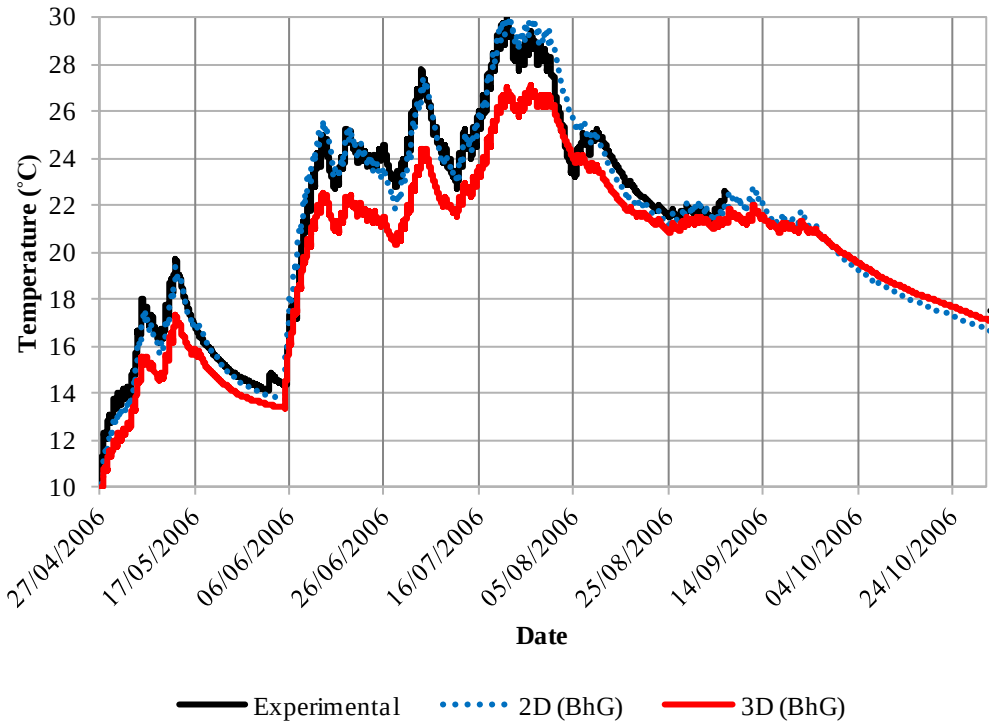

Figure 10-24 - Transient variations in 3D of soil temperature at borehole G at 0.8475 m (storage depth) for the third activation period.

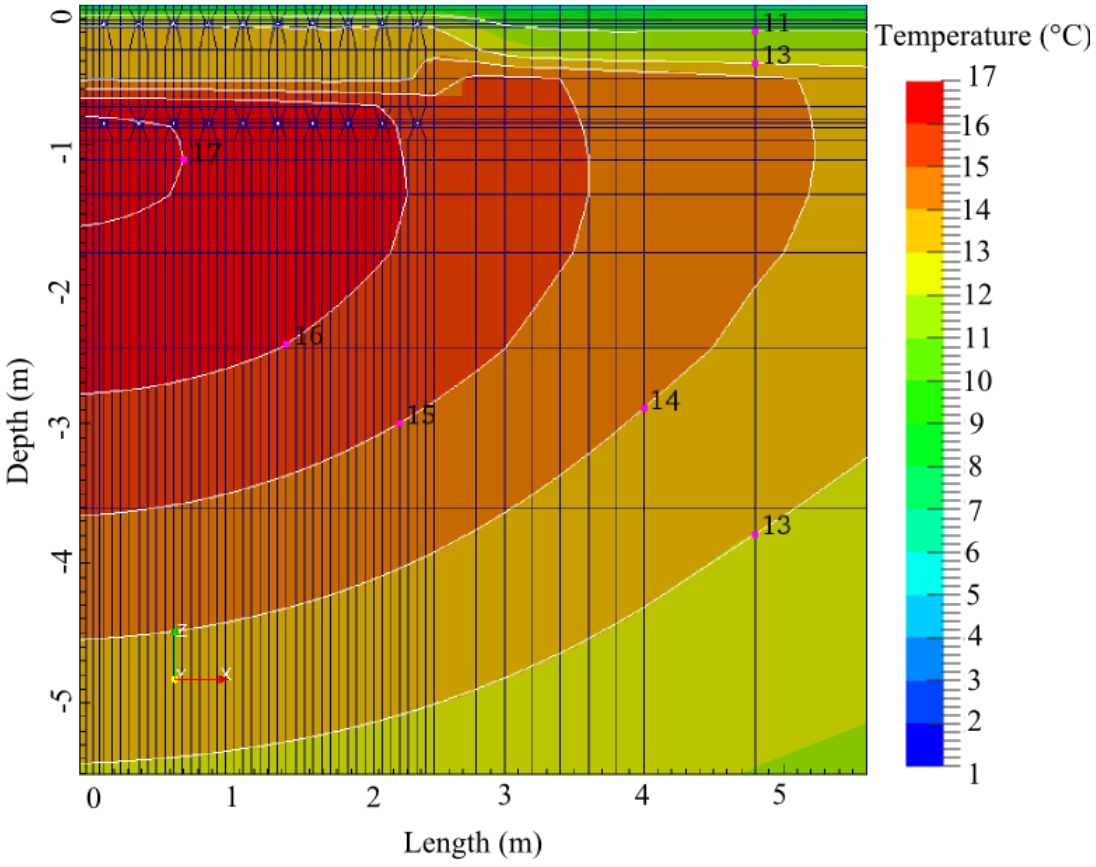

Figure 10-25 - Contour temperature profile near the road surface at y=25 m (Figure 10-3) corresponding to the end of the third activation period (31st October 2006).

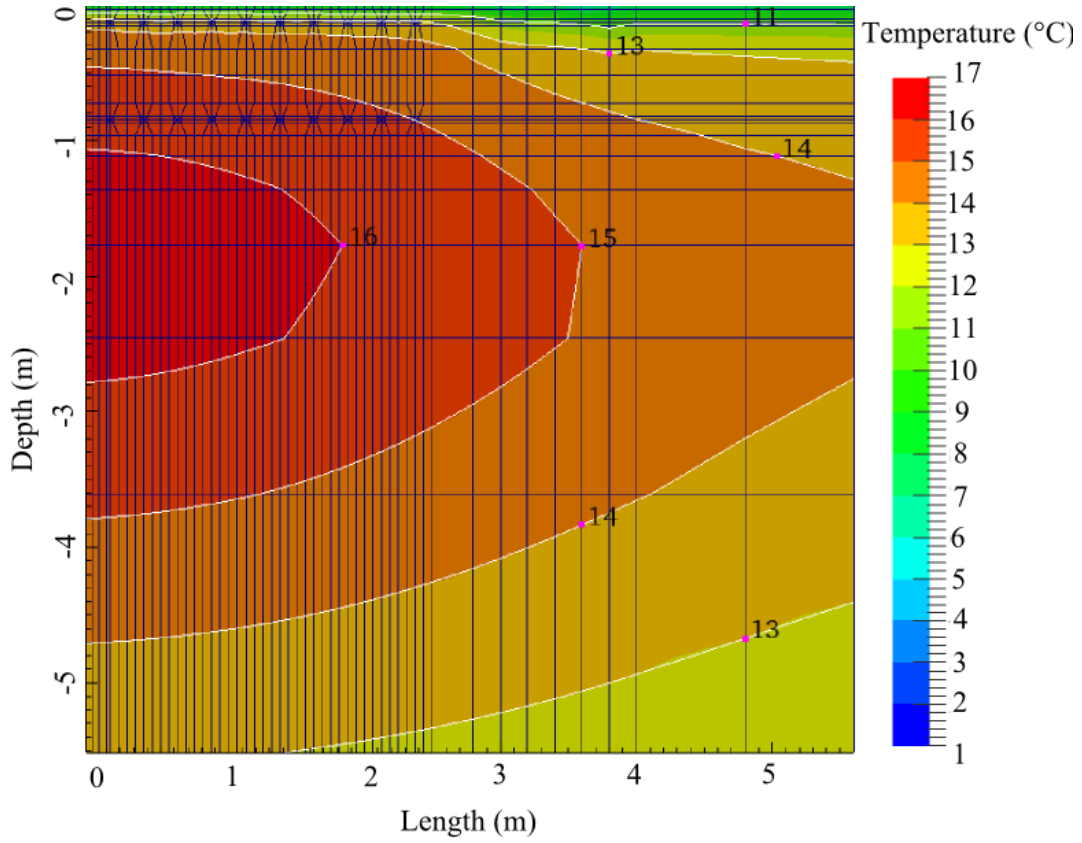

Figure 10-26 - Contour temperature profile near the road surface at y=0 m (Figure 10-3) corresponding to the end of the third activation period (31st October 2006).

10.6.7 Fourth activation period: From 1st November 2006 to 1st March 2007 (usage)

Figure 10-27 shows the comparison of numerical results and experimental measurements for the transient variations of soil temperature at borehole G at 0.1325 m depth (System 2, under road at collector pipes depth) for the fourth activation period. While Figure 10-28 shows the corresponding comparisons at 0.8475 m depth (storage pipes depth). As in the previous usage period (Section 10.6.4), similar predictions are made by 2D and 3D numerical models at collector depth. Both models are affected in a similar way by snowfall events at end of December 2006 and at beginning of February 2007.

Figure 10-29 shows a contour plot predicted by the 3D model of the region near the road surface at plane y=25 m (Figure 10-3) at the end of this activation period. It can be seen how the stored energy in the soil has been discharged after this period. The 3D predictions are similar to the corresponding 2D predictions shown in Figure 9-31 except for slight differences near the edges of the insulation layer. Figure 10-30 shows a similar contour plot for the plane at y=0 m. It can be noticed that in this

region the temperature follows a layered distribution under 2 m depth, while at y=25 m the distribution follows a more elliptical pattern around the storage region and that, for example, the region with temperatures in the order of 9 ˚C is narrower and located closer to the storage pipes allowing regions with slightly higher temperatures than at y=0 m (of about 5˚C) been located closer to the surface under the edge of the insulation layer. This thermal energy could potentially be used for other applications (e.g. building heating).

Figure 34-31 shows a comparison of contour temperature profiles on the plane x=0 (between y=0 to y=25 m) corresponding to the end of the third and fourth activation periods. Span of insulation and pipes in this plane are indicated for reference. It can be seen the effect of the insulation layer, and that the region of influence of the system seems to be restricted to depths above 3 m.

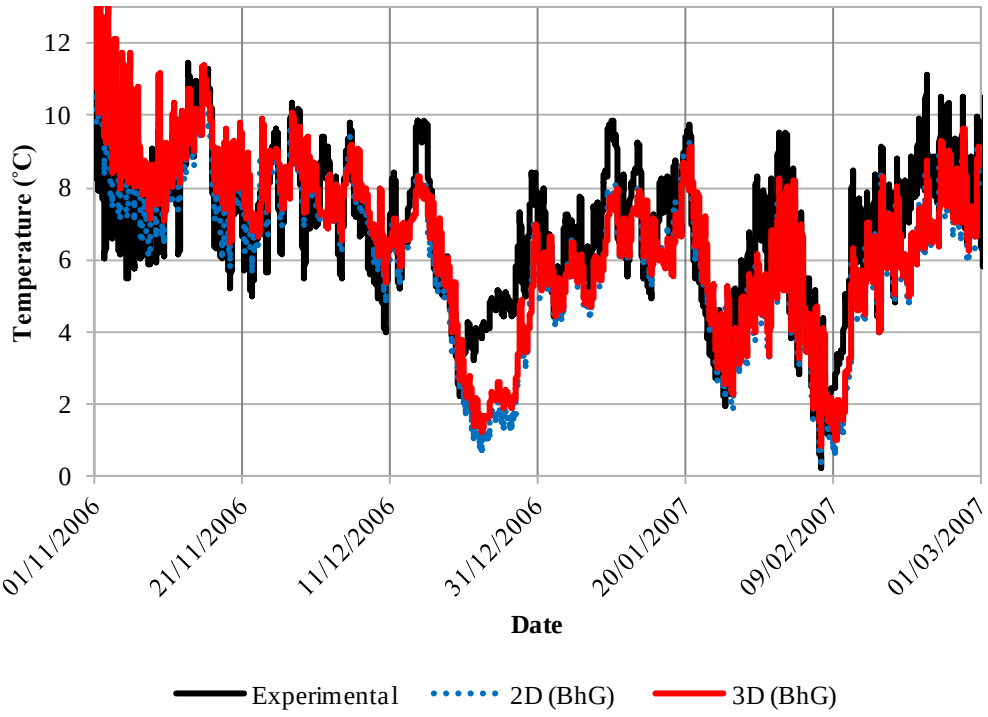

Figure 10-27 - Transient variations in 3D of soil temperature at borehole G at 0.1325 m (collector depth) for the fourth activation period.

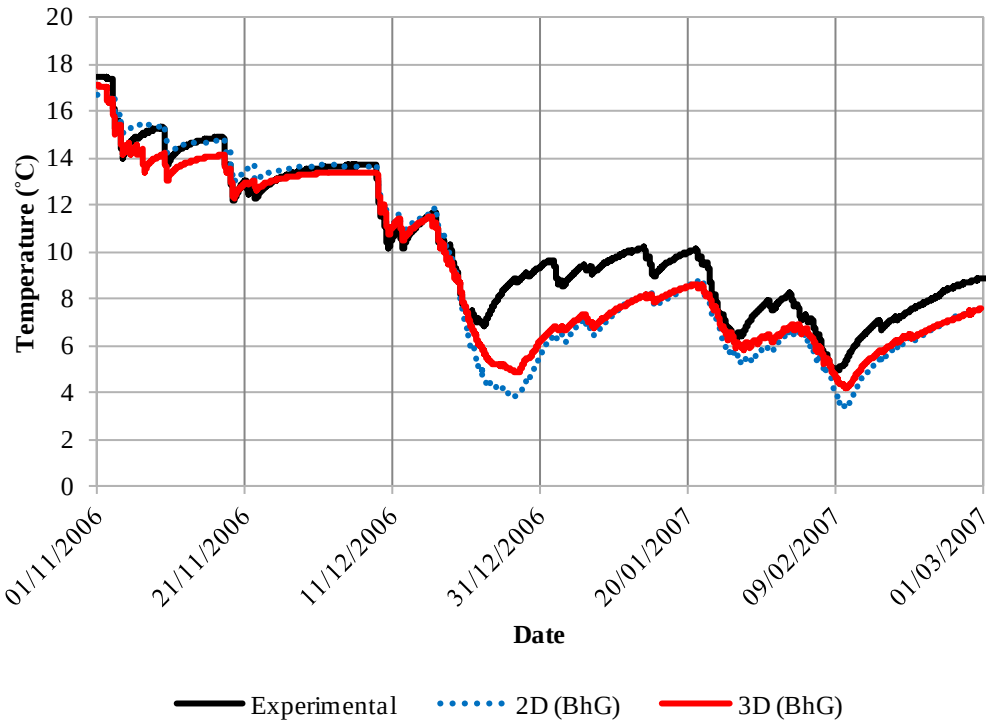

Figure 10-28 - Transient variations in 3D of soil temperature at borehole G at 0.8475 m (storage depth) for the fourth activation period.

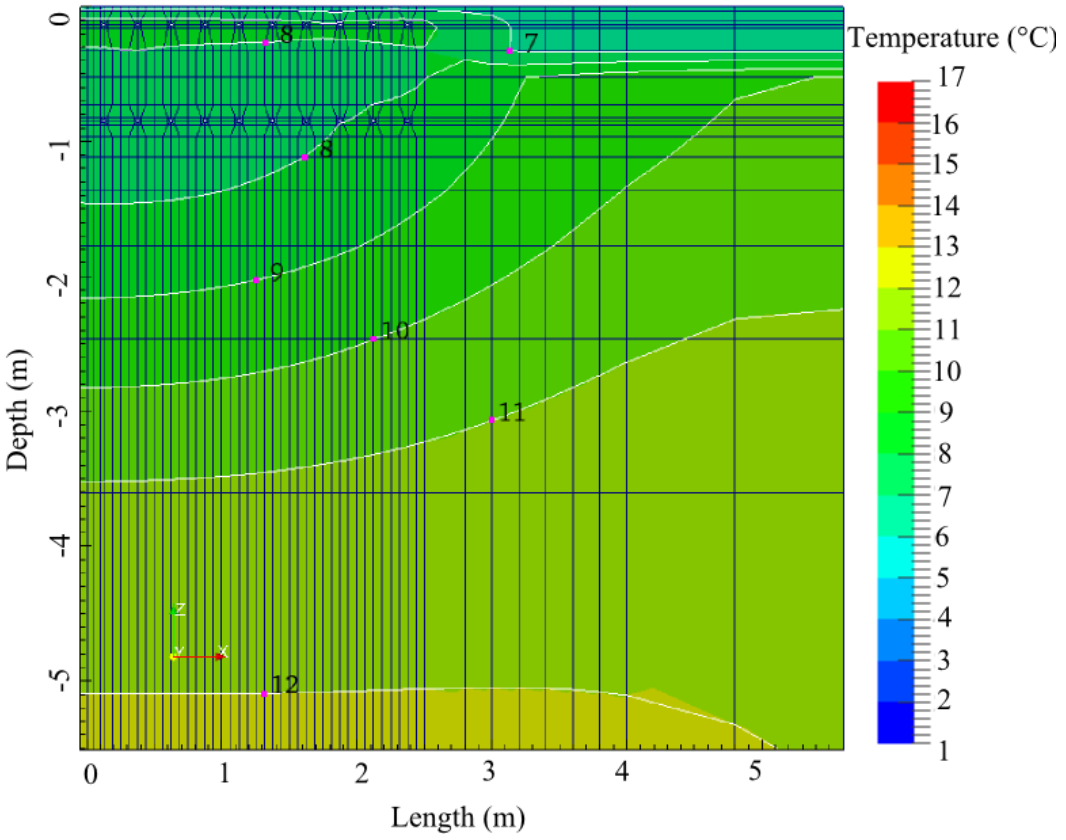

Figure 10-29 - Contour temperature profile near the road surface at y=25 m (Figure 10-3) corresponding to the end of the fourth activation period (1st March 2007).

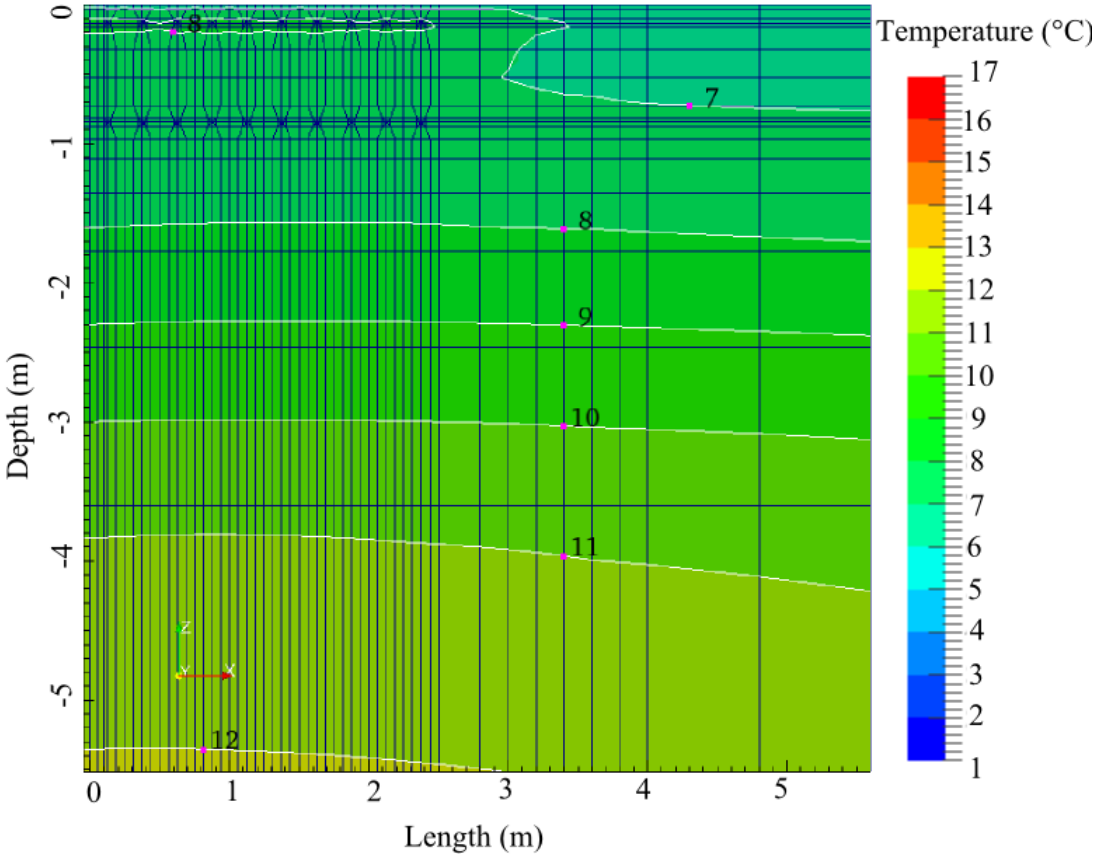

Figure 10-30 - Contour temperature profile near the road surface at y=0 m (Figure 10-3) corresponding to the end of the fourth activation period (1st March 2007).

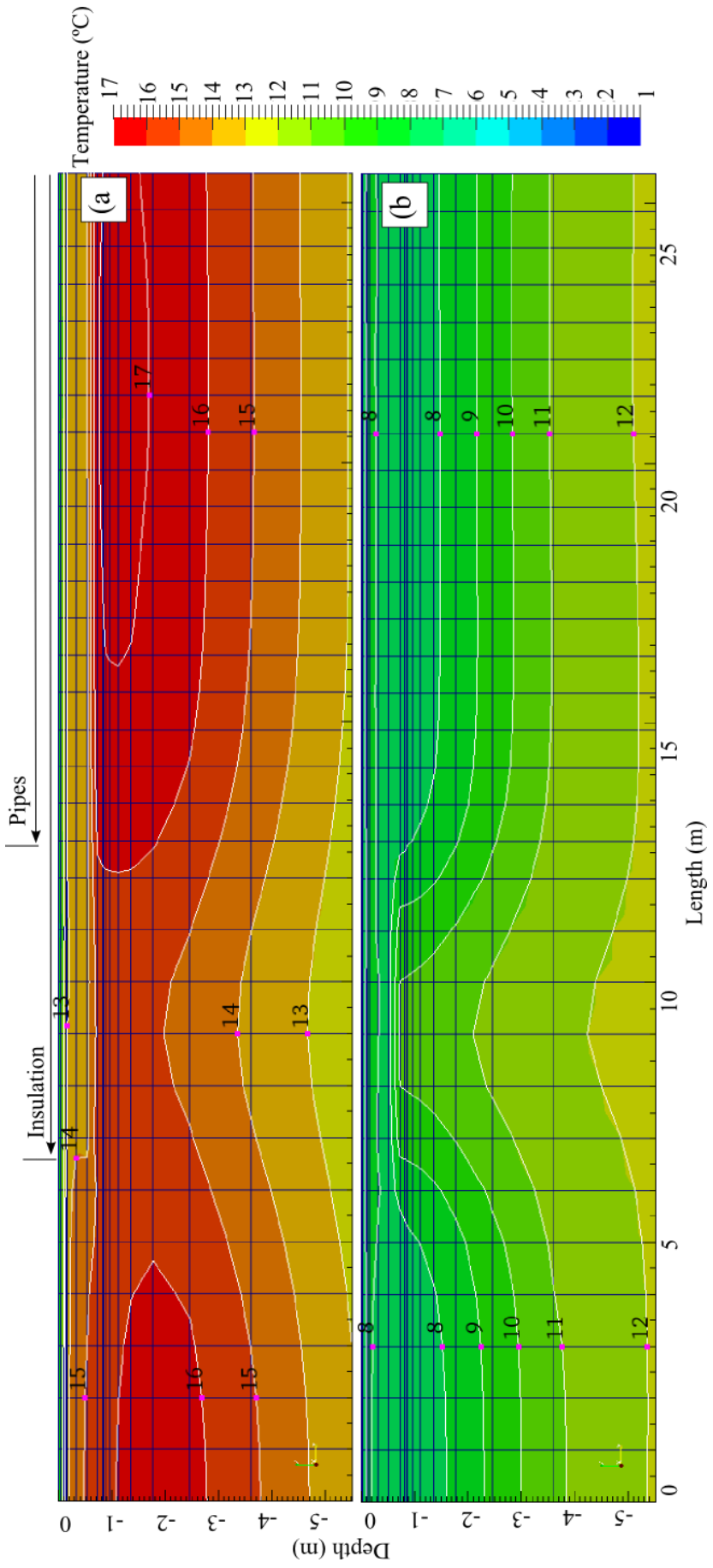

Figure 10-31 - 3D contour temperature profiles near the road surface at the plane x=0 m (Figure 10-3) corresponding to: a) the end of the third activation period (31st October 2006) and the end of the fourth activation period (1st March 2007).. Span of insulation and pipes in this plane are indicated for reference

10.7 Concluding remarks

This Chapter has presented the development of a numerical model in 3D able to represent the process of ground thermal energy storage carried out by buried engineering geo-environmental devices via the use of pipe heat exchangers.

The model solves the transient heat equation in 3D coupled with the transient heat advection equation through boundary and heat generation terms. The heat advection equation enables the model to represent the flow of fluid through pipes considered as 1D domains in relation with the soil domain.

The proposed numerical model has been applied to investigate the case study presented in Chapter 5 that deals with the application of an inter-seasonal heat storage system during a consecutive period of 2 years divided in 2 periods of insulation, 2 periods of thermal energy collection (summer 2005, summer 2006) and two periods of thermal energy extraction (winter 2005-2006, winter 2006-2007). The results obtained have been compared against results obtained with the 2D numerical model described in Chapter 9.

After analysing the different periods where the system was active (under collection or usage settings) including idle periods, the proposed numerical model in 3D has proved to be able to represent successfully the behaviour of inter-seasonal thermal storage devices. In it was found in this Chapter that:

i) the proposed 3D model offers results that are in general comparable with those obtained from a 2D model.

ii) a homogeneous level of shading at 50% (calibrated for the 2D model) seems to be not completely suitable for 3D conditions. This impacts the temperatures predicted in the storage region specially during summer.

iii) a slight improvement in winter performance regarding the matching of experimental measurements was observed in the 3D model as compared with the 2D model. This might be related with the simplifications made in the 2D model that could overestimate the estimated pipe heat fluxes.

iv) the region of influence of the inter-seasonal heat storage system seems to be restricted to depths less than 3 m.

v) in Chapter 9 was suggested that the system was storing a surplus of thermal energy on the soil mass. In this Chapter, this seems to be confirmed with contour temperatures from regions with and without the influence of the storage system. Furthermore, the results seem to indicate that the excess energy is contained in the region under the edges of the insulation layer.

The main limitation found in the 3D numerical model was its inability to deal with snow events. In this way the results are congruent with those obtained in Chapter 9 for the case of a 2D numerical model. Another limitation in the 3D model is the assumption of homogeneous shading on the road surface that might limit the consideration of regions with different levels of solar radiation that are inherent to realistic 3D domains.

10.8 References

Carder, D. R., Barker, K. J., Hewitt, M. G., Ritter, D., and Kiff, A. [2007]. Performance of an Interseasonal Heat Transfer Facility for Collection, Storage and Re-Use of Solar Heat from the Road Surface. PPR302. Transport Research Laboratory.

Chapter 11 Conclusions

11.1 Summary of thesis objectives

The proposed objectives for this thesis have been achieved including the development of numerical models in 2D and 3D capable of simulating the transient behaviour of geo-environmental engineering applications related to the storage of thermal energy in shallow regions of the ground. It has also been accomplished the development of a new analytical approach suitable for the estimation of soil temperature profiles using widely available sources of meteorological data.

Further objectives have been completed in the following deliverables:

- Chapter 2 provided an overview of the scientific literature available related to the storage of thermal energy in soils using shallow heat exchangers. The topics covered included: i) the main physical properties governing the transfer of heat and moisture in the ground, ii) the dependency of these properties with moisture content, iii) the description of three main formulations describing the energy interactions at the soil surface for different soil covers, iv) the process of coupled heat and moisture transfer in a soil and the relative dependence of the hydraulic properties on the temperature field and conversely the dependence of thermal properties on soil moisture content, v) analytical methods for the estimation of the soil temperature profiles and, vi) a brief overview of some scientific works regarding the numerical treatment of buried thermal devices
- Chapter 3 presented the theoretical framework used to describe the governing equations of heat and moisture transfer within soils and heat advection within pipe systems, mass and energy conservation principles and specific relations defining mass and thermal fluxes between the soil and the atmosphere.
- Chapter 4, developed the numerical solution of the theoretical framework presented in Chapter 3. The finite element method was used for spatial discretization and a finite difference time-stepping method was used for time discretization.

- Chapter 5 provided a summary of a field-scale experiment performed by others. This was used to validate the numerical models proposed in this work.
- Chapter 6 provided the results of a laboratory testing schedule used to measure key soil properties from samples obtained from the experimental site described in Chapter 5.

11.2 Main findings

The main findings of this thesis are summarized as follows:

- An analytical solution for the transient heat transfer equation has been developed. The equation was shown to be capable of estimating realistic soil temperature profiles and seasonal variations of thermal energy stored in the ground. A homogeneous free-flux boundary condition at the bottom of the domain and a third-kind boundary condition at the top boundary were employed. This approach minimized the amount of data required by the domain (only thermal properties need to be provided). In addition it also required the development of mathematical expressions describing the daily and annual variation of solar radiation and air temperature. These expressions have been proposed and calibrated using widely available meteorological data. It was demonstrated that the proposed analytical model is able to represent experimental transient variations of soil temperature and thermal energy with reasonable accuracy. A sensitivity analysis of several key variables in the analytical model have shown that the sky emissivity tends to dominate the variations of thermal energy stored in the ground.
- Following the development of the analytical model, a 1D numerical model for the transient heat transfer equation was used to explore the impact that assumptions regarding the boundary formulation at the soil surface had on the seasonal variations of thermal energy stored in the ground. It was found that different surface formulations predict different levels of thermal energy and that it is critical to choose a suitable formulation for the problem under study. It was also found that the main differences in predicted thermal energy were restricted to the region near the surface. Assumptions regarding the bottom boundary condition and initial condition were also considered in terms of their effect on the overall computational effort required to provide

realistic initial states. It was found that if no boundary condition is enforced at the bottom of the domain (assuming a homogeneous free flux boundary condition), at least 8 yearly cycles are required to reach a stationary state, regardless of the initial condition chosen, although in general, steady states are obtained at a faster rate with initial conditions based on experimental measurements. Analytical and uniform initial conditions seems to perform similarly regarding the pace at which a steady state is reached. It was also found that numerical predictions of soil thermal behaviour obtained with meteorological data measured on site are equivalent to those predictions obtained with meteorological data from public sources.

- Numerical models in 2D and 3D were developed and applied to study an experimental test-case related to inter-seasonal heat storage in soils. It was found that both models were able to represent the process of ground thermal energy storage carried out by buried engineering geo-environmental devices via the use of pipe heat exchangers. The main finding in this study was the impact that shade cast upon collection surfaces by nearby objects (e.g. trees) can have on the thermal performance of thermal storage geo-environmental facilities. The results also showed that a 2D simplification of the problem is adequate in this case and requires considerably less computational effort. However, it was shown that a 3D model still offers advantages regarding the detailed description of temperature profiles and heat flow in the domain that could reveal useful regions for further thermal energy extraction. Additionally, if more detailed considerations of the spatial distribution of shading on the surface were taken into account, a 3D model could potentially offer better approximations compared with a 2D model.

11.3 Limitations

As mentioned in the introduction of this thesis, the main limitations of the proposed numerical model are listed as follows:

- No mechanical deformations or chemical reactions were considered in the model.
- The model is applicable for unsaturated conditions. No saturated conditions or combination of saturated/unsaturated conditions were taken into account.

- No snow melting processes are considered, although coupled evaporative processes are taken into account.
- A simplified approach was used to model the shading cast by nearby objects on the soil surface. This approach proved to be suitable in 2D simulations. However, it limits the capabilities of a 3D model that would benefit from a more detailed description of the distribution of shading on the top surface of the domain.
- Regarding the analytical approach proposed in Chapter 7, it was found that main limitation was the inability to take into account cloud cover variations.

11.4 Future work:

The proposed future work is in part related with the limitations previously listed. Suggestions include:

- Improving the prediction of heat energy transfer interactions under extreme weather conditions, in particular snowfalls.
- Further exploration of the implications of long term and/or generalized use of geo-environmental engineering thermal devices on the soil temperature profile.
- Explore in more detail the advantages of using more descriptive shading profiles in 3D simulations.

11.5 Recommendations

Based on the results obtained in this thesis the following recommendations are suggested in relation to the installation and use of geo-environmental engineering devices:

- Care should be taken with the installation area avoiding objects that might cast shades on collector surfaces in systems that rely on solar radiation as primarily heat source.
- Take into account the region of thermal influence of the facility to either better prepare the region or to minimize possible thermal contamination of nearby aquifers. In the case of inter-seasonal heat storage systems this seems to be restricted to 3 m depth.

- Likewise, the region of thermal influence might indicate potential areas where other applications could extract thermal energy without interfering with the main application.
- A canopy cover on the soil surface has a insulation effect reducing the heat fluxes between the soil and the atmosphere. A shallow heat storage system could benefit from having this kind of soil surface in the surrounding area, provided that the vegetation does not influence the mechanisms of heat collection.
- Meteorological data obtained from public sources seems to be suitable to estimate either by analytical or numerical methods the amount of potential energy stored in a given location. This could be useful at planning stages for decision making.

Appendix A Thermal properties of water-ethylene-glycol mixtures

This appendix presents thermal properties of a fluid commonly used in thermal engineering applications: water-ethylene-glycol mixtures. The equations and coefficients used are based on the product description provided by ME Global (2008).

A.1 Thermal conductivity

The thermal conductivity λ_{eg} (W/mK) of an aqueous ethylene glycol solution is given by the equation:

$$\lambda_{eg} = A + BT + CT^2 \qquad \text{(A.1)}$$

where all the coefficients depend on the percentage of ethylene glycol present on the solution and are available on the cited reference. Table A-1 shows the variation of the thermal conductivity of an ethylene-glycol mixture at representative temperatures. It can be seen that the thermal conductivity of the solution decreases with the percentage of ethylene glycol present in it for the same temperature and increases with temperature for the same content of ethylene glycol.

	Thermal conductivity (W/mK)		
Temperature (˚C)	10%	20%	30%
5	0.5343	0.5022	0.4717
15	0.5485	0.5127	0.4787
25	0.5616	0.5221	0.4849

Table A-1 - Values of thermal conductivities of aqueous ethylene glycol solutions for different percentages of ethylene glycol and different temperatures

A.2 Specific heat capacity

The specific heat capacity $c_{p,eg}$ (J/kgK) of an aqueous ethylene glycol solution is given by:

$$c_{p,eg} = A + BT + CT^2 \qquad \text{(A.2)}$$

where all the coefficients depend on the percentage of ethylene glycol present on the solution and are taken from the same reference. Table A-2 shows the variation of specific heat capacity of an ethylene-glycol mixture at representative temperatures. It can be seen that the specific heat capacity of the solution decreases with the

percentage of ethylene glycol present in it for the same temperature and increases with temperature for the same content of ethylene glycol.

	Specific heat capacity (J/kgK)		
Temperature (˚C)	10%	20%	30%
5	4074.90	3926.20	3774.26
15	4082.92	3942.93	3795.85
25	4091.41	3959.66	3817.43

Table A-2: Values of specific heat capacities of aqueous ethylene glycol solutions for different percentages of ethylene glycol and different temperatures.

A.3 Density and specific gravity

The specific gravity γ_{eg} of the fluid is given by the equation:

$$\gamma_{eg}\left(\frac{T}{15.5C}\right) = A + Bx + Cx^2 \qquad \text{(A.3)}$$

where x is the percentage of ethylene glycol present in the solution where all the coefficients depend on the temperature and are taken from the same reference.

Table A-3 and Table A-4 show the variation of specific gravity and density of an ethylene-glycol mixture at representative temperatures. It can be seen that the specific gravity and density of the solution increase with the percentage of ethylene glycol present in it for the same temperature while the behaviour is non-linear with temperature.

	Specific gravity		
Temperature (˚C)	10%	20%	30%
5	1.013	1.029	1.045
15	1.042	1.028	1.042
25	1.010	1.024	1.037

Table A-3: Values of specific gravity for aqueous ethylene glycol solutions for different percentages of ethylene glycol and temperatures.

	Density (kg/m^3)		
Temperature (˚C)	10%	20%	30%
5	1011.79	1027.76	1043.74
15	1012.04	1026.76	1040.75
25	1008.80	1022.77	1035.75

Table A-4: Values of density for aqueous ethylene glycol solutions for different percentages of ethylene glycol and temperatures.

A.4 Dynamic viscosity

The dynamic viscosity μ_{eg} (kg/ms) for an aqueous ethylene glycol solution is given by:

$$Log_{10}\left(\mu_{eg}, cP\right) = A - B/\left(x + C\right) \qquad \text{(A.4)}$$

where x is the percentage of ethylene glycol present in the solution where all the coefficients depend on the temperature and are taken from the same reference. Table A-5 shows the variation of viscosity of an ethylene-glycol mixture at representative temperatures. It can be seen that the viscosity of the solution increases with the percentage of ethylene glycol present in it for the same temperature and decreases with temperature for the same content of ethylene glycol.

	Dynamic viscosity x10^3 (kg/ms)		
Temperature (˚C)	10%	20%	30%
5	2.060	2.704	3.604
15	1.450	1.882	2.476
25	1.140	1.456	1.883

Table A-5: Values of dynamic viscosity for aqueous ethylene glycol solutions for different percentages of ethylene glycol and temperatures.

A.5 References

ME Global. [2008]. *Ethylene Glycol - Product Guide [Brochure]*.

Appendix B Convective heat transfer coefficient inside a pipe.

This appendix explores the impact of varying fluid temperature and mean velocities on the convective heat transfer coefficient between the pipe wall and the fluid.

For the purpose of this study, representative mean velocities (0.10 m/s, 0.14 m/s and 0.20 m/s) and temperatures (5 ˚C, 15 ˚C and 25 ˚C), thermal properties of ethylene glycol solutions presented in Appendix A and assumed values of 0.0125 m and 0.002 m for the external pipe radius and pipe wall thickness are used in the theoretical formulation introduced in Section 3.6.1.

B.1 Reynolds number

Table B-1, Table B-2 and Table B-3 show values for Reynolds number calculated using equation (3-30) at different mean velocities and percentages of ethylene glycol present in the aqueous solution inside the pipe. It can be seen that many of the values for the Reynolds number are expected to be in the range defined as transitional flow ($2000 < Re < 4000$).

	Reynolds number - (10%)		
Mean Velocity (l/s)	5 ˚C	15 ˚C	25 ˚C
0.10	3,067.09	4,354.58	5,522.11
0.14	4,293.92	6,096.42	7,730.95
0.20	6,134.17	8,709.17	11,044.21

Table B-1 - Values of Reynolds number at different temperatures and mean velocities corresponding to an aqueous solutions with 10% ethylene glycol.

	Reynolds number - (20%)		
Mean Velocity (l/s)	5 ˚C	15 ˚C	25 ˚C
0.10	2,373.53	3,403.94	4,383.92
0.14	3,322.95	4,765.52	6,137.49
0.20	4,747.06	6,807.88	8,767.85

Table B-2: Values of Reynolds number at different temperatures and mean velocities corresponding to an aqueous solutions with 20% ethylene glycol.

	Reynolds number - (30%)		
Mean Velocity (l/s)	5 ˚C	15 ˚C	25 ˚C
0.10	1,807.68	2,623.21	3,434.16
0.14	2,530.75	3,672.50	4,807.83
0.20	3,615.36	5,246.42	6,868.32

Table B-3: Values of Reynolds number at different temperatures and mean velocities corresponding to an aqueous solutions with 30% ethylene glycol.

B.2 Prandtl number

Table B-4 show results for Prandtl number calculated using equation (3-32) for different percentages of ethylene glycol present in the solution and for different temperatures.

	Prandtl number		
Temperature (˚C)	Ethylene Glycol (10%)	Ethylene Glycol (20%)	Ethylene Glycol (30%)
5	15.70	21.14	28.83
15	10.80	14.48	19.64
25	8.31	11.05	14.83

Table B-4: Values of Reynolds number at different temperatures and mean velocities corresponding to an aqueous solutions with 30% ethylene glycol.

B.3 Friction factor

Table B-5, Table B-6 and Table B-7 show results for the friction factor calculated using equations (3-33), (3-34) and (3-35), and the Reynolds values presented in section B.1 .

	Friction factor *f* - (10%)		
Mean Velocity (l/s)	5 ˚C	15 ˚C	25 ˚C
0.10	0.033861	0.040332	0.037455
0.14	0.040512	0.036347	0.033880
0.20	0.036280	0.032736	0.030621

Table B-5: Values of friction factor at different temperatures and mean velocities corresponding to an aqueous solutions with 10% ethylene glycol.

	Friction factor *f* - (20%)		
Mean Velocity (l/s)	5 ˚C	15 ˚C	25 ˚C
0.10	0.03115	0.03626	0.04025
0.14	0.03564	0.03920	0.03627
0.20	0.03925	0.03517	0.03267

Table B-6: Values of friction factor at different temperatures and mean velocities corresponding to an aqueous solutions with 20% ethylene glycol.

	Friction factor *f* - (30%)		
Mean Velocity (l/s)	5 ˚C	15 ˚C	25 ˚C
0.10	0.03540	0.03166	0.03650
0.14	0.03139	0.03848	0.03909
0.20	0.03799	0.03805	0.03508

Table B-7: Values of friction factor at different temperatures and mean velocities corresponding to an aqueous solutions with 30% ethylene glycol.

B.4 Nusselt number

Table B-8, Table B-9 and Table B-10 show results for the Nusselt number obtained using equation (3-31) and the results for presented in previous sections for Reynolds number, Prandtl number and friction factor. Note that the relations for laminar flows are not required since the assumed conditions for the fluid put it in transitional and turbulent states.

	Nusselt number Nu - (10%)		
Mean Velocity (l/s)	5 ˚C	15 ˚C	25 ˚C
0.10	25.66	40.55	47.60
0.14	45.45	57.79	66.46
0.20	66.38	81.95	92.93

Table B-8: Values of Nusselt number at different temperatures and mean velocities corresponding to an aqueous solutions with 10% ethylene glycol.

	Nusselt number Nu - (20%)		
Mean Velocity (l/s)	5 ˚C	15 ˚C	25 ˚C
0.10	18.04	30.20	41.17
0.14	32.98	49.55	58.66
0.20	56.23	71.64	83.16

Table B-9: Values of Nusselt number at different temperatures and mean velocities corresponding to an aqueous solutions with 20% ethylene glycol.

	Nusselt number Nu - (30%)		
Mean Velocity (l/s)	5 ˚C	15 ˚C	25 ˚C
0.10	12.73	20.97	30.96
0.14	22.54	38.66	50.44
0.20	42.87	61.02	72.89

Table B-10: Values of Nusselt number at different temperatures and mean velocities corresponding to an aqueous solutions with 30% ethylene glycol.

B.5 Pipe convective heat transfer coefficient

Finally, Table B-11, Table B-12 and Table B-13 summarize the results of convective heat transfer coefficients calculated using equation (3-29) and the results presented in the previous sections for the Nusselt number.

It can be seen that in general h_f decreases when the percentage of ethylene glycol in the solution increases. For a given content of ethylene glycol, the higher values for h_f are obtained with increasing the mean velocity in the tubes and the temperature of the solution. This can be appreciated more easily in Figure B-1, Figure B-2 and Figure B-3, where the convective heat transfer coefficient, for different percentages

of ethylene glycol, has been plotted against temperature for three fluid mean velocities.

	h_f - (10%)		
Mean Velocity (l/s)	5 ˚C	15 ˚C	25 ˚C
0.10	672.00	1,090.36	1,310.40
0.14	1,190.35	1,554.15	1,829.58
0.20	1,738.69	2,203.69	2,558.33

Table B-11: Values of convective heat transfer coefficient, h_f, at different temperatures and mean velocities corresponding to an aqueous solutions with 10% ethylene glycol.

	h_f - (20%)		
Mean Velocity (l/s)	5 ˚C	15 ˚C	25 ˚C
0.10	444.22	759.07	1,053.98
0.14	812.06	1,245.32	1,501.61
0.20	1,384.40	1,800.64	2,128.74

Table B-12: Values of convective heat transfer coefficient, h_f, at different temperatures and mean velocities corresponding to an aqueous solutions with 20% ethylene glycol.

	h_f - (30%)		
Mean Velocity (l/s)	5 ˚C	15 ˚C	25 ˚C
0.10	294.27	492.04	735.95
0.14	521.17	907.19	1,199.03
0.20	991.30	1,432.11	1,732.69

Table B-13: Values of convective heat transfer coefficient, h_f, at different temperatures and mean velocities corresponding to an aqueous solutions with 30% ethylene glycol.

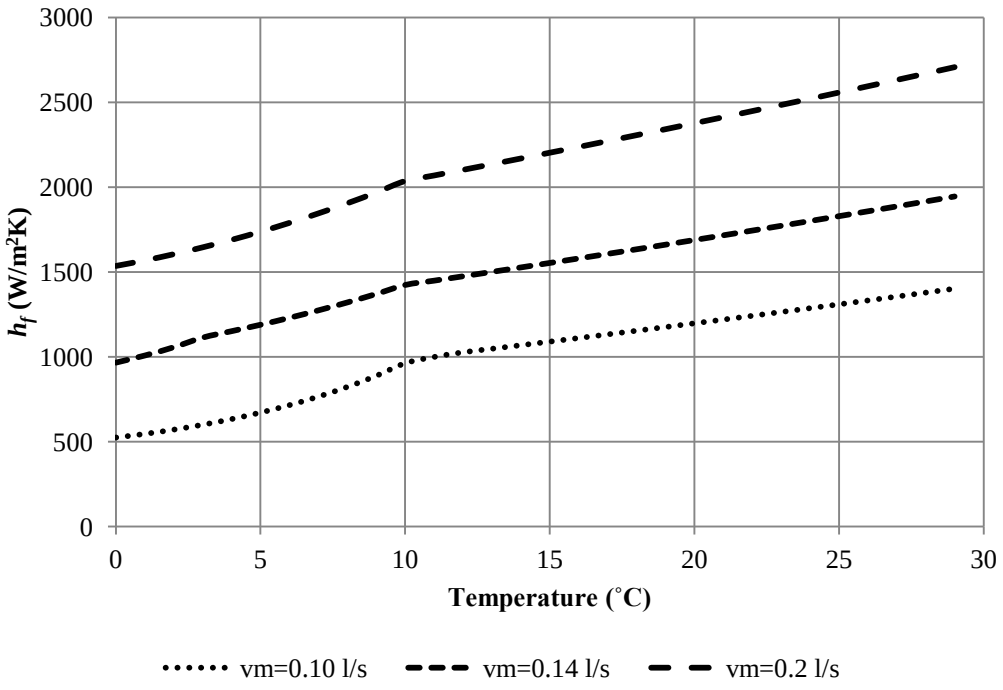

Figure B-1: Variation of the convective heat transfer coefficient with temperature at three fluid mean velocities for an aqueous solution of ethylene glycol at 10%.

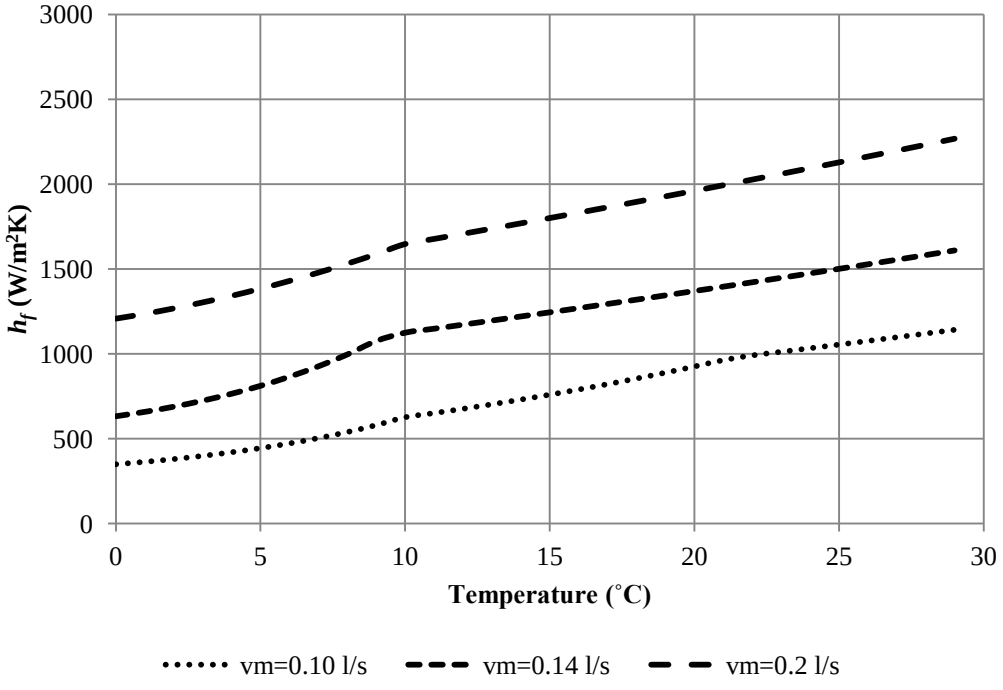

Figure B-2: Variation of the convective heat transfer coefficient with temperature at three fluid mean velocities for an aqueous solution of ethylene glycol at 20%.

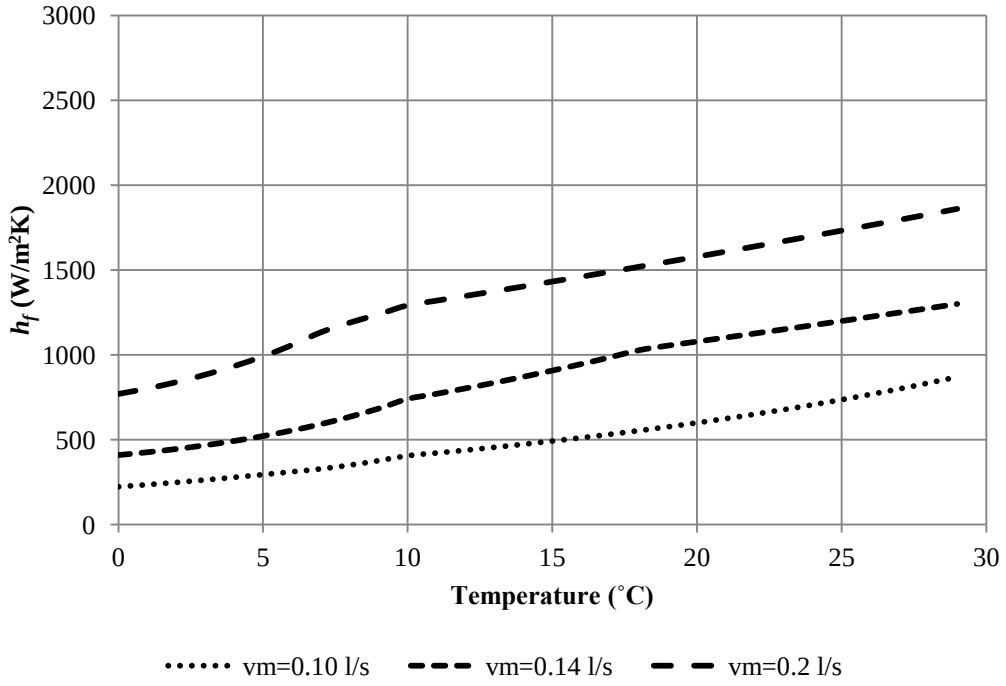

Figure B-3: Variation of the convective heat transfer coefficient with temperature at three fluid mean velocities for an aqueous solution of ethylene glycol at 30%.